NASA CR-112149

TECHNOLOGY DEVELOPMENT OF A BIOWASTE RESISTOJET

VOLUME I

by

D.G.Phillips

Prepared Under Contract NAS 1-9474 by

The Marquardt Company
Van Nuys, California

for

NATIONAL AERONAUTICS AND SPACE ADMINISTRATION
LANGLEY RESEARCH CENTER

June 1972

TECHNOLOGY DEVELOPMENT OF A BIOWASTE RESISTOJET

VOLUME I

BY

D. G. PHILLIPS

Prepared Under Contract NAS 1-9474 by

The Marquardt Company
Van Nuys, California

for

NATIONAL AERONAUTICS AND SPACE ADMINISTRATION
LANGLEY RESEARCH CENTER

June 1972

TABLE OF CONTENTS

LIST OF FIGURES

LIST OF FIGURES. - Continued

LIST OF FIGURES. - Continued

LIST OF FIGURES. - Continued

LIST OF FIGURES. - Continued

LIST OF TABLES

TECHNOLOGY DEVELOPMENT OF A BIOWASTE RESISTOJET

By D. G. Phillips

SUMMARY

This report summarizes the materials research effort conducted in support of a NASA-sponsored biowaste resistojet development program. The resistojet concept under development is the concentric tube design wherein the final pass of the gases through the thruster is through the resistance heated center tube. To produce high specific impulses, this center tube must operate at very high temperatures and it is this element that is most critical in the design. Because of the corrosive nature of the biowaste gases at high temperature, and because of the limited data available for many potential materials, the subject materials study was conducted.

This report is divided into two major divisions, the first being the REQUIREMENTS AND SELECTION CRITERIA, which included a literature search, and the second being the EXPERIMENTAL PROGRAM. The resistojet propellant composition, resistojet environmental considerations and candidate materials study are discussed under the first part.

The two major materials categories that were investigated were the superalloys and the noble metals. The superalloy metals were too limited in their upper operating temperature and therefore experimental effort concentrated on platinum and its alloys. Considerable use was made of the superalloy, Hastelloy X, when testing with methane, since thermal cracking and resulting carbon deposition limits the operating temperature with propellants containing methane. During the high temperature tests, metal temperatures up to 1700°K (3060°R) were investigated with the platinum alloys.

During the early phase of the program, the projected biowaste gases included CO_2, CH_4, H_2O, H_2 and only traces of O_2 and N_2. However, during 1971, it became evident that oxygen concentrations might be on the order of 0.5 to 1.0% by weight. This increase in oxygen concentration eliminated from consideration, otherwise attractive materials that are subject to significant oxidation.

The earliest platinum alloy investigated in detail was platinum-rhodium. This alloy was relatively oxidation resistant, had good strength properties and it was relatively easily to obtain in small tube form. For the 10 mlb resistojet under development, the center rube has an inside diameter of 0.1016 cm (0.040 in.) and a wall thickness of about 0.01778 cm (0.007 in.). Unfortunately, early testing showed that tubes made from Pt-20Rh, (20% rhodium in platinum) suffered from severe carbonyl reactions when operated at high temperature with CO_2. Evidently the CO_2 dissociates, forming CO which reacts with the rhodium forming volatile oxides. This reaction results in a relatively rapid depletion of the rhodium, and severely weakens the tube and causes it to leak.

Later tests indicated that the addition of 1.5% oxygen to the CO_2 suppresses the formation of CO and effectively inhibits the carbonyl reaction. The addition of 0.25% oxygen may be insufficient to suppress carbonyl reactions, however. Also, reducing the rhodium content to 5% appears to minimize carbonyl reactions. When Pt-Rh is maintained at high temperatures for long periods of time, considerable grain growth results and oxygen addition does cause oxidation and some reduction in tube wall thickness.

When the projected biowaste gases contained only trace amounts of oxygen, platinum-iridium appeared very attractive for biowaste applications. Platinum-iridium, although somewhat difficult to work, has high strength and is not subject to significant carbonyl reactions. However, when oxygen concentrations from 0.25 to 1.5% were added to the CO_2, excessive oxidation occurred with resulting tube failures in relatively short times.

Other materials that were tested included platinum-palladium, pure platinum and thoriated platinum. Platinum-palladium (Pt-Pd) does not have as high strength as does Pt-Rh or Pt-Ir but it does not suffer from carbonyl reactions and is relatively resistant to oxidation. However, evaporation of the palladium is excessive at temperatures much above 1500°K (2700°R) and therefore thruster performance would suffer if Pt-Pd were used.

Pure platinum is carbonyl and relatively oxidation resistant but has low strength. Its use would require modifications to the basic concentric tube resistojet design. Such modifications would be acceptable when necessary. Experimental results indicate that at temperatures above 1500°K (2700°R) significant oxidation of pure platinum occurs with a gas mixture of CO_2 and 1.5% oxygen.

Thoriated platinum (TD-Pt) appears to offer the best promise for biowaste resistojet applications. Experimental results indicated little or no carbonyl or oxidation problems. Low temperature strength of TD-Pt is slightly better than pure platinum, but its high temperature strength is much superior. The dispersed thoria is very effective in minimizing grain growth and therefore tube integrity can be maintained for long durations at high temperature.

Grain growth was evident after 1500 hours at 1700°K (3060°R) but grain boundaries were not straight lines and therefore tube strength was maintained. The dispersed thoria is also effective in suppressing oxidation and vaporization of the platinum. After 1500 hours at 1700°K with either pure CO_2 or CO_2 with 0.25% oxygen added, no measurable reduction in wall thickness occurred due to oxidation. However, with CO_2 and 1.5% oxygen, a 5% reduction in wall thickness occurred after 1000 hours at 1600°K. With the maximum projected oxygen content in biowaste gases of 1.0%, the wall reduction would be less.

INTRODUCTION

Resistojets have been under development at The Marquardt Company for the past ten years. Some of this effort has been government-sponsored and some has been conducted under Independent Research and Development programs. Various applications have identified certain design concepts as optimum and generally the specific propellants define materials of construction. This final report summarizes only the materials effort conducted between September 1969 and June 1972 on a biowaste resistojet technology development program* conducted for the National Aeronautics and Space Administration, Langley Research Center, under Contract NAS 1-9474. The engine development phase of the program is summarized in Volume II (Reference 1).

Potential Application

Reference 2 reported the selection of the biowaste resistojet system for simultaneous orbit-keeping and control moment gyro desaturation for the Manned Space Station/Base Concept. This and similar application studies identify desirable resistojet characteristics, define operational requirements and sometimes impose certain restrictions or requirements upon thruster operation that require improvements or significant changes to available thruster designs.

Program Objectives

The objectives of this technology development program included the design, fabrication, and demonstration of electrically heated 10 millipound thrusters utilizing, as propellant, typical by-products of spacecraft life support systems. Since high temperature materials, resistant to these propellants, and having suitable manufacturability characteristics are required to achieve high specific impulse, high thermal efficiencies and long life, materials studies were included. This report summarizes only the materials portion of this program. The materials study phase of the program is published as a separate volume because it should be of more general interest than the engine development phase and hopefully, the information will be useful in other applications or technology areas.

Resistojet Concept

The biowaste resistojet design utilized under this program has resulted from ten years experience at Marquardt in the development of high performance resistojets ranging in thrust from ten millipounds to one pound. The Marquardt design is based upon use of a concentric tube heat exchanger configuration which has the following advantages: (1) high thermal efficiency for low power consumption, (2) final gas

temperature close to maximum wall temperature for high specific impulse, and (3) minimized creep stresses with zero hoop-creep stress in the hottest inner element for long life.

Figure 1 shows the 10 millipound resistojet concept as developed for the MORL (Reference 3). It consisted basically of two functional parts: (1) an electric-gas heat exchanger, and (2) a nozzle for accelerating the resultant high temperature gas to produce thrust. The electrical flow was through the outer case, case end, nozzle and inner heating elements. A strut connector provided an electrical connection between the two main heating elements while concurrently allowing gas to flow through the engine. Approximately seventy-five percent of the ohmic heating took place in the inner heating element.

The gas flowed between the inner and outer case, intercepting the radial-thermal flow and carrying much of the heat back toward the center of the device. The gas then passed through the annulus between the inner and outer heating elements where a significant amount of gas heating took place. The final gas pass was down the inner heating element (center tube), where the gas very closely approached the wall temperature. The gas was then expanded through the nozzle.

The inner heating element is the critical component that necessitated the materials research phase of this program. This tube was small in diameter, I.D. = 0.016 cm (0.040 inches), with a thin, 0.01778 cm (0.007 inches) wall. This tube is approximately 4.24 cm in length. As is evident from Figure 1, the propellant gas flows on both sides of the center tube and therefore there is little pressure drop across the tube. The second tube is exposed to propellant gas on one side and vacuum on the other and therefore must withstand a higher ΔP, but its temperature is lower than that of the center tube.

REQUIREMENTS AND SELECTION CRITERIA

Propellant Composition

Definition of the specific propellant combinations for biowaste development is extremely important because of the corrosive nature of these gases at high temperature. Unfortunately, these gases cannot always be defined rigorously because of the experimental nature of and associated development of the biowaste life support systems. Early in the program, typical biowaste propellants included CO_2, H_2O, H_2, CH_4, other hydrocarbons and trace gases such as N_2 and O_2. It was expected that several of these gases would be available as mixtures.

Contact with personnel from McDonnell Douglas, Huntington Beach, during the latter part of 1971 indicated that the most probable biowaste gases for use with resistojets would contain about 1.0% oxygen instead of just a trace amount. The estimated gas composition, based upon a 90 day life support test was:

97%	CO_2
2%	N_2
1%	O_2

Other typical gas composition could be mixtures of CO_2 and CH_4 with smaller amounts of N_2, O_2 and H_2O. The early materials studies and tests were concerned with biowaste gases containing only trace amounts of oxygen whereas, later tests were conducted with propellants containing significant amounts of oxygen as a result of the change in projected gas composition.

Environmental Considerations

Temperature environment - To achieve high performance, heater tube surface temperatures may be as high as 1700°K (3060°R) while gas temperatures will extend from 1500 to 1600°K. These high temperatures can cause reactions to occur in either the gas or the tube or both. Because of the type of gases, the inner heating element must be resistant to both oxidizing and reducing atmospheres. Elemental carbon and hydrogen may form from the hydrocarbons, therefore, heater parts must resist both carburization and hydrogen embrittlement. Nitriding may be a consideration in the case of steels when nitrogen is present. Carbon monoxide (which can form from CO_2, hydrocarbon with oxygen or water, etc.) may be present as a contaminant gas. If it occurs it can form carbonyls with many elements including iron, nickel and rhodium.

Oxidizing environment - Initially, it was generally believed that very little oxygen would be present in typical biowaste gases. However during 1971, it was concluded that several of the propellant combinations may result in an oxidizing environment. The initial oxygen in the propellant may vary from essentially zero to as much as 1.0%. Oxygen also will be present from dissociation of oxygen bearing materials such as CO_2 or H_2O. Other chemical reactions can occur, depending on the kind of atmosphere, temperature and metal composition. One that has been found to be extremely detrimental to some metals is the formation of carbonyls. Decomposition of CO_2 results in CO which can combine with various elements (Pt, Rh, Ni, Fe, etc.) forming carbonyls which are relatively volatile and result in metal depletion.

The dissociation of CO_2 can be described as follows:

$$2\ CO_2 \rightleftharpoons 2\ CO + O_2 \qquad (1)$$

If a resistojet were operating on pure CO_2, the bulk chemical composition would be expected to be CO_2, since the kinetic of dissociation at a gas temperature of 1700°K or lower are so slow that the dwell time of the gas within the resistojet is not sufficient to reach thermodynamic equilibrium (Reference 4). However, the dwell time of the gas at the interface between the hot wall and the boundary layer is much longer, allowing the dissociation reaction of Equation (1) to proceed to some extent. Also, it is believed that the platinum alloys can act as a catalyst and may result in near equilibrium values. Computations were made to determine the chemical equilibrium of pure CO_2 and H_2O. These results are presented in Figures 2 and 3. Under the temperature condition of interest (1700°K), the amount of CO is significant.

Following the realization that significant amounts of oxygen may be present in the biowaste gases, computations were run to determine how effective the presence of the oxygen might be in suppressing the formation of CO in the tubes. The results of these calculations are shown in Figures 4 and 5 for initial oxygen concentrations of 0.5 and 1.0 weight percent, respectively.

The computer programs used to generate the majority of data of Figures 4 and 5 are written for single precision, limiting accurate calculations of CO mole fractions to values above 0.00001. Therefore, hand calculations of the amount of CO resulting from CO_2 dissociation with 1% O_2 in the initial mixture were made for temperatures below 1500°K. This was done for an initial mixture of 99% CO_2 and 1% O_2 at 40 psia. The result of this computation is shown in the lower portion of Figure 5. (The results of the hand calculations at temperatures below 1200°K are shown in Figure 6 along with predictions for pure CO_2.)

The calculated mole fraction of CO corresponding to the test conditions used for several Pt-20 Rh tubes discussed later, is also shown in Figures 4 and 5. This mole fraction of 0.00025 was calculated for an initial composition of 100% CO_2, a pressure of 40 psia and a temperature of 1500°K. At that condition, a Pt-20 Rh tube had failed because of carbonyl reaction after 570 hours. It is shown in Figures 4 and 5 that an order of magnitude reduction of CO is predicted at 1500°K for the oxygen bearing biowaste product studied. The effectiveness of O_2 in suppressing CO_2 dissociation increases with decreasing temperature, with ratios of 10:1, 20:1, 37:1, and 75:1 at temperatures of 1500, 1400, 1300 and 1200°K, respectively. The effect of the initial O_2 on the kinetics of formation of CO might give an additional improvement in the severity of the rhodium carbonyl reaction. However, the kinetic effects have not been evaluated.

Reducing environment. - Several of the biowaste propellants may result in a reducing atmosphere for the resistojet heating elements. These biowaste propellants include H_2, CH_4, mixtures of CH_4 and H_2O or CH_4 and CO_2 with small amounts of nitrogen. With some mixtures, the ratio of the ingredients determine whether it is oxidizing or reducing.

Experimental results have shown that the decomposition of CH_4 can result in serious carbon deposition and resultant tube plugging. While carbon deposition must be avoided in resistojet thrusters, an understanding of the deposition phenomenon is helpful in order to determine at what condition the carbon actually becomes a problem. Rapid deposition presents a failure mode. Deposited carbon can block gas flow passages, change the electrical characteristics of the thruster heater, and may result in a corrosion problem (carburization). Fracturing of deposits away from heater tube surfaces and subsequent nozzle throat blockage presents the worst type of failure mode. In order to maximize thrusting performance (high specific impulse) it is desirable to establish to what temperature the heater can be operated without a long term carbon problem. Carbon deposition is an exponential phenomenon with temperature. Rather than design for absolute zero rate of deposition, it is more practical to define a threshold temperature of operation in terms of long term-tolerable-minimum deposition rates. For example, a deposition rate of 0.2 micro-inches per hour would result in a 0.002 inches (2 mils) deposit in 10,000 hours. During that time, chemistry conditions would probably be cyclic and at times would strip away any carbon. Thus a 0.2 micro-inches per hour rate would be considered a practical threshold value.

Carbon deposition in resistojet thrusters is an undesirable phenomenon and is considered a potential failure mode. Most of the literature dealing with carbon deposition is in a positive sense where carbon coatings are desired as a final product. Carbon deposition by the pyrolysis of hydrocarbon gas can most simply be described as chemical vapor deposition. With some compounds, the chemistry of vapor deposition is relatively simple. For hydrocarbons, the process is extremely complex and not yet fully understood. Appendix A summarizes some of the theories and observations of the investigations regarding carbon deposition.

It is appropriate to mention briefly that carbon deposits can be removed, and in certain propellant circumstances, performance may be increased. If biopropellants to be used are of fixed composition and contain methane in quantities to present a carbon deposition problem, then operation of the thruster must be strictly limited to a threshold deposition rate acceptable for long term operation (i.e. 0.2 micro-inches per hour). On the other hand, if propellant chemistry is cyclic, higher temperature operation may be possible by taking advantage of the carbon removal properties of carbon dioxide.

Gasification of carbon proceeds rapidly with carbon dioxide at sufficiently high temperatures. Figure 7 presents data from Reference 5 showing carbon removal rate in units of micro-inches per second. Carbon deposition rates discussed in this report are given in units of micro-inches per hour in keeping with the slow rates

observed. In a thruster operated with biopropellant containing methane, temperature will be limited to some threshold level. Maximum carbon deposition rates will occur at maximum (threshold) temperature locations. If the temperature were set for a deposition rate of 1.0 micro-inches per hour and the thruster were operated with a methane mixture for 100 hours, the resulting maximum carbon deposition thickness would be 100 micro-inches or 0.0001 inches. If subsequently the thruster were operated on CO_2 at full power with a surface temperature between 1500 and 1600°K, the carbon removal rate would be above 1.0 micro-inches per second. The above deposit would be removed in less than two minutes. Water should also work as a carbon gasifier. References 6 through 8 give additional data on gasification of carbon with carbon dioxide.

Candidate Materials Study

Selection criteria. - The principal criteria for selection of a resistance heating material may be summarized as follows:

1. Adequate mechanical strength (elastic modulus and yield) and ductility at room temperature following repeated thermal cycling.

2. Excellent high temperature endurance properties such as phase stability, stress, rupture, creep, etc.

3. An electrical resistivity commensurate with practical voltage-current ranges.

4. Low emissivity.

5. Low coefficient of thermal expansion.

6. Ease of fabrication (forming, machining, welding, etc.)

7. Compatibility with supporting structural materials.

8. Resistance to sublimation, oxidation, and other detrimental reactions with the propellant at high temperature.

Practical considerations limit the concentric tube resistojet material selection list to one of relatively ductile materials. Mechanical properties must be considered relative to the space vehicle launch environment and again relative to in-space thrusting. Sufficient cold strength properties are necessary to withstand launch vibration and acceleration loads. Since the engines will be heated during acceptance testing, the critical inner element will be in an annealed condition at the time of launch. Yield strength, the elastic modulus and fatigue strength enter into the dynamic load design. During thrusting operation in space, mechanical loads which include thermal expansion loads (both longitudinal and circumferential on the heater tubes compounded by thermal cycling) are greatly reduced relative to launch environment loads. Adequate creep strength at high temperature is a necessary requirement during in-space operation.

Physical properties which are most important include the melting point, electrical resistivity and emissivity of the material. Of lesser importance are density (a low density is desirable to reduce inertia loads of structural parts), thermal expansion coefficient (thermal expansion may be taken care of by an expansion bellows) and thermal conductivity (gas side thermal resistance is predominate making structural material thermal conductivity of little consequence). The melting point must necessarily be higher than the operating temperature by more than 100°K. An operating temperature around 1600-1700°K appears to be a reasonable goal. It is desirable to have a high electrical resistivity in order that heater tube wall thickness not be too thin to achieve a reasonable voltage-to-current relationship for the thruster.

The heater tube wall thickness is made thinner on the innermost tube in order to generate most of the I^2R heating in the heater core. It is desirable to dissipate 60 to 80 percent of the total power in the innermost heater tube. With high heater wall tempeatures, there is a substantial radiant heat flux potential from the core to the outer case of the thruster. To minimize this outward heat flux, a low emmissivity is desirable. This consideration is even more significant in the higher temperature hydrogen-ammonia resistojet thrusters.

Fabrication factors must also be considered; however, these tend to be secondary considerations except for metallurgical control. The fabrication and parts joining techniques must not degrade those material properites important to long life and reliability at high temperatures.

In the selection of a high temperature-biowaste resistojet heater material, perhaps the most important consideration involve chemical properties of the material relative to corrosion including the effects of thermal cycling and stress. Specifically, high temperature corrosion is a major criteria in heater material selection.

Corrosion is the wasting away of structural material by any one or combination of mechanisms. Corrosion can be uniform on the material surface or irregular causing pitting and cracking or it can occur within the material itself. Unlike ambient temperature corrosion, diffusion in solid phases becomes an important factor in high temperature corrosion. Constituents of the surrounding atmosphere such as oxygen, carbon and hydrogen can diffuse into the material and conversely, metal ions and electrons can diffuse outward causing internal corrosion.

Dry oxidation is a common type of high temperature corrosion in which corrosion products remain on the surface of material and offer resistance against continued corrosion. The term "dry oxidation", used in Reference 9, is a convenient one. It offers a distinction between materials which are precoated with protective material, those whose oxides and corrosion products evaporate away, and the dry oxidation materials which form their own protective coating during exposure to corrosive atmospheres. The effectiveness of dry oxidation materials resistance to corrosion depends on the integrity of the protective film or scale. Superalloys, for example, rely on this protective mechanism in oxidizing atmospheres. The protective scale must be nonporous and adherent, and remain so, under thermal shock and mechanical stress, if it is to be effective. With an effective oxide coating, corrosion proceeds at a slower rate by diffusion.

The term dry oxidation can be defined more specifically as the loss of electrons by a constituent in a chemical reaction and may, therefore, involve other forms of attack besides combination with oxygen. Carburization and nitriding may be included in dry oxidation reactions. It is important to realize that the biowaste propellants and mixtures include a wide variety of chemical substances, and as such, offer a full range of atmospheric environments. These include oxidizing, reducing, carburizing and nitriding. Waste materials from man include sulfur compounds. It is conceivable

that traces of sulfur compounds could find their way into biowaste propellants. Sulfidation could then become a biowaste resistojet heater material problem. Sulfur compounds are particularly harmful to many materials at high temperature. The selection of heater materials must not be made on the basis of oxidation resistance alone. The other types of atmospheres must be considered. A material which is very attractive in an air atmosphere may be very poor in oxidizing atmospheres containing smaller amounts of oxygen than exists in air or in reducing or carburizing atmospheres.

For the biowaste resistojet, oxidizing atmospheres will not include air as such. Oxygen will be recovered and be presented in concentrations from a trace gas to 1.0%. Oxygen will also be present from dissociation of oxygen bearing materials, such as carbon dioxide and water. An atmosphere which contains a very small quantity of oxygen may be oxidizing to one constituent of an alloy while reducing to another.

Methane, hydrogen, nitrogen, and carbon monoxide are likely biowaste propellants. These form reducing atmospheres. A reducing atmosphere is one that will reduce iron oxide on steel. The protective oxides formed in the presence of reducing gases are entirely different from the usual in-air-oxide and generally are relatively ineffective as a protective film.

Decomposition of methane, carbon dioxide and carbon monoxide release free carbon which in turn can result in carburization of the heater material. Carburization is used here to mean the impregnation of a metal with carbon from a surrounding atmosphere containing carbon bearing constituents. The fact that the carbon content increases in a material may not directly result in corrosion. Indirectly, corrosion may occur as the result of an alteration in the oxidation resistance, for instance, or a lowering of the melting temperature of the new higher carbon content material. A reverse phenomenon, called decarburization, may also be harmful by depleting necessary carbides in some alloys.

Hydrogen can enter into the corrosion picture by causing subsurface damage. Hydrogen may diffuse deep into the material, combine with carbon and form methane which will be trapped and cause internal voids and stressing referred to as embrittlement. Atomic hydrogen can recombine in the material, again, causing voids and stresses. Similarly, unstable nitrides can be formed by the diffusion of nitrogen into the metal and cause intergranular attack and embrittlement.

There are many chemical reactions which can occur, depending on the kind of atmosphere, temperature and metal composition. One that has been found to be extremely detrimental to rhodium in Pt-Rh alloy is the formation of carbonyls. Decomposition of carbon dioxide results in carbon monoxide which can combine with various elements (Pt, Rh, Ni, Fe, etc.). Rhodium is particularly susceptible to the formation of metal carbonyls. This problem was dramatically demonstrated by tests

which will be described later. Grain stabilization of such alloys as Pt-Rh was considered to slow down the carbonyl depletion of rhodium from the alloy. However, if rhodium diffuses essentially by a bulk process, grain size would not be of primary importance relative to carbonyl attack.

The above discussion relates to the more serious chemistry problems which can plague resistojet heater materials. The problem is made more severe when compounded by the following phenomena:

1. These effects may be superimposed resulting in more complex and accelerated behaviors.

2. The type of atmospheres may be changing or alternating which generally has a catastrophic effect on metals.

3. Thermal cycling can disturb the metal internally as well as externally to again accelerate corrosion.

4. Mechanical stresses aggravate the corrosion problems, both internally and externally.

Relative to the many parameters involved in the general biowaste resistojet application, the selection problem was extremely difficult because of the lack of high temperature effects data relative to the various atmospheres. A case in point is platinum and its alloys. These materials do not depend on any substantial oxide film for protection. Rather, they are relatively inert to oxygen and hence, noble. There was relatively little data on platinum alloys in reducing and carburizing atmospheres. Based upon the literature, platinum is not always recommended for reducing atmospheres.

References 10 and 11 are suggested for additional information on corrosion phenomenon relative to specific materials.

Oxidation resistant material classifications.- Several classes of materials, including nonmetallics, are recognized as oxidation resistant materials. These are summarized in Figure 8 and in Table I. Of these, the stainless steels fall short of the temperature goal (1700^{o}K) for biowaste resistojet operations. The nickel or cobalt based superalloys are marginal in that they are suitable only for the lower region of the projected temperature range for biowaste resistojets. The temperature goal exceeds the melting points of most of the superalloys. The refractory metal alloys such as tungsten, molybdenum, and rhenium require protective coatings. The small size of resistojet thrusters, however, tends to preclude the use of adequate coatings. The ceramic materials are characterized by brittleness and poor shock resistance. Thus, the refractory metals and ceramic material are not being considered for the current application.

Three general classes of metals having sufficient ductility for the biowaste resistojet design have been considered in depth. These include the following:

1. Those metals which rely on dry oxidation for corrosion protection.

2. The noble metals which are inherently inert and do not require appreciable self-generated coating for corrosion protection.

3. Dispersion strengthened metals of the first two classes.

The dry oxidation class can be subdivided as follows:

1. Stainless steels
2. Iron-chromium - aluminum steel
3. Nickel-chromium steels
4. Nickel-base alloys
5. Cobalt-base alloys

Nickel (except dispersion strengthened nickel discussed later) and nickel-iron alloys are not being considered since they are generally inferior to all of the above metals for high temperature applications.

The stainless steels have been replaced by the superalloys for very high temperature applications. In the next section, however, one of the better austenitic steels, Type 310, and a ferritic steel, Type 446, will be considered for comparative purposes. Iron-chromium-aluminum alloys have long been used for electrical resistance heater elements. These have excellent resistance to oxidation because reaction with oxygen forms a protective layer of alumina. N-155 or Multimet which can be classified as a nickel-chromium steel can be considered for this class of steel. Generally referred to as "superalloys" are many nickel-base and cobalt-base alloys. These are very complex alloys containing closely controlled amounts of several other elements. Generally, oxidation resistance of these materials has been compromised for mechanical properties suitable for jet aircraft engine structures. Several of the better or typical superalloys are compared.

Of the noble metals and their alloys, oxidation resistance considerations suggest platinum and platinum-rhodium alloys. Mechanical considerations generally find pure platinum unsuited structurally. Carbon dioxide is a major constituent of the biowaste propellant spectrum and can result in extremely rapid destruction of platinum-rhodium at elevated temperature. Platinum-iridium alloys are less resistant to oxidation but iridium offers greater resistant to carbonyl attack while possessing attractive mechanical properties. Platinum-palladium alloys have relatively good oxidation properties, are not prone to carbonyl attack, but have lower mechanical strengths and lower melting points than rhodium or iridium alloys.

Dispersion strengthened materials considered included already commercially available TD-Ni and TD-NiCr as well as some development dispersion strengthened noble metals. TD-NiCr is essentially a thoria dispersion strengthened Nichrome. Nichrome has served as a leading commercial electric resistance heater material for applications above 1300°K. TD-Ni is inferior to TD-NiCr relative to oxidation and reduction type of atmospheres. TD-Ni properties are presented, however, and are useful in drawing some conclusions about dispersion strengthened metals. TD-Pt offers great promise for biowaste resistojet application.

References 12 through 57 can be referred to for more detailed information on the materials discussed in this report. It is not possible to include here the vast amount of experimental data available. In many instances, such data are misleading because they relate to specific environmental conditions for specific materials. It is difficult, with the exception of exposure to air, to compare all of the candidate materials. While oxidation is a consideration, reliance on this effect alone can be especially misleading relative to the biowaste resistojet application.

Corrosion data in the literature are presented in many different forms and immediate comparisons are often difficult. Very often, dry oxidation type corrosion data are presented as weight changes in the tested materials. Material weight can increase as oxygen, carbon, etc. are absorbed and/or reacted and retained by the material. Spalling of scale and evaporation of the metal and/or oxides results in a weight loss. Relative to resistojet applications, oxide coatings will not present mechanical strength advantages nor generally contribute to the conduction of electrical current.

Scale and coatings are to be considered a hazard should they subsequently spall and flake away into the gas stream and block the thruster nozzle throat. Corrosion data should be compared on the basis of the actual depletion (or recession) of the parent metal (or surface). Thick coatings should be viewed with caution and a selection of such a material should only be made after extensive environmental testing including thermal, atmospheric, and mechanical stress cycling to evaluate the integrity of such coatings. This caution tends to direct specific attention to the noble metals and their alloys.

Candidate material properties. - Because of the large number of possible materials and physical and chemical properties, some repetition in discussion is unavoidable. Summary type tables will be presented first, following by more detailed discussions.

General properties: Some physical and mechanical properties of typical candidate materials are compared in Table II. Values given are rounded off and where conflicting data exist, the conservative value is given. These data should be used for candidated material selection and not for design purposes. These data are typical since some superalloys are not included which may be superior in some respects to those listed. The alloys listed are generally the more common alloy for a specific

combination of elements or those for which data are more readily available. Certainly, if a specific alloy composition appears outstanding a more comprehensive evaluation should be made of immediate relatives. For example, the British alloy Nimonic 90 has been improved by an increase in the Al and Ti content (Nimonic 95) and again by the addition of more Al and Co with less Cr and Ti (Nimonics 100 and 105). Nimonics 100 and 105 offer greater resistance to oxidation and improved creep strength. Udimet 700 can be considered the United State's Nimonic 105 with still better creep properties.

Hafnium-tantalum alloy is included in Table II. References 25 through 27 discuss the hafnium-tantalum development studies of several investigators. This material does not appear to offer the oxidation resistance of many of the superalloys and noble metals.

Molybdenum disilicide is included in Table II as a curosity. It has already been rejected on the basis of brittleness. Note, however, its high melting point of 1950°C. Density is relatively low at 6 grams per cubic centimeter which is good. Electrical resistivity increases a factor of 6 from room temperature to 800°C. This is favorable and would permit a relatively thick walled innermost element. Improved strength of $MoSi_2$ has been demonstrated by bonding with metal powders. The behavior of $MoSi_2$ in the biowaste atmospheres remains to be evaluated.

Silicon carbide is another tempting material relative to many of its properties, particularly corrosion resistance. Like $MoSi_2$, it is a brittle material. SiC and $MoSi_2$ still present structural problems with respect to the concentric tube resistojet geometry.

The melting point temperatures listed in Table II generally exceed, by a sufficient margin, the useful corrosion resistance temperature and are of little importance. Densities of the steels and superalloys are lower than the noble metals by a factor of two or more. At the same time cold mechanical strength of the noble metals (with the exception of 20 and 30 percent iridium alloy) is inferior to the steels and superalloys. In this respect the steels and superalloys have the advantage relative to inertia load capability. Mechanical strength values reported are generally for the annealed condition and for the weaker structural form of the material. Resistojet heater tubes with 5 mil wall thicknesses generally do not have the advantages of repeatable strength obtainable in the more conventional structural shapes.

With the exception of TD-Ni and the noble metals, electrical resistivity is desirably high. While Nichrome, TD-Ni and TD-NiCr are not superalloys, they have been placed in the nickel base (less than 5 percent cobalt) class for convenience. The Nichrome and TD-NiCr physical properties listed in Table II are essentially the same as for superalloys, however. TD-Ni cold short term strength is relatively low as is the modulus for TD-NiCr.

For the noble metals, Table II shows iridium alloy to have superior strength and higher electrical resistivity than platinum and Pt-Rh alloys. The resistivity change on a percentage basis is higher for platinum followed by the platinum-rhodium aloys. Melting point is greater for both the rhodium and iridium alloys compared to pure platinum.

Comparative creep strengths for the candidate metals are presented in Table III. These data indicate the general improvement in hot temperature strength of the superalloys. In-100 and Mar M-200 lead the superalloys in this category. In-100, Mar M-200 and Mar M-302 are casting alloys. Nichrome (80 Ni - 20Cr) has a surprisingly good rupture stress but rates low in long term creep. This means its geometry will be changed significantly by light loads at high temperature. TD-NiCr which is essentially Nichrome with dispersed thoria offers even better stress to rupture and should have a significantly improved 1% creep strength. These data are not available; however, the creep strength advantage is reflected by the 4 kpsi for TD-Ni at 1210^{o}C, a condition at which pure nickel would be mechanically useless.

Emissivities of some of the candidate materials are listed in Table IV. The emissivity of platinum, which should be representative of the platinum alloys as well, is seen to be generally low. On the other hand, the steels and superalloys have generally high emissivities if any oxide coating is present. TD-Ni fairs in about the middle. TD-NiCr should have an emissivity close to that for Nichrome. The emissivity of thoria is shown and seen to be generally low. Thus, small additions of thoria to platinum for instance, should not significantly affect its emissivity. Dispersion strengthening with thoria is discussed in more detail in the next section. The emissivity of graphite is also listed in Table IV to indicate the harmful effect carbon deposition can have on noble metals and TD-Ni relative to radiant heat transfer.

Reference 12 presents a discussion very appropriate to this subject entitled: "The Selection of Material for Electrical Heating Alloys". A table is presented (Reference 12, page 622) comparing the life of various heating element materials in different atmospheres including oxidizing, reducing and carburizing. Nickel-chromium, nickel-chromium-iron and iron-chromium-aluminum are listed under alloys. Molybdenum, tantalum, tungsten and platinum are listed under pure metals and silicon carbide and graphite are listed under nonmetallic materials. Only graphite is recommended for carburizing atmospheres. Silicon carbide and the Ni-Cr and Ni-Cr-Fe alloys are recommended for reducing atmospheres. All but the refractory metals and graphite are recommended for oxidizing atmospheres.

For the ductile materials, the above recommendations in Reference 12 exclude carburizing type atmospheres. This has already been recognized as a problem from the carburization point of view as well as carbon deposition point of view. On the basis of deposition, resistojet operating conditions will be backed off to 1090^{o}K (see the Carbon Deposit Experiments Section). Carburization effects will be greatly

lessened at this lower temperature. The Reference 12 recommendations caution against the use of platinum for reducing atmospheres.

Dry oxidation resistant metals: Of the major components used in stainless steels and superalloys, chromium is the most important in establishing oxidation resistance. Chromium forms chromium oxide which adheres to the surface and reduces the rate of further oxidation. Chromium oxide spalls easily under thermal cycling. Nickel is added to minimize spalling. Figure 9 indicates how increased nickel and chromium content greatly affects the corrosion in air of steels under severe cyclic conditions. Nichrome is shown also for comparison. Figure 10 is a common presentation technique to show the trade-off between chromium and nickel to achieve low metal loss from corrosion. In general, as the nickel content is reduced, the chromium content should be increased for optimum corrosion resistance. At the other extreme, chromium content should not fall below 10 percent for good corrosion resistance.

Nichrome consisting of 80 percent nickel and 20 percent chromium appears about optimum in Figure 10 on the right hand margin of the diagram. Nichrome is one of the best alloys for commercial applications requiring oxidation resistance. This alloy has been improved by adding small quantities of various elements. Up to 3 percent silicon is sometimes added to increase lifetime at temperature. Many nickel base alloys have been developed for high temperature thermocouple service. Article 19 in Reference 13 presents work by Potts and McElroy with considerable data, including photomicrographs, on many of these alloys. Loss in wire diameter is presented for a dozen alloys including nickel for 500 hours exposures to 1000^{o}C. Chromel-A, which is Nichrome with 1.5 percent Si, has the lowest diameter loss at about 0.3 percent.

Nimonic 80A is essentially Nichrome with Ti and Al added for increased high temperature resistance. Oxidation of Nichrome proceeds slowly along grain boundaries. Carburization, with the formation of chromium carbides, can be extensive in water gas (chiefly CO and H_2) while not generally presenting a problem with carbon dioxide and carbon monoxide alone. Nitrogen will penetrate into the material forming chromium nitrides.

The Ni-Cr-Fe alloys generally behave like Nichrome but with reduced scaling resistance. Both Ni-Cr and Ni-Cr-Fe alloys are subject to embrittlement when alternately exposed to high temperature oxidizing and reducing atmospheres. Such atmospheres may contain hydrogen or carbon monoxide as reducing agents and water or carbon dioxide as oxidizers. Oxide coatings are not stable against reducing gases. Grain boundary material is reduced and oxidized rapidly under the very destructive alternating atmospheric conditions.

Some other general, and pertinent, corrosion phenomenon that have been observed with steels and nickel-base alloys include the following:

1. Oxidation in CO_2 is small but increases rapidly with increased H_2O content.

2. CO_2 in the presence of H_2O may result in decarburization of nickel alloys.

3. Hydrogen attack resulting in decarburization is reduced by the addition of elements such as Cr, Mo, W, Ti and Cb.

4. High nickel content is desirable to minimize carburization effects. Addition of Ti, Nb and Al improve resistance to corrosion by carburization.

5. Iron improves corrosion resistance in combustion gas type atmospheres. Table 7.49, page 7.106, of Reference 11 shows that replacing 20 percent of the nickel in Nichrome with iron greatly improves corrosion resistance in a water gas type atmosphere. Therefore, Hastelloy X and Inconel 601 should behave well in this atmosphere.

Before discussing the more compex superalloys, mention should be made of the uniqueness of iron-chromium-aluminum electrical resistance alloy. In an oxidizing atmosphere, this alloy forms a protective layer of 95 percent pure alumina giving it excellent resistance to corrosion by oxidation. This alloy is lacking in high temperature strength, however, Reference 12 presents data for Fe-20Cr-5Al 0.5 Co wire and indicates a useful cyclic life of 1000 hours for a 10 mil wire at 1800°F. While superior to Nichrome relative to oxidation resistance, the Fe-Cr-Al alloy is not suitable in reducing atmospheres. This implies destruction by diffusion through the alumina coating since alumina is generally good in H_2, CO, CH_4 and NH_3 atmospheres.

Data are presented on Page 699 of Reference 10 for the lifetime of 80Ni-20Cr, 60Ni-18.5Cr-18Fe, 34Ni-20Cr-43Fe and 63Fe-30Cr-5Al in air, CO_2, N_2, city gas, O_2, H_2 and water gas. Testing temperatures of 1050°C are quoted for the Ni-Cr and Ni-Cr-Fe alloys and 1200°C for the Fe-Cr-Al alloy. The CO_2, city gas and water gas atmospheres are particularly interesting and represent typical biowaste propellants. These tests were cyclic and conducted on small diameter wires. Lifetimes were short because of the small wire sizes (spirals 0.0157 inches in diameter). The pertinent data are summarized as follows:

		Cyclic Lifetime in Hours		
Alloy	Temperature, °C	CO_2	City Gas	Water Gas
80Ni-20Cr	1050	200	130*	> 400*
60Ni-18.5Cr-18Fe	1050	100	130*	360
34Ni-20Cr-43Fe	1050	50	-	140
63Fe-30Cr-5Al	1200	140	110	60

*Test discontinued

These data generally indicate superiority of the 80Ni-20Cr and 60Ni-18.5Cr-18Fe alloys to these atmospheres.

The superalloys contain many additional constituents which are generally employed to improve high temperature strength at the expense of oxidation resistance. Superalloys, particularly the precipitation - hardenable nickel-base alloys, are susceptible to intergranular oxide penetration. Intergranular oxidation can be a serious problem, particularly for thin structural sections. Fortunately, intergranular oxidation takes place only at relatively high temperatures. Internal preferential oxidation of chromium might occur in atmospheres that are oxidizing to chromium and reducing to nickel. Internal oxidation might take place under a surface that has previously been carburized.

The oxidation resistance of the nickel and cobalt base alloys is considered relatively good. Oxides formed are tightly adherent and protective. Extensive data are presented on the oxidation resistance of the nickel and cobalt base superalloys in Reference 20. These data show the new British Nimonics 100 and 105 to have superior oxidation resistance during continuous and cyclic heating over Nimonic 80A (essentially improved Nichrome). Nichrome looks good against the nickel-base superalloys. In general the nickel-base alloys appear to be on a par with colbalt base alloys. Hastelloy X fairs well and is considered a good high temperature superalloy.

A vast amount of data on corrosion of nickel and cobalt base alloys for gas turbine applications are presented in Reference 24 (a compilation of papers from the 69th Annual Meeting of the ASTM). These data include exposure to sulfur compounds and in some cases, also to sea salt. In a paper by Bergman, Sims and Beltran (page 38, Reference 24), the conclusions state that the best cobalt base alloys show a similar resistance to attack at 1750^{o}F as the best nickel base alloys. At 1900^{o}F the cobalt base alloys are more resistant. Among the nickel base alloys tested, Hastelloy X fairs well in the Bergman et al tests.

Stress plays an important role in the effectiveness of protective oxide coatings. This factor is discussed in Reference 20. Data are presented to indicate stress levels that result in rapid oxidation rate increases for typical superalloys at high temperature. Similar data are presented in Reference 19. These show, for example, that oxide penetration in 100 hours for a Nichrome type alloy doubles at 1800^{o}F when a stress of 1750 psi is applied. At 2200^{o}F, a 315 psi stress doubles the oxide penetration.

Stresses in gas turbine blades run high in absolute values. Turbine blades are rather "beefy" structural elements relative to the innermost heating element of a biowaste resistojet. Strains in the resistojet are completely different and more severe. Finding a dry oxidation type heater material whose protective film can withstand thermal mechanical resistojet conditions is a formidable problem which

is further compounded by the chemistry. Materials which are good for prolonged high temperatures in gas turbines will not necessarily work in resistojet environments. Likewise, thermocouple wire material in the form of thin walled long tubes will not necessarily work. This is to say that extensive resistojet testing and/or good simulation testing would be required with any candidate dry oxidation type material.

Platinum metals: The platinum metals are easier to project into a resistojet design than are the other metals. They do not accumulate significant oxide films while having good oxidation resistance. There are some unknowns, however, as to how well they will hold up in the other atmospheres (carburizing and reducing). Data on the effects of these other atmospheres on the noble metals are scarce. The noble metals generally have oxidation resistance which is very competitive with the dry oxidation materials. This is true of pure platinum and the platinum-rhodium and platinum-palladium alloys. With large additions of iridium in platinum, reduced oxidation resistances result.

Considerable oxidation data are given in the literature on the platinum metals (References 9 - 13, and 28 - 44 for example). Figures 11 and 12, from Reference 10, present some typical data. These show how weight loss increases when the surrounding atmosphere is in motion. Oxide vapors of the metals are swept away by the moving atmosphere thus accelerating the metal oxidation process. Rhodium alloying is seen to have little effect on oxidation of platinum while 10 percent iridium in platinum increases the weight loss an order of magnitude.

The data in Figures 11 and 12 can be converted to inches per year by dividing MDD (milligrams per square decimeter per day) by density and an appropriate conversion factor. Since the density of Pt and the Pt-Rh and Pt-Ir alloys are all about equal, then

$$(\text{Inches/Year}) \simeq (70 \times 10^{-6})\ \text{MDD}$$

At 1200°C in moving air the surface recession becomes about 0.0007 inch per year for platinum and 0.007 for Pt-10Ir. It is difficult to compare these values to those for a dry oxidation material. How the protective oxide coating holds up for a year becomes a variable. The values above for the platinum metals are fairly realistic for a one year period while a similar calculation from dry oxidation material data is academic. As expected, the inches per year values above increase with temperature. According to the Figures 11 and 12 data for platinum, the recession would increase about a factor of 4 from 1200°C to 1400°C.

The other noble metal alloy to consider is platinum-palladium (Pt-Pd). Palladium exists as a solid solution in platinum in all proportions. Palladium has a lower melting point (1825°K) than platinum (2042°K). However, the melting point

of alloys of Pt containing 10% or 20% of Pd would be close to that of pure Pt. Palladium forms a superficial oxide film when heated in air or oxygen at temperatures up to about 1073°K. The palladium oxide (PdO) is a dark blue or green. At higher temperatures, the PdO decomposes and the Pd surface is clear.

The oxidation resistance of Pd is superior to Pt in the temperature range 1173°K to 1473°K. At 1573°K the weight losses due to oxidation of platium and palladium are about the same (Reference 53). At higher temperatures, the weight loss of Pd increases relative to Pt; however, this is due (Reference 39) primarily to the greater evaporation of Pd. At 1773°K, the weight loss of Pd increases only 20% by changing the atmosphere from inert to O_2. There is no evidence of a carbonyl reaction with palladium in the available literature. Palladium differs from platinum in its characteristic of absorbing oxygen in solution, with maximum solubility of 0.63 atom percent (Reference 53).

Pt-Pd alloys show no visible internal oxidation at temperatures as high as 1673°K. However, there is some loss in mechanical strength of Pt-Pd alloys after heating at elevated temperatures. Figure 13 taken from Reference 55 shows the effects of heating Pt-Pd alloys in air at 1200°C (1473°K). Initially, a Pt-20% Pd alloy has a tensile strength nearly twice as great as pure platinum. After heating nearly 1000 hours, the tensile strength of the alloy would still be stronger than pure platinum, but by a smaller factor of about 1.5:1.

Mechanically, platinum is lacking in required strength. Chemically, platinum-rhodium alloy suffers severe carbonyl attack and platinum-iridium alloys oxidize more readily than Pt. Palladium alloys may be a good compromise but require operation at a lower temperature than 1700°K.

Reference 13 includes several author's discussions on the uses of the noble metals for thermocouples. These authors agree that data are lacking for platinum metals in atmospheres other than oxidizing. It is recognized, however, that Pt and Pt-Rh deterioriate under high temperature reducing conditions by absorption of gases. Relative to corrosion other than oxidation, iridium increases the resistance of platinum. A general discussion on the effects of various atmospheres is presented by Zysk beginning on Page 145 of Reference 13. The carbonyl problem with rhodium is not recognized, however. It is mentioned that hydrocarbons cracking in contact with platinum results in damage and that silica is considered very harmful to platinum. The corrosion books (References 9 - 11) and "The Metals Handbook" (Reference 12) each have chapters on noble metals and are worthy references relative to corrosion in general.

A technique developed by the British and used in this country by Engelhard Industries to retard grain growth and, hence, improve creep strength significantly is described in Article 9 of Reference 13. This article discusses the development and properties of Fibro Platinum as used for thermocouple wires. A composite

structure is made from a 1/2 inch diameter pure platinum tube filled with 0.020 inch diameter pure platinum wires and swaged into small diameter Fibro platinum wire. Stress-to-rupture data at 1450°C indicate the Fibro Platinum wire to be about as good as 5 and 10 percent additions of rhodium to platinum. This technique might be extended to tubes but has not been seriously considered as a resistojet heater material.

Dispersion strengthening: Dispersion strengthening of metals began in the early 1900's when thoria was introduced into tungsten for electric lamp filament lifetime improvement. Since then many metal particle systems have evolved with oxides the most common dispersoid. Carbides of the refractory metals have also been found to be effective dispersoids. Some one dozen techniques are used to effect particle dispersions in metals and alloys. These are well summarized in Table I of Reference 47. These range from mechanical mixing of powdered constituents to reduction of mixtures of various chemical compounds of the metal(s) and dispersoid.

Among the "jet age" materials, TD-Nickel and TD-Nickel-Chromium are perhaps the most commonly known dispersion strengthened materials. These are described in References 47 through 50 and can be considered commercially available production materials. Some pertinent properties of TD-Ni and TD-NiCr have been shown in Tables II, III and IV. Essentially, the effect of thoria in Ni and NiCr is to significantly improve the high temperature mechanical properties without having a significant effect on the physical properties. In Reference 47, a factor of 3.8 improvement in ultimate tensile strength at 1600°F (870°C) is indicated for 3.7 percent thoria in nickel. Strength data at room temperature does not indicate any significant change over pure nickel without thoria. The dispersoid effects grain stabilization in the material. This has a marked effect on the integrity of protective oxide coatings and hence, on oxidation resistance and on high temperature strength.

One of the mechanical properties of TD-Ni and TD NiCr which appears to be adversely affected by the thoria addition is the elastic modulus. This parameter is extremely important for dynamic loading by vibration, acceleration and/or shock. A primary concern in the concentric tube resistojet design (shown in Figure 1) under dynamic load is the inertia loading of the inner heater parts floated axially by the expansion bellows. The critical load on the small diameter inner tube is a column load which is proportional to the elastic modulus.

The elastic modulus E for Nickel 200 (99% Ni) and NiCr are about 30 million psi. Reference 47 gives E for TD-Ni at about 30 million psi based on some preliminary data. More recent data from another source reported in Reference 15 gives a range for E from 16 to 18 million psi. Reference 49 gives the E for TD NiCr as 22 million psi. It appears that the introduction of 2 percent thoria in Ni and NiCr have resulted in about a one-third reduction in the elastic modulus E. The selection of these thoriated materials in any design requires a close examination of the effect of a lower elastic modulus.

The British extended inert oxide dispersions into the platinum metals in the early 1940's. They later expanded their work to include carbides (Reference 51) for dispersoids. As with the Ni and NiCr metals, dispersions were being used to improve the high temperature mechanical properties of platinum metals.

Reference 52 presents data on the improved strength obtained with 0.25 percent dispersions in Pt-10Rh alloy wire. Also discussed in the Fibro Platinum (discussed in the previous section) based on a technique developed by the British (British Patent 849,431). Knight and Taylor (Reference 52) show ultimate tensile strength (UTS) at room temperature to increase from 90 to 96 thousand psi with the thoria addition. They attribute this improvement to increased cold work hardening remaining in the TD alloy. Their creep strength data at 1400°C show that for a stress causing failure in 10 hours in the non-thoriated alloy, the thoriated material lasted 1000 hours. They indicate that the increase in strength obtained by grain stabilization with thoria is equivalent to a rise in temperature of 350 to 400°C for equal time to failure. They also point out that the advantage of thoriated alloy may be lost at 1500°C, however. Regarding fabrication, Knight and Taylor point out that it is more difficult to obtain improved mechanical properties in strip material than in wire. Forming techniques are critical on the final properties of these materials.

More recent work on thoriated platinum metals is reported in Reference 54. Included are data for alumina and ceria dispersoids. Volume percent of dispersant ranged from 8 to 12.5 percent. Two techniques, (1) decomposition and (2) mixing, were used to form the thoriated platinum. Decomposition involves decomposing inorganic salts on metal powder to form composites while mixing involves blending of the fine elemental powders with a refractory oxide powder followed by compaction and hot working. In all cases, only platinum was used for the metal. Bufferd, et al, (Reference 54) reported very significant increases in the room temperature tensile strength of pure platinum as follows:

Composition	Tensile Stress, psi
Platinum	30,000
Platinum + Al_2O_3	40,000 - 47,000
Platinum + ThO_2	46,000 - 164,000
Platinum + CeO_2	55,000

Their creep data, for example, showed a factor of 15 (from 180 to 2800 psi) increase in a 100 hour rupture stress at 1300°C with 12.5 percent thoria.

It was these data that prompted early experiments on TD platinum for biowaste resistojets. Attempts were made to obtain TD-Pt with 10% thoria. Neither the major platinum metal sources, nor the Reference 54 group responded to a 10%, 5%, or even 2% level of thoria. Engelhard Industries did respond and supply material with their

recommended maximum thoria content of 0.7%. Evaluation of some of these materials is reported in a later section of this report. Material which was purchased as containing 0.2% thoria was later analyzed and found to contain 0.7%.

In Reference 55, one of the authors of Reference 54 stated that later work showed that a 2 to 3 percent level of thoria appeared to be optimum for strengthening platinum. This would agree with the work of Frazer, et al, on TD-Ni reported in Reference 47 which indicated an optimum in high temperature UTS with about 3% thoria. In view of Reference 55, care should be used in interpreting the Reference 54 data.

Reference 56 presents the work by the Johnson Matthey and Company on dispersion strengthening of platinum metals with titanium carbide. Darling, et al, (Reference 56) claims that carbides strengthen platinum more effectively than oxides and require smaller amounts of dispersant so that physical properties are less affected. Less than 0.1% by weight of carbide was used. Their micrographs on platinum wire with 0.04% TiC show a more favorable micro-structure as compared to platinum containing 0.2% thoria. They suggest that inclusions obvious in the Pt-0.2 ThO_2 are the result of the tendency of thoria to agglomerate.

Stress rupture data are given in Reference 56 for pure platinum and Pt-10Rh and their TiC dispersion strengthened counterparts. The following rupture times were found at temperature for various tensile stresses:

		Time to Rupture, Hours		
Material	Form	700 psi	1400 psi	2800 psi
Pure Pt	Wire	1/2 - 1	-	-
Pure Pt	Sheet	1/2	-	-
Pt-0.04 TiC	Wire	1,000	800	30
	Sheet	150	30	-
Pt-10Rh	Wire	50	10	1
Pt-10Rh + TiC	Wire	1,000	1,000	100

While not absolutely clear from the writing in Reference 56, it appears these data are for 1400°C. This would agree with other data they present as well as the data of other investigators. Note the difference between wire and sheet confirming the findings of Knight and Taylor.

Physical and mechanical properties for the above materials are listed in Reference 56. These show the following:

1. Density of the dispersion strengthened (DS) material is about 99.5% of the pure material.

2. Electrical resistivity increases about 15% for the DS material. This is desirable for resistojets.

3. Temperature coefficient of resistance drops to 90 to 95% for the DS material.

4. The UTS (annealed) increases about 40% for DS Pt and 10% for DS Pt-10Rh.

5. The modulus of elasticity increases from 22 to 23 million psi for DS Pt and from 27 to 28 million psi for DS Pt-10Rh.

Based upon these results with Pt and TiC, this material looked promising. However, later contact indicated that these results could not reliably be duplicated.

Additional work on thoriated platinum was done by Engelhard Industries. This effort, reported in Reference 57, was sponsored by NASA and was in direct support of biowaste resistojet development. The conclusion reached from this effort was that 0.6% thoria was the optimum dispersion in platinum from the manufacturing and usage standpoint. The tests reported showed that there is relatively little effect of 0.6% thoria on the room temperature mechanical and electrical properties of platinum. For all practical manufacturing purposes the thoriated material behaved as does commercially pure platinum. The advantage of adding thoria showed up in the high temperature, long term properties. The stress-rupture tests showed that in this type of testing, the platinum - 0.6% thoria alloy has a much greater life than platinum - 40% rhodium. In earlier testing, the platinum - 40% rhodium alloy had been found to be the best commercial alloy in stress-rupture tests at 1450°C. Figure 14 is a plot (taken from Reference 57) of stress vs. time-to-rupture for platinum - 0.6% thoria and some platinum-rhodium alloys, at 1450°C. The superiority of platinum - 0.6% thoria in this type of testing is clearly evident in this plot. Since platinum iridium alloys are more readily oxidized, they would show up as inferior to both the platinum - 0.6% thoria and platinum-rhodium alloys.

As reported in Reference 57, the metallographic cross sections of platinum - 0.6% thoria on test for extended periods at 1450°C showed an elongated grain structure. This elongated structure is quite different from platinum or platinum-rhodium wrought alloys held at high temperatures for extended periods. In the latter case the recrystallized grains would be equiaxed, and as time progressed the grain growth would result in very large grains.

Reference 57 continues: "The observation in dispersion hardened materials of relatively unaffected room temperature properties and enhanced high temperature properties has been reported for other materials such as nickel and copper. While the theoretical basis for improved high temperature properties has not yet been

firmly established, the most recent publications tend to focus on the particles in the grain boundaries, their interactions with dislocations and their modification of the grain boundaries as sources and sinks for vacancies. The action of the grain boundaries is obviously crucial in any theoretical development since this is the principal difference in cross sections of wrougth versus dispersion strengthened materials. Particularly so since it is observed that the fracture in the stress rupture testing invariably follows the grain boundaries. On a phenomenological basis, it can be observed that since the fracture follows the grain boundaries, a stable, elongated, fine grain structure presenting a minimum of grain boundary perpendicular to the applied stress would be the most desirable. This, of course, describes the platinum - 0.6% thoria alloy, and while not a fundamental explanation of the high temperature properties, it does help to rationalize the improvement in these properties.

The joining tests demonstrate that the platinum - 0.6% thoria alloy can be reliably fabricated by a number of techniques other than simple fusion welding. The particular method to be employed in a given situation will depend on the structure to be fabricated. However, when the alloys are properly joined, the weld will be as strong as the parent metal. Brazing is feasible with platinum-gold alloys, the choice of alloy being governed by the operating temperature required and the degree of temperature control which can be exercised in the brazing operation."

Based upon the work reported in Reference 57, it appears that thoriated platinum (TD-Pt) is a very strong contender for biowaste resistojet development although the material still has low strength properties in the annealed condition at room temperature.

Mention is made in Reference 30 of the strengthening of iridium by tungsten and thoria. The following tensile strengths are given for material annealed at 1300°C:

Material	Tensile Strength, psi	
	Room Temperature	1000°C
Pure Ir	101,000	22,400
Ir-5W	155,000	79,000
Ir-0.25 ThO_2	150,000	49,500

These data are not qualified as to work hardness condition. It would appear that the difference between the UTS of pure Ir and TD-Ir is in the temper condition. The UTS on drawn Ir wire can go to 300,000 psi. Ir oxidation properties were not discussed.

As with TD-Ni and TD-NiCr, investigators of dispersion strengthened platinum metals warm of the detrimental effect of melting the material as in welding. Dispersants agglomerate under these conditions creating voids and weakening the material. Joints to be welded must be located at lower temperature, lower stress location, otherwise, brazing techniques or mechanical joints must be used.

From the foregoing discussions, it is obvious that a significant experimental materials effort was necessary to evaluate the various promising materials under actual biowaste resistojet conditions before a final material could be selected. Even with experimentation, it is evident that the specific material can change with the specific application or by changes in geometry of the basic resistojet concept. The remainder of this report deals with the materials tests conducted in conjunction with this materials study.

EXPERIMENTAL PROGRAM

To aid in selecting the best material for the critical heating tube in the concentric tube resistojet, material tests were conducted in the Marquardt bell jar facility. The following section describes this facility.

Facility Description

At the start of this program, Marquardt had a single bell jar in which to conduct resistojet materials tests. Later the facility was improved and expanded to two bell jars. In the bell jars, the tubes made of candidate materials are resistance heated with the tubes exposed externally either to vacuum conditions or to one atmosphere as desired. Propellants are passed through the tubes to duplicate the chemical environment as well as the hydrostatic load conditions experienced in the thruster. Figure 15 shows the original bell jar test setup which includes three test samples. A closeup view of the tubes while being heated is shown in Figure 16. The tube samples can be supplied with different propellants. In the test illustrated in Figure 16, CO_2, CH_4, and H_20 are being supplied to the tubes from front to back. A water boiler is shown on the inlet side of the water supplied tube.

Figures 17 through 20 show the dual bell jar - resistojet heater tube test facility. The two bell jars are seen on the left and right in Figure 17. On the far right are a stack up of 6 power supplies to permit simultaneous operation of 6 sample tubes independent of one another. Gaseous propellant flow control is handled by the panel located between the two bell jars. An optical pyrometer in the foreground is used to measure tube surface temperatures. Immediately to the right of the right hand bell jar is a Milroyal precision water pump used to provide accurate water flow metering down to 0.005 grams per second. Miscellaneous equipment on the shelf behind the bell jars include vacuum monitoring equipment, a power control and meter for a steam generator and a temperature recorder. Behind the flow control panel is a 4 foot high gas humidifier column used in some of the experiments. Vacuum pumps, plumbing and wiring are located under the bell jar bench. Figure 18 shows another view of the bell jars and flow control panel. On the shelf can be seen clocks which total the time accumulated on each tube being tested. In Figure 18, two tubes are seen glowing in the left hand bell jar. These are of platinum-iridium alloy and are at maximum temperatures of 1590 and 1645^{o}K (2860 and 2960^{o}R) with a reducing atmosphere.

Close-ups of the bell jars are shown in Figures 19 and 20. The small diameter (typically 0.052 inches O.D.) - 2 inches long - sample tubes are mounted in 1/8 inch diameter support tubes and are seen in Figures 19 and 20 between the numbered - vertical electrical connector straps. The electrical connectors provide electrical current flow through the sample tubes. Propellants are fed by the 1/8 inch tubes from right to left in Figures 19 and 20. The left side bell jar shown in Figure 19 is plumbed for gaseous propellant mixtures. The right hand bell jar is shown with a steam generator. As shown in Figure 20, methane and water (boiled to steam) are being mixed and metered through small 0.012 inch diameter flow distributing orifices to the sample tubes. A mixing chamber on top of the boiler column insures uniform chemistry conditions. All tests are being conducted at tube internal pressures of 2 atmospheres. The steam generator-mixer is operated with a 533^{o}K (960^{o}R) outlet temperature. The plastic tubing connected to fittings near the base of each electrical connector strap provides water cooling for the straps. This prevents overheating of the vacuum feed through seals. A vacuum can be maintained in the bell jar of less than 20 microns of mercury. This imposes a hydrostatic bursting load on the tubes to aggravate the corrosion test conditions and give a more conservative test relative to actual resistojet conditions.

Pressure switched relays (high and low) and vacuum relays are used to provide automatic shut-down in the event one tube fails. Interlocking relays prevent restarts after power failure shut-downs. This preserves the data available in the remaining tubes. Temperature control is important for meaningful data in this test series. Generally, maximum temperature settings are found to hold within $\pm 10^{o}K$ with carbon deposition tests and $\pm 5^{o}K$ with corrosion tests on a day to day basis. Prior to setting operating conditions, tube samples are burned in with CO_2, for example, to ensure a dry starting condition and to establish tube outside surface emissivities used in interpreting optical pyrometer readings. Small 0.0025 inches diameter wires approximately 0.015 inches long are capacitance welded to the outside of the sample tubes. These are located transversely at 0.4 inch intervals along the 2 inches long sample tubes to provide precise temperature measurement reference locations for the optical pyrometer. In the vacuum condition, these reference wires do not affect tube wall temperatures since they have relatively negligible thermal losses. Thermocouples have been tried for tube wall temperature measurements and found to be unreliable. Thermocouple induced thermal losses can be significant. More importantly, electrical potential along the sample tubes is typically 1.0 volts per inch. This can induce large signal errors in the thermocouple junction even when care is taken to attach the wires at the same circumferential location.

Tube Inspection Techniques

An important part of any materials investigation is to know the condition of the material in question before and after testing. Although the vast majority of the tubes tested in the bell jar experiments behaved more or less as expected, a few of the tubes failed in an entirely unexpected and sometimes unexplained manner. For example, two of the tubes failed during the initial heatup. This failure was evidenced by a pop and the shattering of a short section (approximately 3/8 inches) of the tube. The tubes that failed in this manner must have been defective. To preclude this type of failure, several methods of nondestructively determining tube integrity were investigated.

It was also of interest to determine if nondestructive tube inspection techniques could be used to determine if inner granular corrosion had occurred inside the tubes during the tests. The techniques that were examined were Ultrasonic Inspection, Eddy Current Inspection, and Fluorescent Inspection. None of these techniques appear suited for inspection of inner granular corrosion that has occurred on the inside of the tubes. All methods can be used to detect external cracks in the tubing. It did not appear that the Ultrasonic or Eddy Current Inspection techniques offer any advantage over the Fluorescent Inspection technique. In the final analysis, however, it appears that the best approach to ensure tube integrity is to initiate testing and if no failures occurred during the first 10 hours of testing, the tube can be assumed to be free of mechanical defects.

Following testing, the tube condition was determined by cross-sectioning the tube at various locations. Prior to cross-sectioning, the tube condition, including deposits or corrosion inside the tube, was preserved by potting the tube inside and outside with a clear casting epoxy (Maraglas Type A, Marblette Corporation). The epoxy was outgassed before casting and was cured slowly over about 16 hours to minimize shrinkage and brittleness after casting. The potted tube could then be cross-sectioned, polished and etched as desired for inspection under a microscope and with photomicrographs. Photomicrographs were also made of a section of the end of the tube before the tube was mounted in the test fixtures to serve as the before test or "as received" condition of the tube. These photomicrographs and their interpretation served as the primary source of information for determining the effects of the biowaste gases on the tube materials under simulated resistojet conditions.

Test Results

In the concentric tube thruster, the innermost heater element is heated to approximately 1700°K. This element does not have a significant hydrostatic load since propellant flows along both the inner and outer surfaces of the tube. In addition, small leakages in this element are tolerable. The next heater element adjacent to the innermost element, is exposed to vacuum on one side and receives a substantial hydrostatic load. This tube must not leak. While the structural temperature of this tube is lower (about 1500°K) than that of the innermost tube, the structural requirements are more severe. The majority of the bell jar tests were conducted with vacuum conditions in the bell jar. These tests are more representative of conditions experienced by the second tube. Some of the later tests were conducted with one atmosphere of the test gas in the bell jar which more closely represent conditions for the center tube. In all tests, pressures in the tubes were maintained in the region of 2 to 3 atmospheres.

The high temperature tests (1500-1700°K) were all conducted with platinum or platinum alloy tubes. Most of the lower temperature carbon deposition tests were conducted with Hastelloy X tubes but included some platinum alloy tubes. The carbon deposition tests are discussed first and then the high temperature tests with each tube material are discussed.

Carbon deposition tests. - To provide an understanding and an appreciation of the test procedures and results, some of the early tests with Hastelloy X tubes are described in considerable detail. Tubes having an inside diameter of 0.037 inches were used to simulate the resistojet innermost heater element. The purpose of the first test on Hastelloy X tube samples was to evaluate the effect of a long term exposure to methane with a stay time representative of an actual biowaste thruster (3 milliseconds). Two tubes were tested, one flowing CO_2 to serve as a reference condition (no carbon) and the other flowing CH_4. Both tubes were heated to 1250°K with 579 and 509 hours, respectively accumulated on the CO_2 and CH_4 test samples.

Pressure drop across the CH_4 test sample was monitored and indicated that no significant carbon blockage occurred throughout the test. The tube samples were 2 inches long followed by a long (6 to 8 inches) length of cold 0.030 I.D. tubing. Had a significant amount of carbon been present in the bulk gas or been swept along in the gas to wall interface, a downstream blockage would have likely occurred and been reflected as pressure drop.

Photomicrographs of the tube samples tested are shown in Figures 21 through 23. The tube samples were made from 0.093 inches O.D. by 0.037 inches I.D. Hastelloy X tube stock. The O.D. was reduced to 0.051 inches by centerless grinding for a nominal wall thickness of 0.007 inches. Slight nonconcentricity resulted in a wall thickness variation of typically 0.006 to 0.008 inches.

Figure 21 compares the "as received" tube to the maximum temperature ($1250^{o}K$) section of the tube exposed internally to CO_2. The dark pits are not defects in the material but rather carbides which fell out during etching of the material sample. The material structure actually appears to have been improved by the long high temperature test. Slight roughening of the inner and outer diameter surfaces occurred but are not considered significant. Hastelloy X appears to be an attractive material for CO_2 propellant.

Figures 22 and 23, on the other hand, reveal some problems with pure methane propellant. In the top photomicrograph in Figure 22, a deposit buildup is seen on the thin wall side over approximately one-half of the inner wall circumference. A thin ring like pattern in the parent metal about one mil deep is noted around the complete circumference. A light gray layer about one mil thick appears to cover the tube inner circumference over the parent metal and the deposit. Some parent metal is seen to have been displaced inward with the deposit. The deposit contains a soft blackish material belived to consist essentially of carbon. The light blotch near the center of the tube hole is an identification chip of copper placed in the metallographic mounting material and can be ignored.

The outer two-thirds of the tube wall thickness appears to have retained good structural qualities. The grain structure is different than that of the CO_2 test sample (Figure 21) and is believed to be due to carburization (formation of carbides) of the material. The deposit appears much like a blister. To check this possibility, the tube sample was resectioned 0.030 inches deeper (Figure 23); however, the deposit is seen to still be present. Thus, the deposit grew considerably in a longitudinal direction and yet did not become thicker than about 0.003 inches in 500 hours of testing. Micro-hardness tester marks are shown in the bottom of Figure 23 and revealed considerable softening near the tube inner wall where the material appears to be spongy. Hardness measurements near the wall center and outer wall indicated the same hardness as in the "as received" condition, contradicting any assumption of carburization. This could be explained in terms of actual carburization with resultant loss in hardness if the sponginess extended throughout the wall. That is,

the formation of carbides apparent in the photomicrographs should result in a significant increase in hardness. It is suggested that the sponginess, obvious near the inner wall, extends throughout the wall resulting in a compensating softening effect.

The second test with Hastelloy X samples involved three tubes operated at three different temperatures with a mixture of CO_2 and CH_4. A mixture ratio of CO_2 to CH_4 of 1.1 by weight was used to provide an excess of methane. Average stay times in the tubes was seven milliseconds. The tubes were operated at steady temperatures with two atmospheres of internal mixture pressure and a bell jar pressure of 25 microns. Each tube was cross-sectioned for metallographic examination at two locations of different temperature after 250 hours of continuous operation.

The following stations were examined:

Tube No.	Station, Distance from Propellant inlet, inches	Temperature at Station, ^{o}K (^{o}R)
1	1.5	1320 (2380)
1	1.0	1255 (2260)
2	1.5	1230 (2220)
2	1.0	1145 (2060)
3	1.5	1115 (2005)
3	1.0	925 (1660)

Pyrolytic graphite deposits were noted in all of the samples except the 925^{o}K sample. The degree of deposit increased consistently with temperature. Four of the photomicrographs are shown in Figures 24 and 25 in the polished condition and under polarized light.

The 925^{o}K section was found to be clean and free of carbon. Some dark spots at the I. D. shown in Figure 24 are voids in the potting compound used. Short radial lines at the I. D. are surface irregularities in the original material. Comparing the successive temperatures in Figures 24 and 25, the increase in pyrolytic graphite thickness with increasing temperature is obvious. Effects of carburization on the tube inside wall are seen in Figure 25 resulting in some material depletion and a sponginess similar to that observed in Figures 22 and 23.

The Figures 24 and 25 cross sections show the effect of temperature on methane decomposition and deposition at the gas to solid interface resulting in a build-up of pyrolytic graphite. Rather than decomposition occurring in the gas stream and then carbon depositing, methane is being adsorbed by the gas-to-solid interface and subsequently decomposes. Gas kinetics at these test temperatures would indicate trivial amounts of carbon in the bulk gas stream. This is substantiated by no significant blockage in the downstream cold 0.030 I. D. connecting tube.

As this program progressed, a large number of carbon deposition tests were conducted. Table V summarizes the tests conducted when only the single bell jar facility existed. As is evident from the table, ten different tests were conducted. The results shown in Figures 21 through 23 were from Tests VI and VII of Table V and results of Figures 24 and 25 were from Test VIII.

The objectives of exposing sample heater tubes to a methane rich mixture of CO_2 and CH_4 were as follows:

1. To determine the rate of carbon deposition with a typical bio-waste mixture.

2. To determine the threshold temperature at which carbon deposition occurs.

3. To determine the structural nature of the carbon formation.

4. To determine if catalytic activity of the tube surface affects the carbon deposition.

In order to arrive at meaningful answers for the above objectives, it was necessary to obtain a sufficient number of experimental data points with a minimum number of variables. During the carbon deposition test series (VIII through X), only two tube materials were used, Hastelloy X and platinum-rhodium alloy, and exposed to one type of propellant mixture.

The metallographically observed carbon deposition rates in Table V are compared in Figure 26 as a function of tube wall temperature. Contrary to previous expectations, the data indicate an apparent faster carbon buildup in the less active Hastelloy X tube than the catalytically active Pt-20Rh tube. Sufficient data points were obtained to establish a threshold wall temperature of 1090°K (1960°R) for a typical rich methane-carbon dioxide mixture. With the exception of one amorphous carbon deposition data point for a Pt-20Rh tube, all deposits were found to consist of pyrolytic graphite. A maximum observed deposition rate line is shown in Figure 26 for the Hastelloy X tubes. Similarly, a curve is indicated for the Pt-20Rh tube data points. Only one high deposition rate point is available for interpretation of the Pt-20Rh data. The three points at 1255°K (two pyrolytic and one amorphous) are sufficient to indicate the possibility of a significant deposition rate difference for the more catalytically active Pt-20Rh as compared to the less active Hastelloy X tube.

Intermediate reactions would tend to be more or less affected by the catalytic activity of the tube surface and could account for the apparent difference in deposition rates of Hastelloy X and Pt-20Rh. It would seem, however, that once a light coating of carbon appeared on the surface of the tubes, deposition rates might become

equal with a gas to carbon interface in both cases. The data of Figure 26 then suggests that a diffusion mechanism is letting the gas see the tube material in a way to affect the carbon deposition.

The data of Figure 26 include low points relative to the line fit for Hastelloy X at 1230 and 1255°K. Randomness in the carbon deposition process at these temperatures is to be expected and can generally be attributed to surface conditions and contamination. The propellants used were commercial grade CO_2 and technical grade CH_4. These may have differed from bottle to bottle to account for random effects. The low Hastelloy X point at 1255°K was obtained with the same propellant as the 1255°K Pt-20Rh points (three), therefore again, caution must be used in interpreting the Figure 26 data.

Of the four above listed objectives of the sample heater tube tests, the first three are answered with some degree of confidence. Relative to a 1.0 to 1.1 mixture weight ratio of CO_2 to CH_4,

1. The rate of carbon deposit is conservatively depicted by the Hastelloy X curve in Figure 26.

2. Tube walls can be operated to 1090°K (1960°R) without long term carbon deposition problems. This would correspond to resistojet chamber gas temperatures of 1000°K (1800°R).

3. The deposited carbon is generally of a pyrolytic form but can be amorphous. Both deposits, and particularly the pyrolytic one, have good structural integrity. Whether or not thermal and stress cyclic loads would cause spalling of carbon deposits would require additional testing.

To gain additional information on the effect CO_2 has on the deposition of carbon with CO_2-CH_4 mixtures, an additional test (not included in Table V) was attempted at a mixture ratio of 3 to 1. This test was conducted with a TD-Ni, a TD-NiCr and a Pt-30Ir tube. A maximum temperature of 1445°K (2600°R) was set for all three tubes operating simultaneously. After 43 hours a failure (blow hole) occurred in the TD-NiCr tube. Before these tubes were examined metallographically, the bell jar test was started again with the same propellant mixture and with one Pt-30Ir and one Pt-20Rh tube. Maximum temperature was set for 1600°K (2880°R). This test ended in 24 hours with no flow due to blockage in the tubes and subsequent overheating to about 1750°K (3150°R).

Carbon production in the tubes was not expected on the basis of experience with the Mark I biowaste thruster reported in Reference 1. The metallographic report of extensive carbon blockage in addition to the hole in the TD-NiCr tube for the set of three tubes came through in the same hour that the set of two platinum alloy

tubes overheated. Each of the tube samples were approximately 2 inches long and were brazed into 1/8 inch diameter supply and exhaust tubes. The following is a summary of the extent of carbon formed in each case:

For the first set of three tubes:

1. TD-Ni - No carbon in the tube sample. Complete blockage at the exhaust tube braze joint.

2. TD-NiCr - Approximately 0.001 inch thick pyrolytic carbon at a 1370°K location with no carbon at the downstream maximum temperature location. The maximum temperature location had indications of corrosive pitting with some oxide like coating present. The exhaust tube was found to be essentially unrestricted.

3. Pt-30Ir - Pyrolytic carbon buildup to almost complete blockage at a 1250°K location, then decreasing in thickness to 0.003 to 0.004 inch at the downstream maximum temperature location decreasing further downstream to 0.002 inch near the exhaust tube braze joint where temperature was about 920°K. Immediately downstream of the braze joint, complete blockage occurred.

For the second set of two tubes:

1. Pt-20Rh - No carbon in the tube sample or inlet tube. Complete blockage at the exhaust tube braze joint.

2. Pt-30Ir - Complete blockage near the inlet tube braze joint, generally no carbon in the sample tube except in the region of maximum temperature where a 0.002 inch pyrolytic carbon coating occurred. Almost complete blockage at the exhaust tube braze joint.

In all cases, carbon deposits in the exhaust tube braze joint appeared to consist of both pyrolytic and amorphous carbon. An examination of the exhaust plumbing (water cooled) indicated large (of the order of 0.1 inch diameter) particles of sooty-light-amorphous carbon. Pyrolytic carbon deposits are the result of an ordered deposit of carbon molecules and occurs when a carbon bearing molecule is adsorbed on a surface and subsequently decomposed leaving a carbon molecule behind. Amorphous carbon is considered to be due to deposition of free carbon molecules carried along by the bulk gas.

It should be mentioned that the TD-Ni sample tube suffered small circumferential wall cracks which progressed to the tube O.D. causing short longitudinal cracks to appear early in the test. The TD-NiCr blow hole failure was apparently due to weakening by corrosion where pitting extended halfway through the wall. These data are preliminary and are not considered conclusive in view of the nature of the test. These failure modes were apparent at the maximum temperature location (1445 ^{o}K) whereas both materials looked good at 1370^{o}K locations.

These test results have posed many questions regarding the carbon deposition problem with methane in any concentration with carbon dioxide. Relative to the Figure 26 carbon deposition rates, it appears deposition is accelerated by the increased CO_2 content.

These early tests, both on heater tube samples and the biowaste thrusters were conducted with technical grade methane. This grade contains about 2.5 mole percent of ethane C_2H_6. Carbon deposition rates are greater for ethane than for methane and a given amount of carbon deposition per unit time occurs at a lower temperature with ethane than for methane. References 58 and 59 discuss the thermal decomposition of light hydrocarbons and suggest some incipient thermal decomposition temperatures based upon a one percent decomposition rate per hour. References 58 and 59 present the following calculated thermal decomposition temperatures:

Hydrocarbon	Reference	Decomposition Temperature, ^{o}R
Methane	73	1865
Ethane	73	1715
55% Methane 45% Ethane	73	1400
Methane	74	1770
Ethane	74	1400

The mixture decomposition temperature was calculated using activation energy and rate constant (or frequency factor) obtained by molar-average values of the constituents. Differences in the calculated temperatures by the two references stem from differences in the activation energies and rate constants used. Reference 59 used a decomposition temperature for a methane-ethane blend the same as for pure ethane.

Reference 59 presents a detailed discussion of the thermal decomposition of light hydrocarbons. Pertinent information is summarized here. The products of pyrolysis are considered to include larger species as well as elemental carbon. For instance, methane yields hydrogen, ethane, ethylene, acetylene, propylene, and (at higher temperatures) elemental carbon. Ethane yields ethylene and hydrogen. It is known that ethylene breaks down rapidly to form carbon. Pyrolysis takes place over

a range of temperatures. The decomposition of hydrocarbons at high temperature leads to the formation of pyrolytic carbon. Decomposition rate is proportional to the first power of pressure, suggesting that thruster pressure be kept low.

Of particular interest, Reference 59 mentions an investigation conducted by the Russians (Reference 60) which claims that platinum exhibits a small accelerating effect while metals of the iron subgroup show marked catalytic activity. The data presented in Figure 28 suggests that carbon deposition rates may be less for platinum alloy than for a Ni-Cr-Fe steel. Reference 60 also mentions that quartz becomes catalytically active above about 1300°K (2300°R).

At this time in the program, the facility was expanded to two bell jars. Tests similar to that represented by Figure 26 were conducted using chemically pure grade methane which contains only 1/10 of the ethane that is contained in technical grade methane. An instrument grade methane also was available with even less ethane, however, its use could not be justified because of cost considerations. Table VI presents the data obtained in the left hand bell jar of the expanded facility. The test number designation refers to the bell jar (left or right) and the consecutive test number in that bell jar. For instance, L2 is the second test in the left hand bell jar. Data point numbers identify the tube position 1, 2, or 3 in the bell jar and the letters refer to locations along each tube which were examined metallographically. These letter stations do not correspond from one test to the next.

It was mentioned previously that, for the threshold carbon deposition experiments with temperatures to about 1300°K at least, chemistry changes along the tubes do not affect deposition rates. The amount of propellant being reacted in the tubes is so small (typically 15 billionths) that downstream stations should not be affected by upstream deposits and/or reactions. In the Table VI data, many data points occur on one tube at a particular temperature which corresponds to identical conditions at a significantly different axial station on another tube. These cross check points are displaced from 0.3 to 0.5 inches on adjacent tubes and, in general, carbon deposition rates agree.

In most cases of deposited carbon, clean coatings were found. A typical coating is shown in Figure 27 for data point 3E from test L6. This photomicrograph shows an enlarged (500 X) portion of the inside wall of a platinum-iridium tube sample. The mean deposit thickness measured was 550 micro-inches. The Figure 27 location was chosen to show a typical carbon film, in this case of pyrolytic carbon, and also to show how deposited carbon fills holes or cracks in the tube wall. The hole midway along the tube wall in Figure 27 is 500 micro-inches deep. Of interest are the fact that the hole is well filled as seen in the bright field photomicrograph. Also, the hole did not necessarily cause an indentation in the deposited carbon surface. Rather, the total thickness (even relative to an extension of the normal wall line) is seen to be thicker than normal. And, finally, the hole results in a weakening of the

carbon coating as evidenced by a large delamination starting near the hole. The columnar structure of the carbon is obvious in the polarized light photomicrograph. To the left and near the wall is a large delamination or separation. This is typical of thermal contraction separation.

Figures 28 and 29 present three photomicrographs of more unusual carbon deposits which were found. The Figure 28 deposits occurred with chemically pure grade methane and are of amorphous carbon. The L4-3B data point photo shows amorphous carbon as a gray outer coating and show some scattered amorphous carbon that has formed in the Hastelloy X tube wall to a depth of about 600 micro - inches. Between the tube inside wall surface and the outer gray carbon-coating is another film which appears that the light film is softer than the carbon film because it seemed to be missing as though it had fallen out in some cross sections like in the L4-1B photomicrograph.

There were cases where a thin carbon coating was found to be spaced uniformly distant from the tube wall in which case a separation must have occurred. In Figure 28, L4-1B, the gap is nonuniform indicating the prior existence of the light material. The L4-1B photomicrograph is shown because of the unusually long fiber which grew from the wall coating. This is amorphous carbon with a cross section measuring 1500 micro-inches long by 100 micro-inches wide. It is the only one observed at the 1B location and must have grown from a micro-thin fiber extending from the wall. It seems unreasonable that no nucleation sight was present and that 1500 micro-inches of growth occurred radially compared to a mean film growth of only 100 micro-inches. At a station 1A 0.4 inches downstream from 1B, many smaller fibers were observed the maximum of which measured 300 by 40 micro-inches. Of 9 stations examined in test L4, 3 stations (1A, 2A and 3A) contained many fine fibers. In test L5, fine fibers were noted at stations 1B, 2A, 2C and 3B. The photomicrograph in Figure 29 shows the L5-2C carbon film which is rough, contains many fibers extending 1400 micro-inches from the tube wall, and consists of both amorphous and pyrolytic carbon. In 18 stations examined from test L6, only one (2D) had fibers which extended 800 micro-inches. Fibers were not detected at any of the stations examined from tests L1, L2, and L3.

Figure 30 presents a photomicrograph from the carbon deposition tests reported in Table V. This is shown to stress the importance of avoiding thick carbon deposits. This tube was exposed to $CO_2 + CH_4$ for 241 hours at 1440°K (2590°R). The thick carbon coating was thermally shocked only once at test termination. Large delamination fractures are seen and emphasize the nozzle throat blockage potential of large carbon deposits.

Figures 31 through 33 present the Table VI carbon deposition data for tests L1 through L6. Test L4 data for methane is shown in Figure 31. Two curve fits are shown, one for the gray coating of amorphous carbon, the other for the combined gray plus light or separation space where the separation is not due to thermal contraction. Figures 22 and 23 showed photomicrographs of a Hastelloy X tube sample

exposed to CH_4 for 509 hours at 1250°K (2250°R). A blister-like deposit occurred over a portion of the tube, however, most of the tube inside wall was seen to have a relatively uniform coating of amorphous carbon and a lighter coating which appeared to be metallic material formed from or separated from the tube itself.

The original tube inside diameter of the Figure 22 and 23 sample corresponds to what is essentially the tube. The light film is believed to be composed of metallic constituents from the Hastelloy X which have migrated to the tube inside surface and formed a film. This would explain the general appearance of void-like spaces to a depth of 600 micro-inches in the Figure 28 case and which appear to have filled with carbonaceous material. In the Figure 22 and 23 case, the light film is seen to have separated and filled with a relatively large deposit of carbonaceous material which now is believed to be a mixture of pyrolytic and amorphous carbon. The gray film extending completely around the tube is amorphous type carbon.

In view of the above observations, it appears that the Hastelloy X tube material is effecting the deposits which are formed. Metallic constituents appear to be trading places with deposited carbon, or voids left by metallic constituents are being filled by carbon deposition directly. The light coating was only evident in test L4 with pure methane. In the tests with a CO_2-CH_4 mixture, voids filled with carbon were found within about 1.2 mil of the inside wall surface, however, no light metallic-like coatings were noted.

Figure 32 compares the test L1 and L3 data for a CO_2 and CH_4 mixture ratio of 1.1 and 3.0, respectively. These data correlate well indicating a deviation in rate as temperature increases above 1100°K. The mixture ratio of 3.0 condition is considered lean with sufficient CO_2 present to theoretically prevent free carbon formation. It must be concluded that for the temperatures tested, thermal decomposition of CH_4 is proceeding while oxidation by CO_2 is not significant to completely gasify the carbon. The spreading of the two curves fit such a conclusion. With higher temperatures, carbon deposition would tend to continue with the rich mixture ratio of 1.1. It seems intuitively possible that the mixture ratio of 3.0 curve would level off and possibly decrease to zero at sufficiently high temperature for oxidation reactions to proceed rapidly.

The fact that the lean mixture deposition may cease at high temperatures is not a cure-all for resistojets. Any heater configuration necessarily has a range of temperatures including the 1100 to 1300°K range for which carbon deposition rate is becoming significant. A much leaner mixture might and should, however, result in lower tolerable deposition rates. In terms of an acceptable deposition rate of 0.2 micro-inches per hour, the Figure 32 threshold temperature is seen to be about 1055°K (1900°R). It should be noted that all of the Figure 32 data points contained pyrolytic carbon.

Figure 33 presents data from three test runs for a CO_2 to CH_4 mixture weight ratio of 2.0. L2 and L5 data are for Hastelloy X tubes while L6 data are for platinum-iridium tubes. The data were reviewed carefully to determine whether or not operating condition differences existed to explain the L2-L5 data differences. The only factor uncovered was that tube samples for tests L1, L2 and L3 were prepared as a group but at a different time than the tubes prepared as a group for tests L4 and L5. With the exception of the two points shown at 0.1 micro-inches per hour, the test L2 data line up well. The higher temperature point (1B) at 1305°K, however, consisted of amorphous carbon unlike the pyrolytic carbon found at the L1 and L3 data points. It appears that the L2 test fits the L1-L3 data reasonably well while the L5 data reflects some unusual phenomenon. Photomicrographs of the deposits from these two test runs do not indicate differences as far as contamination or tube wall surface texture. More amorphous carbon was formed in the L5 test, however. This is attributed to the high (above 1.0 micro-inches per hour) deposition rate occurring at relatively low temperature 1000 to 1130°K.

During tube sample preparation, care is taken to not contaminate the tubes by using excess brazing flux. Brazing stop-off is not used as it is a potential contaminate. Tubes are thoroughly cleaned after assembly by flushing with solvents, boiling water and passivation. It is believed that the L5 test samples were in some way contaminated relative to the L1 through L3 test samples. The L5 data in Figure 33 are considered unusual reflecting possible contamination and catalytic effects. These data should serve as a warning that carbon deposition rates are not absolutely predictable and that surface preparation is very critical.

Considerable scatter exists in the test L6 data for platinum-iridium tubes. A mean fit correlates well with the tests L1 through L3 data however. In Figure 33, a conservative fit curve is taken relative to the L2 and L6 data and indicates a threshold temperature of about 1000°K (1800°R). In the lower temperature range (data from 995 to 1115°K) many amorphous carbon data points are noted in the L6 data. It should be pointed out that for deposits which are very thin (less than 100 micro-inches) it is difficult under polarized light to absolutely classify the carbon. The type carbon callouts in Table VI are the metallographers best estimate for the very thin deposits.

The scatter in the L6 data indicates a possible catalytic effect. Recall, however, that in Reference 60, experiments indicated a small catalytic effect for platinum compared to iron subgroup metals. Possibly iridium in the alloy tested in the L6 test affects the deposition rate. These will have to remain questions as the L6 data are not conclusive relative to differences between the platinum-iridium alloy and Hastelloy X. If there is a difference, it might be said that it appears to be small.

Figure 34 is a composite of the curve fits used in Figures 31, 32, and 33. At the high temperature end, the mixture ratio of 2 data correlate with the 1.1 and 3 data. A mean fit rather than a conservative fit used for the Figure 33 data would correlate better in the Figure 34 plot.

Four tests of three heater sample tubes each were completed with water-methane mixtures in the right hand bell jar. Conditions of these tests are summarized in the following table:

Test No.	Material	Weight Mixture Ratio, H_2O/CH_4	Exposure Time, hours	Temperature Range ^oK	^oR
R1	Hastelloy X	1.13	161.5	955-1250	(1720-2250)
R2	Hastelloy X	0.5	164.8	945-1240	(1700-2230)
R3	Hastelloy X	0.26	140.4	1028-1308	(1850-2355)
R4	TD-Platinum	0.49	97.8	1043-1418	(1880-2550)

The first test, R1, was conducted with a mixture ratio of 1.13 corresponding to a stoichiometric mixture based upon equation.:

$$H_2O + CH_4 \rightleftharpoons CO + 3\,H_2. \qquad (2)$$

This is perhaps an academic definition of stoichiometry involving H_2O and CH_4 since other reactions are involved including those having elemental carbon in the products.

Metallographic examinations along the three tubes from test R1 at three stations up to and including the maximum temperature stations revealed no carbon. It was decided to try mixtures richer in CH_4 relative to the above equation for subsequent tests R2 and R3. Test R2 examinations revealed trace amounts of carbon at three stations examined up to and including the maximum temperature locations. The greatest carbon deposition rate detected was 0.2 micro-inches per hour. This is the minimum rate at which accurate resolution is possible. All carbon deposits were identified as containing both pyrolytic and amorphous type carbon. In test R3, the Hastelloy X temperature was pushed to 1308^{o}K (2355^{o}R) in an attempt to obtain larger deposits for more accurate deposition rate measurements. The Hastelloy X tubes cannot be operated at too high a temperature, otherwise corrosion mechanisms can occur and present an influencing factor in the carbon deposition process.

Carbon deposit rates observed in tests R2 and R3 did not correlate with temperature. The following table compares some typical data to indicate this point:

Test	Tube Station	Temperature, ^oK	Approximate Deposition Rate, Micro-inches per hour
R2	2A	1063	0.2
R2	2B	1137	0.1
R2	2C	1182	0.06
R3	3A	1110	0
R3	3B	1172	0.2
R3	3C	1200	0.14

Deposition rates are qualified as approximate because the rates given are no more than the 0.2 micro-inches per hour resolution for these experiments. Stations A, B, and C, in both cases are in order of flow direction from A to the maximum temperature station, C. Figure 35 presents a typical temperature distribution taken during test R3 with data point stations indicated.

Test R4 with TD platinum tubes was undertaken in order to obtain higher test temperatures, and therefore, higher carbon deposition rates. The data obtained for tests R1 through R4 are tabulated in Table VII. Deposition rates are plotted in Figure 36. In each test, data point stations D were also examined at the exit end of the heater sample tubes where they connect to a larger 1/8 inch O.D. support tube. These sections revealed carbon deposits which correlate well with tube wall temperature as seen in Figure 36. Thus, relative to tube wall temperature, deposition rates at station D are higher by more than an order of magnitude than the station A, B, and C data seen scattered about in Figure 36. Similar downstream stations were examined during test L6. Those stations, called D at the junction of the sample tube and support tube and F 0.015 inches upstream of D are plotted along the curve fit in Figure 33. The carbon was identified as the amorphous type.

Figure 37 shows a set of photomicrographs from test R3 at station D, and indicates the systematic increase in carbon thickness from tube 3 to 2 to 1 corresponding to increasing temperature. The rounded bumpiness along the surface of the carbon reflects nodules of pyrolytic carbon among amorphous type carbon. The nodules were positively identified with polarized light.

Figure 36 shows that a significant difference exists in deposition rate for the TD platinum versus Hastelloy X tube material. The station D data reflect an order of magnitude lower deposition rate with TD platinum. The A, B, and C station data for TD platinum correlate well and fit, somewhat, the general scatter in the Hastelloy X A, B, and C data. It appears that oxidation with Hastelloy X has an effect on deposition rates relative to the TD platinum. Some oxides appeared to be present with the carbon deposits seen in the photomicrographs taken. It is not known whether the oxidation was the result of oxygen freed from the water molecules and/or that oxidation was the result of dissolved oxygen (air) in the water supply system. The deposition rates for the TD platinum are considered more representative of rates to be found with biowaste resistojets. The curves in Figure 36 for TD platinum indicate 0.2 micro-inches per hour threshold temperatures of 1235^{o}K and 1085^{o}K for the heater and nozzle throat, respectively. Here the station D correlation is taken as representing a nozzle throat where the station A, B, and C stations are equated to the heater proper.

Figure 38 is a plot showing the Marquardt data (from Figure 34) and data of other investigators. The Carley-Macauly and Mackenzie curve from Reference 7 is a composite fit to several investigator's data for CH_4 interpreted at 2 atmospheres pressure. The Bokros data (Reference 67) are from fluidized bed experiments

using helium as a diluent. Curves for two different bed charge and one atmosphere pressure are shown. The AVCO curve is from recent methane data (Reference 62) apparently plotted against ^{o}C in error. Temperatures given in ^{o}C are interpreted as ^{o}R, otherwise the platinum-rhodium wires used in those tests would have melted. The AVCO tests were short time tests ranging from about one to a few hundred minutes. The curve presented in Figure 38 is from the AVCO 2 atmosphere data. A data point in Reference 62 for 1 atmosphere reflected a factor of 5 lower deposition rate from the Figure 38 AVCO curve, conflicting with the first power of pressure theory proposed by other investigators. The Bokros data extended to lower temperature and the Carley-Macauley and Mackenzie data compare favorably with the Marquardt data while the AVCO data appears high in deposition rate.

Four data points are plotted from nozzle throat deposition rates observed with the Mark I and II biowaste resistojet thrusters (reported in Reference 1). Deposition rate was calculated as a nozzle throat surface buildup corresponding to observed decreasing thrust rates. These in turn are plotted in Figure 38 against estimated maximum structural temperature. The nozzle throat temperature is not accurately known and is not necessarily equivalent to the maximum structural temperature. Therefore, these thruster points are indirectly correlated. They do, however, fit the sample heater tube data suggesting that the tube data may serve to predict thruster threshold temperature conditions with reasonable accuracy. The data points numbered 3 and 4 are particularly interesting in that they occupy appropriate relative positions for their chemistry. Point 4 with a mixture ratio of 2.5 is seen to be below point 3 with a mixture ratio of 2.

The data from Figure 36 were not included in Figure 38 because of space and data clutter considerations. However, the station D line for TD-Pt in Figure 36 would represent a close approximation to Data Point 2 (Mark II resistojet) shown in Figure 38. While many questions remain relative to these specific materials and how they affect carbon deposition, it is evident that a carbon deposition threshold condition sufficiently accurate for setting resistojet operating conditions can be found from the Figure 34 data fits. It is recommended that the lower, amorphous coating only, curve for methane be used to represent methane with resistojet heater materials. It was obvious that great care must be exercised in maintaining clean heater surfaces in order to obtain predictable deposition rates. Care must be exercised during operation of the thruster not to affect adverse contamination if operating conditions are to be pushed to the threshold temperatures reflected in Figure 34.

After having tested 18 tubes for many hundreds of hours in the left hand bell jar, the exhaust plumbing was examined for traces of sooty carbon which might have carried along in the gas stream. Some bell jar tests at temperatures above $1400^{o}K$ resulted in gas-phase carbon deposition and much sooty carbon in the exhaust plumbing. This occurred with run times from 24 to 48 hours in some tests. A close examination of the 1/8 inch diameter mounting tubes on the exhaust end of the tested samples revealed the following:

1. No carbon for CO_2-CH_4 mixture tests for temperatures to 1200°K.

2. Sooty type carbon for all tubes tested with pure methane.

The absence of sooty carbon in these threshold temperature experiments with CO_2-CH_4 mixtures and maximum temperatures to 1200°K agree with the observations of Tesner (Reference 63). Therefore, spacecraft contamination from gas-phase carbon should not present a problem with resistojet heater temperatures as high as 1100 to 1200°K provided CO_2 is mixed with the CH_4. Carbon dioxide appears to inhibit gas-phase deposition relative to pure CH_4 for comparable wall deposit thicknesses.

During the early tests (Table V), technical grade methane containing 2.5 mole percent of ethane was used. The data reported in Table VI were obtained using chemically pure grade methane containing an order of magnitude less ethane. A factor of 2 reduction in deposition rate has been noted in the Table VI test data for CO_2-CH_4 equal to one as compared to the Table V data for the same mixture ratio. This reflects the autocatalytic effectiveness of ethane mentioned by other investigators (References 59 and 63).

Comparing the test L1 and L3 data using CO_2 + CH_4 against the test L4 data using CH_4 only, it appears that the addition of carbon dioxide promotes very effectively the formation of pyrolytic carbon at the low threshold temperature. It is suggested that the CO_2 + CH_4 mixture be considered for vapor deposition of pyrolytic carbon at temperatures as low as about 1100°K or 800°C.

The following summarizes the observations made for the various methane/methane mixture tests conducted on sample heater tubes in the bell jar facility. For pure CH_4 propellant:

1. All carbon deposits observed were found to be of the amorphous type. The maximum test temperature was 1255°K (2260°R).

2. The carbon deposition threshold temperature was found to be about 950°K (1700°R).

For CO_2-CH_4 mixtures:

1. The addition of CO_2 resulted in pyrolytic type carbon deposits.

2. The carbon deposition threshold temperature was found to be from 1000 to 1055°K (1800 to 1900°R).

3. Carbon formed even for a high weight mixture ratio of CO_2 to CH_4 of 3.0.

4. For heater temperatures to 1200°K (2160°R), carbon deposition was found to be a surface reaction with virtually no carbon particles in the gas phase. Deposition rates followed local wall surface temperatures and were not dependent on the flowing history.

For H_2O/CH_4 mixtures:

1. The addition of H_2O resulted in a mixture of pyrolytic with some amorphous type carbon with the pyrolytic type becoming dominant at the higher temperature.

2. The carbon deposition threshold temperature was found to depend on flowing gas history. Heater sample tubes used in the carbon deposit experiments had an axial-gradient in wall temperature to a maximum value followed by a decreasing temperature to a cooler value at the tube exit. In effect, the sample tube simulated a resistojet thruster with the cooler exit condition likened to a thruster nozzle throat. For example, in a typical test, temperatures increased gradually with axial distance to 1200°K (2160°R) and then fell rapidly to an exit condition of 1030°K (1850°R). Deposition rates to the maximum temperature point correlated with wall temperature indicating a threshold temperature of 1235°K (2225°R). However, deposition rates at the exit station correlated to a lower threshold temperature of 1085°K (1950°R). This lower value should be used in determining thruster operating conditions with H_2O/CH_4 mixtures.

3. Carbon formed even for a theoretically stoichiometric weight mixture ratio of H_2O to CH_4 of 1.13. Mixture ratios of 0.26 to 1.13 were tested. These large amounts of H_2O did not prevent carbon deposition.

4. In view of the observed difference in deposition rate at the maximum wall temperature station versus the exit station, deposition rate is considered dependent on flowing gas history. Relative to the CO_2/CH_4 mixture, it appears that gas phase carbon particles are more likely to be present with H_2O/CH_4 mixtures at temperatures above the threshold temperature. The increased deposition rate at the colder downstream station is believed to be due to condensation of gas phase carbon.

Platinum-rhodium tests. - One of the earliest platinum alloys selected for the high temperature elements in the biowaste application was platinum rhodium (Pt-Rh). This material was selected because of its oxidation resistance and strength properties at high temperature. Although rhodium is oxidation resistant, it soon

became evident that it was severely affected by carbonyl reactions when exposed to CO_2 at high temperature.

Two Pt-20Rh (platinum with 20% rhodium) tubes were tested as is shown by Test Nos. I and II of Table V. After the cumulative period of 500 hours at three temperature levels for sample 1 and 570 hours at 1500°K for sample 2, the tubes developed leakage (evidenced by a slight increase in bell jar pressure). Post-test examination revealed that rhodium carbonyls were formed in the presence of CO_2 which resulted in depletion of the rhodium from the alloy. Figure 39 shows the surface of the Pt-Rh tube after testing and reveals extensive grain growth. Metallographic examinations, shown in Figure 40, show the extent of grain growth and reveal the formation of large voids within the grains. Results of an electron microprobe scan of the Pt and Rh concentration are shown in Figure 41. The scan reveals a large depletion of rhodium from the inner surface of the tube. A discussion of the formation and effects of carbonyls is presented in Appendix B.

A Pt-30Rh wire sample also was tested in the bell jar by flowing CO_2 at one atmosphere past the hot wire. Figure 42 shows the external surface of the wire after 500 hours exposure at 1707°K to CO_2. Considerable surface roughness is apparent. A cross-section enlargement of the maximum temperature region of the wire is shown in Figure 43. The roughness, most apparent on the leading edge, indicates depletion of the alloy as a result of carbonyl formation and subsequent vaporization.

As was discussed in an earlier section of this report, results from computer programs indicated that the presence of a small amount of oxygen mixed in with the CO_2 would suppress the formation of CO (see Figures 4-6). This trend was at least partially verified by test. During Test R6 a Pt-10Rh tube was subject to CO_2 with 1.5% O_2 at a temperature of 1700°K for 500 hours. Photomicrographs of the Pt-10 Rh tube before testing and after 500 hours at a maximum temperature of 1700°K are shown in Figures 44 and 45, respectively. Very large grain growth is evident but no real evidence of carbonyl reaction is present. The grain boundaries and general tube cross section are clean, in contrast to the results with pure CO_2 shown in Figure 40. There was some reduction in wall thickness, however.

During test R6 in the right hand bell jar and L10 in the left hand bell jar, and nearly all subsequent tests, pressure in the bell jar was maintained at one atmosphere instead of under vacuum. After the test, gas mixture passed through the tubes, at about 32 psia, it was ducted back into the bell jar at one atmosphere. This technique has three advantages over previous tests where a vacuum was maintained in the bell jar.

These advantages are:

1. More representative of the actual engine which has gas flowing over both sides of the tube.

2. Reduced hoop stress (engine has zero hoop stress).

3. One atmosphere pressure on outside of tube will greatly reduce evaporation of the platinum at high temperature.

One side of each of the other tubes in the concentric tube resistojet engine is exposed to vacuum in space but these tubes operate at lower temperatures than the center tube. They also can be made any thickness desired. The disadvantage of this test technique was that it was more difficult to detect small tube leaks. Small leaks were detected by periodically shutting down the electrical power and evacuating the bell jar.

Next, a Pt-10Rh tube was subjected to CO_2 plus 0.25% oxygen. The tube was maintained at a maximum temperature of 1700°K for 1500 hours with no tube failures or leakage. Although there was no leakage, there was evidence of attack in the grain boundaries. Figure 46 shows the results at the 1600°K station. The etched photomicrographs reveal voids in the grain boundaries. Figure 47 shows results at the 1700°K station where significantly more grain boundary attack occurred. It appears that tube leakage would have occurred in another 500-1000 hours. The results appear to indicate that with tubes containing 10% rhodium, 0.25% oxygen is insufficient to prevent carbonyl reactions in the grain boundaries.

Another potential method of reducing potential carbonyl reactions was to minimize the amount of rhodium in the tubes. To investigate this affect, a Pt-5Rh tube was subjected to pure CO_2 for 1500 hours at 1700°K. The tube in its "as received" condition is shown in Figure 48. As is evident, there was considerable roughness on the inner surface of the tube as a result of the fabricating process. The results from this test are presented in Figures 49 and 50 for the 1600°K and 1700°K stations, respectively. These photographs reveal no evidences of carbonyl or grain boundary attack and raises the question as to how the Pt-5Rh tubes would stand up under 0.25 to 1.5% oxygen addition. Time did not permit an investigation of this question under the subject program. These results indicate that Pt-5Rh may be a very attractive material for biowaste use but additional tests should be conducted.

Platinum-iridium tests. - Platinum-iridium alloys appeared to be very attractive materials for biowaste operation when it was thought that the oxygen concentration in the biowaste gases would be less than 50 ppm. However, as will be shown by the experimental results, when the oxygen content of the gases increased to around 1.0%, oxidation rates of the Pt-Ir tubes were excessive.

Because the properties of Pt-Ir were not completely documented, the initial tests were conducted with wire specimens to evaluate the potential carbonyl formation characteristics of the alloy. The wire tested contained 30% iridium and was maintained at about 1725°K for 500 hours in a CO_2 atmosphere. Figures 51 and 52 are photographs of the wire after the test. Comparing these photos with those of the Pt-30Rh wire (Figures 42 and 43) indicate that little if any carbonyls are formed under this condition with iridium. Significant grain growth is evident but little metal depletion or vaporization occurred.

Following the wire test, a platinum-30% iridium tube was tested with CO_2. This test is listed as Test II-1 in Table V. This tube successfully completed 706 hours exposure at about 1550°K.

Figure 53 shows the outside tube surface condition of a Pt-20Rh and the Pt-30Ir tube at similar temperature conditions. The Pt-20Rh tube surface photograph is from Test No. 1. The Pt-30Ir tube surface in Figure 53 is seen to be in excellent condition with a duller - higher emissivity finish than for the Pt-20Rh tube. Surface grain boundaries of the Pt-30Ir tube were examined under a microscope and found to be very fine, representing tight boundaries having excellent structural characteristics.

Figure 54 shows 500X photomicrographs of the Pt-30Ir tube as received and at the maximum temperature location. These can be compared to similar photomicrographs for the Pt-20Rh tube shown in Figure 40. The Pt-30Ir as received grain size is seen to be larger than for the Pt-20Rh alloy. In addition, deeper surface pitting is indicated for the Pt-30Ir. This reflects the more difficult-to-form nature of the Pt-30Ir alloy. Larger grain size in the Pt-30Ir case is attributed to the more extensive annealing required in working the Pt-30Ir alloy.

Of particular interest are the post-test cross sections shown in the bottom half of Figure 40 and in Figure 54. For the Pt-20Rh alloy, the depletion of rhodium due to the carbonyl corrosion mechanism was obvious and shown as large voids in the remaining tube wall structure. The post-test condition of the Pt-30Ir tube is seen to be in excellent condition. While grains have become large as with the Pt-20Rh tube, grain boundaries are tight and clean indicating no grain boundary attack. Small spots on the etched surface are the result of etching and not defects in the material. Neither carbonyl nor oxidation forms of corrosion were apparent for the Pt-30Ir material exposed to CO_2 for 706 hours at 1550°K wall temperature.

Following the carbon deposition tests with CH_4, which were discussed in the previous section, additional high temperature tests were conducted with platinum-iridium alloys. A 720 hour test on two Pt-20Ir tubes with a reducing atmosphere was completed and is designated as Test L7 in Table VIII. Mass flow rate for each tube was 8×10^{-4} grams per second. The propellant mixture passed through the

tubes at 2 atmospheres pressure while the tubes were exposed to a vacuum of 5 microns of mercury in the bell jar. Maximum temperatures of 1690°K (3040°R) and 1640°K (2950°R) were maintained for 734 hours with a weight mixture of 73% of hydrogen, 22% carbon dioxide and 5% of water. Water and CO_2 were included to represent a typical biowaste-reducing type atmosphere.

Figure 55 shows a photomacrograph of the outside surface of the 1690°K station. The shiny mosaic-like surface is due to significant grain growth. Figure 56 shows photomicrographs of a cross-section of the same station unetched and etched. The unetched section is most representative of the post-test condition of the alloy with a few small pits or voids evident. Etching brings out these voids by enlarging them and makes other smaller ones appear. The voids are generally located toward the tube O.D. indicating a reaction with the bell jar vacuum environment (air at about 5 microns of mercury). The voids appear to be filled spaces with an unknown material which falls out during polishing, and are further disturbed by the etching process. In hard vacuum, the spots in Figure 56 should not be as profuse. Based on the unetched Figure 56 photomicrographs, the Pt-20Ir alloys should be capable of a service lifetime measured in thousands of hours with temperatures to 1690°K (3040°R) for reducing type atmospheres.

At about this time in the program, questions began to arise regarding the concentration of oxygen in the biowaste gases. The concentration was believed to be small but oxidizing atmosphere tests were conducted on two Pt-20Ir tubes. Maximum temperatures of 1700°K (3060°R) and 1600°K (2880°R) were set on tubes numbered 3 and 2, respectively. A mixture of CO_2 and O_2 was humidified to represent a typical biowaste-oxidizing atmosphere. Weight percent of oxygen varied from 1.2 to 1.5 and water vapor content was estimated to be 0.4 percent with CO_2 varying from 98.1 to 98.4 percent. Tube number 3 began leaking after 160 hours as the result of longitudinal cracks while tube 2 developed a prominent circumferential crack after 136 hours. Figure 57 shows the failure sections in photomacrographs. The crack in test L8-2B was further aggravated upon removal of the tube from the bell jar as evidenced in Figure 57. The leaks in both tubes occurred at stations upstream of the maximum temperature points as indicated in Figure 57. The reason the major failure points did not occur specifically at the maximum temperature stations, may be the result of oxygen being consumed along the flow path and being partially depleted at the maximum temperature station.

In the case of tube 3, other cracks occurred in addition to the one shown in Figure 57. A second major crack occurred downstream of the maximum temperature location where the temperature was 1630°K (2930°R). The test L8 photomacrographs in Figure 57 indicate a duller surface finish than for test L7 (Figure 55). This is attributed to exposure to bell jar pressure increased to about 40 microns of Hg some 10 to 20 hours before test termination. That is, actual leakage began 10 to 20 hours before the total test times of 160 and 136 hours quoted above.

Figure 58 shows unetched and etched photomicrographs of the cross section at the major failure location of the tube No. 1 and Figure 59 shows photomicrographs of the L8-3B station at which a major leak had developed due to a longitudinal crack. The degree of corrosion should be judged from the unetched sections. Etching enlarges voids and grain boundaries and is used to identify the grain boundaries relative to corrosion sites. It is clearly evident in the etched cross sections that corrosion is along the grain boundaries and the grain size is seen to be large with some grains having dimensions comparable to the tube wall thickness Results of this test caused concern that the performance of Pt-20Ir tubes would not be adequate in oxidizing atmospheres. Further examination was done to determine the degree of oxidation attack of Pt-20Ir as a function of temperature. Sections of the tube were examined at progressively colder areas toward the tube inlet. At a location corresponding to about 1330°K (2400°R), the tube wall still exhibited grain boundary attack completely through the wall. This is shown by the lower photograph in Figure 60. Surface oxidation was not as severe as that noted at the hottest location, however, it is quite apparent that the oxidation had proceeded completely through the tube wall with resultant tube leakage only a matter of time at that location. From Figure 60, it appears that the oxidation attack in the grain boundaries was as severe near the outside of the tube wall as near the inside.

In contrast with the oxidation experienced at the 1330°K and 1700°K locations, examination of an adjacent section which had been at a temperature of approximately 1245°K (2240°R) showed there was only slight evidence of oxidation attack. Photographs of this location are shown in Figure 61. Again the attack near the outside surface appears as significant as that near the inside. The line of demarcation between those zones which were significantly attacked during the 160 hour test period appears to be quite sharp indicating that the oxidation may be associated with material properties.

Referring to the unetched sections in Figures 58 and 59, intergranular corrosion is generally evident to a depth of about 1/3 of the tube wall thickness. A few locations reflect a complete breakdown into leakage paths. These can be associated with slight mechanical defects in the original tube suggesting a non-homogeneous tube material was used or that the tube was overworked introducing minute fractures. Three samples were taken from the Pt-20Ir tubes as received and were examined micrographically. These revealed generally sound material with some grain enlargement due apparently, to hot working. Etched sections indicated some not so tortuous paths from I.D. to O.D. These details would not reproduce well enough for this report. More obvious crack-like paths were found in a more difficult to work alloy containing 30% iridium (Pt-30Ir). A typical section is shown in Figure 62 and reveals a few not so tortuous paths through not so fine a grain structure.

Briefly, the following pertinent observations were made while using drawn tubes of Pt-20Ir and Pt-30Ir:

1. The easier to work Pt-20Ir resulted in heater parts having greater mechanical quality.

2. Some Pt-30Ir parts were found to have fine longitudinal cracks, some of which would not pass a helium leak check.

3. Frequently, in attempting to weld or braze a Pt-30Ir or Pt-20Ir part, cracks would open up in the material exposed to thermal stress. This indicated that built-in mechanical defects existed in both alloys.

Since it was suspected that some of the failures in the Pt-Ir tubes might be due to mechanical defects in the tubes due to working during the drawing process, defect-free tubes were prepared by eloxing tubes from Pt-Ir bar stock. The tubes were then compared during a 100 hour test. The nominal test conditions are tabulated below:

Test Number - R5

Tube Material - #1 Pt-Ir (drawn)
#3 Pt-Ir (eloxed)

Test Duration - 100 hours

Tube temperature (max) - 1570^{o}K (2826^{o}R)

Propellant
Composition - CO_2 - 95.68%, N_2 = 3.32, O_2 = 1.0%
Pressure - 37 psia
Flow rate - 24.6 gm/sec

Bell jar pressure - 8-12 microns

Figure 63 shows photomicrographs of the tube cross sections at the 1400^{o}K section. These photos show essentially no evidence of oxidation attack on the inside of the tubes. The irregularities in the surface of Tube 1 are typical of drawn tubes. The eloxed tube shows an imperfect alignment in the eloxing operation as evidenced by the variation in tube wall thickness.

Figure 64 shows the cross sections at the 1500^{o}K section, In comparing Figures 63 and 64, there is some evidence of chemical attack. This attack is more pronounced in Figure 65 at the 1570^{o}K section.

The photomicrographs after the tubes have been etched show the large grain growth, especially at the highest temperature, but reveal no significant differences between the eloxed tube and the drawn tube. Figures 66 and 67 are photomicrographs taken at X500. The eloxed tube had slightly more oxidation attack in one area than

did the drawn tube. This localized area is shown in Figure 69 at X500. Figures 66 and 67 show that there was no preferential grain boundary attack as was experienced previously in Test L8. Also grain growth during Test R5 was greater. The reason for these differences has not been determined. Two known differences between the tests that may be significant are:

1. Test L8 propellant was humidified, containing about 0.4% H_2O, whereas Test R5 propellant was not.

2. Test R5 propellant contained 3.32% N_2 whereas propellant L8 did not contain nitrogen. Additional tests would have to be run to establish if either of these differences are significant.

Based upon the results of this test (R5) and the oxidation shown in Figure 65, it appears that the oxidation had penetrated approximately 0.001 inches into the inner surface of the drawn Pt-Ir tube.

Assuming this oxidation rate remained constant, this tube would have failed in about 700 hours if maintained at 1570°K. Since in the concentric tube resistojet, oxidation occurs on both sides of the tube, the Mark II resistojets could be expected to fail in about 350 hours if it operated with the same propellant mixture and maintained a center tube temperature of 1570°K.

These results indicate that unless some method is used to eliminate the presence of oxygen, Pt-Ir materials are not suitable for the resistojet center tube using the currently projected biowaste gases.

Platinum-palladium tests. - Since Pt-Rh and Pt-Ir alloys did not appear suitable for resistojet application with biowaste gases containing either pure CO_2 or CO_2 with significant amounts of oxygen, a third platinum alloy, platinum-palladium was examined.

A 500 hour test was conducted on the first Pt-20Pd tube. This test was designated as Test R6 in Table IX. No tube failures were encountered during test R6. However, the pressure in the tubes rose gradually with time. This pressure rise was traced to a small buildup of dark material in the valve downstream of the Pt-Pd tube. A thin coating of similar material also slowly accumulated on the inside surface of the bell jar. Samples of this material were collected and subjected to X-ray defraction analysis. The results of this analysis showed the material was finely divided palladium. Evidently at temperatures above 1500°K, significant amounts of the palladium will vaporize.

The gas mixture employed was CO_2 with sufficient air to supply 1.5% oxygen and the Pt-20Pd tube was maintained at a temperature of 1600°K for 500 hours. After

500 hours at 1600°K had been accumulated, this tube was removed for examination. Figure 68 shows the "as received" condition of the tube. The two lower photographs show the fine grain structure prior to heating. Figure 69 shows the tube at the 1600°K point after the test. The photographs reveal that the grain structure on the outer tube surface is still relatively small, but that the grains have grown very large in the bulk of the tube. In many places, there is effectively one grain across the tube.

This large grain growth did not result in tube failure and the results indicate that the test could have continued for a longer period of time, although there was some vaporization of metal.

A second Pt-20Pd tube was maintained at about 1500°K for 1003 hours with a CO_2 plus 1.5% oxygen mixture. Figure 70 shows results from this test. The results are not too different from that of Figure 69 although there appears to be more oxygen attack (creating voids) from the 1003 hour test. Both Figures 69 and 70 show a reduction in wall thickness when compared to Figure 68. A comparison of the wall thicknesses indicates that a 20-25% reduction in wall thickness could be expected in 1500 hours at 1500°K.

This temperature limit, large grain growth and high material vaporization rate make the Pt-Pd alloys unsuited for potential resistojet application unless low performance (< 1500°K) can be tolerated.

Platinum tests. - Since pure platinum is not subject to carbonyl reactions and is relatively resistant to oxidation, this material was evaluated, realizing that the material could only be used in a resistojet design that was specifically tailored for low strength materials. The first platinum tube was evaluated at the start of Test L10. The tube was subjected to CO_2 plus air to provide 1.5% oxygen for 125 hours at a tube temperature of 1600°K.

After 125 hours of operation, the platinum tube was removed and cross-sectioned for examination. The "as received" condition is shown in Figure 71. The etched photomicrographs reveal a fairly fine grain structure. Figure 72 shows the tube condition following the 125 hours. A comparison of the unetched cross sections reveals no metal depletion or corrosion. The etched cross section reveals significant grain growth, which was expected. It was not known whether the dark spots at the grain boundaries near the wall were significant or not.

Following removal of this tube from the bell jar, another Pt tube was inserted and testing was resumed. This platinum tube accumulated 765 hours at 1600°K when test L10-3 was stopped and then accumulated an additional 24 hours during Test L11 at which time the tube began to leak. This leak was entirely unexpected because

Test R6-3 was being conducted simultaneously and that Pt tube had already accumulated more hours at 1700°K without evidence of leakage. The results from Test L10-3 are presented in Figures 73 and 74. The cross section at 1500°K (Figure 73), shows slight evidence of oxidation attack whereas the 1600°K section (Figure 74) shows severe evidence. In addition to severe inside surface attack, the lower right hand photo shows grain boundary attack completely through the tube wall.

Figures 75 and 76 show results from Test R6-3 where a Pt tube was maintained for 1000 hours at 1700°K and no grain boundary attack occurred. The inside diameter of the tube shown in Figures 75 and 76 has increased considerably over the "as received" tube shown in Figure 71, which indicates a relatively uniform oxidation and resultant vaporization of the surface. No explanation can be given at present for why grain boundary attack occurred during Test L10-3 but not in Test R6-3. These results indicate that pure platinum should be limited to about 1500°K when operating with biowaste gases containing 1.5% oxygen. Actual biowaste gases are not expected to contain more than 1.0% oxygen and therefore the results obtained with 1.5% oxygen should be conservative.

Thoriated platinum tests. - Relatively early in this program, a sample of TD-Pt, platinum with about 0.7% thoria added, was evaluated in the bell jar (Test III of Table V). The samples were generally of questionable quality as may be noted by the generally hexagonal pattern of the inside diameter of the sample shown in Figure 77. This characteristic was indicative of the experimental nature and fabrication problems associated with this material during the early stages of this program. Nevertheless, the TD-Pt tube was operated for 429 hours at an average maximum temperature of 1509°K with CO_2 inside and a vacuum outside of the tube. Figure 77 shows the cross-sectional microstructures of the thoriated platinum tube sample tested in the as received and after exposure conditions. Essentially no change in grain size is apparent indicating that there was no loss in structural integrity of the material. There was no apparent change in the outside surface appearance. Although these results appeared very encouraging, additional developmental effort was undertaken by Engelhard Industries under NASA sponsorship. During 1971, Engelhard supplied Marquardt (TMC) with samples of TD-Pt containing 0.6% thoria. At the request of TMC, Engelhard conducted tensile tests on the TD-Pt material. The tests were conducted on 0.020 inch diameter wire. The wire was annealed at 1000°C and tested on a table model Instron tensile tester. The average of four tests gave a proportional limit (departure from a straight line on the stress-strain-chart) of 10,800 psi, and a yield strength (0.2% offset) of 13,400 psi. As indicated by Engelhard, these values are nearly equivalent to those of pure platinum.

Upon receipt of a length of the TD-Pt tube (0.040 inches I.D. with a wall thickness of 0.007 inches), photomicrographs were taken of the material. Figure 78 shows a cross section of the tube. It is evident from Figure 78 that the grain structure is quite fine. The thoria can be seen as dark specks. Although the tube

structure appears sound, macrographs of the external surface of the tube revealed surface irregularities which are assumed to be mechanical scratches. Figure 79 shows typical photographs of the exterior tube surface. Although the surfaces appeared rough, there was no evidence that these surface irregularities caused tube failures.

As part of Test R5, a 100 hour test was conducted on the TD-Pt containing 0.6% thoria. The tube was maintained at a maximum average temperature of about 1570°K. The propellant was CO_2 with sufficient air to result in 1.0% oxygen. Figure 80 shows the average tube temperature distribution. Figures 81 through 83 show micrographs of cross sections at various temperature stations. There is no evidence of oxidation attack, metal evaporation and little if any evidence of grain growth. Figure 84 shows X500 photos and again, a comparison of the "as received" photo in Figure 78 reveals little change. These results are in sharp contrast to the other tubes (Pt-20Ir) tested at the same time (shown in Figures 66 and 67).

As a result of the encouraging performance of the TD-Pt tubes in Test R5, the left bell jar was set up to run long duration tests using three TD-Pt tubes with a mixture of CO_2 and air resulting in 1.0% oxygen. All of the tubes contained 0.6% thoria in platinum. Approximately 10 hours after full temperature (1700-1800°K) had been reached, one of the tubes failed. The tube developed a longitudinal crack approximately 0.2 inches long in the highest temperature region. The upper photo in Figure 85 is a photomacrograph of the high temperature region showing the crack. The lower photos show the tube cross section in the region of the crack.

Testing was continued with the other two tubes, but they also failed by developing longitudinal cracks. The tube at 1700-1800°K failed in about 17 hours and the tube at 1600-1700°K failed in about 26 hours.

These failures were unexpected, based upon Test R5 and long duration - high temperature tests conducted by Engelhard Industries. Close liaison was being maintained with Engelhard Industries and a sample of the tube shown in Figure 85 was returned to Engelhard for analysis. Results from Englehard indicated that thoria in the tubes had been reduced to thorium. This reduction reaction can occur at high temperature in the presence of carbon with platinum acting as a catalyst. The furnace used at Marquardt to braze these tubes to the larger support tubes was graphite cloth-lined and it might be possible that some reduction could have occurred during the brazing process. This same furnace has been used to successfully braze all of the other platinum alloy tubes since pure platinum and its alloys are not affected by graphite.

While the failure mode investigation was underway, an additional TD-Pt sample (obtained during 1971) was prepared for bell jar tests. This tube was brazed in a furnace that did not contain graphite. In addition, Engelhard Industries supplied an additional length of TD-Pt tubing.

This experience with TD-Pt raised the question of operation of the material with biowaste gases containing methane or carbon monoxide. However, normal operation with CH_4 would be at substantially lower temperatures than those experienced in the braze furnace in order to stay below the carbon deposition threshold. Additional studies and tests were conducted to determine if restrictions other than carbon deposition threshold temperature must be imposed when operating with these gases.

The TD-Pt tube that was brazed in the TMC "clean" furnace was evaluated during Test L10-2 with CO_2 plus sufficient air to result in 1.5% oxygen. The tube was maintained at 1600°K for 1007 hours before it was cross-sectioned. When initially heated in the bell jar facility, all of the platinum alloy tubes developed an oxide type film on the tubes. This dark coating evaporates at the higher temperature regions of the tubes and has not appeared to have any affect upon the tubes other than affecting the tube local emissivity. Figure 86 shows the temperature distribution of the tube and Figure 87 shows external views of the tube prior to cross sectioning it. An examination of these two figures reveals that the transition from dull to bright finish occurred at a temperature of about 1500°K.

Figures 88, 89, and 90 show cross sections at temperatures of 1450°K, 1500°K and 1600°K. There is evidence of oxidation attack on the outside of the tube at the 1450°K station and some inside and outside at 1500°K, but none at the 1600°K station. Why this apparent oxidation attack occurred is not known as it is the only instance of TD-Pt attack to date. It may be associated with the surface film. Since the unetched photos do not reveal any grain boundary attack, the affect on the grain boundaries must be very minor. In actual resistojet application, the center tube is expected to operate between 1600 and 1700°K and therefore this condition should not exist. Also, no evidences of surface films have been noted in the biowaste thrusters operated in the TMC high vacuum facility. This film has been noted in the bell jars, both when vacuum conditions and one atmosphere have been maintained in the bell jar. A comparison of the wall thickness from this test and that of Figure 78 reveals that there was only about a 5% reduction in wall thickness after 1000 hours at 1600°K. This is a significant improvement over any of the other materials that have been tested. The large dark specks seen clearly in Figure 90 have not been precisely identified but are probably thorium oxide. How or why this material agglomerates is not known, but it does not appear to be detrimental to the life of the tubes.

The additional TD-Pt tubes supplied by Engelhard Industries were of larger diameter (0.094 inches) than the previous tubes (0.054 inches) but had about the same wall thickness (0.007 inches). Figure 91 shows a cross section of the "as received" tube. As is evident from the photograph, the wall thickness varied somewhat because of a non-smooth inner surface. The 0.6% thoria apppears to be dispersed in a satisfactory manner.

During Test L11-2, the effect of 0.25% oxygen on one of the new TD-Pt tubes was investigated. This tube was maintained at 1700°K for 1500 hours. Figure 92 shows external views of the tube. As can be noted, the majority of this tube is clean with only dark coatings at the cool ends. Figures 93 and 94 show cross sections at 1600 and 1700°K stations. Although the grain size appears large, with one grain across the wall, no attack in the grain boundaries occurred. Also, the grain boundaries are irregular in shape rather than being straight. Very little if any reduction in wall thickness occurred.

Tests also were conducted to determine if during thruster operation, carbon or CO might cause reduction of the thorium to thoria. To evaluate the effects of carbon, two carbon deposition runs were made using CH_4 followed by carbon stripping runs with CO_2 + 1.5% O_2. During Test R8-1, CH_4 was run for a total of 189 hours with a tube temperature of 1200°K (2160°R) followed by 313 hours with CO_2 + 1.5% O_2 at 1600°K. The tube was then subjected to an additional 1213 hours with CO_2 at a tube temperature of 1600°K. This resulted in a total time at 1600°K of about 1526 hours. Figure 95 shows cross sections of the tube after this test. The photos reveal no detectable reduction in wall thickness but some evidence of grain growth. At least the grains are easier to identify. There also appears to be more and larger black specks. The tube integrity appears excellent after 1500 hours at 1600°K. This tube also had about 189 hours of time at 1200°K with methane. The carbon deposition does not appear to have affected the tube in any way.

Figure 96 shows a longitudinal cross section at the 1600°K location. As was expected, the grains are elongated in a direction along the tube. These photographs, Figures 95 and 96, look essentially identical to the annealed sections presented as Figures 7 and 8 of Reference 57.

The TD-Pt tube in Test R8-2 was subjected to pure CO_2 for 1500 hours at 1700°K. Figure 97 shows the 1700°K section after the test. Again no significant reduction in wall thickness is evident although the non-smooth inner surface in the "as received" condition makes it more difficult to accurately measure the wall thickness. The tube is still in excellent condition as is evident by the photographs. Although photographs are not included here, tube R8-1 was also sectioned at the 1400 and 1500°K sections and tube R8-2 was sectioned at the 1600°K section. These lower temperature sections also confirm that the tubes were in excellent condition.

From the experimental results obtained with TD-Pt, it is obvious that TD-Pt is the best of the noble metals for biowaste resistojet applications. Not only does the dispersed ThO_2 greatly improve the hot strength properties, but it also inhibits grain growth and appears to suppress oxidation and vaporization of the platinum.

CONCLUSIONS AND RECOMMENDATIONS

1. Candidate materials for biowaste resistojet applications can be considered in two broad categories. These include the nickel or cobalt based superalloys and the noble metals. When considering all of the desired resistojet properties for the central heater tubes, only the platinum based materials apply.

2. The biowaste gases available for propellant include CO_2, CH_4, O_2, N_2, H_2, and H_2O in various proportions. Experimental results indicate that thoriated platinum can be successfully used with any of these propellants. During some periods, it will be desirable to operate with all propellants at the highest attainable specific impulse (maximum thruster temperature). However, because of thermal decomposition and resulting carbon deposition, it will be necessary to limit the thruster temperature when operating with propellants containing methane.

3. When operating with CH_4 containing propellants, Hastelloy X tubes can be used because of the temperature restriction. The nobel metal tubes can operate with non-methane propellants at temperatures up to 1700°K (3060°R).

4. Excessive carbon deposition is undesirable for a resistojet because of potential nozzle throat blockage from fractured carbon presenting a failure mode. Light coatings, on the other hand, are considered tolerable, especially when the carbon coating has good structural integrity. It is suggested that a tolerable deposition rate of about 0.2 micro-inches per hour be considered in determining a nominal carbon deposition threshold temperature. Operation for 5,000 hours at this deposition rate would result in a total carbon thickness of one mil (0.001 inches). The carbon deposition threshold temperatures for several CH_4 containing propellants are as follows:

Propellant	Threshold Temperature, °K (°R)
CH_4	950 (1700)
CO_2-CH_4	1000 to 1055 (1800 to 1900)
H_2O-CH_4	1235 (2225)

5. Although Pt-Rh alloys offer good strength and high temperature properties, alloys with 20% rhodium concentration suffer from severe carbonyl reaction when operating with pure CO_2 at high temperatures. When the rhodium content is reduced to 10% and when 1.5% oxygen is added to the CO_2, carbonyl reactions are minimized or eliminated, although some surface oxidation occurs.

Carbonyl reactions still occur when only 0.25% oxygen is added. With a rhodium content of 5%, carbonyl reactions are minimized with CO_2 but the effect of oxygen addition was not investigated.

6. Platinum-iridium alloys also offer high strength and good high temperature properties but suffer from excessive oxidation when used with biowaste gases containing appreciable amounts (0.25-1.5%) of oxygen.

7. Platinum-palladium alloys offer more strength than platinum but operating temperature is limited to about 1500°K because of excessive vaporization of the palladium above this temperature.

8. Pure platinum is not subject to carbonyl reaction but significant oxidation occurred at temperatures above 1500°K (2700°R) when CO_2 plus 1.5% oxygen was tested. This oxidation may occur either on the surface or in the grain boundaries.

9. Thoriated platinum (0.6% ThO_2 dispersed in Pt) offers the best potential of meeting the desired requirements of a biowaste resistojet. Sample tubes have operated continuously at 1700°K (3060°R) for 1500 hours with no deterioration with pure CO_2 and when 1.5% oxygen was added, only a 5% reduction occurred after 1000 hours at a tube temperature of 1600°K (2880°R). No measurable reduction in wall thickness occurred after 1500 hours at a temperature of 1700°K (3060°R) when the oxygen content was 0.25%. Evidently the thoria not only inhibits grain growth but also suppresses oxidation and vaporization of the platinum.

REFERENCES

1. Phillips, D.G., Technology Development of a Biowaste Resistojet, Vol. II.

2. Bliss, J.R. and Greco, R.V., Design and Operational Characteristics of an Integrated Biowaste Resistojet System, AIAA Paper 71-686, AIAA 7th Propulsion Specialist Conference, Salt Lake City, Utah, June 1971.

3. Pisciotta, A., Report of the Development of the Manned Orbital Research Laboratory (MORL) System Utilization Potential; Task Area IV MORL System Improvement Study. Douglas Aircraft Co., (MSSD) Report SM-48819B, January 1966.

4. Gaubatz, W.A., James, N.E., and Page, R.J., Chemical Nonequilibrium Effects in Biowaste Thruster Performance. AIAA Paper presented at the 7th Propulsion Joint Specialist Conference, Salt Lake City, Utah, June 1971.

5. Ladd, I.R., and Walsh, P.N., Complex Temperature Dependence of the Oxidation of Pyrolytic Graphite by CO_2. Carbon, Vol. 4, pp. 539-541.

6. Golovina, E.S. and Kihavstovich, G.P., The Interaction of Carbon with Carbon Dioxide and Oxygen at Temperatures up to 3000°K. Eighth Symposium (International) on Combustion, The Combustion Institute, pp. 784-792, 1962.

7. Mentser, M. and Ergun S., Kinetics of Oxygen Exchange Between CO_2 and CO on Carbon. Carbon, Vol. 5, pp. 331-337, 1967.

8. Reif, A.E., Mechanism of the Carbon Dioxide-Carbon Reaction, J. Phys. Chem., Vol. 56, pp. 785-788, June 1952.

9. Corrosion Resistance of Metals and Alloys. Edited by F.L. LaQue and H.R. Copson, 2nd Edition, Reinhold Pub. Co., N.Y., 1963.

10. Corrosion Handbook. Edited by H. H. Uhlig, John Wiley and Sons, N.Y., 1948.

11. Corrosion: Vol. 1 - Corrosion of Metals and Alloys. Edited by L.L. Shrier, John Wiley and Sons, N.Y., 1963.

12. Metals Handbook, Vol. 1, Properties and Selection of Metals. Eighth Edition American Society for Metals, 1961.

13. Temperature, It's Measurement and Control in Science and Industry - Part 2, Applied Methods and Instruments. Vol. 3, Reinhold Pub. Co., N.Y., 1962.

14. Aerospace Structural Metals Handbook, Vol. I, Ferrous Alloys. AFML TR-68-115, March 1968.

15. Aerospace Structural Metals Handbook, Vol. IIA, Non-Ferrous Alloys. AFML TR-68-115, March 1968.

16. Goldsmith, A., Waterman, T.E., and Hirschhorn, H.J., Handbook of Thermophysical Properties of Solid Materials. Armour Research Foundation, MacMillan Co., N.Y., 1961.

17. High Temperature Technology. Edited by I.E. Campbell, John Wiley and Sons, N.Y., 1956.

18. Lund, C.H., Physical Metallurgy of Nickel-Base Superalloys. Battelle Memorial Institute, DMIC Report 153, May 5, 1961.

19. Wagner, H.J. and Hall, A.M., The Physical Metallurgy of Cobalt-Base Superalloys. Battelle Memorial Institute, DMIC Report 171, July 6, 1962.

20. Lund, C.H. and Wagner, H.J., Oxidation of Nickel and Cobalt-Base Superalloys. Battelle Memorial Institute, DMIC Report 214, March 1, 1965.

21. Eiselstein, H.L., and Skinner, E.N., American Society Testing Materials. Spec Tech Report No. 165, 1954.

22. Gibeaut, W.A. and Ogden, H.R., Summary of the Seventh Meeting of the Refractory Composites Working Group. Battelle Memorial Institute, DMIC Report 184, May 30, 1963.

23. Gibeaut, W. A. and Bartlett, E.S., Properties of Coated Refractory Metals. Battelle Memorial Institute, DMIC Report 195, January 10, 1964.

24. Hot Corrosion Problems Associated with Gas Turbines. ASTM Special Technical Publication No. 421, 1967.

25. Marnoch, K., High Temperature Oxidation Resistant Hafnium-Tantalum Systems. Third Quarterly Report on Contract AF33(615)-1628, Marquardt Corporation Report No. 25,157, February 1965.

26. Marnoch, K., High Temperature Oxidation Resistant Hafnium-Tantalum Alloys. Paper presented at the 94th AIME Annual Meeting, Chicago, Illinois, February 14-18, 1965; Marquardt Corporation MR 20, 314.

27. Marnoch, K., Some Properties and Applications of the Hafnium-Tantalum Alloy. Pages 283-301 of the Summary of the Thirteenth Refractory Composites Working Group Meeting, May 1968. Tech. Report AFML TR-68-84.

28. Platinum - The Metal, Its Properties and Applications. The International Nickel Co., Inc., Bulletin A-445, January 1968.

29. Rhodium - The Metal, Its Alloys, Chemical Compounds and Catalytic Properties. The International Nickel Co., Inc., Bulletin A-402, January 1966.

30. Iridium - The Metal, Its Alloys, Chemical Compounds and Catalytic Properties. The International Nickel Co., Inc., Bulletin A-370, March 1965.

31. Siller, R.H., Oates, W.A. and McLellan, R.B., The Solubility of Carbon in Palladium and Platinum. J. of the Less-Common Metals, Vol. 16, 1968, pps 71-73.

32. Bartlett, R.W., Platinum Oxidation Kinetics with Convective Diffusion and Surface Reaction. J. Electrochem. Soc. Vol. 114, June 1967, pps. 547-550.

33. Fryburg, G.C. and Petrus, H.M., Kinetics of the Oxidation of Platinum. J. Electrosoc. Soc., Vol. 108, 1961, pps. 496-502.

34. Wise, E.M., The Platinum Metals - Alloys and Compounds. The International Nickel Co., Inc. Interscience Encyclopedia Inc., N.Y.

35. Platinum Metal Products. J. Bishop and Co., Bulletin 964R, 1962.

36. The Platinum Group Metals in Industry. The International Nickel Co., Inc., Bulletin A-347, March 1964.

37. Chaston, J.C., Reaction of Oxygen with the Platinum Metals: I - The Oxidation of Platinum. Platinum Metals Review, Vol. 8, No. 2, 1964, pps. 50-54.

38. Hill, J.S. and Albert, H. J., Loss of Weight of Platinum, Rhodium and Palladium at High Temperatures. Engelhard Industries, Inc. Technical Bulletin Vol. IV, No. 2, Sept. 1963, pps. 59-63.

39. Alcock, C.B. and Hooper, G.W., Thermodynamics of the Gaseous Oxides of the Platinum Group Metals. Proceeding Roy. Soc., London, Vol. 254A, 1960, pps. 551-561.

40. Betteridge, W. and Rhys, D.W., The High Temperature Oxidation of the Platinum Metals and Their Alloys. First International Congress on Metallic Corrosion, 1961, pps. 186-192.

41. Phillips, W.L., Jr., Oxidation of the Platinum Metals in Air. Transactions of the ASM, Vol. 57, 1964, pps. 33-37.

42. Brown, H.L., Armstrong, P.E. and Kempter, C.D., Elastic Properties of Polycrystalline Sc, Re, Ru and Pt-21Ir. J. of the Less-Common Metals, Vol. 11, 1966, pps. 135-140.

43. Sadowski, E.P. (Part I) and Albert, H.J., Accinno, D.J., and Hill, J.S. (Part II), Streee Rupture Properties of Some Platinum and Palladium Alloys. AIME Metallurgical Society Conference Vol. 11, Refractory Metals and Alloys, Interscience Publishers, N.Y., 1961, pps. 465-482.

44. Darling, A.S., Iridium Platinum Alloys - A Critical Review of Their Constitution and Properties. Platinum Metals Review, Vol. 4, 1960, pps. 18-26.

45. Zysk, E.D., Toenshoff, D.A. and Penton, J., Compatibility of Iridium with Other High Temperature Materials at Elevated Temperatures. Engelhard Industries, Inc., Tech Bulletin, Vol. IV, No. 2, Sept. 1963, pps. 52-58.

46. Selman, G.L., Ellison, P.J. and Darling, A.S., Carbon in Platinum and Palladium. Platinum Metals Review Vol. 14, No. 1, Jan. 1970, pps. 14-20.

47. Rice, L.P., Metallurgy and Properties of Thoria-Strengthened Nickel. Battelle Memorial Institute, DMIC 210, Oct. 1, 1965.

48. TD Nickel - A Dispersion Strengthened Metal. Fansteel Inc., Bulletin TD-007-1.

49. TD NiCR - A Dispersion Strengthened Alloy. Fansteel Inc., Bulletin TD-007-2.

50. The Low Radioactivity Factor of Fansteel Metals Contraining Thoria. Fansteel Inc., Bulletin TD-007.

51. British Patent 830,628, Alloys; Powder Metallurgy. Johnson-Matthey and Co. Ltd., July 24, 1958.

52. Knight, J.R. and Taylor, B., Production and Properties of Grain Stabilized Platinum and Platinum Alloys. Powder Metallurgy, No. 10, 1962.

53. Raub, E. and Plate, W., Z. Metall, 1957, 48, 529.

54. Bufferd, A.S., Zwilsky, K.M., Blucher, J.T. and Grant, N.J., Oxide - Dispersion Strengthened Platinum. Inter. J. of Powder Metallurgy, Vol. 3, No. 1, 1967, pps. 17-26.

55. Grant, N.J. of Industrial Materials Tech, Inc., Communication to Marquardt Company, May 23, 1969.

56. Darling, A.S., Selman, G.L., and Bourne, A.A., Dispersion Strengthened Platinum-Improved High Temperature Creep Properties. Platinum Metals Review, Vol. 12, 1968, pps. 7-13.

57. Albert, H. J. and Hill, J.S., Development of a Platinum - Thorium Oxide Alloy for Resistojet Thruster Use. NASA CR-111959, dtd. July 1971.

58. Space Storable Regenerative Cooling Investigation. Pratt and Whitney Aircraft Interim Report PWA FR-2552, NASA CR-72341.

59. Space Storable Regenerative Cooling Investigation. Rocketdyne Report R7338, NASA CR-72360, September 1968.

60. Robinovich, E.Y. and Rodionov, A.V., Formation of Carbon Filaments During Thermal Decomposition of Hydrocarbons. Chemical Abstracts, Vol. 54, 13614, 1960.

61. Bokros, J.C., The Structure of Pyrolytic Carbon Deposited in a Fluidized Bed. Carbon, Vol. 3, pps. 17-29, 1965.

62. Pugmire, T.K., et al, Applied Resistojet Technology. AIAA J. Spacecraft and Rockets, Vol. 8, No. 1, pps. 63-68, January 1971.

63. Tesner, P.A., Formation of Dispersed Carbon by Thermal Decomposition of Hydrocarbon. Seventh Symposium (International) on Combustion, Butterworths, London, pps. 546-553, 1959.

APPENDIX A

CARBON DEPOSITION PHENOMENON

The phenomenon of the pyrolysis of hydrocarbon gases exposed to heated surfaces is not fully understood. This phenomenon is known to be very complex and many theories have been proposed, some of which are conflicting. Reference A1 through A15 discuss various theores and observations of many investigators and are helpful in trying to understand carbon deposition.

Many theories assume that the decomposition of hydrocarbons involves stable intermediates. Deposition of methane for instance may involve the formation of intermediates C_2H_6, C_2H_4 and C_2H_2 and finally carbon. Some investigators suggest that the deposition process involves gas phase dehydrogenation and polymerization of hydrocarbons. Others maintain that carbon formed by thermal decomposition of a hydrocarbon involves the breaking down of molecules on the surface without any necessary reaction in the gas phase. Still others have suggested that both phenomenon are important.

Generally, the theories proposed and conclusions reached are based on experimental results. Experimental conditions are far ranging and very likely there is much truth in most of what has been claimed about carbon deposition. There seems to be universal agreement that particles formed in fluid streams is the result of a two-stage process. The first stage is the formation of nuclei and the second stage involves growth into particles by deposition of material on the nuclei. Growth proceeds readily by reaction with unsaturated or active molecules of gas. Initial nucleation of surfaces is also considered a requirement for subsequent deposition of carbon. It has been suggested that nucleation is provided by large aromatic molecules from the gas phase. Very often these nuclei are referred to as "soot particles".

Tesner (Reference A6) claims that growth of carbon surfaces during thermal decomposition of hydrocarbons is due to direct decomposition of hydrocarbon molecules on the surface. This involves decomposition of active hydrocarbon molecules at active points on the carbon surface. The carbon atoms are assumed not to migrate along the surface as is usually the case in the growth of a crystal lattice. Rather, the atoms are assumed to remain at the reaction sight. These conclusions of Tesner were based on electron microscope measurements of successive accumulations of carbon. Tesner maintains that it is the molecules of the initial hydrocarbon that decompose on the carbon surface and not carbon radicals or bulk-polymerization products.

Other examinations by electron microscopy (Reference A8) revealed particles formed at 1000°C from acetylene to consist of very long chains completely dry of any polymer. These chains were cross linked into networks of spheres. At lower temperatures, 700°C for example, polymer droplets formed and remained stable. Some solid reaction products were also noted and consisted of small particles of carbonaceous material distributed throughout odd-shaped blobs of polymer. This material would be classified as an amorphous carbon. Acetylene was used in the Reference A8 tests and deposition was observed at a temperature as low as 600°C. With methane, this threshold temperature would be higher.

Experimental data reported in Reference A11 indicate a threshold temperature for carbon deposition from the pyrolysis of methane to be 850°C. These investigations conclude that the main part of pyrolytic carbon formed is composed of a mixture of high-molecular hydrocarbons and their free radicals. Reference A11 carbon deposits were obtained at tempeatures from 850 to 1000°C.

In Tesner's experiments (Reference A6) with methane decomposition, carbon formation on surfaces began at 900°C. It is also significant to note that Tesner found that particle formation in the gas stream adjacent to the deposition surface did not begin until 1050°C. Tesner concluded that to form nuclei in the gas stream by the decomposition of hydrocarbon, the gas must be superheated from 150 to 200°C. This is an important observation and one which is now evident in the Marquardt bell jar experiments. It is important because it means a resistojet thruster can be operated at or slightly above the threshold temperature for carbon deposition and still not produce a carbon particle contaminated exhaust plume. This means that spacecraft contamination by the thruster plume will not necessarily set the maximum operating temperature of the biowaste resistojet, rather incipient carbon deposition temperature will determine the operating point of the thruster with biopropellants containing methane.

Bokros (Reference A13) conducted deposition experiments in fluidized beds using methane diluted with helium. He found that a significant fraction of amorphous material or single layers can be present in pyrolytic carbon deposited below about 1700°C. His conclusion is that the low-temperature, high-density, anistropic deposits are built up from planar molecules that are formed in the gas phase, dehydrogenated, and are removed by condensation directly in the bed surface. When deposited, these molecules align themselves parallel to each other and to the substrate. The isotropic low-density structures (which would be considered amorphous) are considered by Bokros to be formed at conditions where general gas-phase nucleation of droplets and soot occurs in the bed.

These observations go on and on from the many experimental investigations conducted on the pyrolysis of hydrocarbons. There is a general sense of continuity and usefulness in these vast amounts of data. However, there is also an ever present degree of confusion. One must be careful in relating his carbon problem to these data as many parameters are involved and are important.

In view of the theory that surface deposition requires initial nucleation, polished surfaces can be used to delay the deposition of carbon. There is the question, however, of the catalytic activity of the surface itself in promoting initial reactions. Experiments reported in Reference A3 showed that: (1) metals of the iron subgroup have a maximum catalytic effect, (2) quartz acts catalytically at temperatures above 1000°C, (3) platinum has a very small catalytic effect; and (4) copper, porcelain and pure carbon have no catalytic effect. Studies conducted by Grisdale, et al (reported in Reference A14) showed that ceramics were coated with dense compact carbon while surfaces contaminated with metal or metal oxides gave loose sooty deposits which could be formed at low temperature. Their experiments ranged in temperature from 930 to 1300°C.

A polished metal surface may hinder initial deposition by forming nucleation sights slowly, however, it can present other problems. If conditions are such that small carbon deposits will occur in time of a magnitude which is tolerable, then the following should be considered. Nucleation on smooth surfaces will tend to be random causing large local carbon deposits and nonuniform carbon structure. The smooth substrate would promote flaking or breaking away of deposits. This is worse than the formation of a slightly thicker amount of carbon with good structural stability. It would be best to have a controlled surface finish which would promote uniform nucleation and result in a more reliable-stronger carbon film. Too rough a surface is to be avoided as this too promotes large crystals to grow which are weaker than fine crystals and may present a fracturing problem.

This discussion centers around the problems to be avoided if a slow carbon deposition rate occurs in a thruster. For instance, if a thruster is operated at carbon threshold temperatures for thousands of hours, small deposits (of the order of a mil) may occur and may not be necessarily harmful. The designer should anticipate this possibility and design accordingly to achieve maximum thruster integrity.

Relative to resistojet thrusters, there are two carbon deposit classifications which are of interest, amorphous and pyrolytic. Amorphous carbon includes isotropic deposits assumed to contain polymers mixed with carbonaceous material which are not optically active under polarized light. Amorphous carbon can be porous and soft. However, in sample heater tube tests conducted at Marquardt, the amorphous deposits found, while softer than pyrolytic deposits, have reasonably good structural integrity. Pyrolytic carbon, on the other hand, is comprised of discrete grains which are optically active under polarized light. Pyrolytic carbon or graphite is anisotropic and generally occurs in either of the following forms:

1. Columnar with radially oriented grains or cones (the most common form).

2. Laminar with parallel planes in the case of flat surface deposits or concentric shells in the case of cylindrical or spherical deposits.

Pyrolytic graphite observed in sample heater tube tests has been of the columnar type with lamination lines reflecting some resemblance to the laminar type.

Figures A1 and A2 present typical columnar pyrolytic graphite deposit photomicrographs. These were obtained from samples of vapor deposited carbon on a Thornel substrate (Union Carbide composite material) and are used here to more clearly show some important features of these type deposits. Similar structures on a much smaller scale have occurred in the long term tests on sample heater tubes, examples of which will be discussed in the experimental section. Figure A1 shows a typical large conical crystal emanating from a nucleus consisting of a particle of amorphous carbon. Adjacent smaller cones began growing from the deposition surface. The nucleus for the large cone was deposited later along a dark line referred to as a lamination. Many typical laminations are seen like the one identified in the large crystal. Laminations are growth rings and result when a very small change in deposition conditions (temperature, chemistry, etc.) occurs and from mechanical straining such as thermal contraction on cool down. The laminations are potential fracture lines as are the crystal planes of large crystals. Note in Figure A1 that even in a bright field, the laminations and the large crystal boundary are evident. Such a large crystal or a portion of it could fracture away from the surrounding carbon coating and present a nozzle blockage problem.

Similar characteristics are seen in Figure A2 where two large crystals are seen side by side. Note here, however, that these crystals grew at the same time that the surrounding crystals began to grow from the substrate surface. The nucleus called out in Figure A2 points to a fine fiber which extends some 2 mils from the substrate surface. This case demonstrates why rough surfaces are to be avoided in order to avoid these large-weaker crystals.

Stresses occurring in vapor deposited materials is a continuing problem with this process. Bonding along the columnar grains tends to be poor. Fracturing and breaking away of deposited material can occur and is aggravated by thermal changes. Fracturing along laminations is referred to as delamination and is the most obvious failure mode in these type of deposits. Separation of the bulk of the coating from the deposition surface also occurs, again, due to thermal expansion and is most apt to occur in thick deposits and/or at sharp corners.

Many factors affect the deposition of carbon. Tesner (Reference A6) found that deposition rate is of first order with respect to hydrocarbon concentration. It is generally agreed that deposition rate increases with the first order of pressure which agrees with Tesner's finding. An interpretation of the effects of pressure or concentration would depend on whether or not both gas-phase and surface deposition were occurring. At the slow deposition rates at threshold temperatures or slightly higher temperatures in resistojet sample heater tube tests, only surface deposition occurs.

Methane decomposition rates are one to two orders of magnitude lower than those for the higher molecular weight hydrocarbons. Gas impurities such as oxygen, nitrogen and water vapor tend to increase nucleation. Hydrogen however seems to retard carbon formation by the chemisorption of hydrogen on the deposition surface. Tesner (Reference A6) presents data for a CH_4-H_2 mixture at 950°C. With 12% H_2 addition, carbon deposition rate is reduced a factor of 5 for example. The hydrogen "H" effect (slowing down of decomposition by the accumulation of H_2) has been observed by many investigators and explains the venturi shaped deposits observed in some of the Marquardt tests. Under conditions of rapid carbon deposition, released hydrogen from hydrocarbon decomposition increases in concentration affecting subsequent downstream deposition rates.

Another important effect resulting from kinetics is referred to as the autocatalytic effect. In the decompositon of methane, ethane may be produced. As the concentration of C_2H_6 increases, so does decomposition. In the carbon deposition threshold experiments conducted at Marquardt, neither the hydrogen nor the autocatalytic effect are important. For example, in a typical test with a carbon dioxide to methane mixture weight ratio of 2 a maximum temperature of 1280°K (2300°R) was held for 185 hours. Carbon deposition reached a thickness maximum of 0.00075 inches at the maximum temperature location. The total amount of carbon accumulated in the tube was integrated and found to weigh 15×10^{-6} grams. During the test, 1333 grams of methane passed through the tube. The ratio of the carbon deposited to the total carbon in the hydrocarbon passed through the tube was found to be 15 billionths (15×10^{-9}). This means that the changes in the gas chemistry due to carbon deposition are negligible in the threshold temperature experiments. On the other hand, any hydrogen mixed with methane in spacecraft biopropellant should be welcomed both as a deposition retarder and I_{sp} increaser. Other impurities may be harmful, however, by reducing threshold temperatures.

APPENDIX A - REFERENCES

A1. Space Storable Regenerative Cooling Investigation. Pratt and Whitney Aircraft Interim Report PWA FR-2552, NASA CR-72341.

A2. Space Storable Regenerative Cooling Investigation. Rocketdyne Report R7338, NASA CR-72360, September 25, 1968.

A3. Robinovich, E.Y. and Rodionov, A.V., Formation of Carbon Filaments During Thermal Decomposition of Hydrocarbons. Chemical Abstracts, Vol. 54, 13614, 1960.

A4. Powell, C.F., Oxley, J.H., Blocher, J.M.,Jr., Vapor Deposition. The Electrochemical Society, Inc., John Wiley and Sons, N.Y., 1966.

A5. Bradshaw, W., and Armstrong, J.R., Pyrolytic Graphite, Its High Temperature Properties. Technical Documentary Report No. ASD-TDR-63-195, March 1963.

A6. Tesner, P.A., Formation of Dispersed Carbon by Thermal Decomposition of Hydrocarbons. Seventh Symposium (International) on Combustion, Butterworths, London, pps. 546-553, 1959.

A7. Johnson, G.L. and Anderson, R.C., An Electron Microscope Study of Carbon Formation in the Pyrolysis of Hydrocarbons. Proceedings of the Fifth Conference on Carbon, Vol. 1, June 1961, Pergamon Press, pps. 395-405, 1962.

A8. Carley-Macauly, K.W., and Mackenzie, M., Studies on the Deposition of Pyrolytic Carbons. Proceedings of the Fifth Conference on Carbon, Vol. 2, pps. 449-459, June 1961.

A9. Stehling, F.C., Frazee, J.D., and Anderson, R.C., Mechanisms of Nucleation in Carbon Formation. Eighth Symposium (International) on Combustion, The Combustion Institute, pps. 774-784, 1962.

A10. Narasimhan, K.S., and Foster, P.J., The Rate of Growth of Soot in Turbulent Flow with Combustion Products and Methane. Tenth Symposium (International) on Combustion, The Combustion Institute, pps. 253-257, 1965.

A11. Syshov, K.I. and Jelikhovskaya, E.I., On the Formation and Composition of Pyrolytic Carbon. Carbon, No. 3, Vol. 5, pps. 201-203, Pergamon Press, 1967.

A12. Schneider, J.A., The Thermal Decomposition of Methane. Chemical Abstracts, Vol. 55, 6996, 1961.

A13. Bokros, J.C., The Structure of Pyrolytic Carbon Deposited in a Fluidized Bed. Carbon, Vol. 3, pps. 17-29, 1965.

A14. Mantell, C.L., Carbon and Graphite Handbook. Interscience Publishers, John Wiley and Sons, N.Y., 1968.

A15. Clark, Ronald K., Simulation of Pyrolysis-Gas Flow through a Char Layer During Ablation. NASA (Langley) TN-D-5464, October 1969.

APPENDIX B

CARBONYL FAILURE MECHANISM

Certain elements are known to form volatile compounds with carbon monoxide gas. Included among these elements are iron, nickel, platinum, iridium and rhodium. For the environmental conditions explored in this study program, rhodium appears to react with CO relatively fast compared to iridium which reacts one order of magnitude slower followed by platinum which reacts at an insignificant rate. Rhodium is known to form several carbonyls*; e.g., $Rh(CO)_3$, $Rh(CO)_4$, and $Rh_6(CO)_{16}$.

The equilibrium decomposition reaction for carbon dioxide,

$$CO_2 \rightleftharpoons CO + (1/2)\,O_2, \qquad (1)$$

is dominantly to the left at nonelevated temperatures. Not until 1630°K does the mole fraction of CO even reach 10^{-3}. Metal carbonyls form at relatively low temperature and decompose at elevated temperatures:

$$Me(CO)_x \underset{500^{\circ}C}{\overset{1100^{\circ}C}{\rightleftharpoons}} Me + xCO \qquad (2)$$

A third reaction involving the oxidation of metal and the formation of a volatile oxide,

$$Me + 2CO_2 \longrightarrow MeO_2 + 2CO \qquad (3)$$

should also be considered. Although this reaction proceeds slowly, it serves to accelerate the formation and loss of carbonyls through production of CO.

Consider the case of a platinum-rhodium alloy (refer to Figure 40). Oxidation of platinum, per Equation 3, can accelerate the production of carbon monoxide. In a stagnant system, the equilibrium pressure of the carbonyls is very low. In a flowing system, however, the carbonyls formed at the metal surface are continually swept away, and the reactions to form carbonyls continue in trying to establish the equilibrium concentration.

When the surface of the Pt-Rh alloy becomes depleted in rhodium, rhodium diffuses from the interior of the alloy in order to maintain thermodynamic equilibrium in the continuous Pt-Rh solid solution system. Ideally, such a system will result in a uniform linear concentration gradient from zero at the surface to the initial concentration. The transition position moves inward as the surface reaction proceeds. In the Pt-Rh system, a typical total solid solution system, additional

*Rhodium, International Nickel Company, Publication A-402, 1966

complications probably occur as the result of grain growth, to which Pt-Rh alloys are especially prone. Further, because atomic movement in solid solutions occurs principally by the vacancy mechanism, large holes are formed by the coalescence of vacancies. The holes are formed within the grain and at the grain boundaries. Because of these added complications, the grain boundary pores may become continuous long before the concentration gradient region extends fully through the alloy tube wall, Thus, failure may be accelerated by the combined effects of grain growth and pore formation. However, if rhodium diffuses essentially by a bulk process, grain size would not be of primary importance relative to carbonyl attack.

EVACUATED CONCENTRIC TUBES RESISTOJET CONCEPT

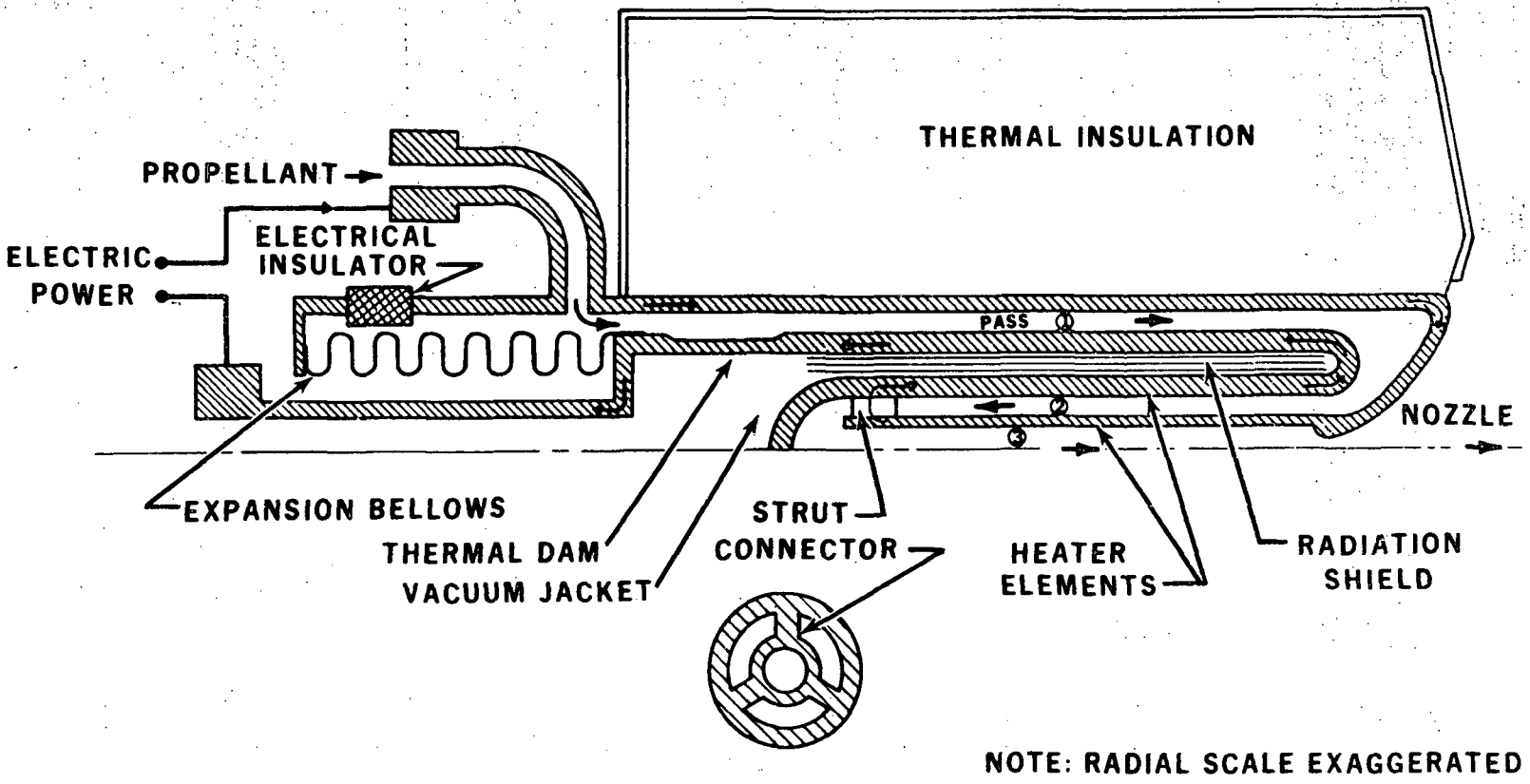

Figure 1

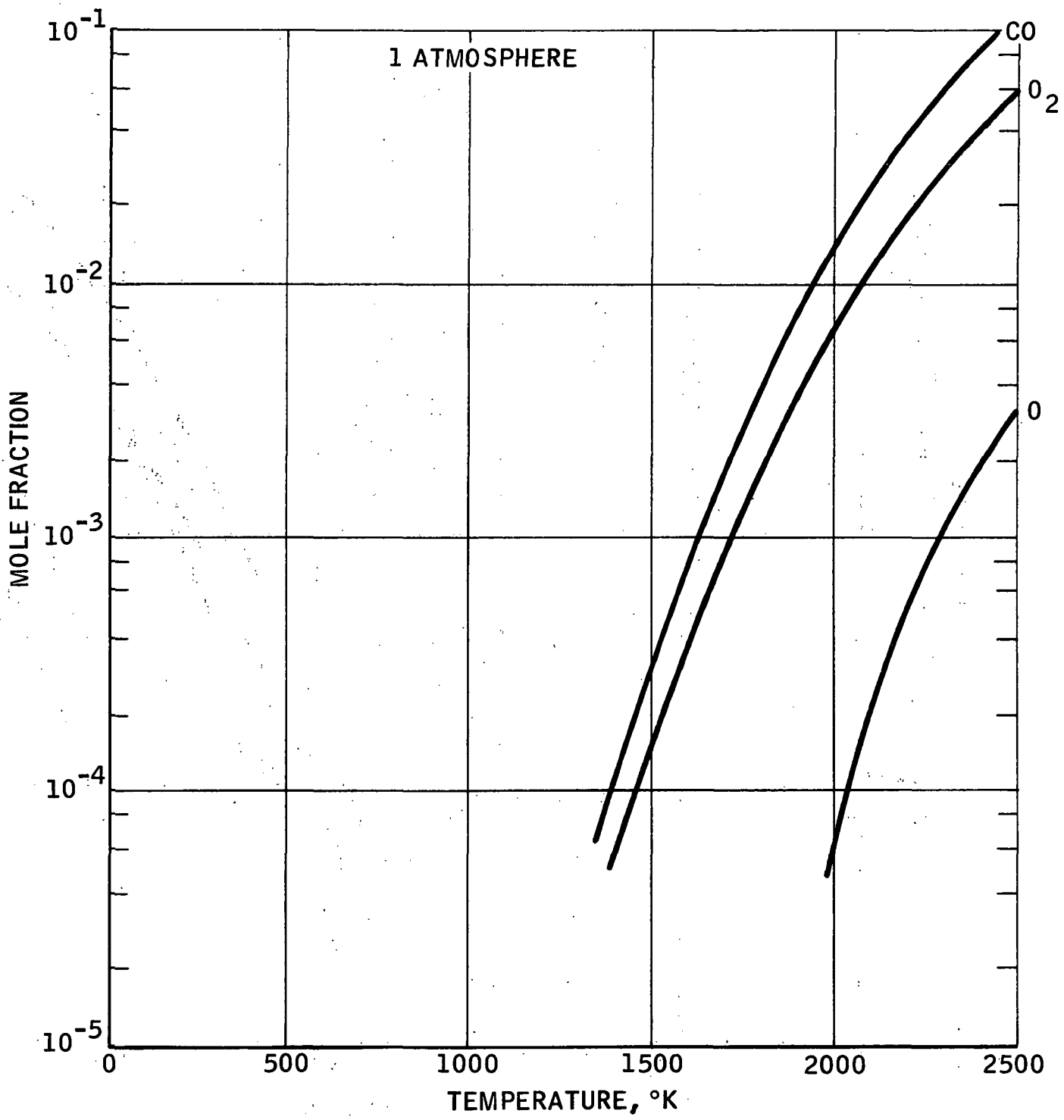
DECOMPOSITION OF CO_2
1 ATMOSPHERE
CO
O_2
O
MOLE FRACTION
10^{-1}
10^{-2}
10^{-3}
10^{-4}
10^{-5}
0
500
1000
1500
2000
2500
TEMPERATURE, °K

Figure 2

DECOMPOSITION OF WATER

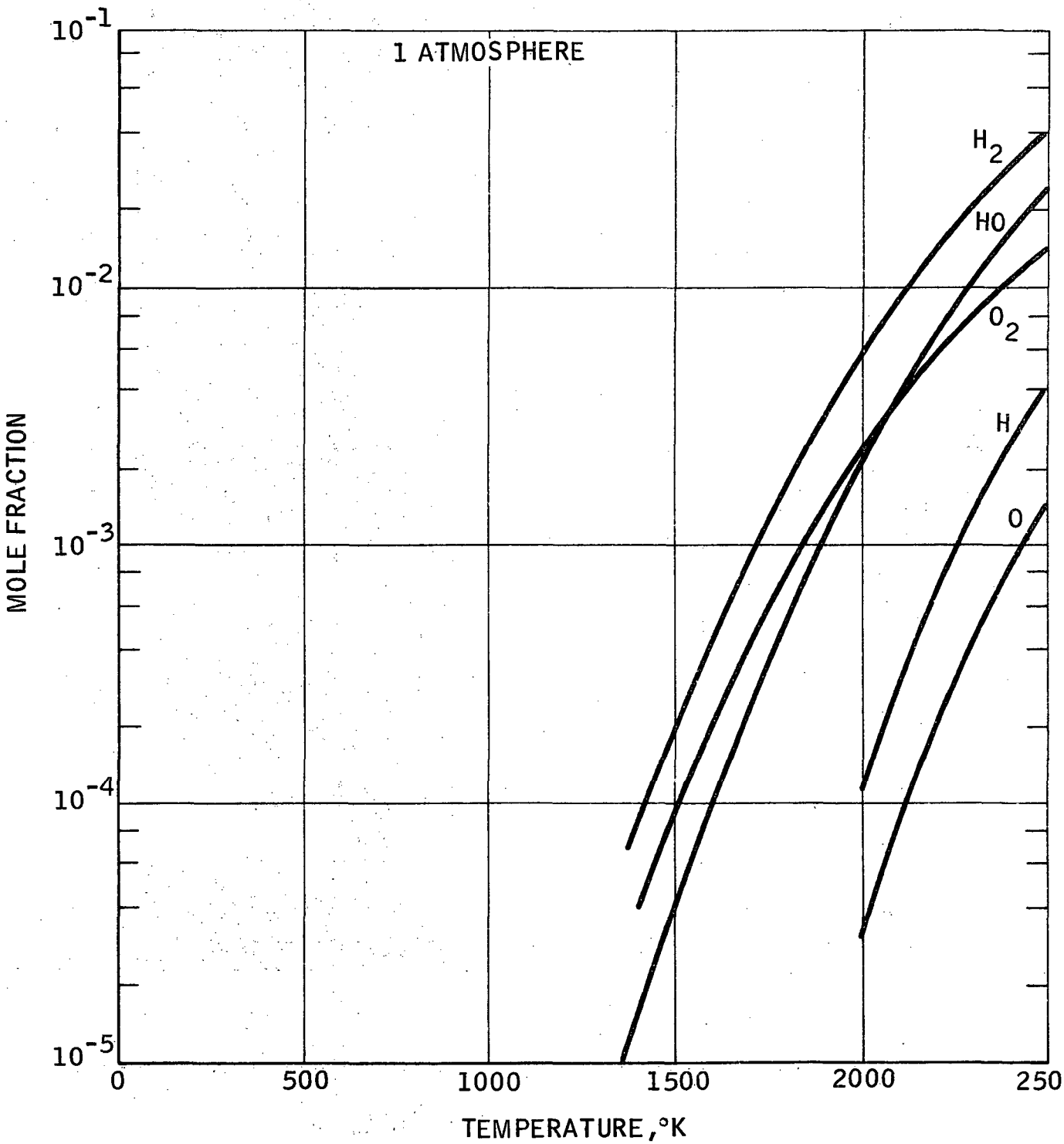

Figure 3

EFFECT OF TEMPERATURE AND PRESSURE ON CO CONCENTRATION

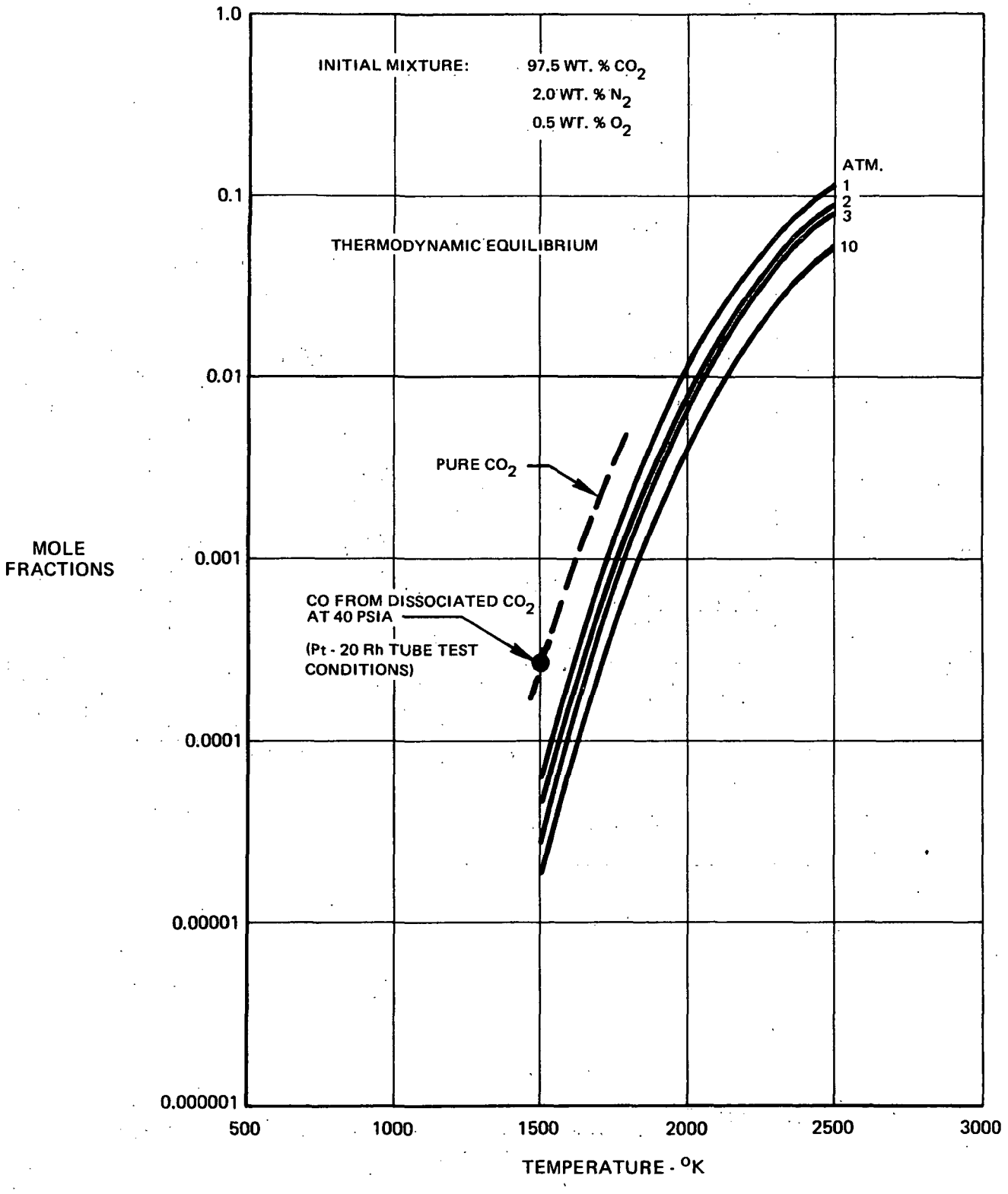

Figure 4

EFFECT OF TEMPERATURE AND PRESSURE ON CO CONCENTRATION

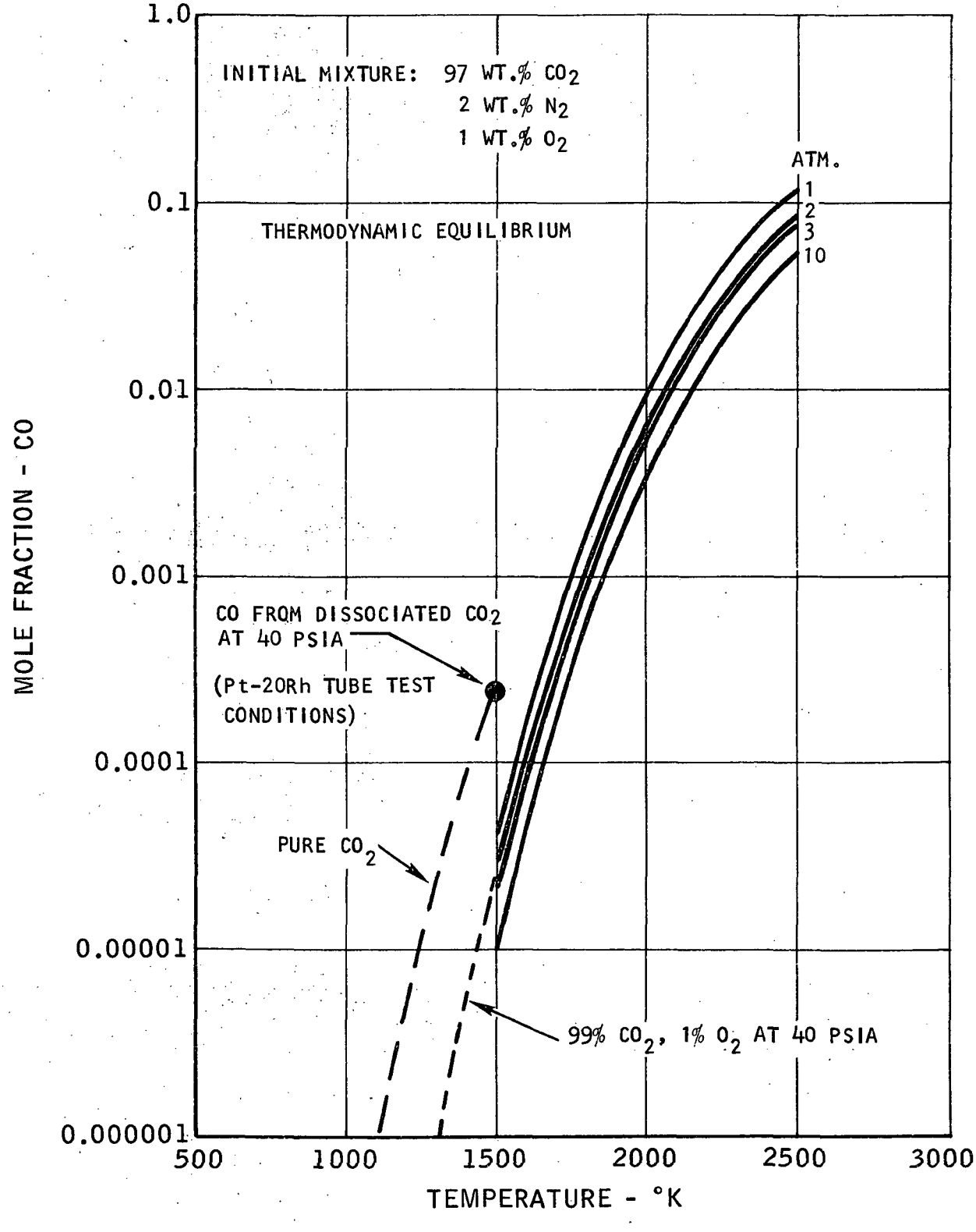

Figure 5

A71-9-089-10

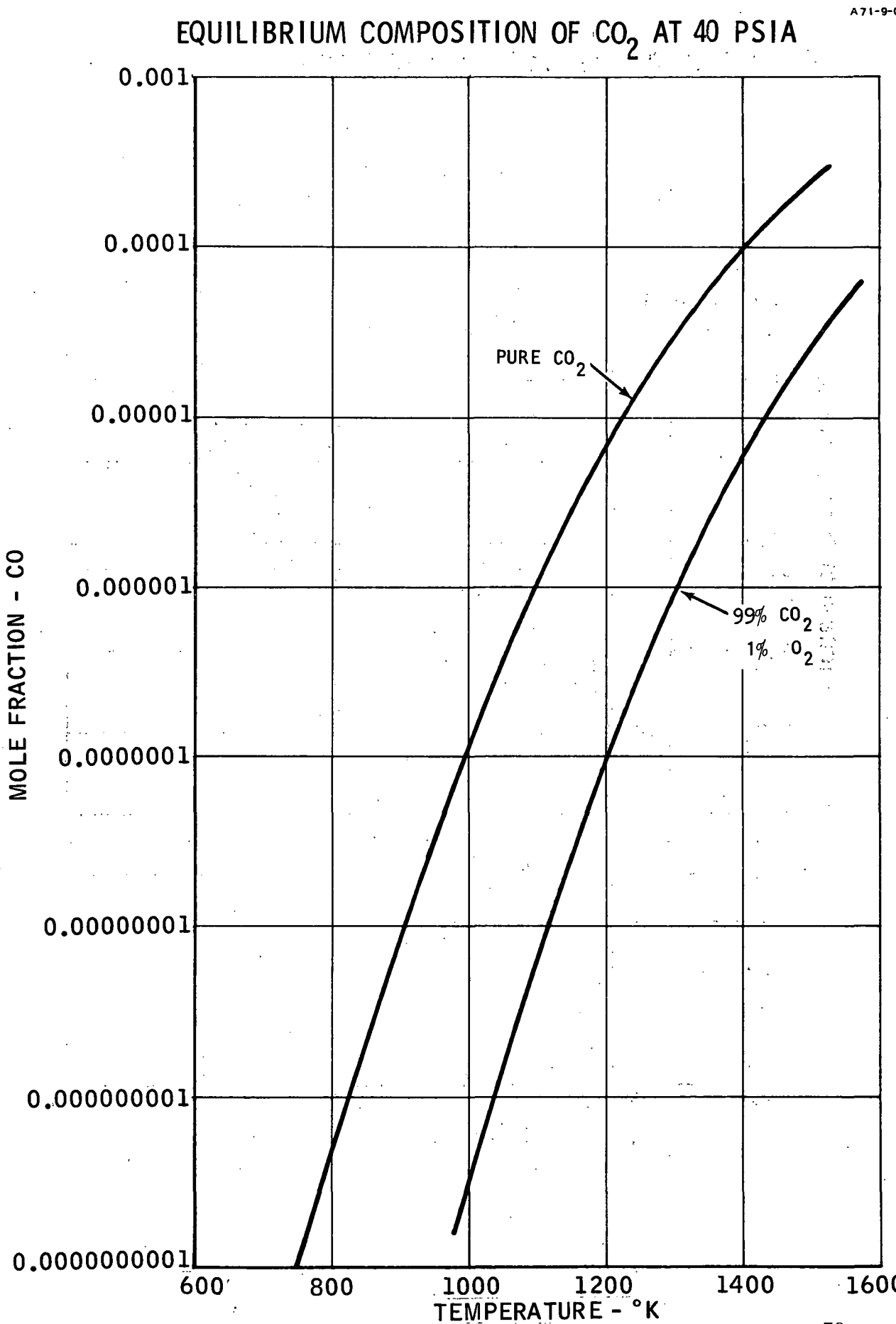

Figure 6

OXIDATION OF PYROLYTIC CARBON BY CARBON DIOXIDE

FROM CARBON, 1966 VOL. 4 pp 539-541 LADD & WALSH

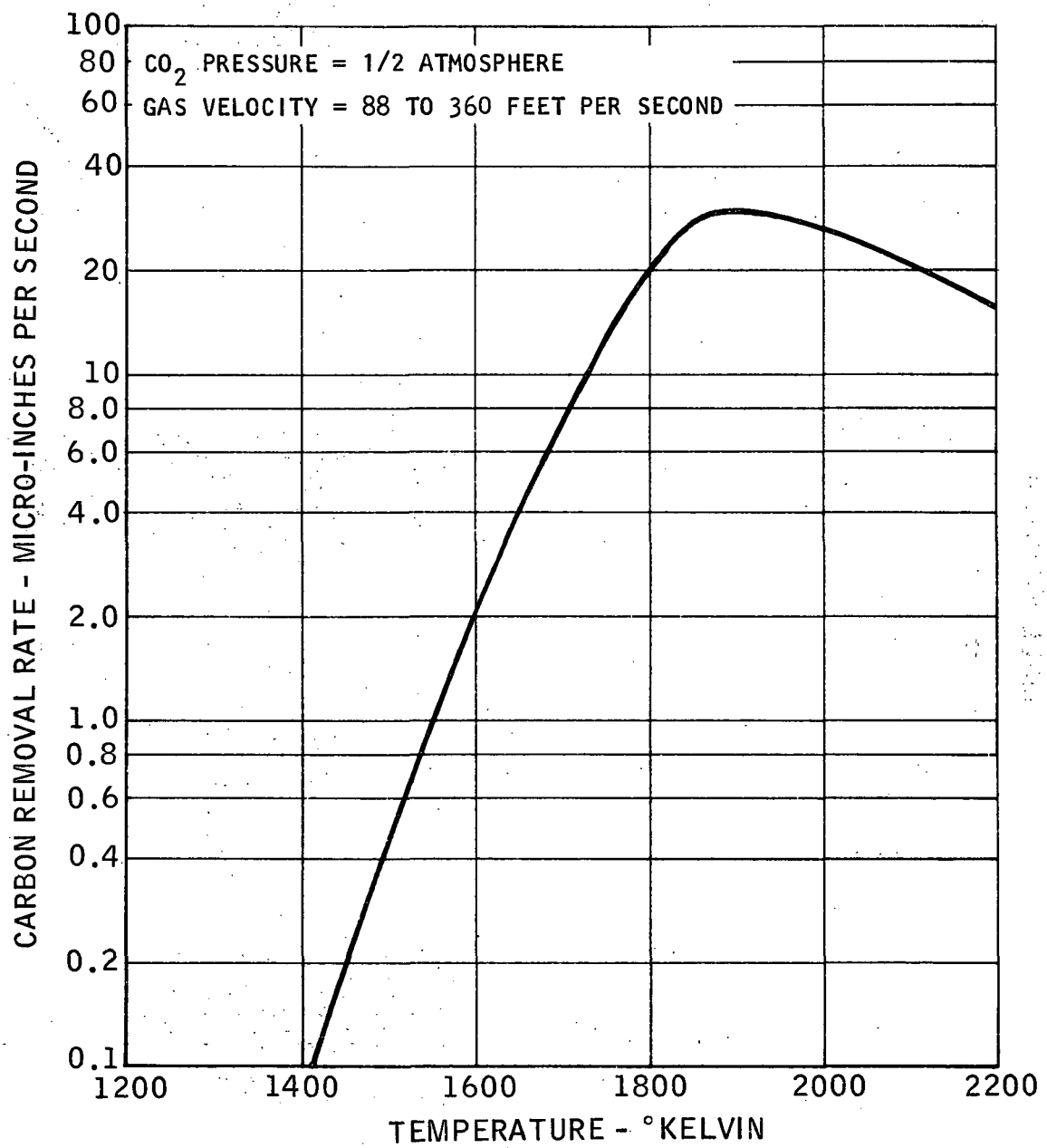

Figure 7

OPERATING TEMPERATURE LIMITS OF VARIOUS OXIDATION RESISTANT MATERIALS

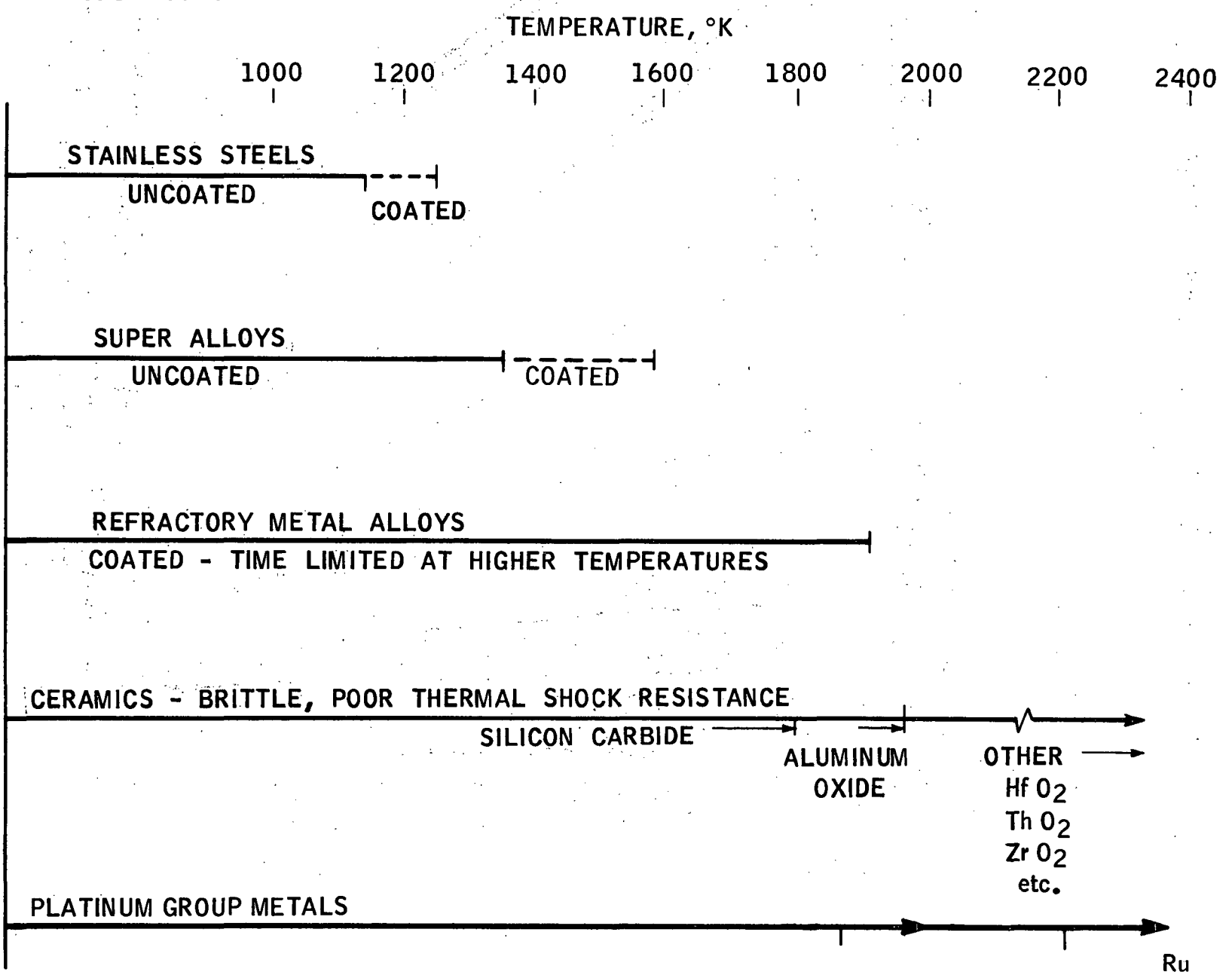

Figure 8

A72-6-276-29

CYCLIC SCALING RESISTANCE OF SOME IRON-CHROMIUM-NICKEL ALLOYS AT 980°C

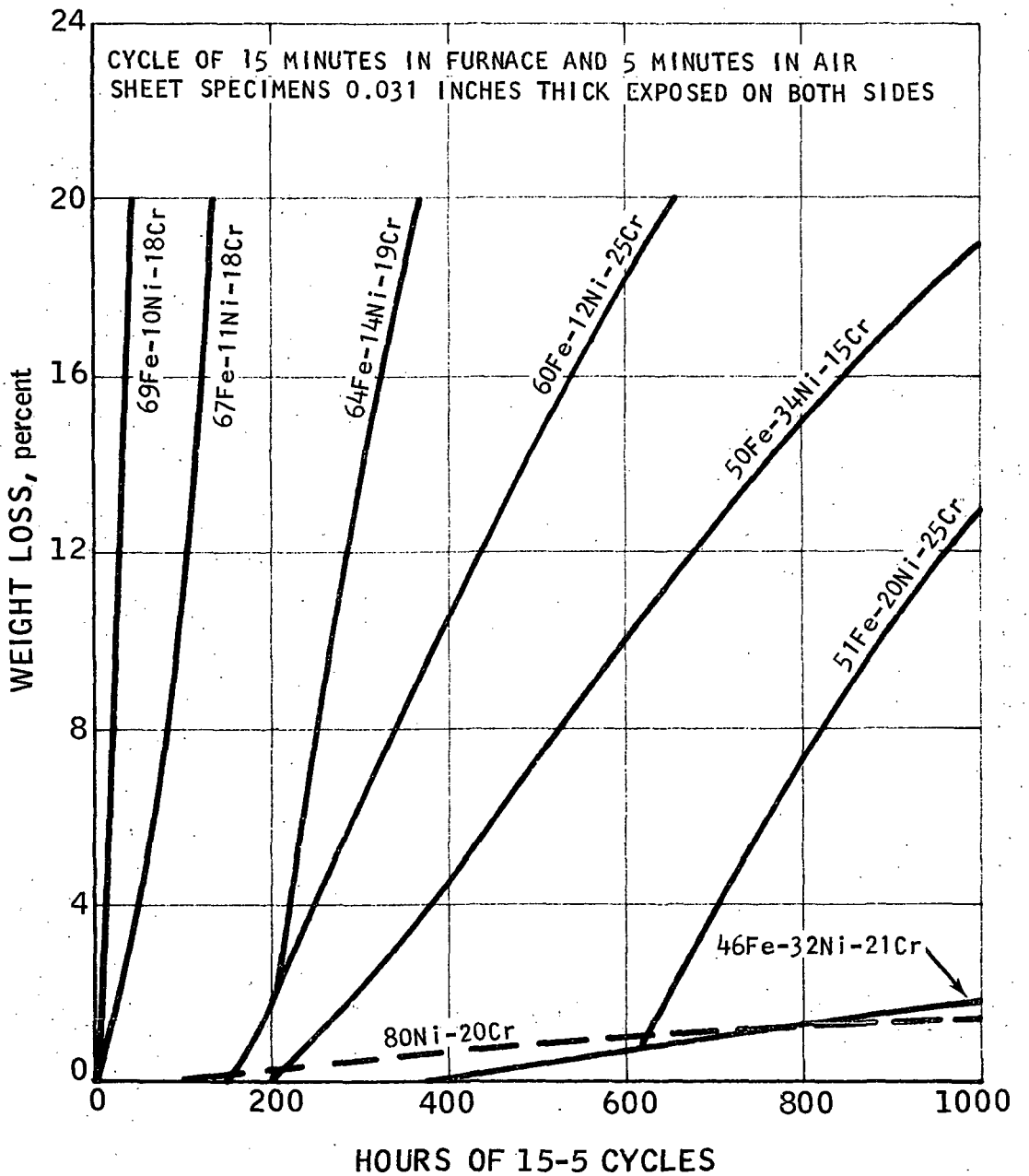

Figure 9

METAL LOSS BY OXIDATION OF NICKEL-CHROMIUM-IRON ALLOYS
AIR CORROSION AT 980°C (1800°F)

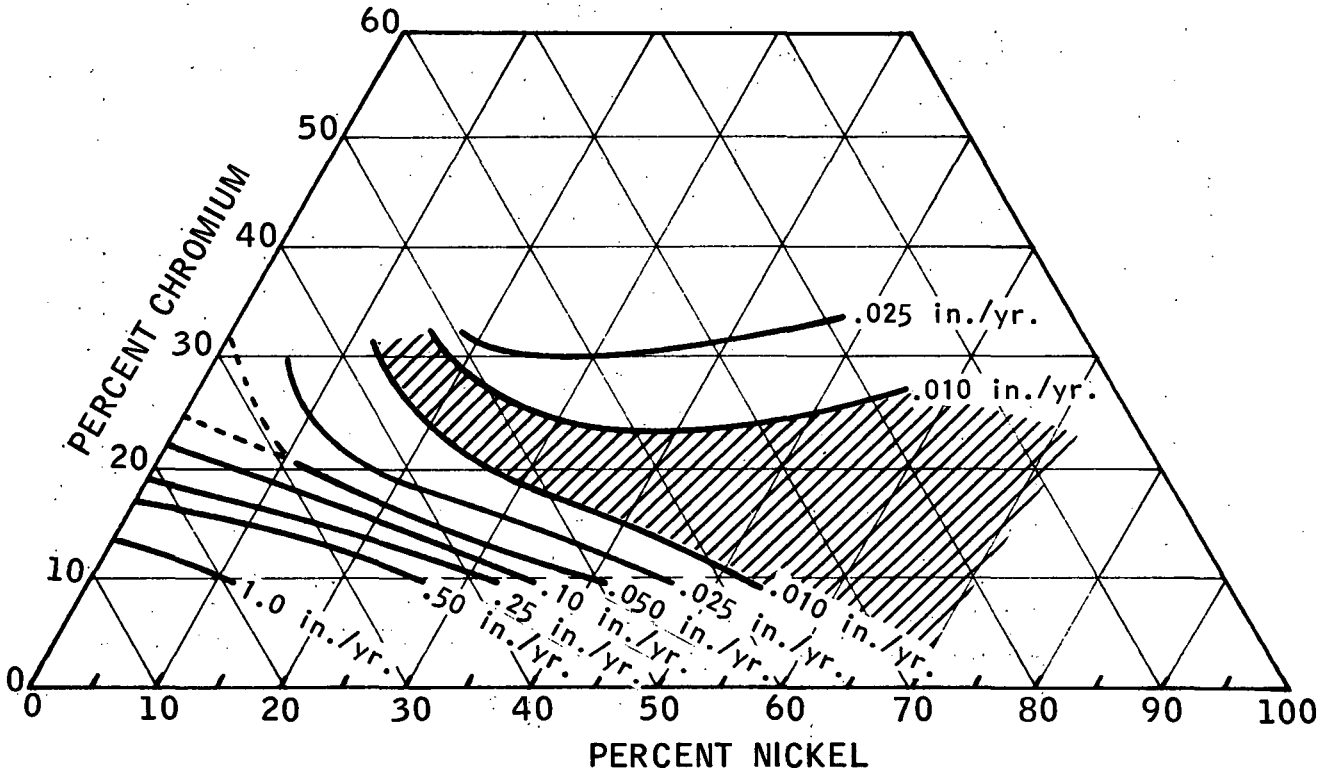

Figure 10

V8093-13

WEIGHT LOSS OF PLATINUM AND SOME PLATINUM ALLOYS HEATED IN AIR, INERT GAS, AND VACUUM

JONES, LANGMUIR, AND MCKAY
× RIDEAL AND WANSBROUGH-JONES
□ KUBASCHEWSKI
● BURGESS AND WALTENBERG
MDD = MILLIGRAMS PER SQUARE DECIMETER PER DAY

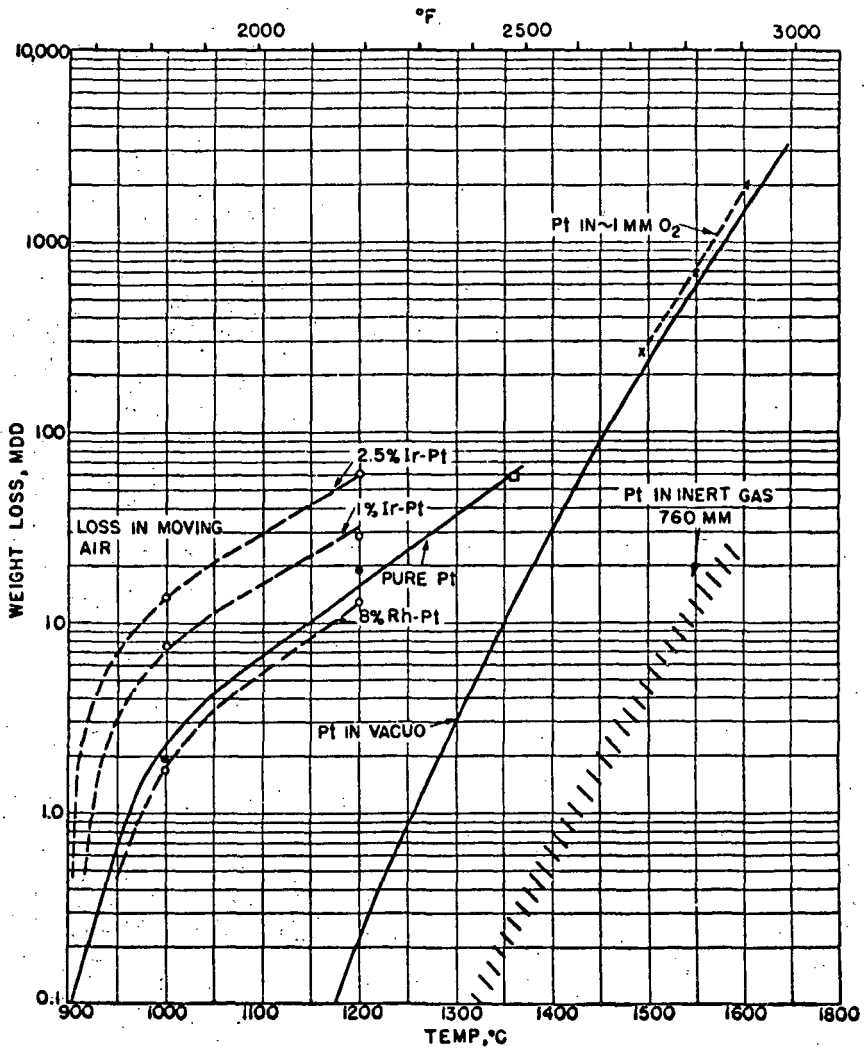

Figure 11

EFFECT OF MOVING AND STILL AIR ON WEIGHT LOSS OF PLATINUM AT VARIOUS TEMPERATURES

MDD = MILLIGRAMS PER SQUARE DECIMETER PER DAY

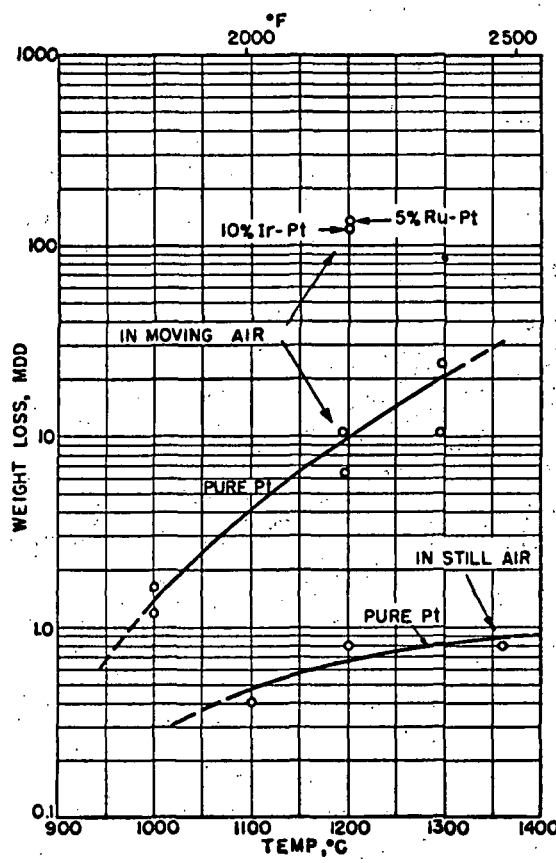

Figure 12

STRENGTH PROPERTIES OF 0.06 IN DIAMETER WIRE AFTER HEATING IN AIR AT 1200° C

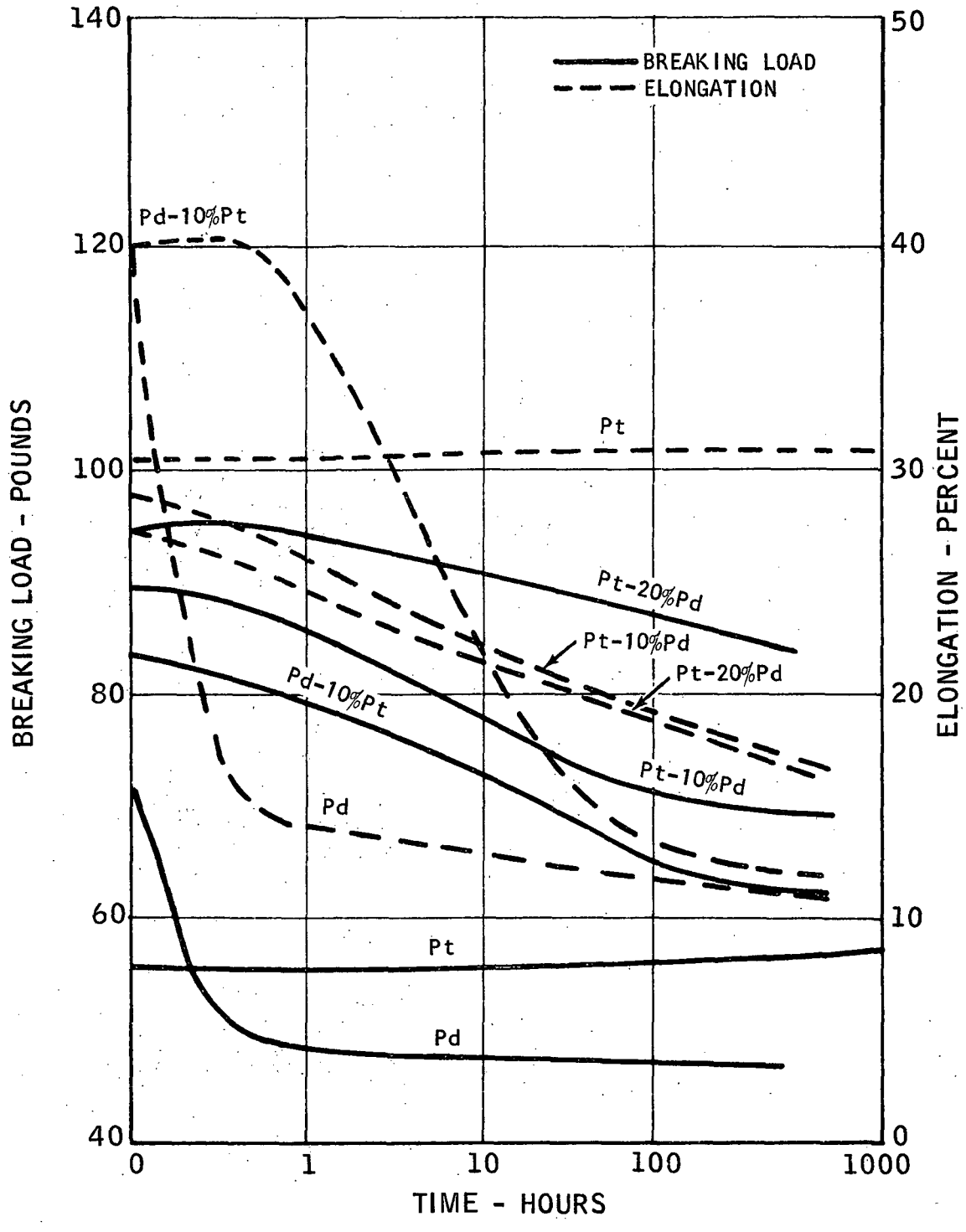

Figure 13

STRESS - RUPTURE CHARACTERISTICS FOR PLATINUM - 0.6% THORIA AND PLATINUM - RHODIUM ALLOYS AT 1723°K IN AIR (3100°R)

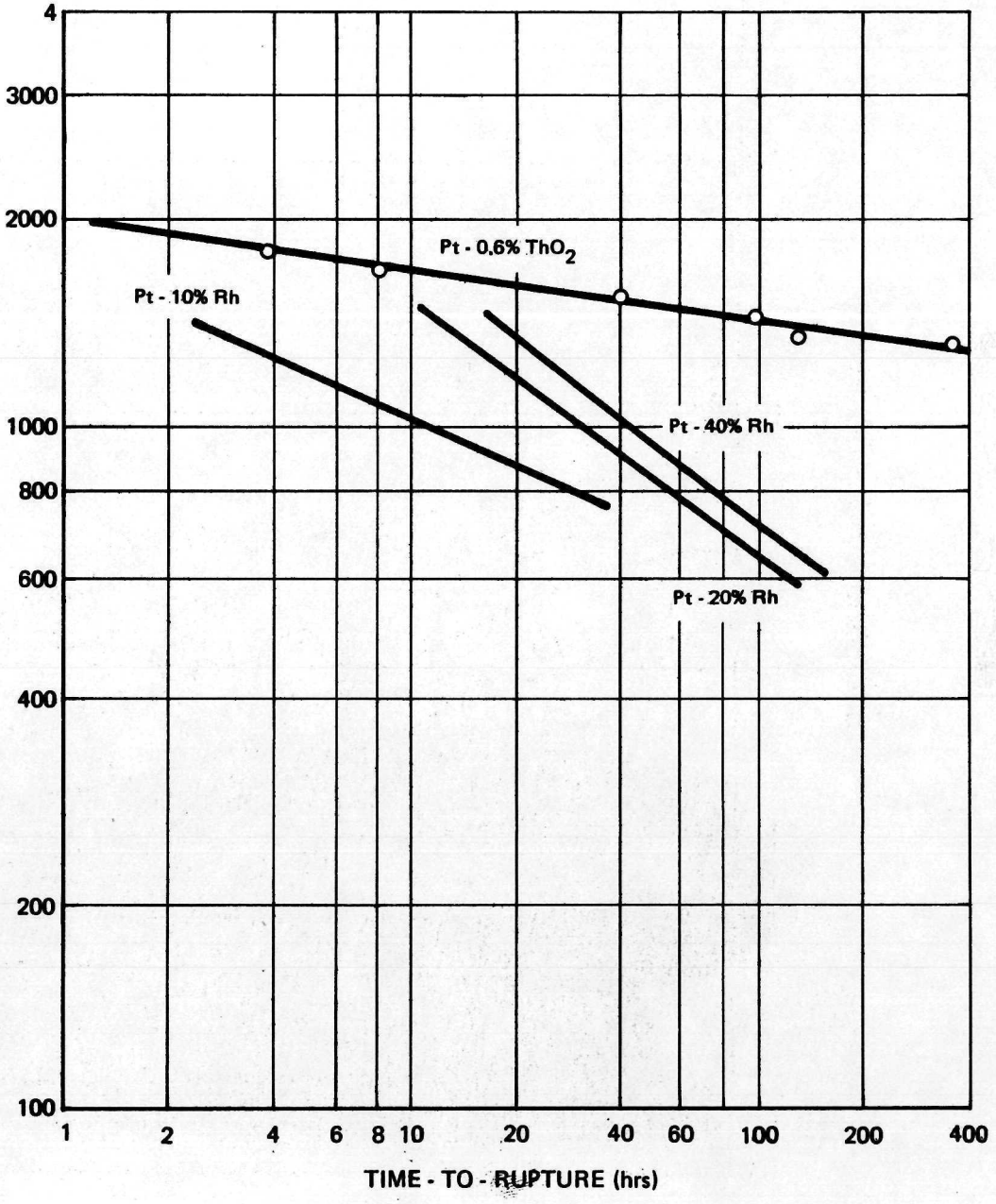

Figure 14

BIOWASTE RESISTOJET MATERIALS EXPERIMENT

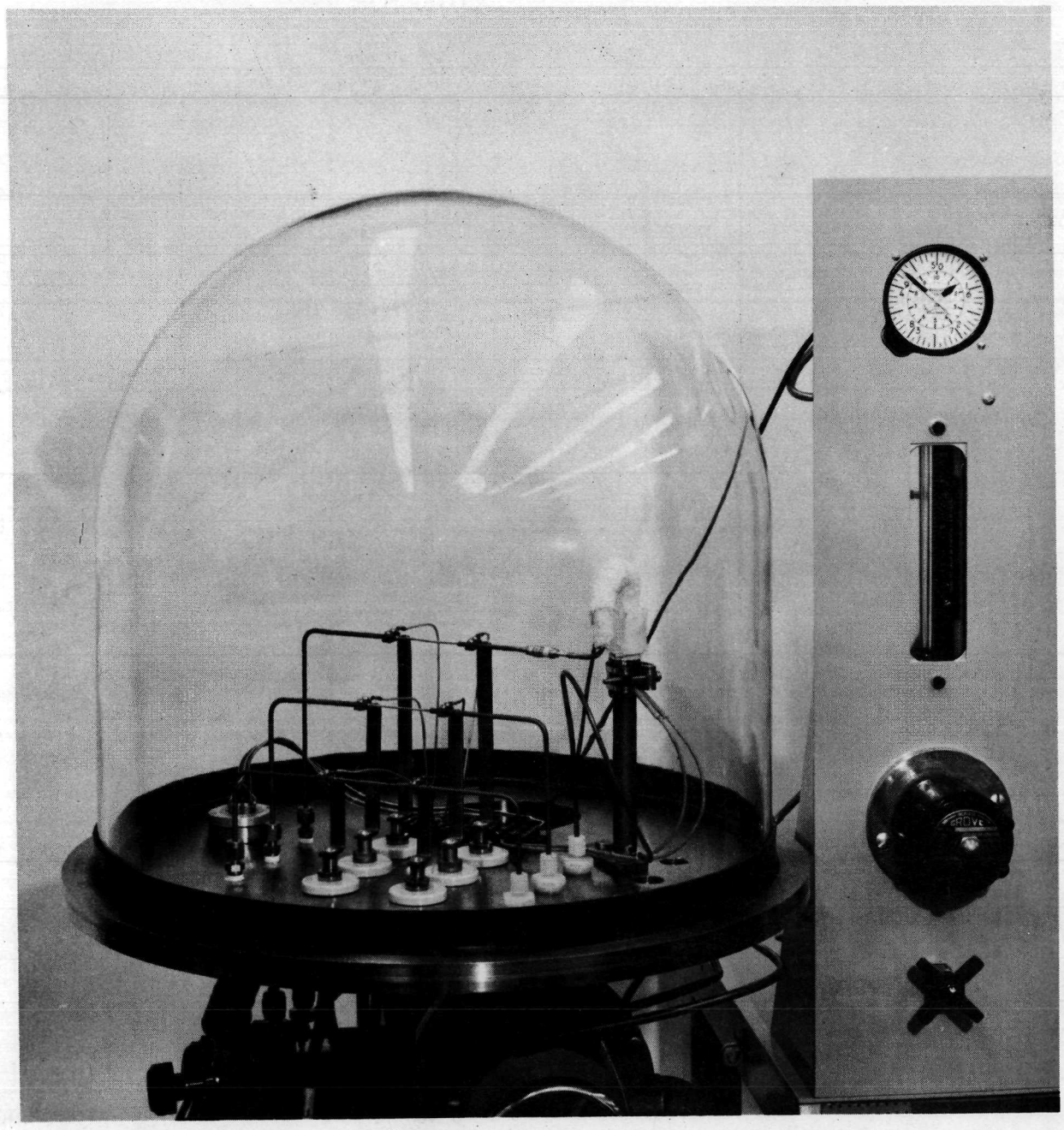

Figure 15

Neg. 9708-1
M-10,037

BIOWASTE RESISTOJET MATERIALS EXPERIMENT

M10,045
Neg. 9713-1

Figure 16

RESISTOJET HEATER TUBE TEST FACILITY

Figure 17

NEG. 9950-4

V8444-

RESISTOJET HEATER TUBE TEST FACILITY

Figure 18

NEG. 9950-3

91

V8444-3

LEFT BELL JAR SETUP
RESISTOJET HEATER TUBE TEST FACILITY

Figure 19

NEG. 9950-1

V8444-1

RIGHT BELL JAR SETUP
RESISTOJET HEATER TUBE TEST FACILITY

NEG. 9950-2

Figure 20

V8444-2

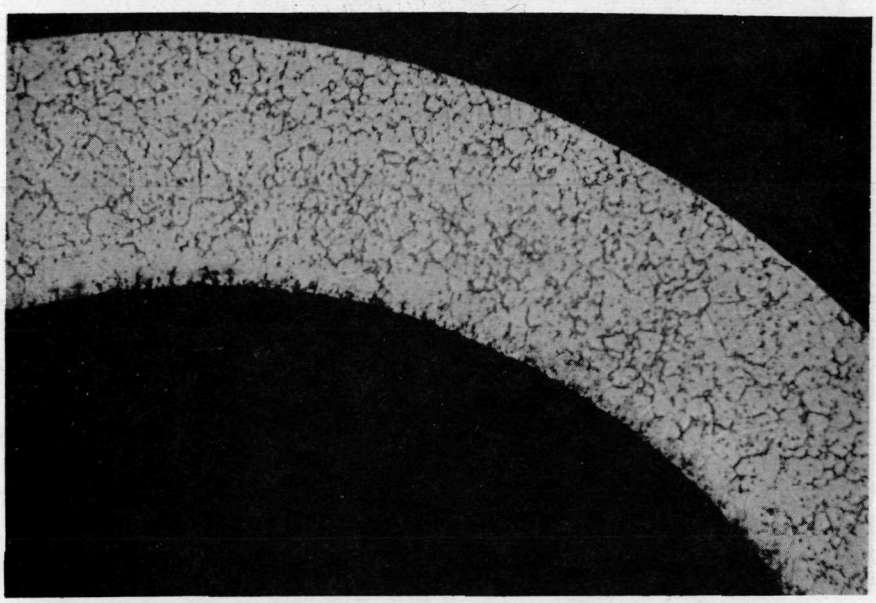

CROSS SECTION OF HASTELLOY X TUBE AS RECEIVED
(200X)

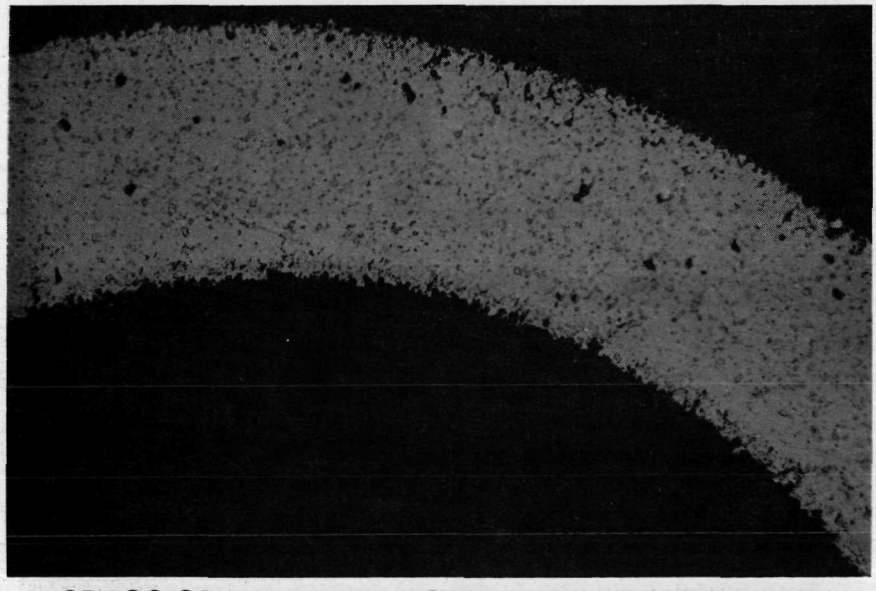

CROSS SECTION OF HASTELLOY X TUBE AFTER
INTERNAL EXPOSURE TO CO_2 AT HIGH TEMPERATURE
(200X)

Figure 21

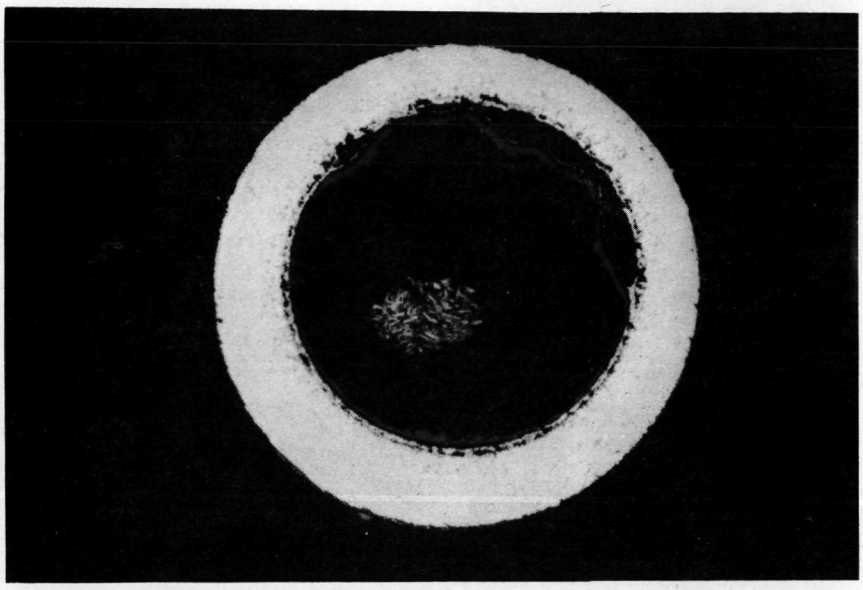

CROSS SECTION OF HASTELLOY X TUBE AFTER INTERNAL EXPOSURE TO CH_4 AT HIGH TEMPERATURE

(50X)

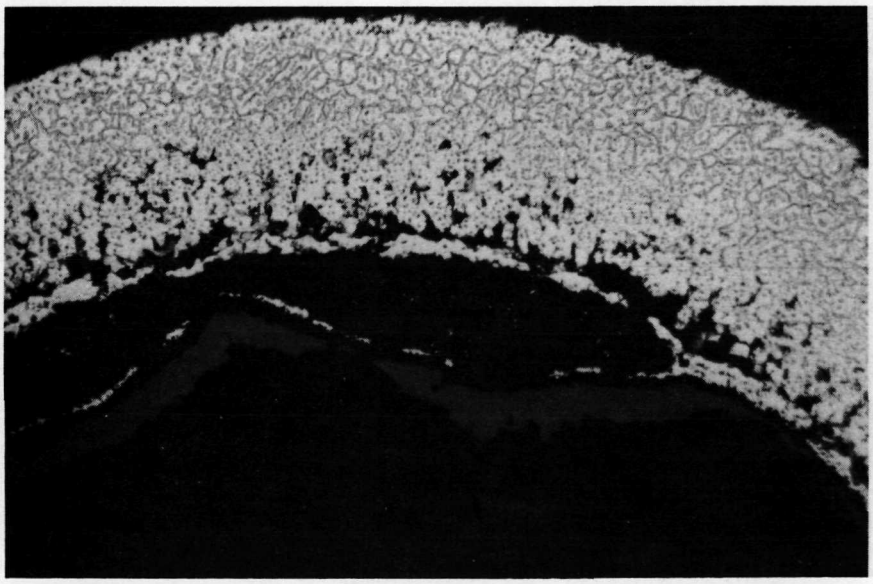

ENLARGED PORTION OF ABOVE CROSS SECTION

(200X)

Figure 22

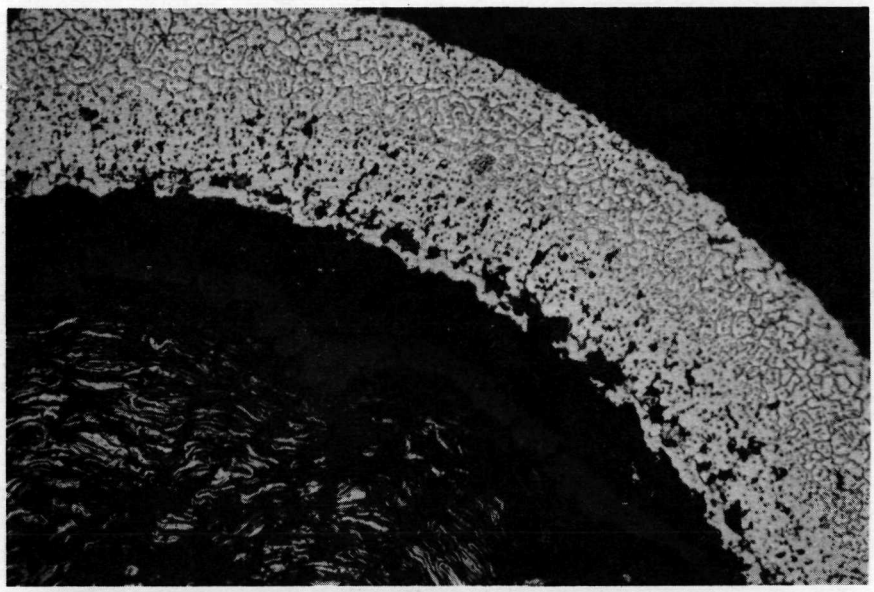

CROSS SECTION OF HASTELLOY X TUBE AFTER
INTERNAL EXPOSURE TO CH_4 AT HIGH TEMPERATURE
(SECTION 0.030 INCHES DEEPER THAN PREVIOUS SECTION)
(200X)

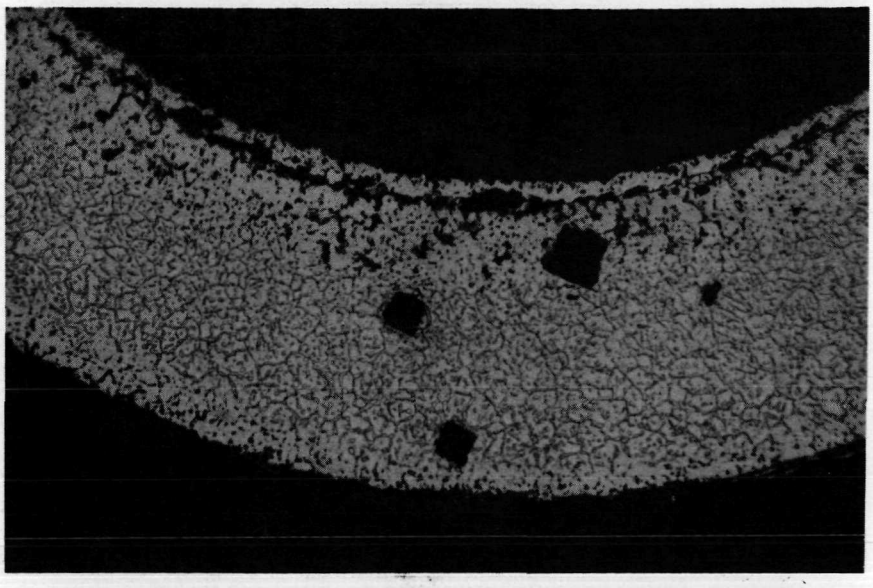

DIAMETRICALLY OPPOSITE SECTION SHOWING
MICROHARDNESS TESTER MARKS
(200X)

Figure 23

CROSS-SECTIONS OF HASTELLOY X TUBES EXPOSED TO CO_2/CH_4 MIXTURE FOR 250 HOURS

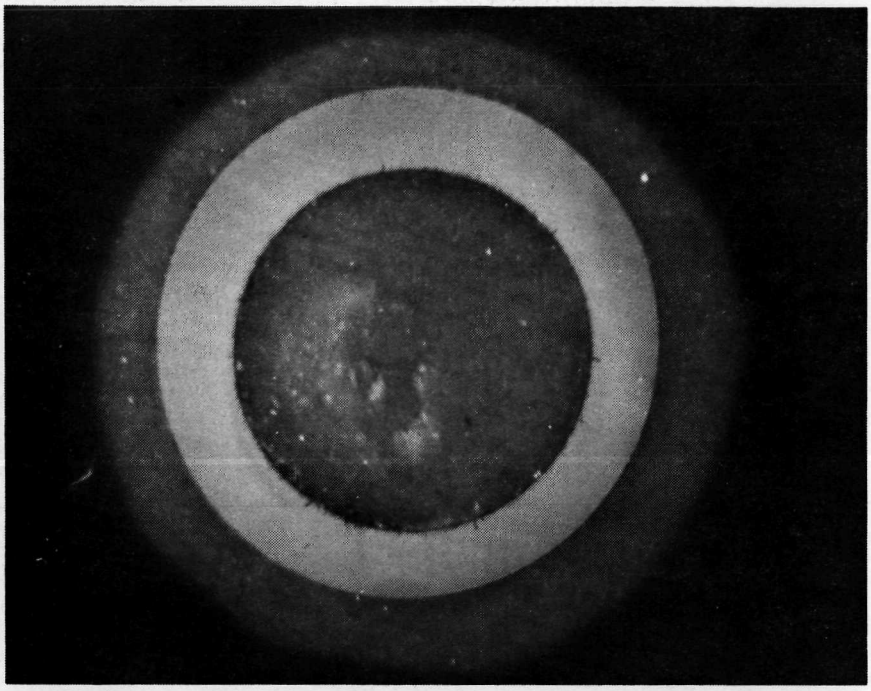

NEG. 9808-3

1660 °R POLARIZED LIGHT 50 X

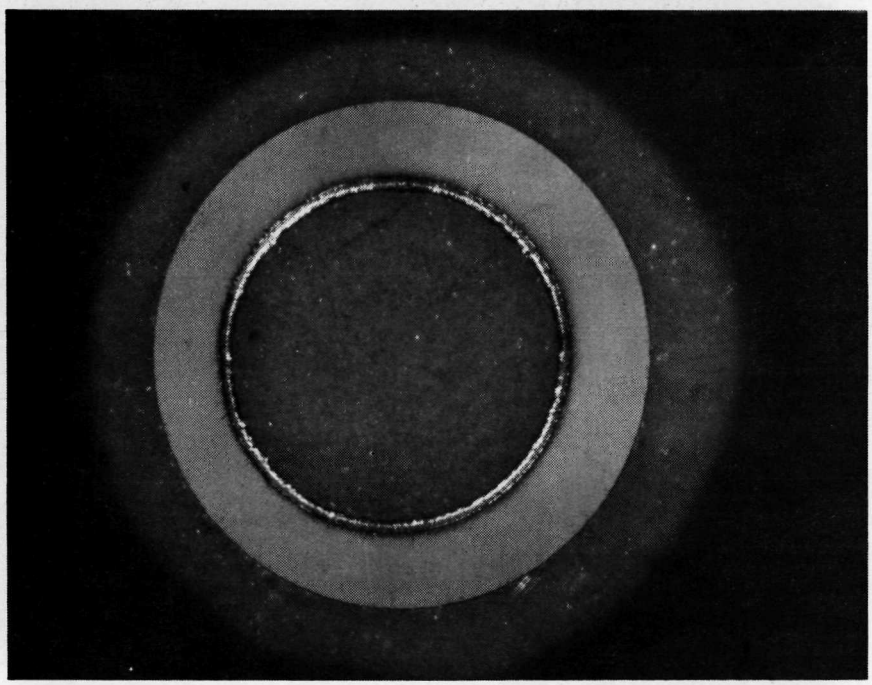

NEG. 9808-4

2060 °R POLARIZED LIGHT 50 X

Figure 24

CROSS-SECTIONS OF HASTELLOY X TUBES EXPOSED TO CO_2/CH_4 MIXTURE FOR 250 HOURS

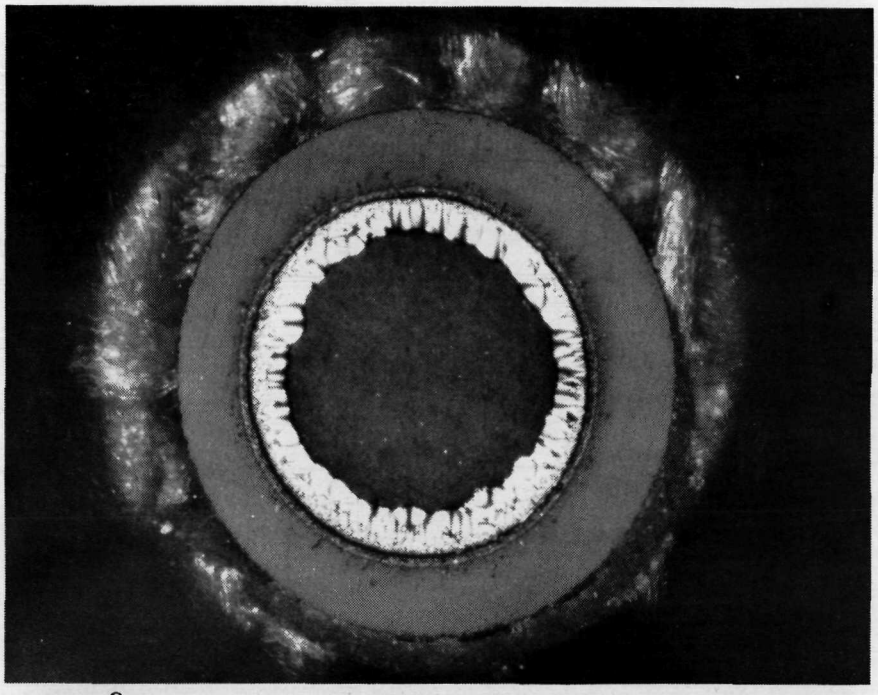

NEG. 9808-1

2260 °R POLARIZED LIGHT 50 X

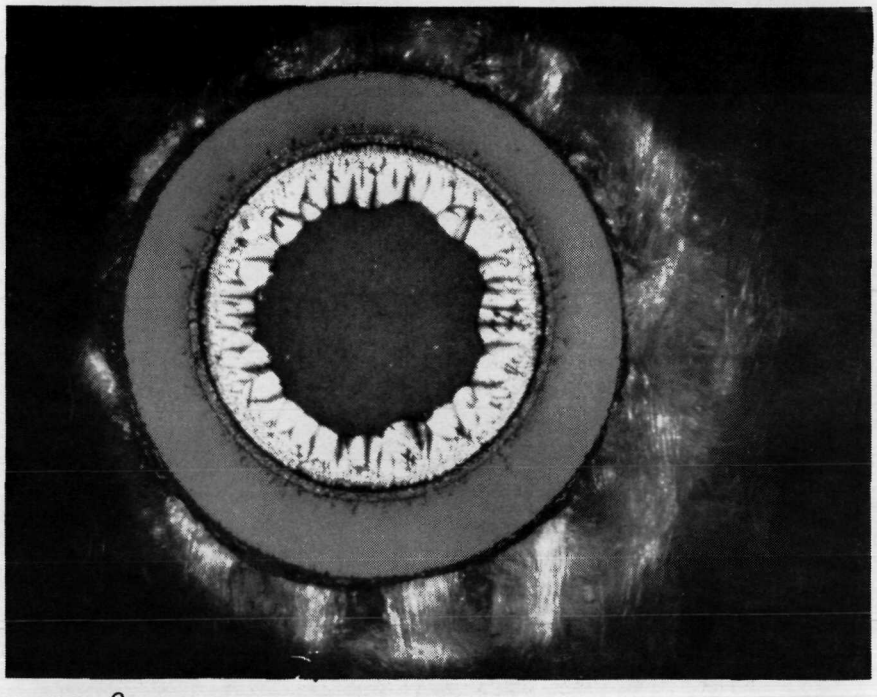

NEG. 9808-2

2380 °R POLARIZED LIGHT 50 X

Figure 25

CARBON DEPOSITION RATE
BIOWASTE RESISTOJET MATERIAL SAMPLE TESTS

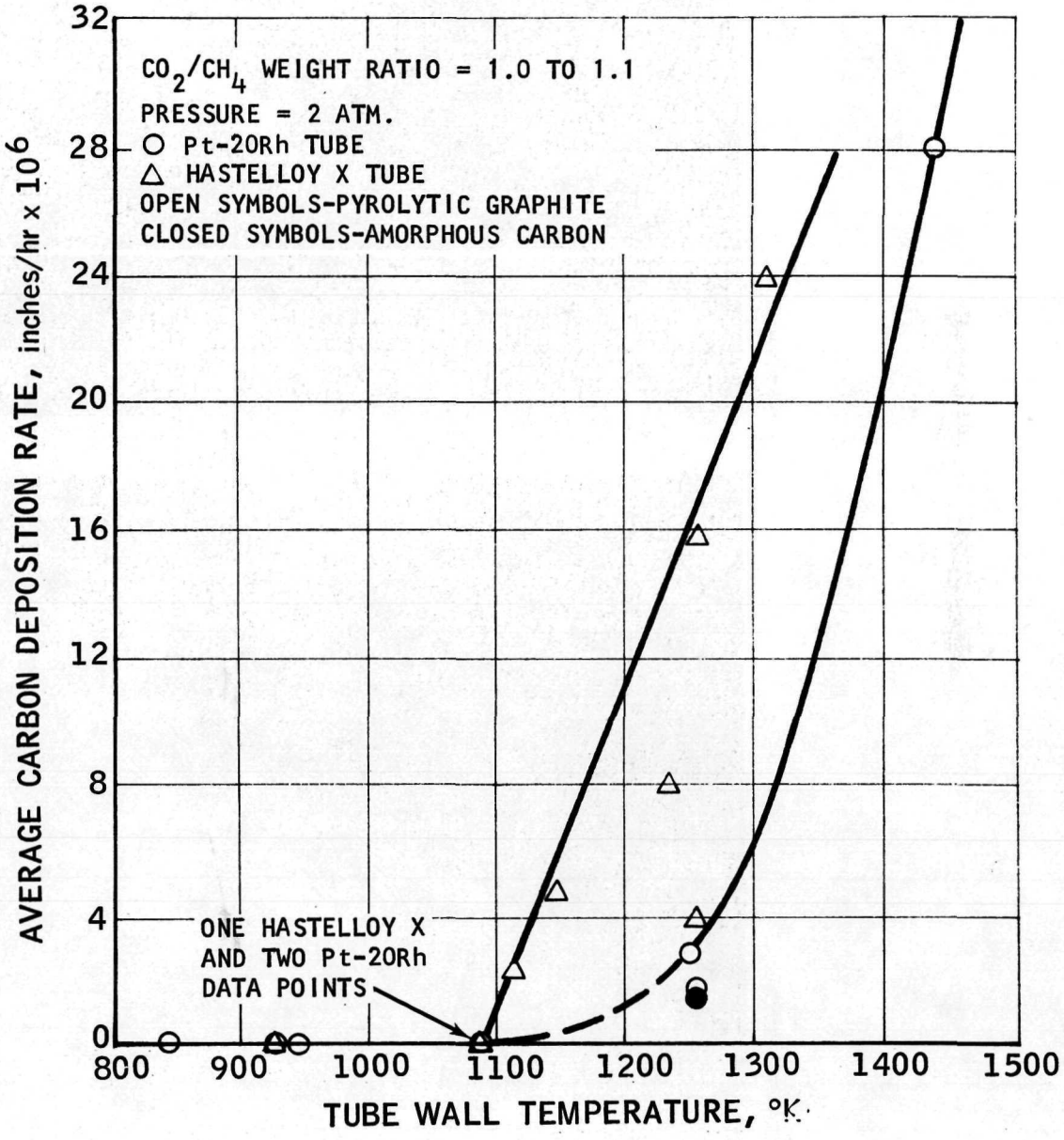

Figure 26

CARBON FORMATION
TEST L6-3E

POLARIZED LIGHT - 500X

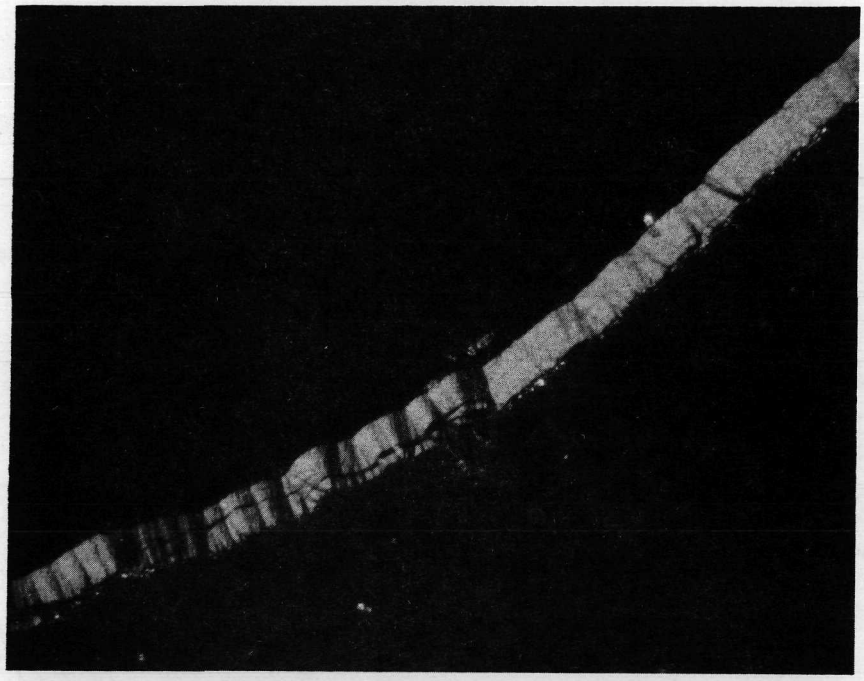

NEG. 9994-6

BRIGHT FIELD - 500X

NEG. 9994-5

Figure 27

CARBON FORMATION
BRIGHT FIELD - 500X

TEST L4-3B

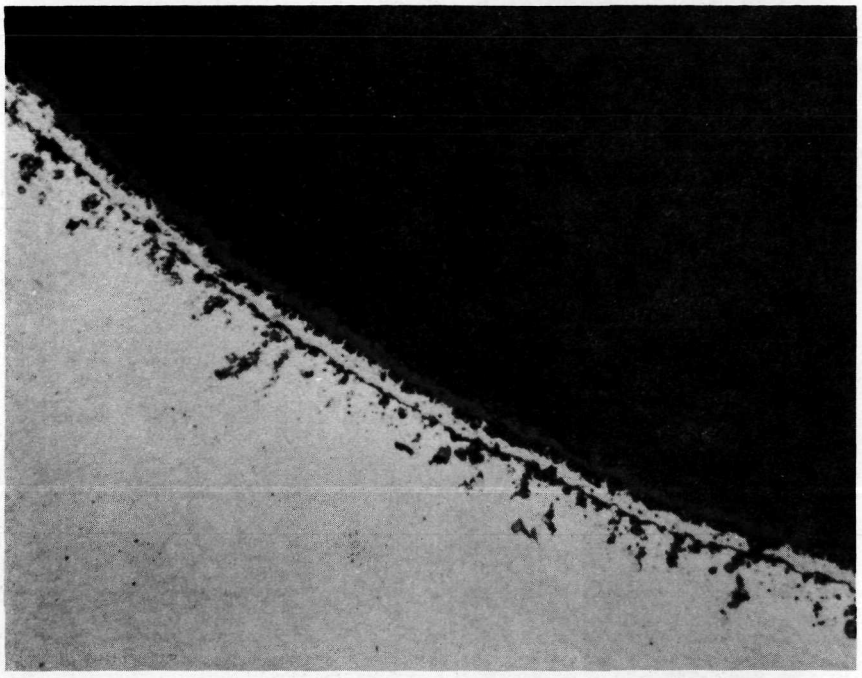

NEG. 9994-3

TEST L4-1B

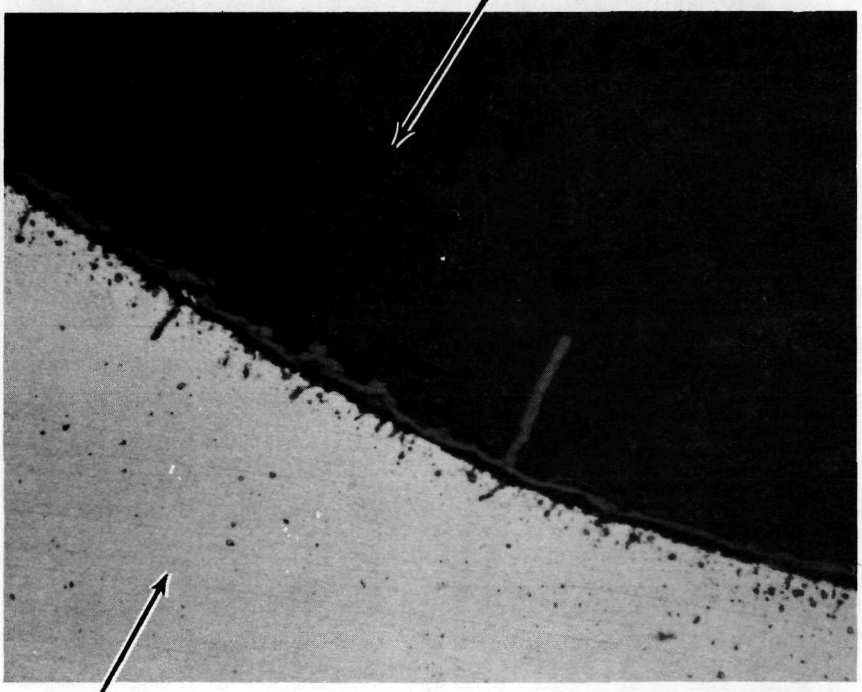

NEG. 9994-2

Figure 28

CARBON FORMATION WITH FINE FIBERS

BRIGHT FIELD - 500X

TEST L5-2C

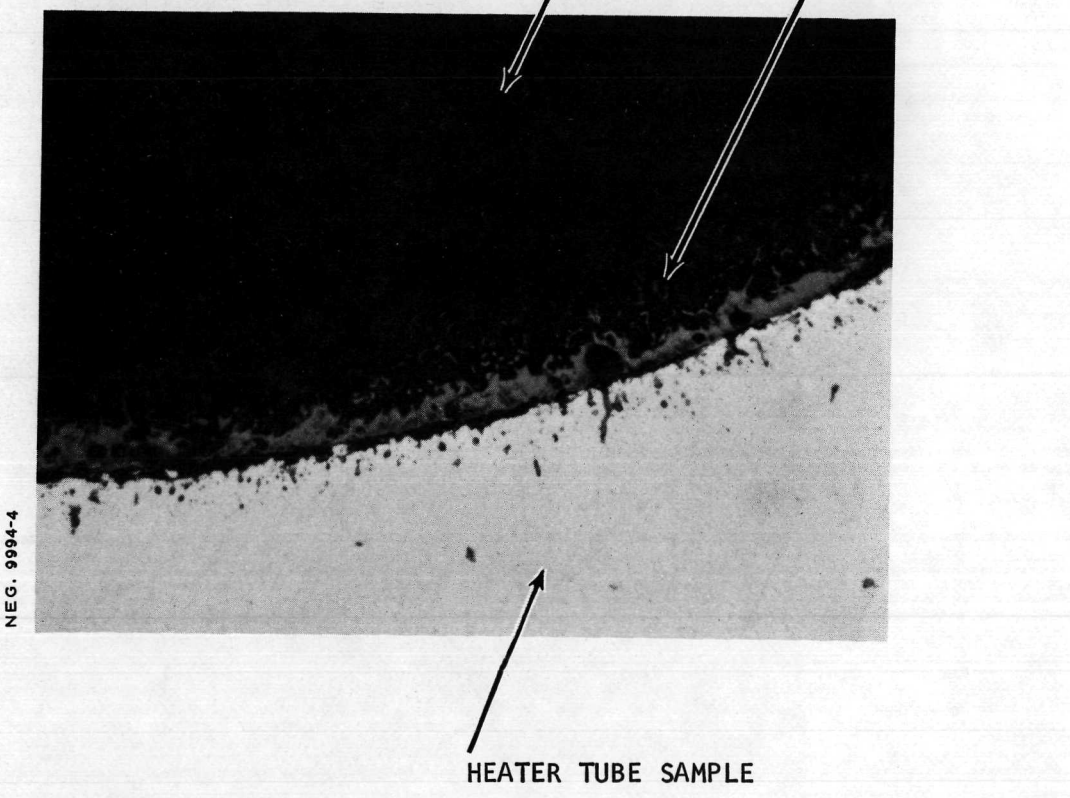

Figure 29

CARBON FORMATION WITH DELAMINATION

POLARIZED LIGHT - 50X

TEST X-3

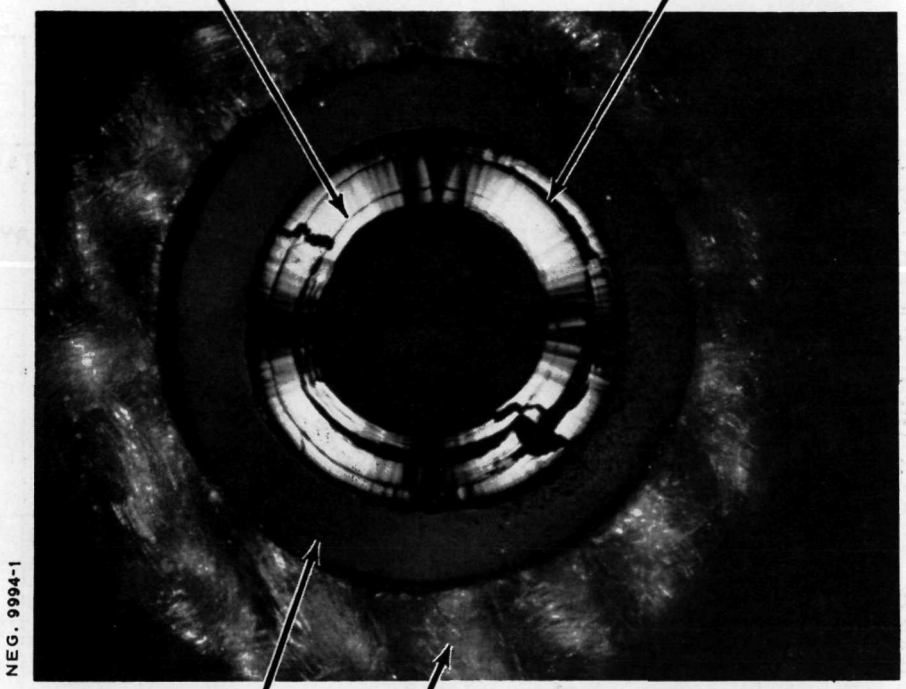

Figure 30

CARBON DEPOSITION RATE

PROPELLANT - CH_4
PRESSURE - 2 ATM.
MASS FLOW RATE - 0.005 GRAMS/SECOND
HEATER TUBE MATERIAL - HASTELLOY X
TEST NO. L4
EXPOSURE TIME 92 TO 122 HOURS

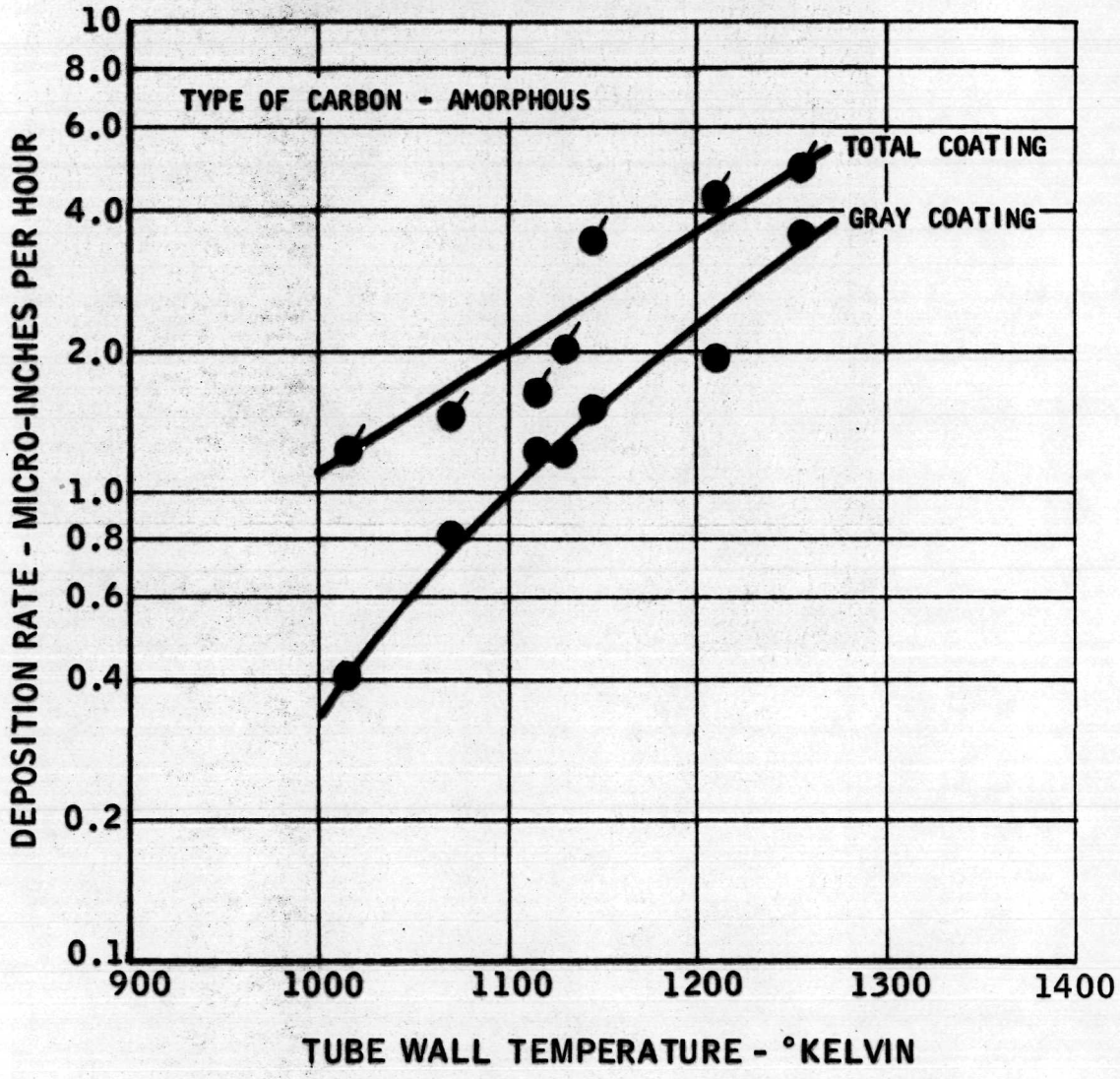

Figure 31

CARBON DEPOSITION RATE

PROPELLANT - CO_2+CH_4
PRESSURE - 2 ATM.
MASS FLOW RATE - 0.006 GRAMS/SECOND
HEATER TUBE MATERIAL- HASTELLOY X

SYMBOL	TEST	EXPOSURE TIME, hrs.
△	L1	113.5
◇	L3	125

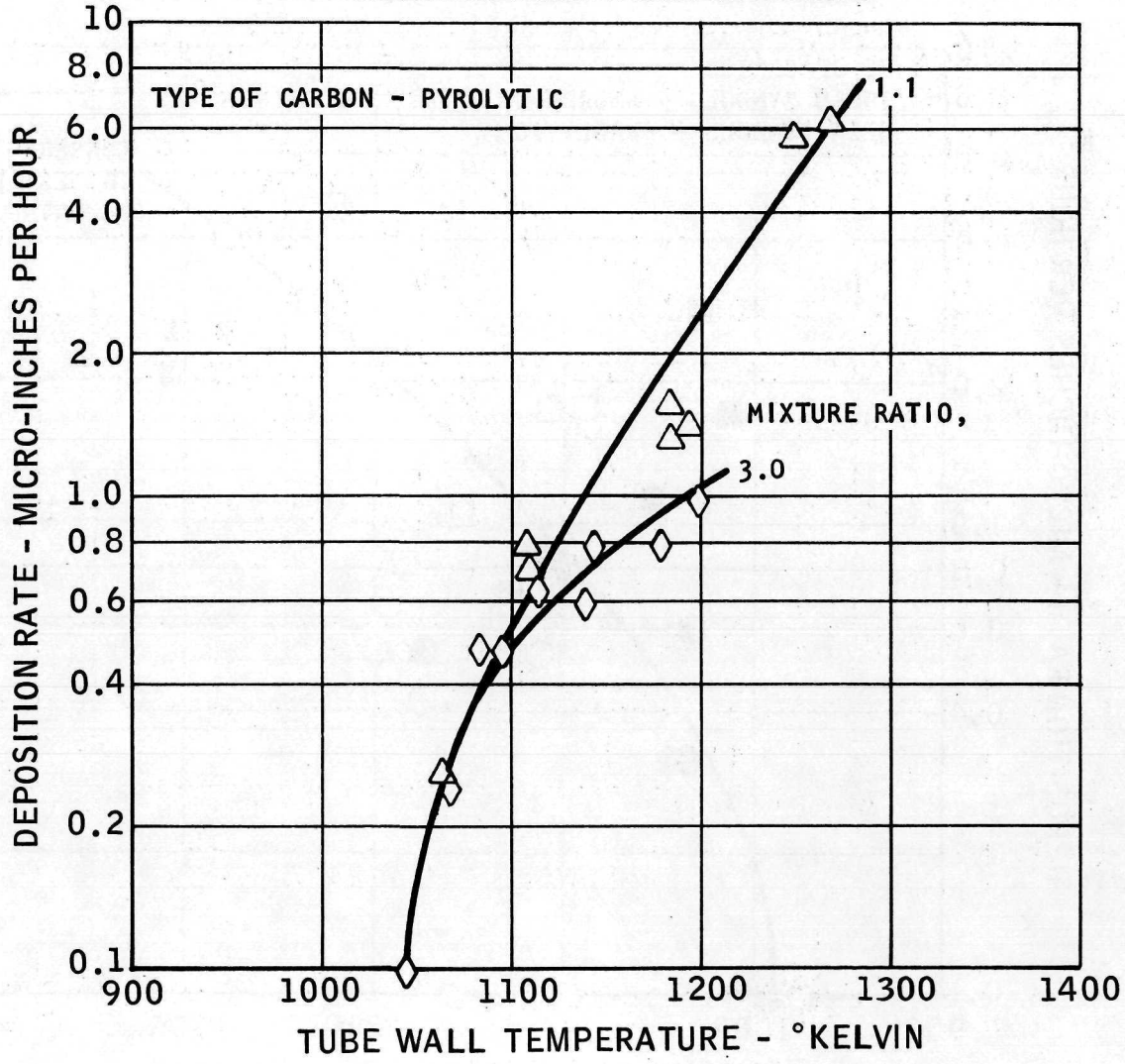

Figure 32

CARBON DEPOSITION RATE

PROPELLANT - CO_2+CH_4 MIXTURE RATIO $CO_2/CH_4 = 2$
PRESSURE - 2 ATM.
MASS FLOW RATE - 0.006 GRAMS/SECOND

SYMBOL	TEST	HEATER TUBE MATERIAL	EXPOSURE TIME, hrs.
□	L2	HAST. X	97.2
◨	L5	HAST. X	140.5
⬡	L6	Pt-30 Ir	185

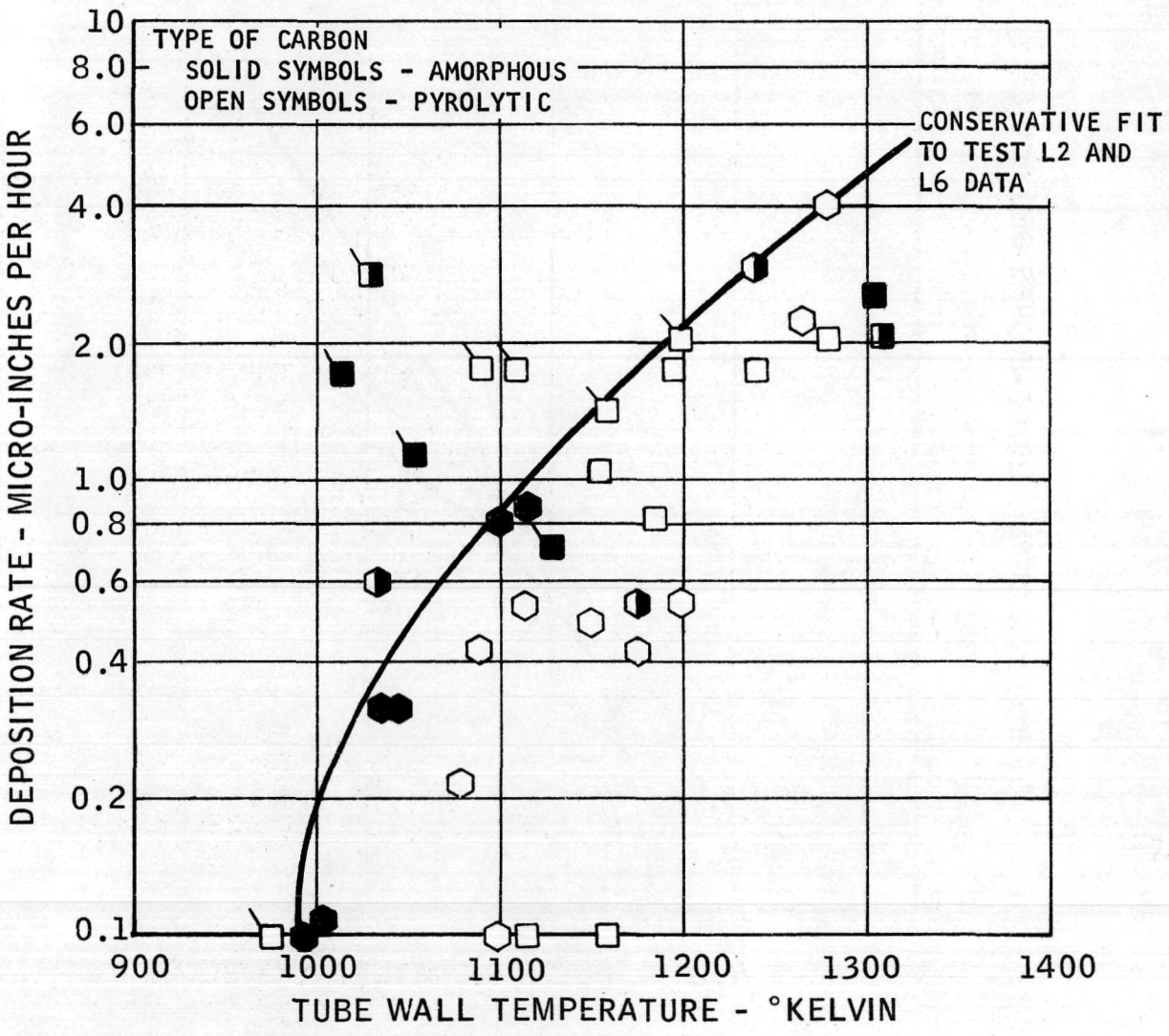

Figure 33

CORRELATION OF MARQUARDT CARBON DEPOSITION DATA

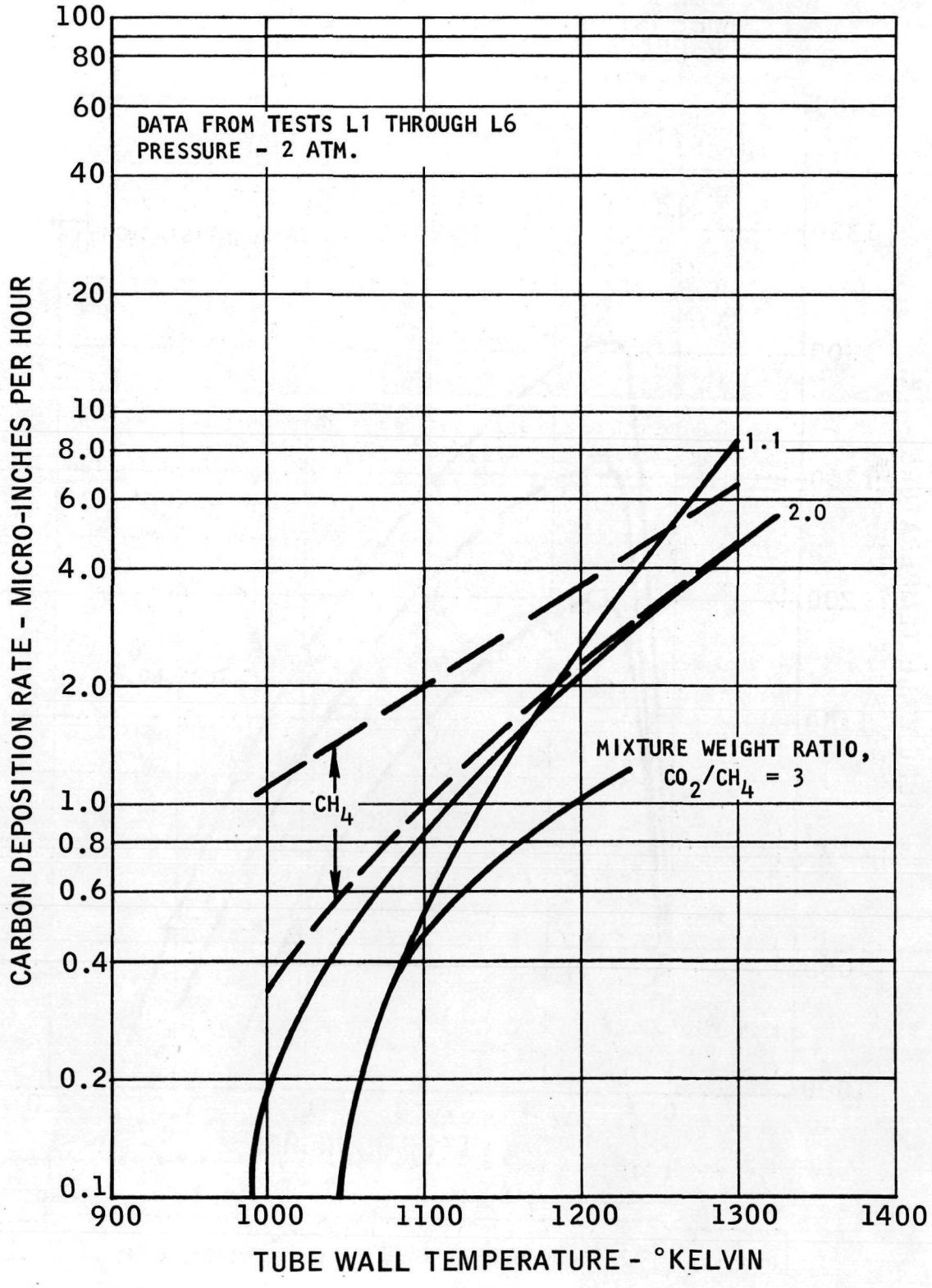

Figure 34

TEMPERATURE DISTRIBUTION ALONG HEATER TUBE SAMPLES

TEST R3

TUBE MASS FLOW RATE - 0.008 GRAMS/SECOND
TUBE INTERNAL PRESSURE - 2 ATM.
PROPELLANT - $H_2O + CH_4$

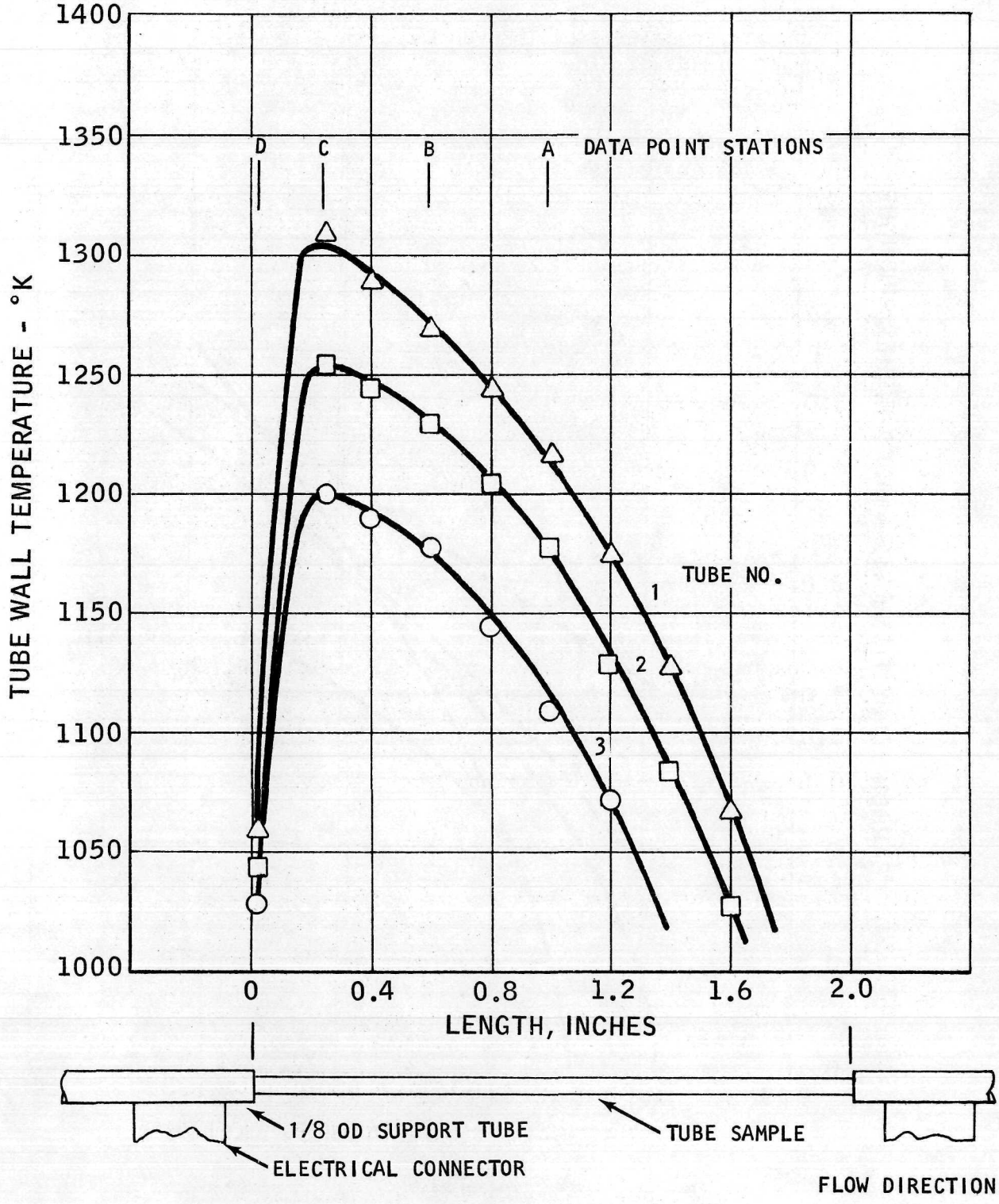

Figure 35

CARBON DEPOSITION RATE

PROPELLANT - $H_2O + CH_4$
PRESSURE - 2 ATM.
MASS FLOW RATE - 0.008 GRAMS/SECOND

SYMBOL	TEST	TUBE MATERIAL	EXPOSURE TIME - HRS.	MIXTURE RATIO H_2O/CH_4
○	R1	HASTELLOY X	161.5	1.13
△	R2	"	164.8	0.50
□	R3	"	140.4	0.26
◇	R4	TD PLATINUM	97.8	0.49

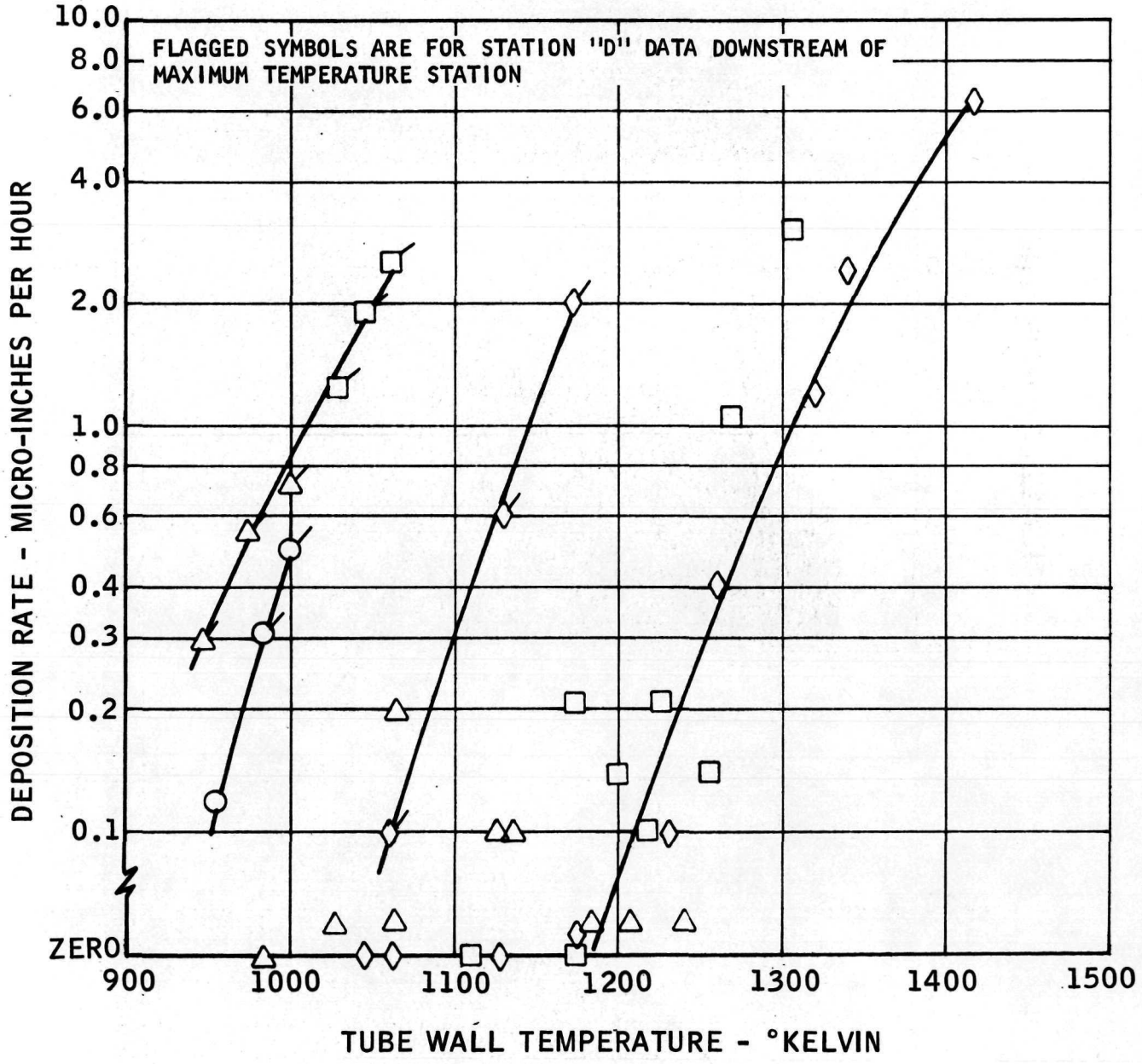

Figure 36

CARBON FORMATION - X500

A71002-6

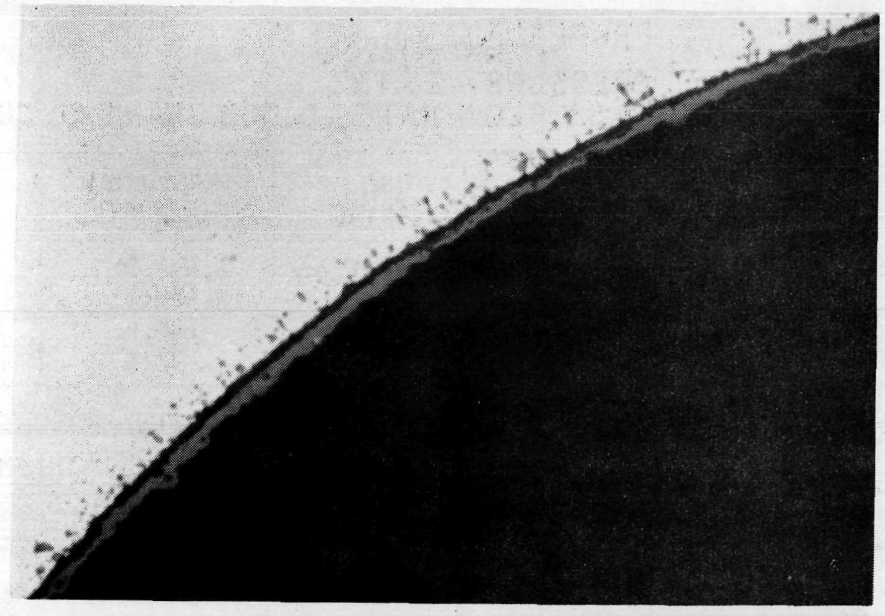

TEST R3-3D

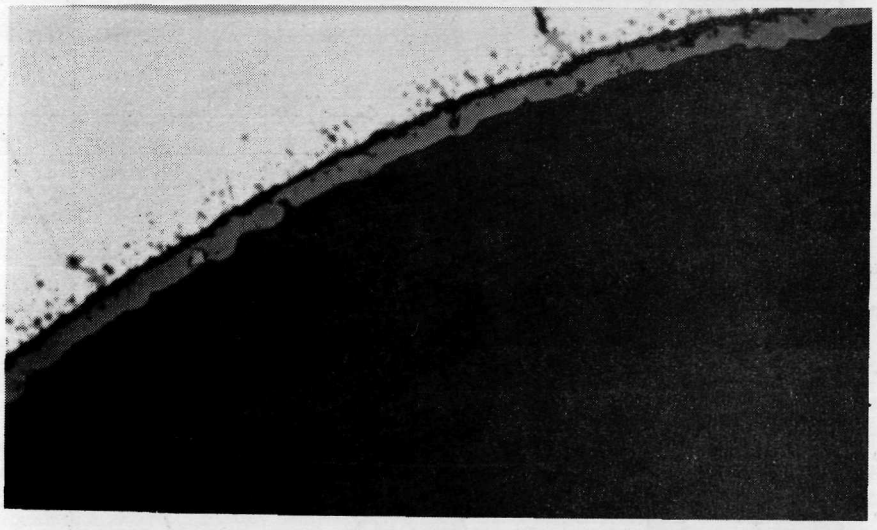

TEST R3-2D

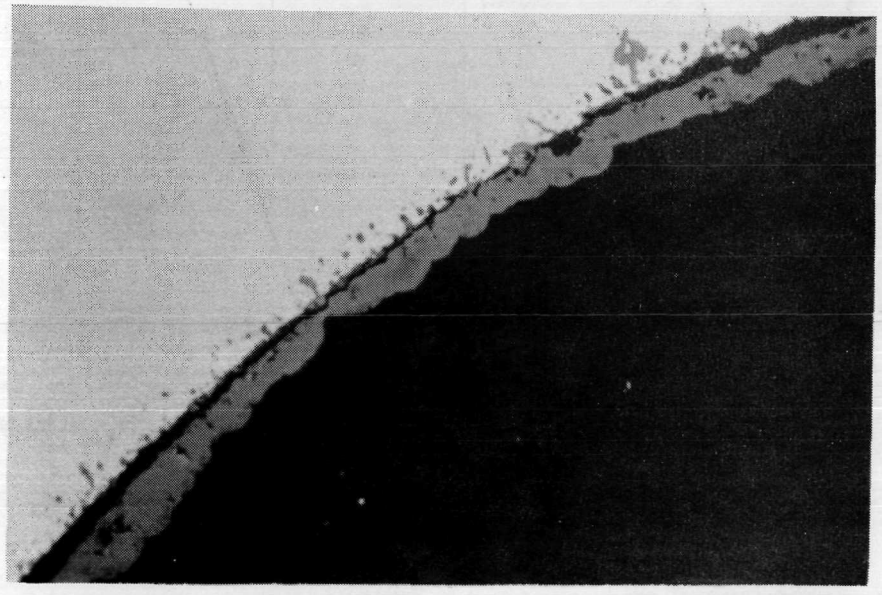

TEST R3-1D

Figure 37

CORRELATION OF CARBON DEPOSITION DATA

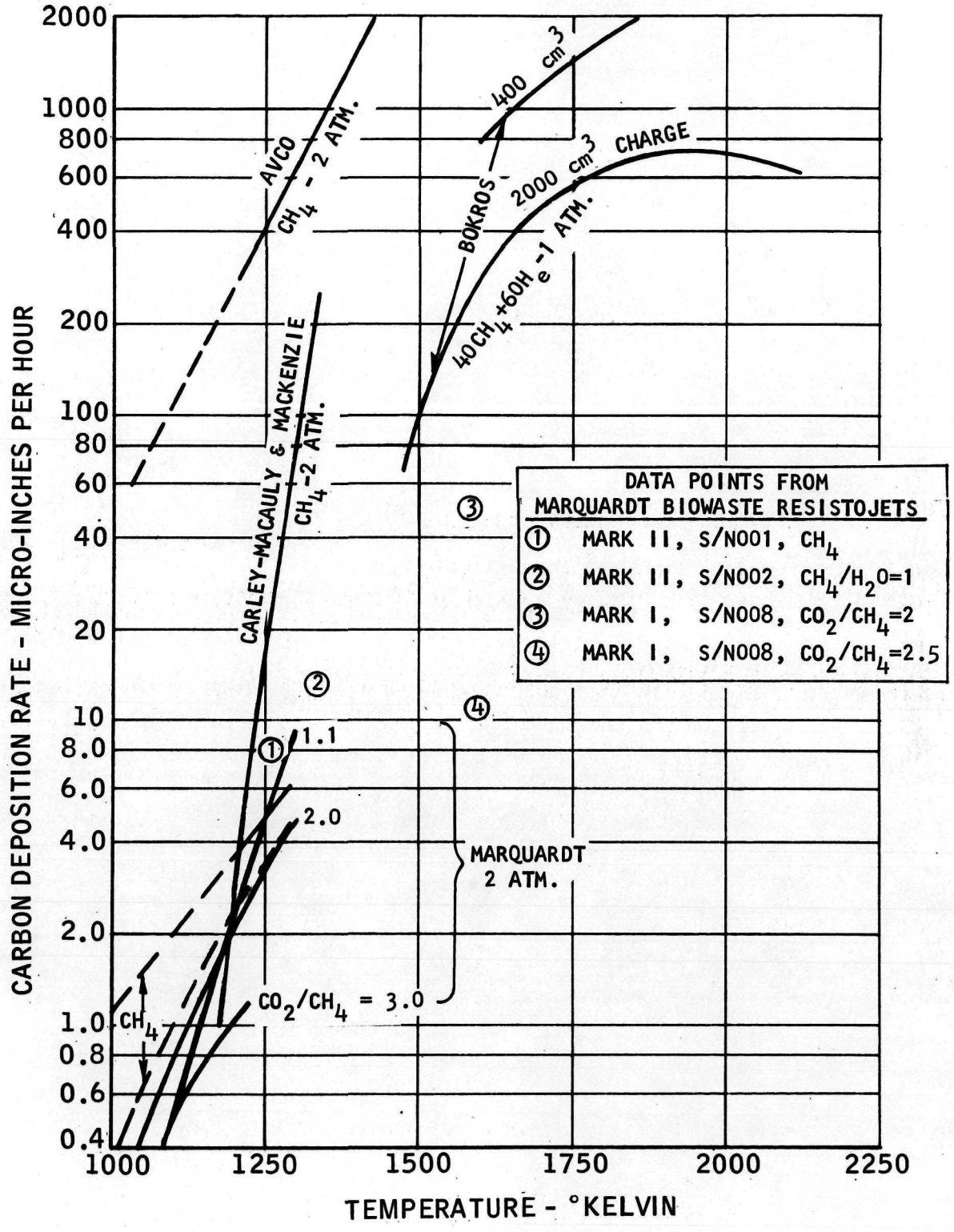

Figure 38

SURFACE OF Pt-20 Rh TUBE AFTER HIGH TEMPERATURE EXPOSURE TO CO_2

570 HOURS AT 1500°K

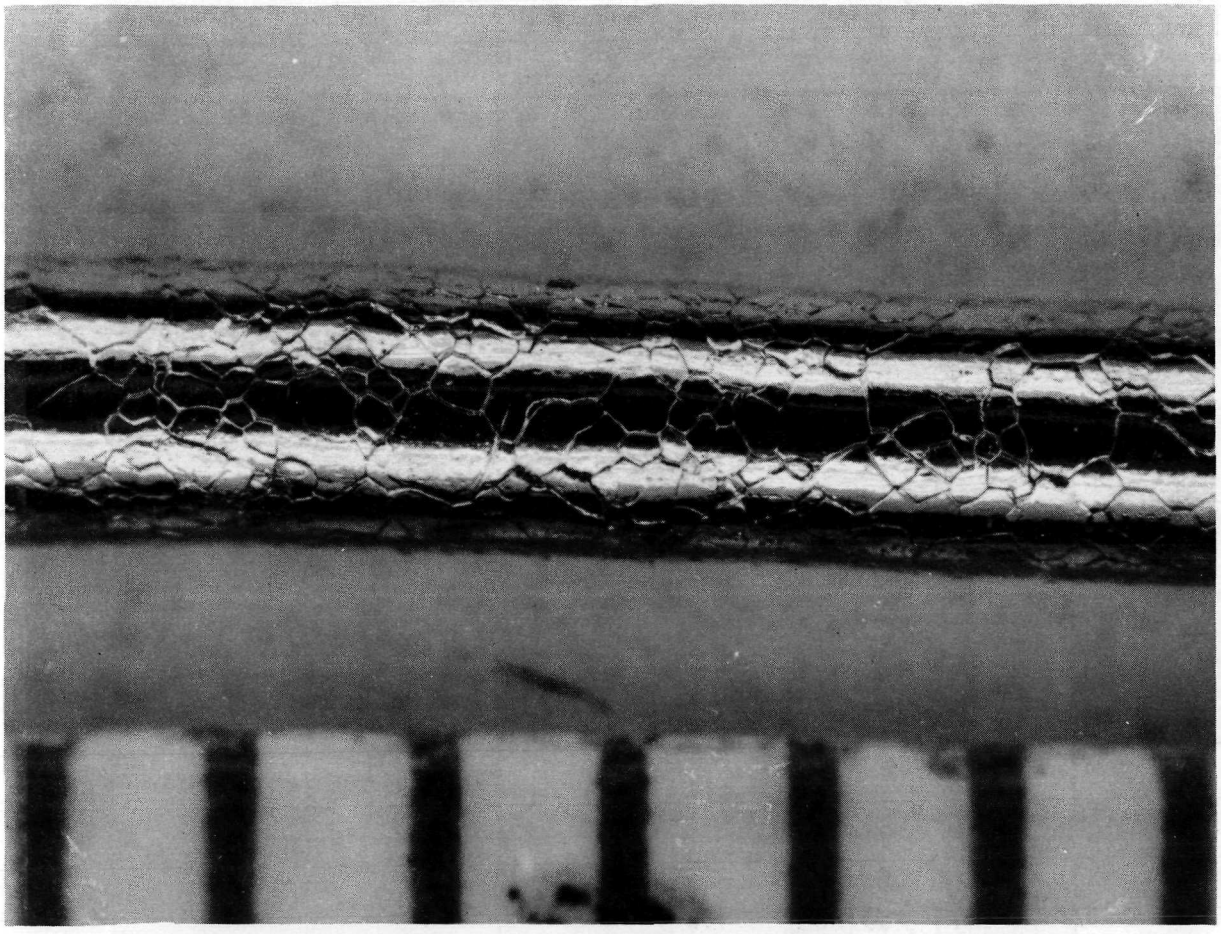

Figure 39

TEST II CROSS SECTIONS OF Pt-20Rh TUBES

X 500 ETCHED

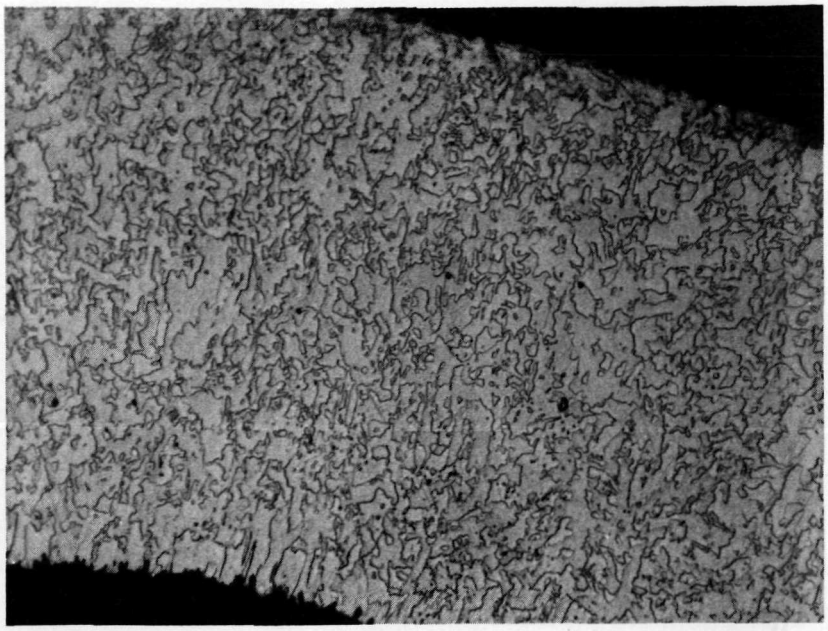

AS RECEIVED

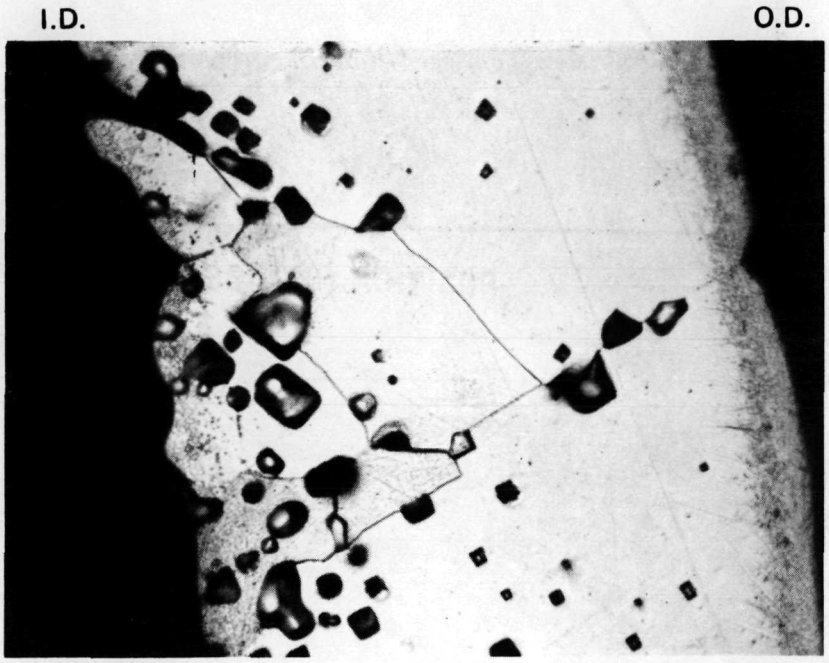

AFTER EXPOSURE TO CO_2 FOR 570 HOURS AT 1500 ^{o}K

Figure 40

DEPLETION OF RHODIUM FROM Pt-Rh ALLOY IN CO_2

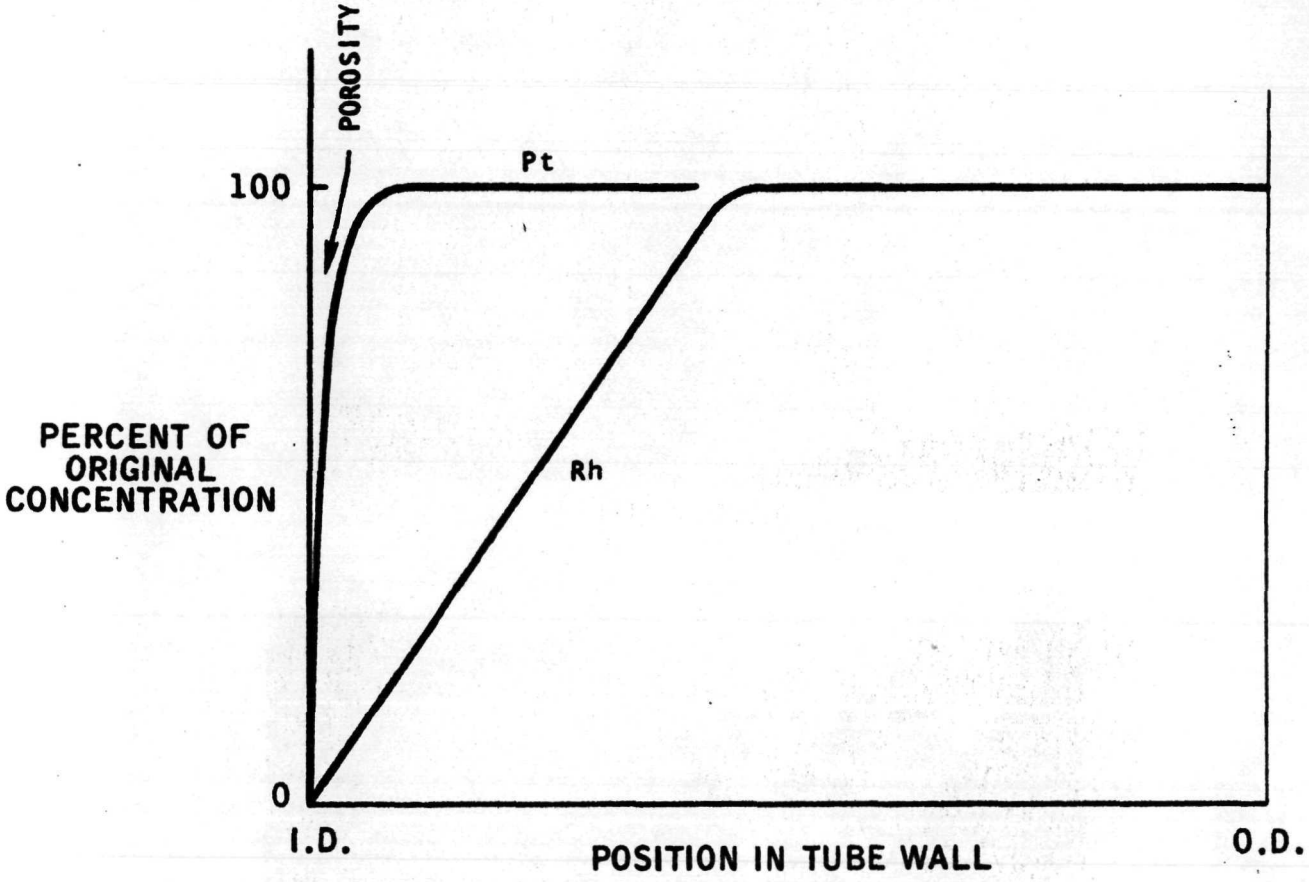

Figure 41

SURFACE OF Pt-30Rh WIRE AFTER HIGH TEMPERATURE EXPOSURE TO CO_2

500 HOURS AT 1707°K

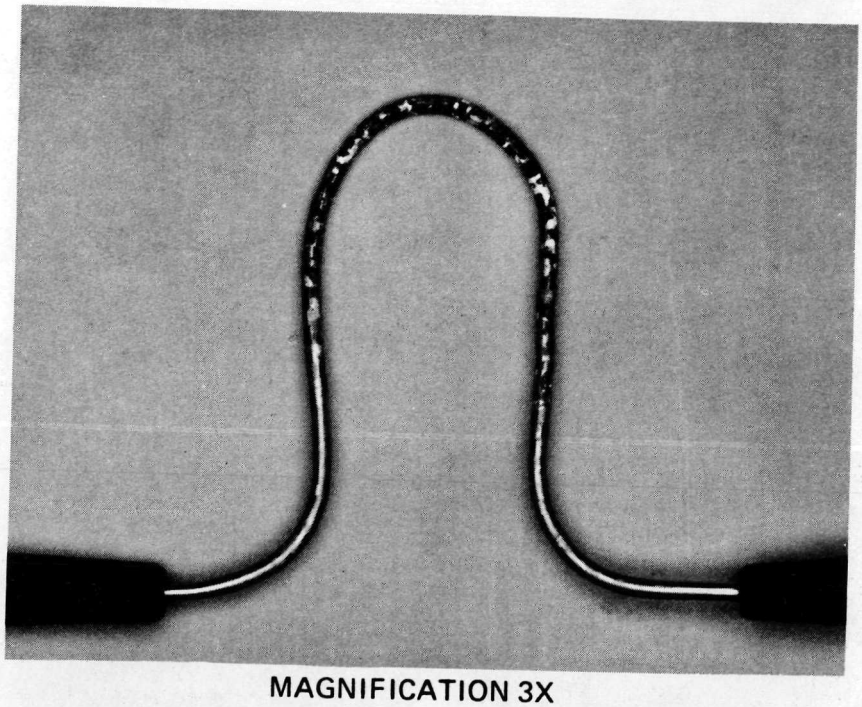

MAGNIFICATION 3X

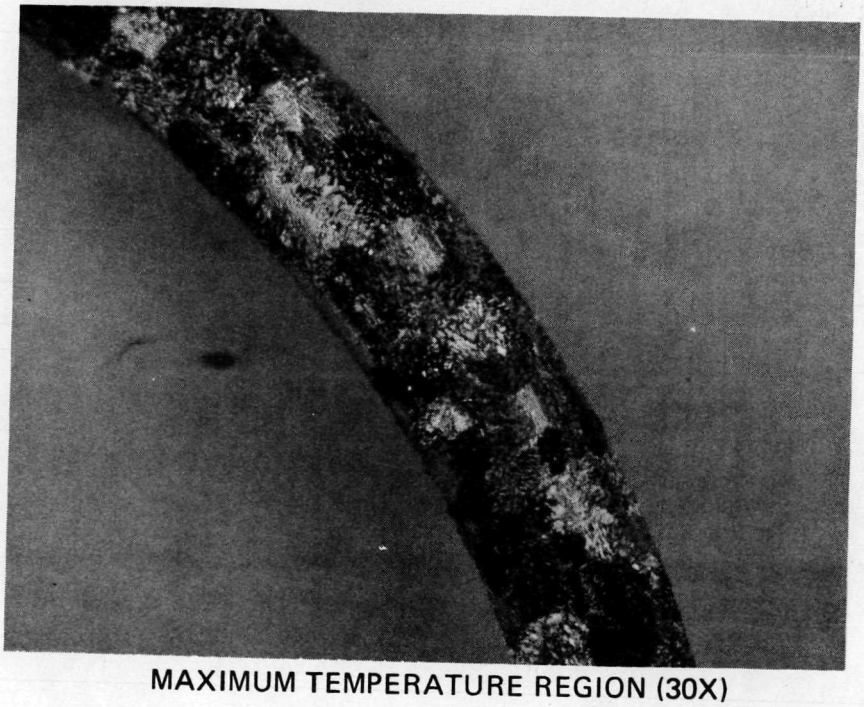

MAXIMUM TEMPERATURE REGION (30X)

Figure 42

CROSS-SECTION OF PLATINUM RHODIUM WIRE AT MAXIMUM TEMPERATURE REGION AFTER EXPOSURE TO CO_2

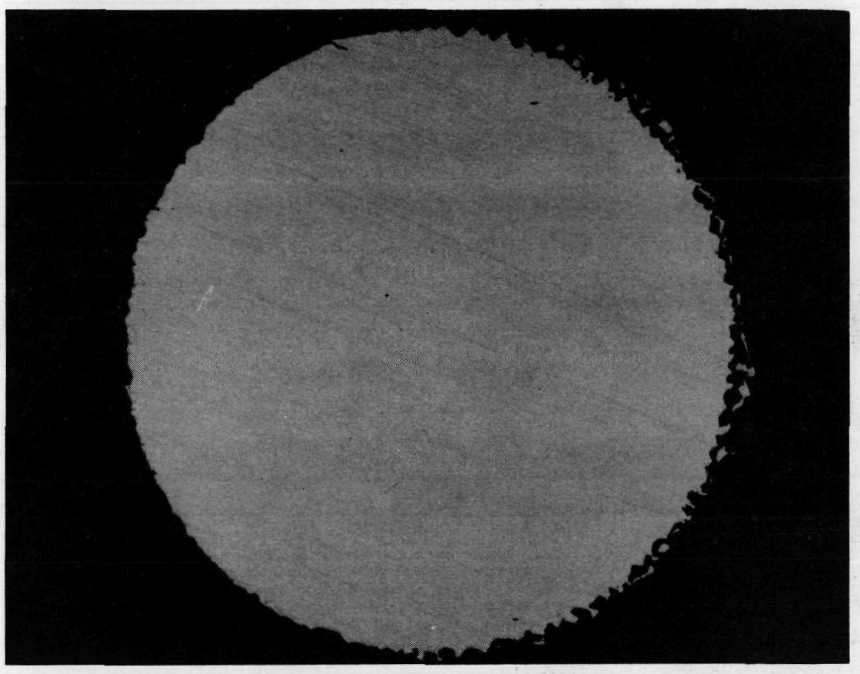

500 HOURS AT 1707 °K

Figure 43

PLATINUM - 10% RHODIUM TUBE PRIOR TO TESTING

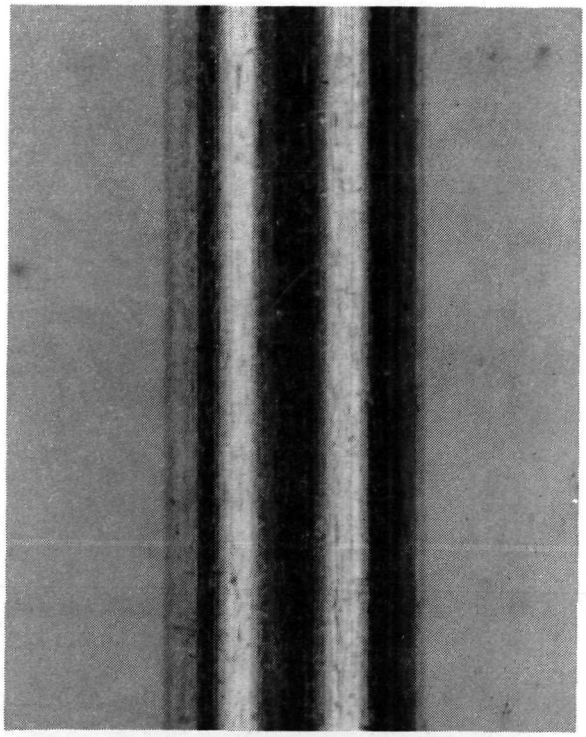

X25

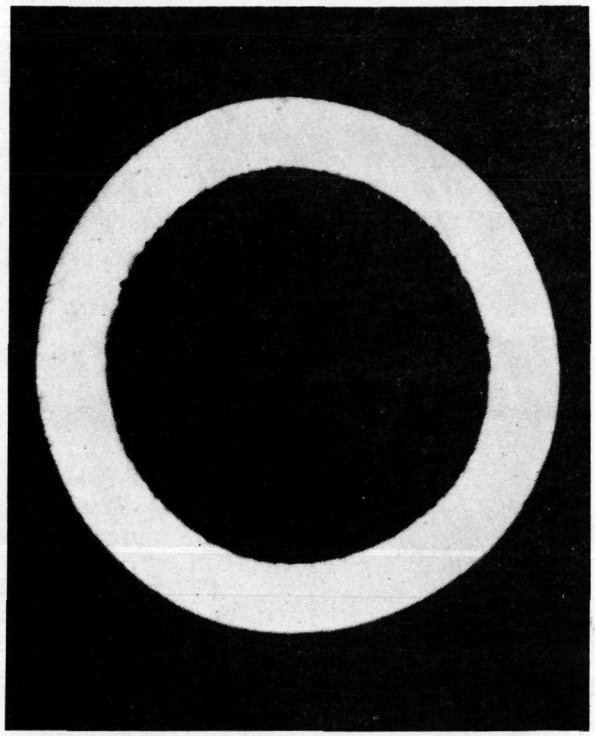

X50

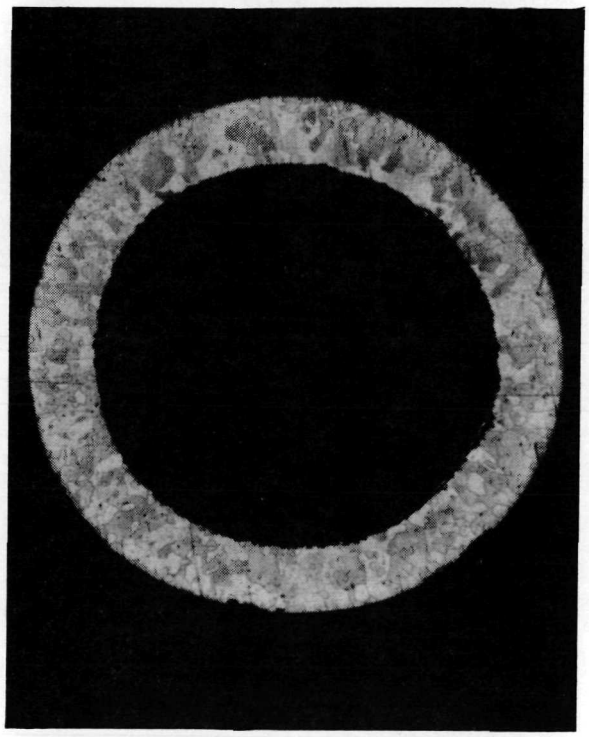

X50 ETCHED

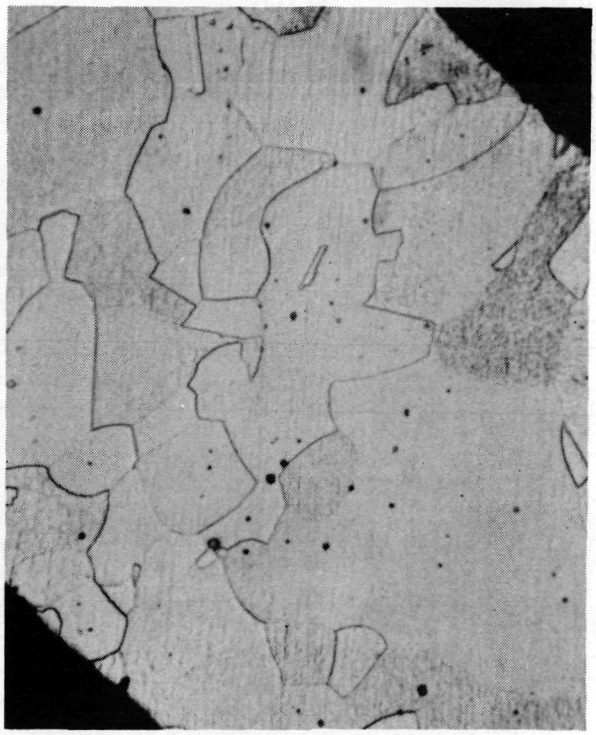

X500 ETCHED

Figure 44

TEST R6 Pt-10Rh TUBE AFTER 500 HOURS AT 1700° K

CO_2 + 1.5% O_2

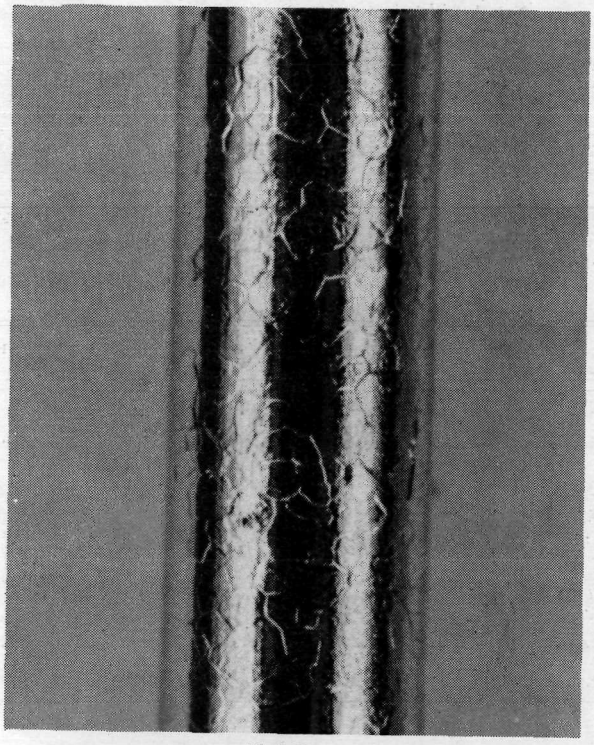

X 25

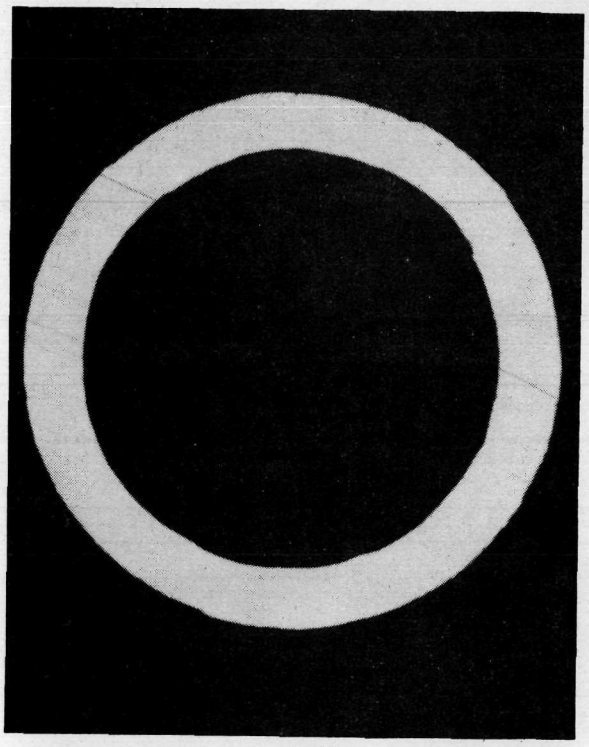

X 50

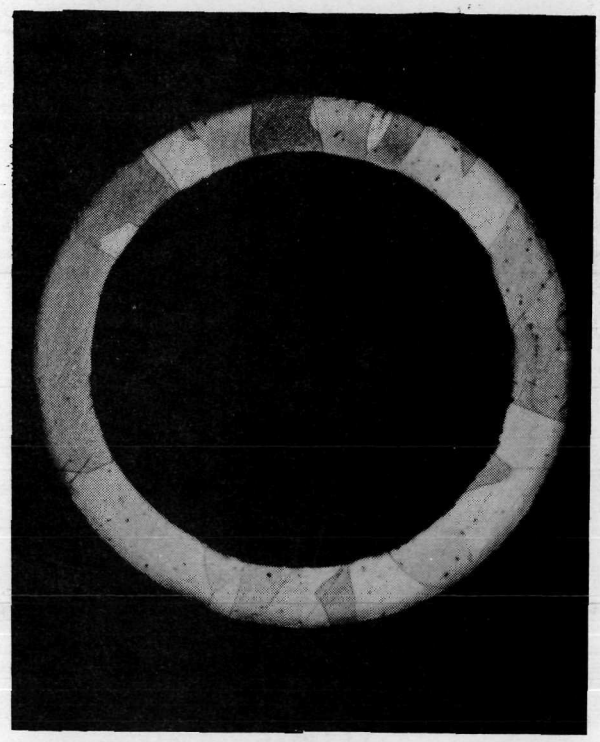

X 50 ETCHED

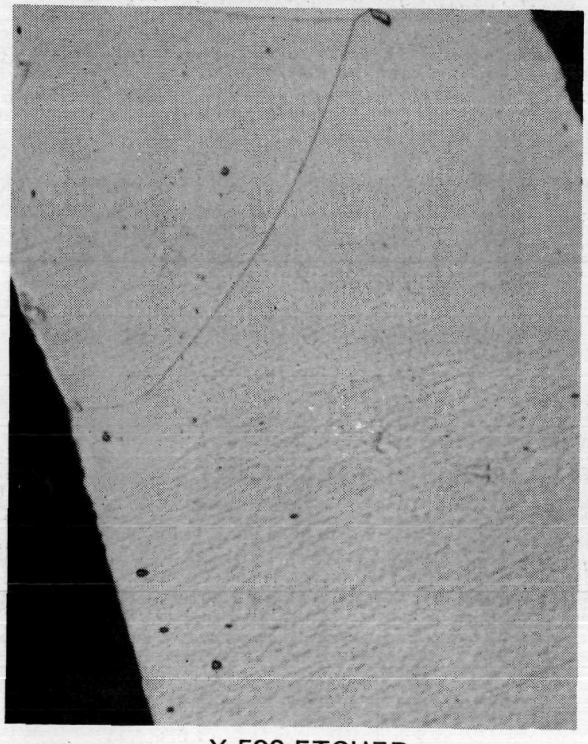

X 500 ETCHED

Figure 45

TEST L11-1 Pt-10Rh TUBE AFTER 1500 HOURS AT 1600° K

CO_2 + 0.25% O_2

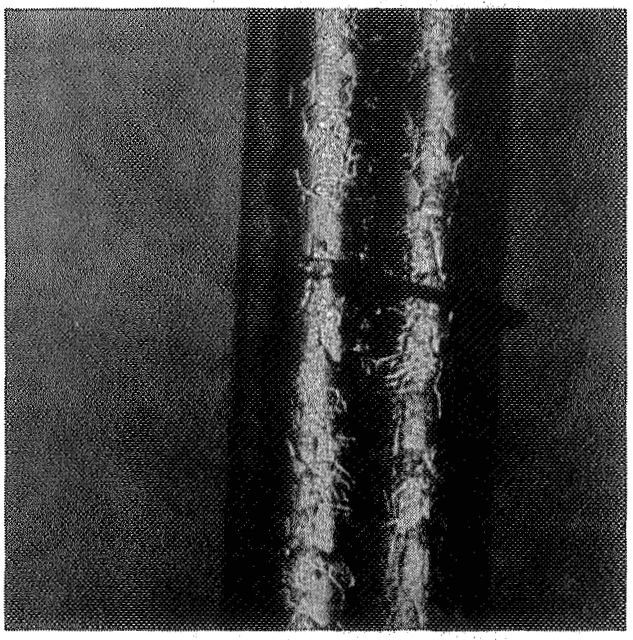

X 25

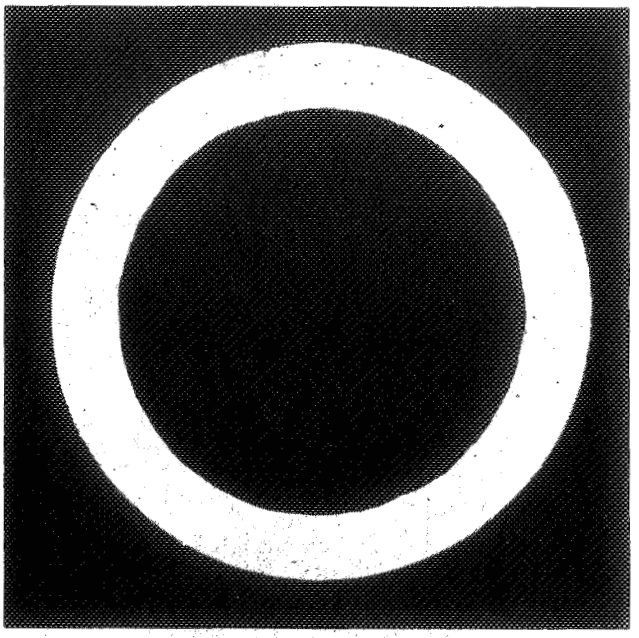

X 50

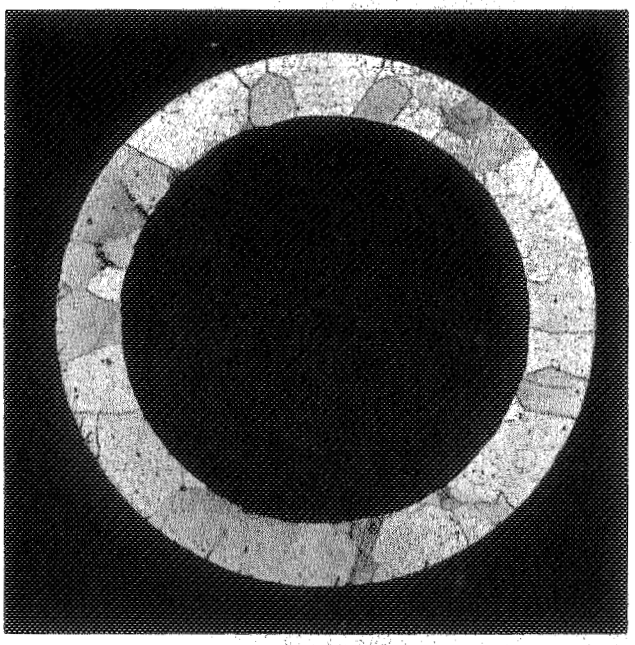

X 50 ETCHED

X 500 ETCHED

Figure 46

TEST L11-1 Pt-10Rh TUBE AFTER 1500 HOURS AT 1700° K

CO_2 + 0.25% O_2

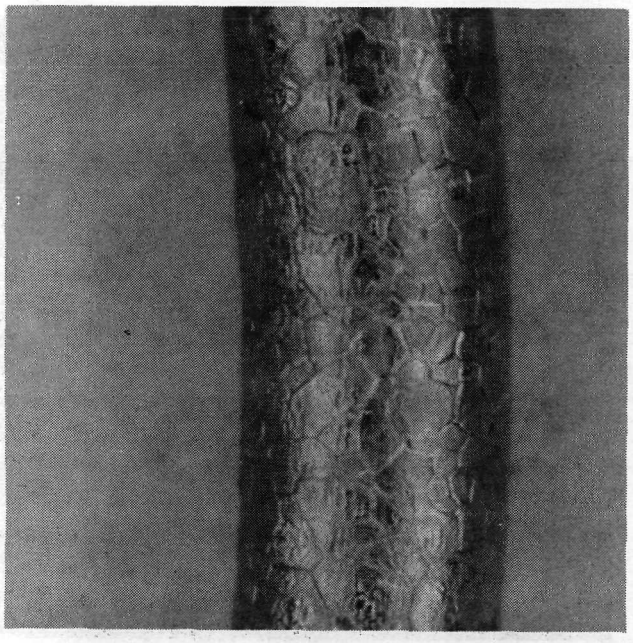

X 25

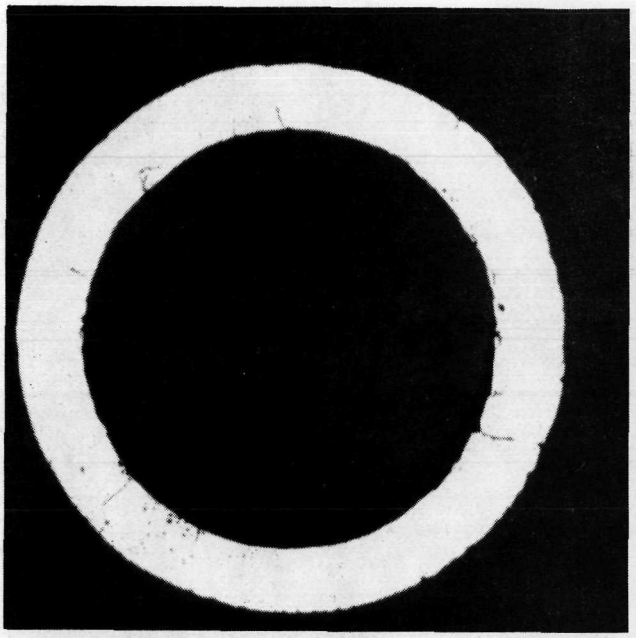

X 50

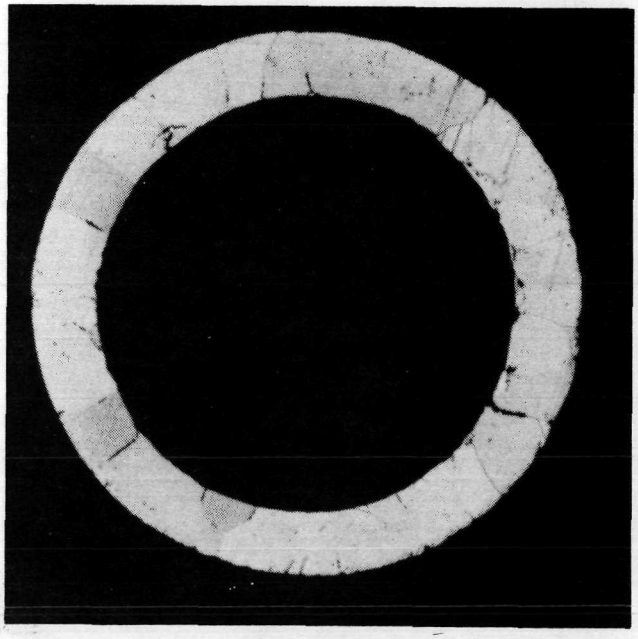

X 50 ETCHED

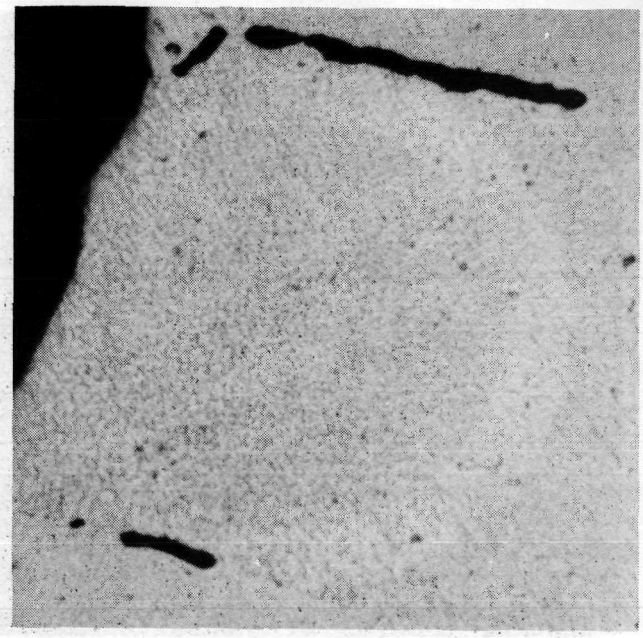

X 500 ETCHED

Figure 47

PLATINUM - 5% RHODIUM TUBE PRIOR TO TESTING

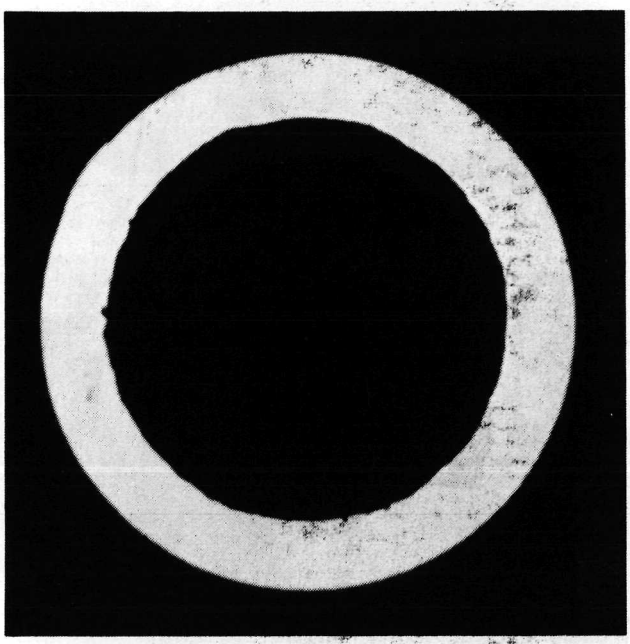

X 50

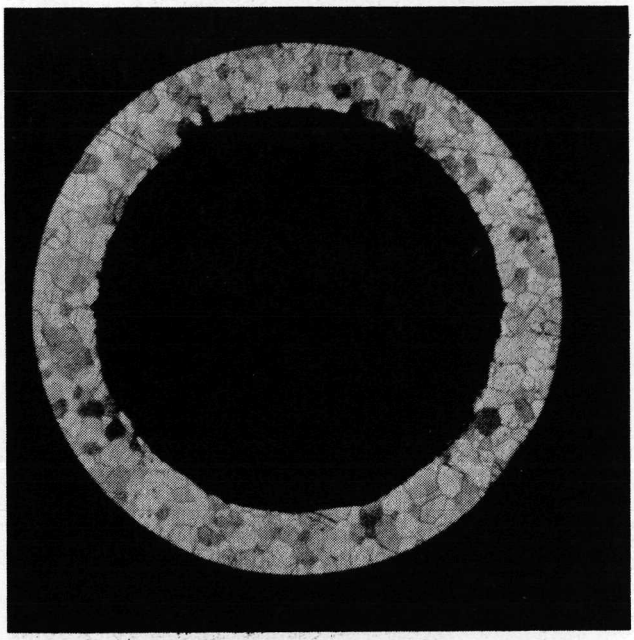

X 50 ETCHED

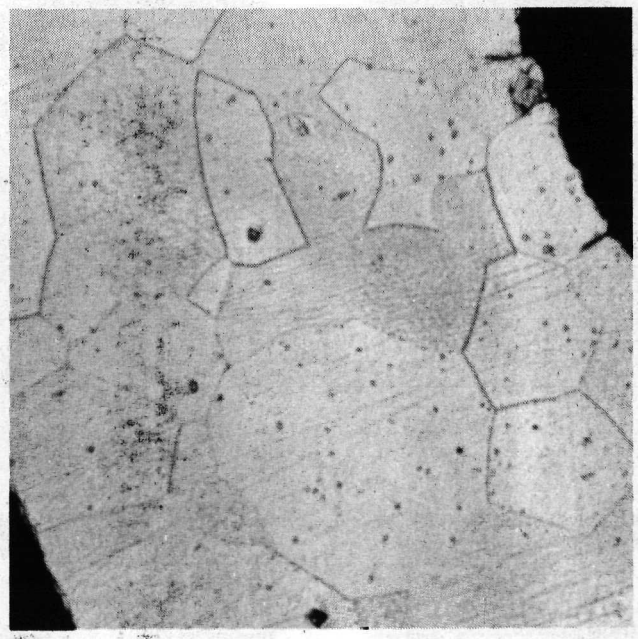

X 500 ETCHED

Figure 48

TEST R8-3 Pt-5Rh TUBE AFTER 1500 HOURS AT 1600° K

CO_2

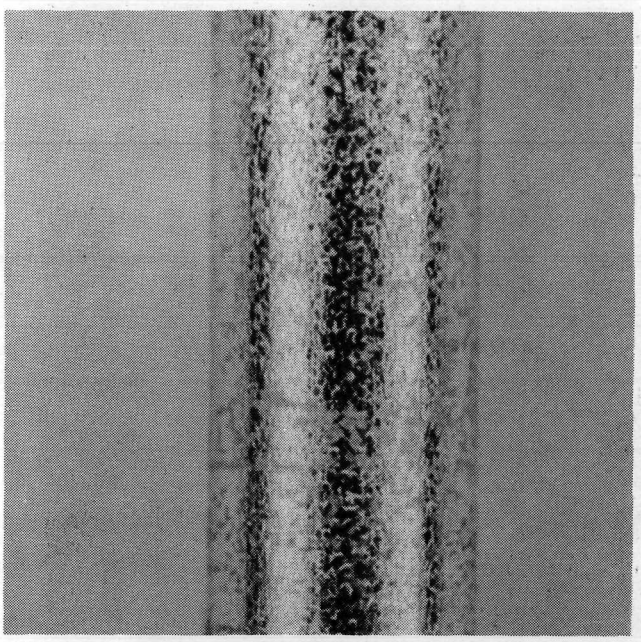

X 25

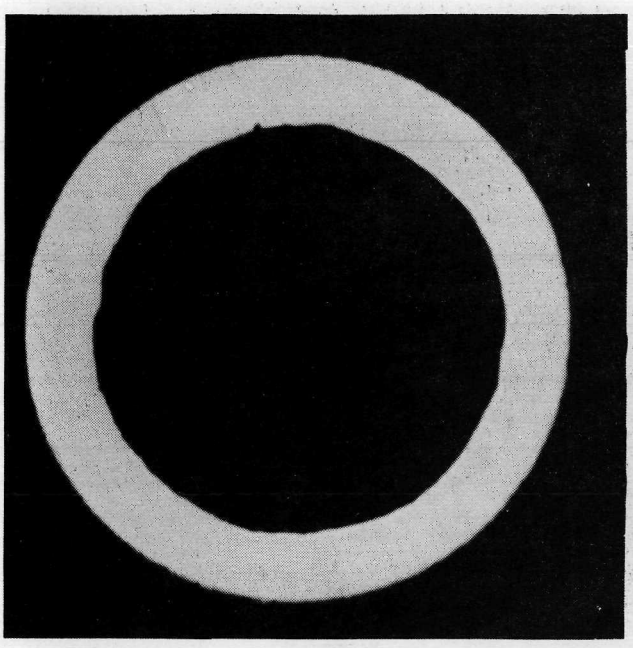

X 50

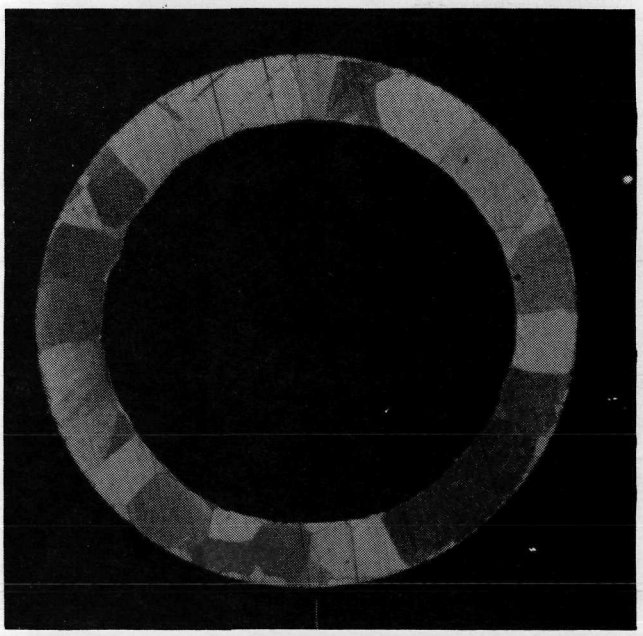

X 50 ETCHED

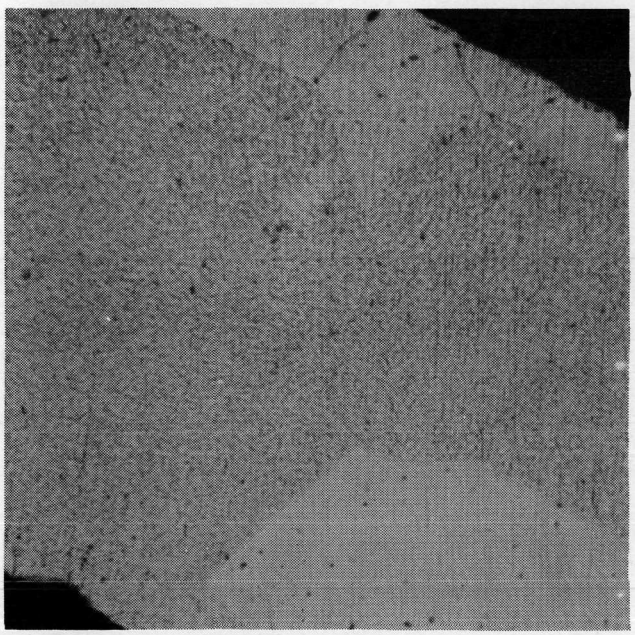

X 500 ETCHED

Figure 49

TEST R8-3 Pt-5Rh TUBE AFTER 1500 HOURS AT 1700° K

CO_2

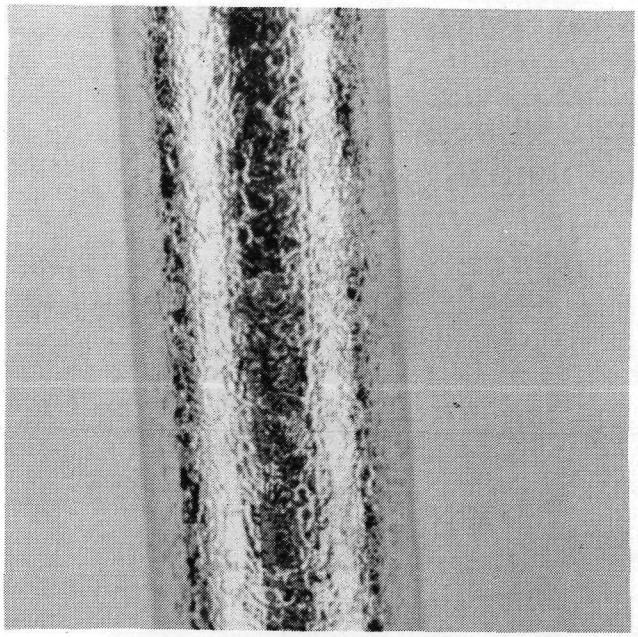

X 25

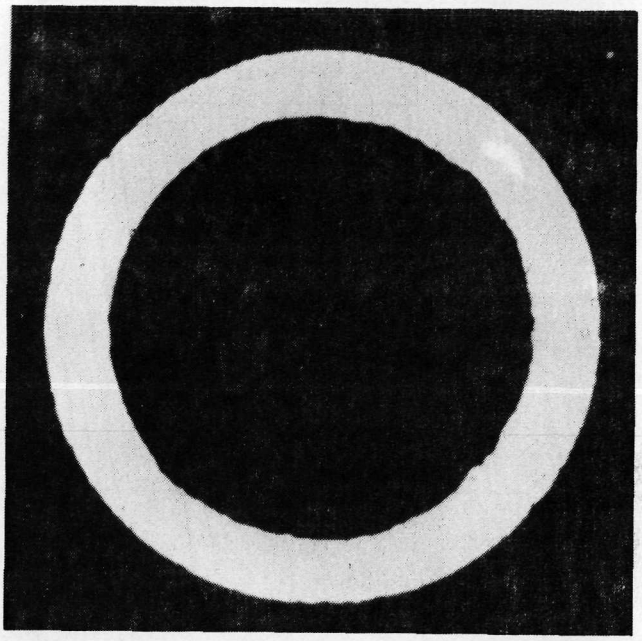

X 50

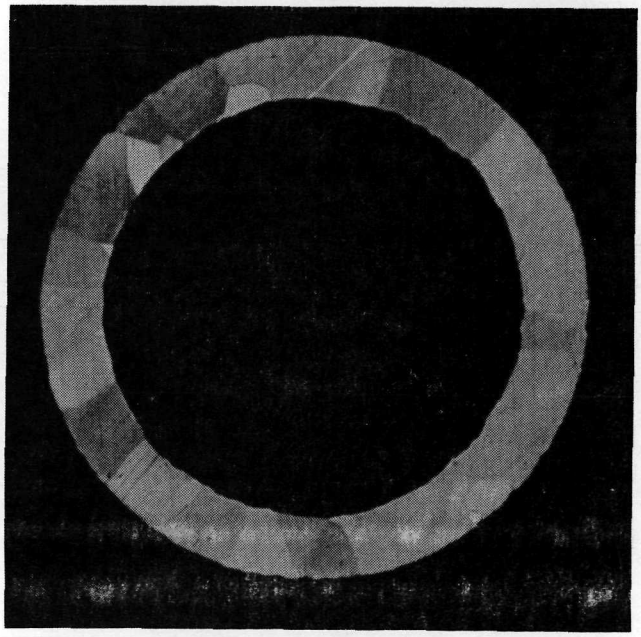

X 50 ETCHED

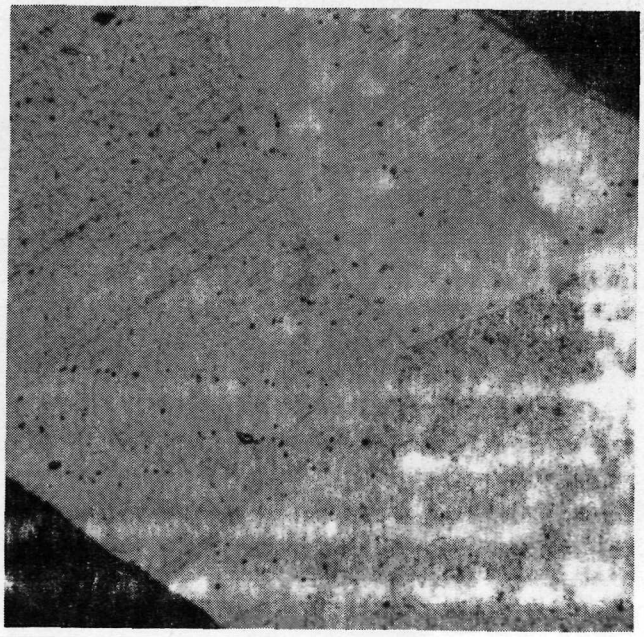

X 500 ETCHED

Figure 50

SURFACE OF Pt-30Ir WIRE AFTER HIGH TEMPERATURE EXPOSURE TO CO_2

500 HOURS AT 1725°K

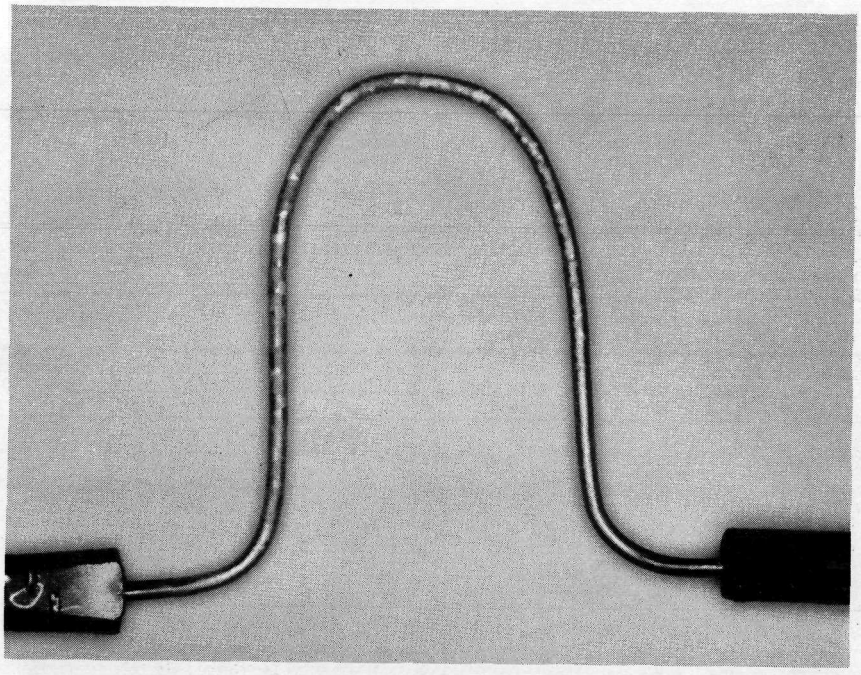

MAGNIFICATION 3X

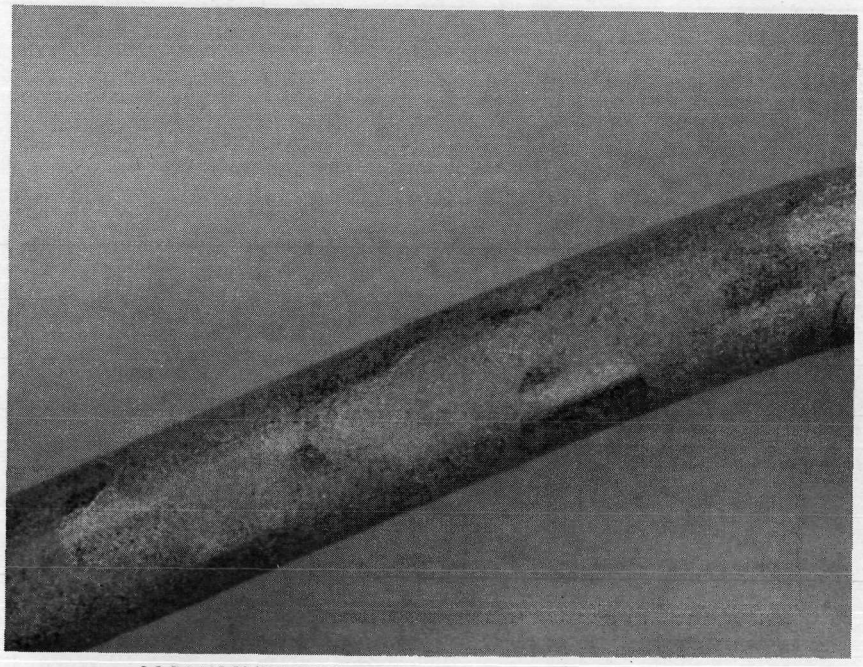

MAXIMUM TEMPERATURE REGION (30X)

Figure 51

CROSS-SECTION OF PLATINUM IRIDIUM WIRE AT MAXIMUM TEMPERATURE REGION AFTER EXPOSURE TO CO_2

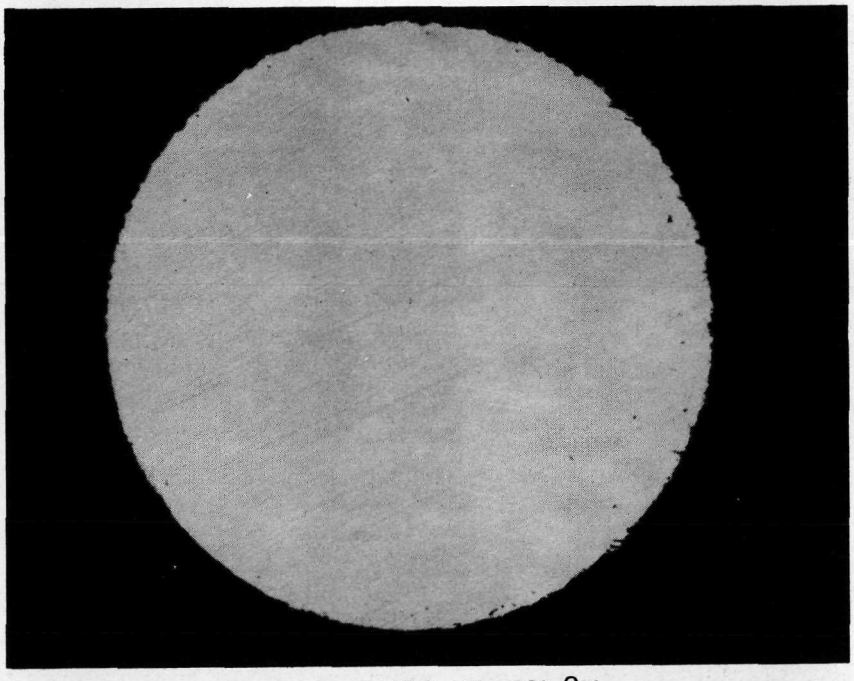

500 HOURS AT 1725 °K

Figure 52

SURFACE OF PLATINUM ALLOY TUBES AFTER HIGH TEMPERATURE EXPOSURE TO CO_2

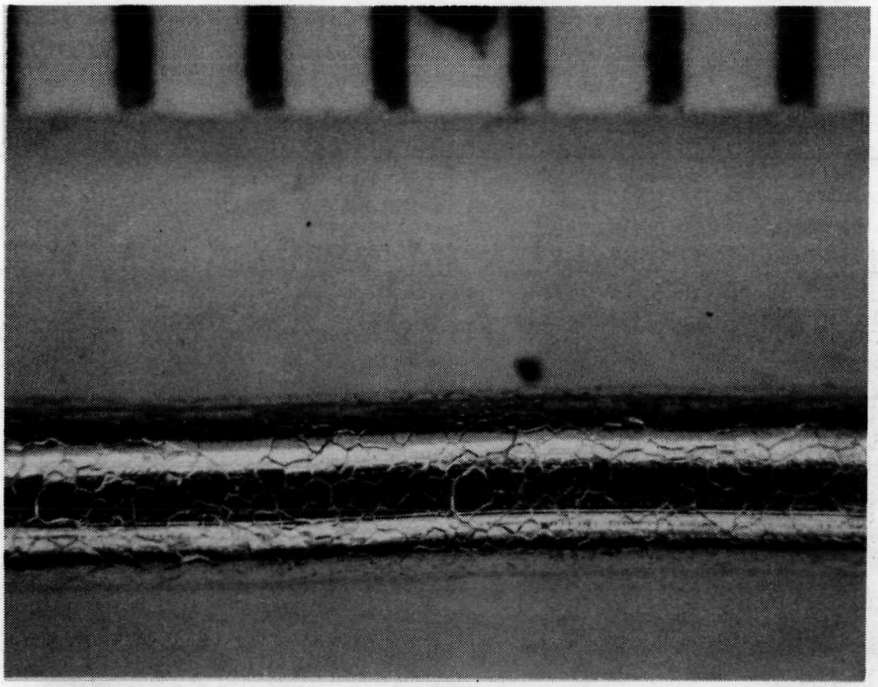

Pt-20Rh 200 HOURS AT $<1400^{\circ}K$
20X 300 HOURS AT $1600^{\circ}K$

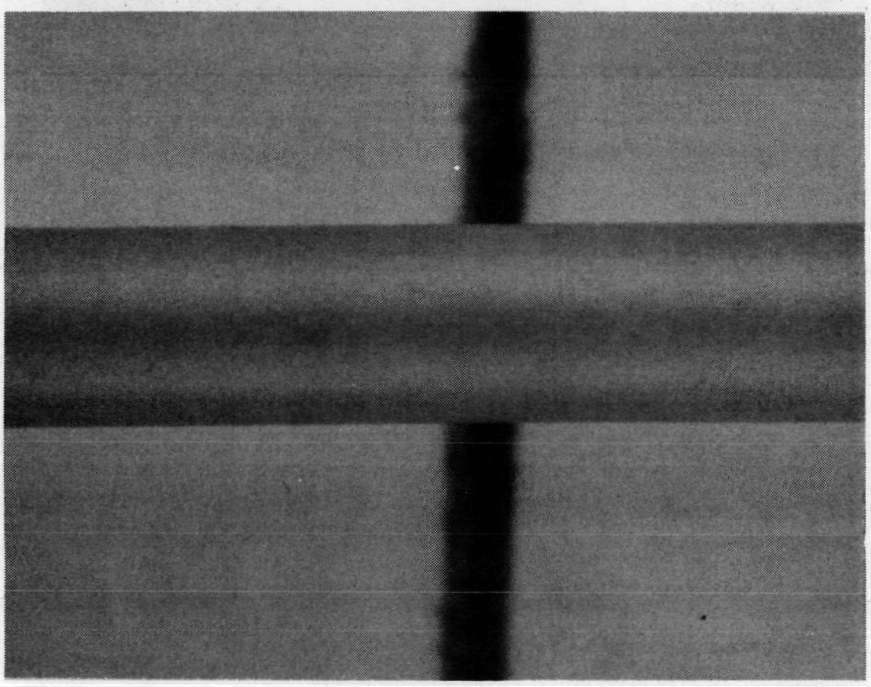

Pt-30Ir 706 HOURS AT $1550^{\circ}K$
20X

Figure 53

Figure 1

TEST 11-1 CROSS SECTIONS OF Pt-30Ir TUBES

X 500 ETCHED

I.D.

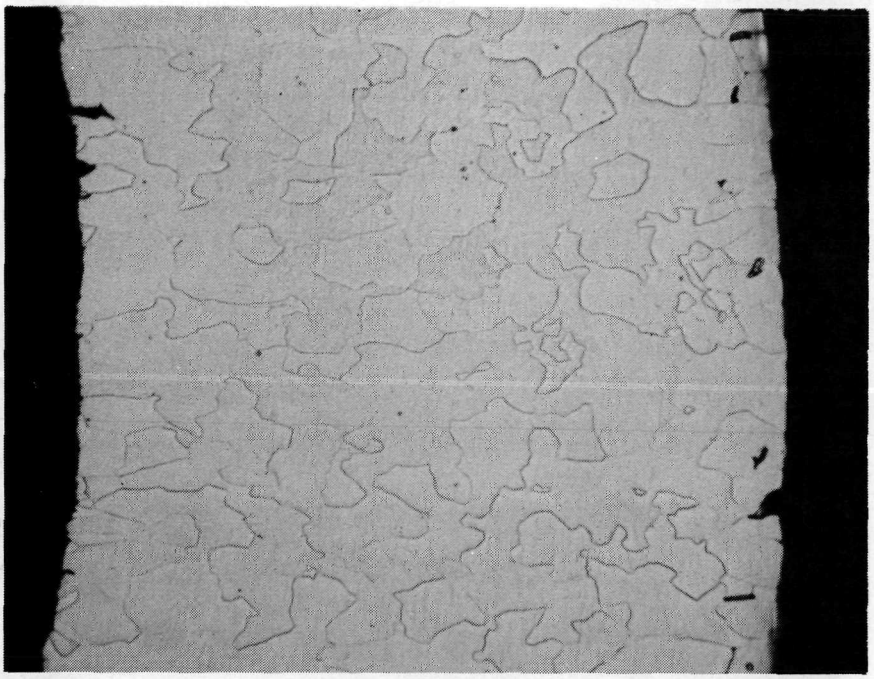

O.D.

AS RECEIVED

I.D

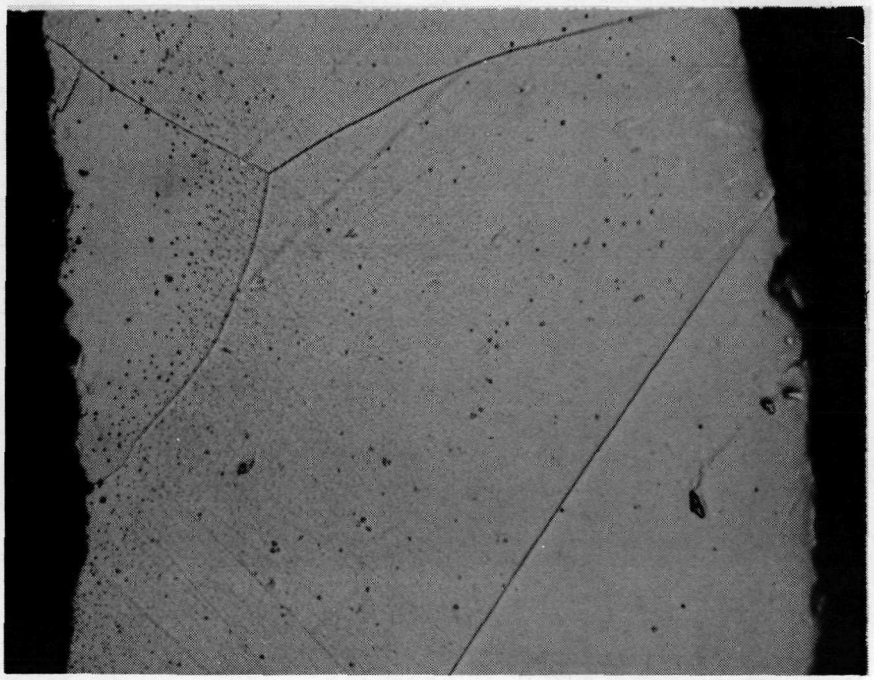

O.D.

AFTER EXPOSURE TO CO_2 FOR 706 HOURS AT 1550 ^{o}K

Figure 54

OUTSIDE SURFACE OF Pt-20Ir TUBES
REDUCING ATMOSPHERE INSIDE
VACUUM OUTSIDE
734 HOURS
1690 °K

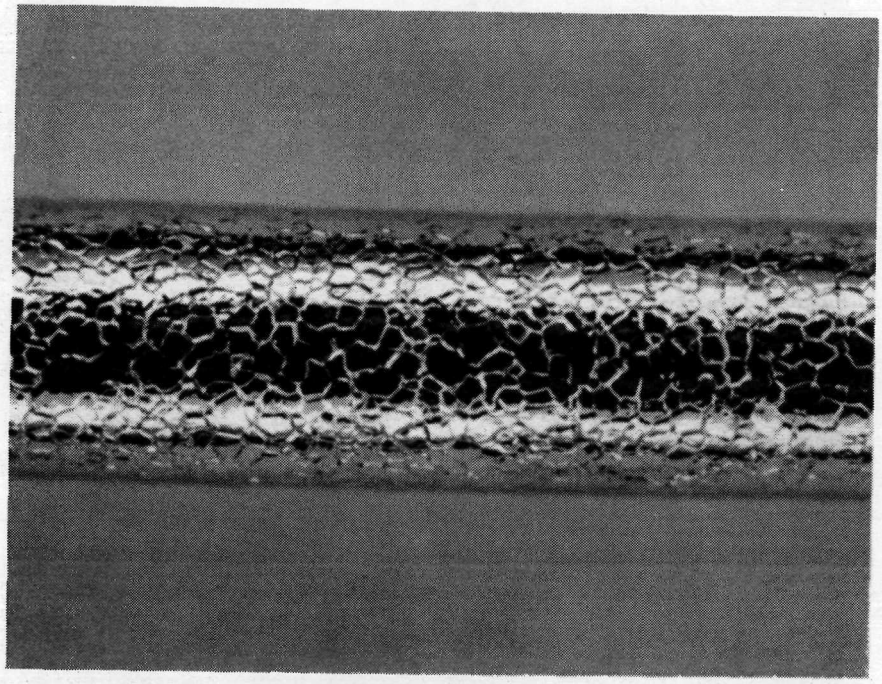

TEST L7-3C - X27

Figure 55

Pt-20Ir TUBE AFTER 734 HOURS WITH REDUCING PROPELLANT

1690 °K
X50

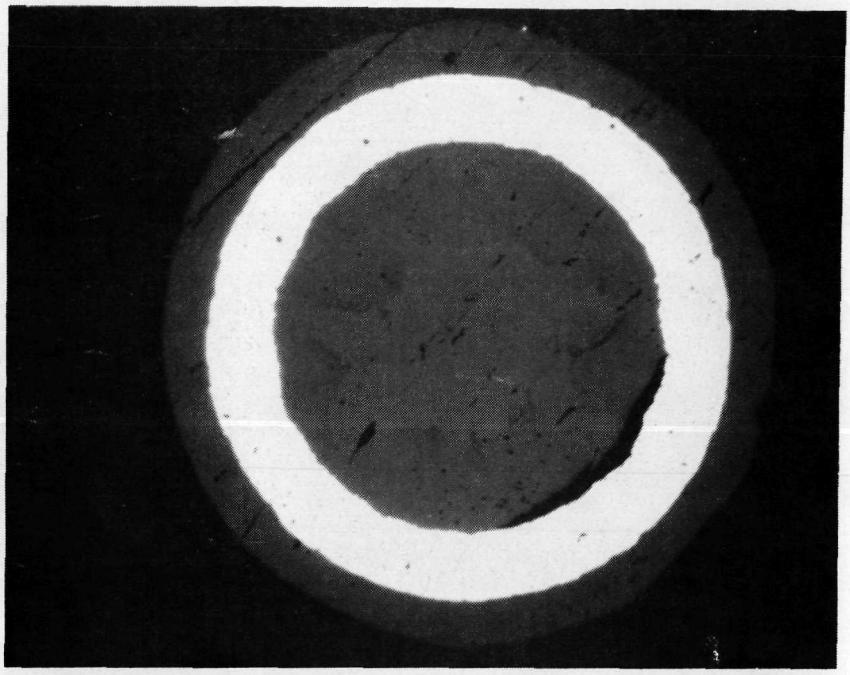

TEST L7-3C UNETCHED

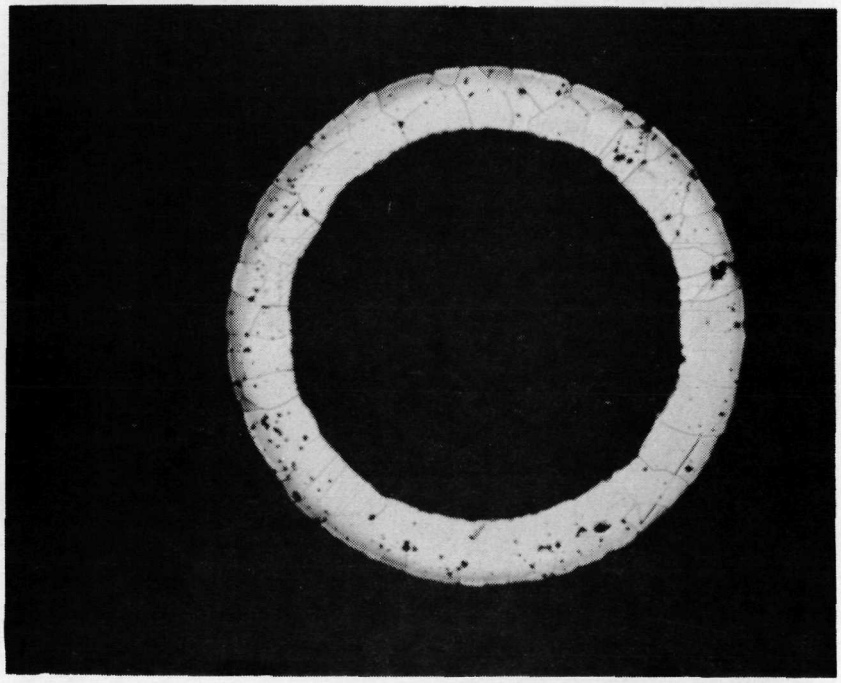

TEST L7-3C ETCHED

Figure 56

OUTSIDE SURFACE OF Pt-20Ir TUBES
OXIDIZING ATMOSPHERE INSIDE
VACUUM OUTSIDE
X27

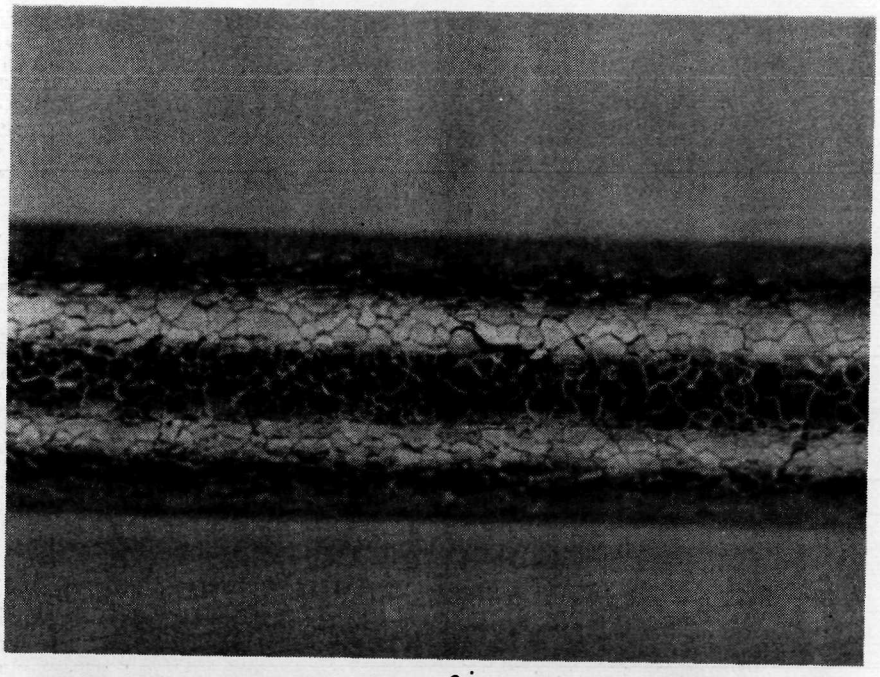

TEST L8-3B 1645°K 160 HOURS

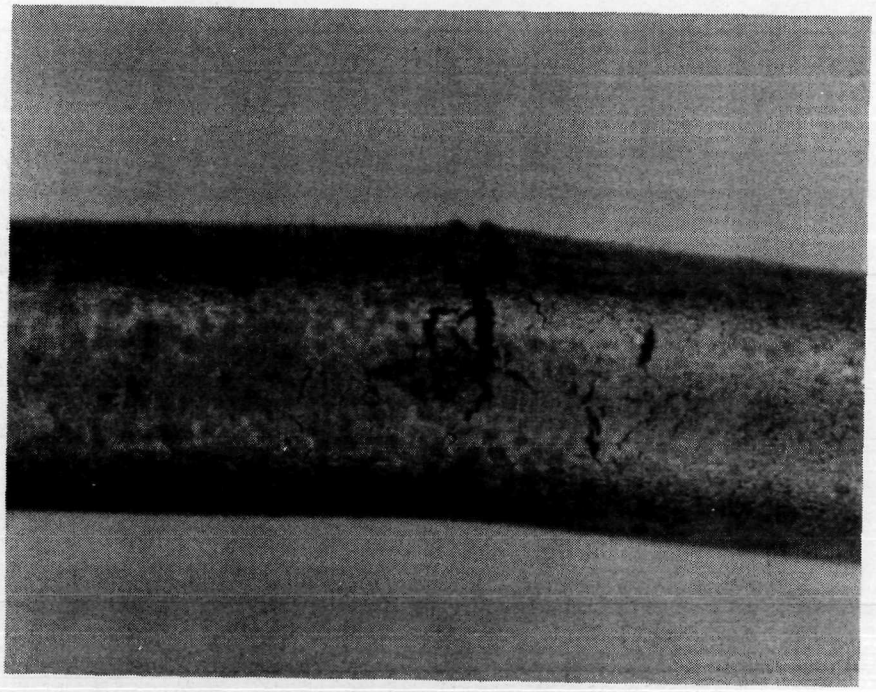

TEST L8-2B 1465°K 137 HOURS

Figure 57

Pt-20Ir TUBE AFTER 160 HOURS AT 1700° K WITH OXIDIZING PROPELLANT X50

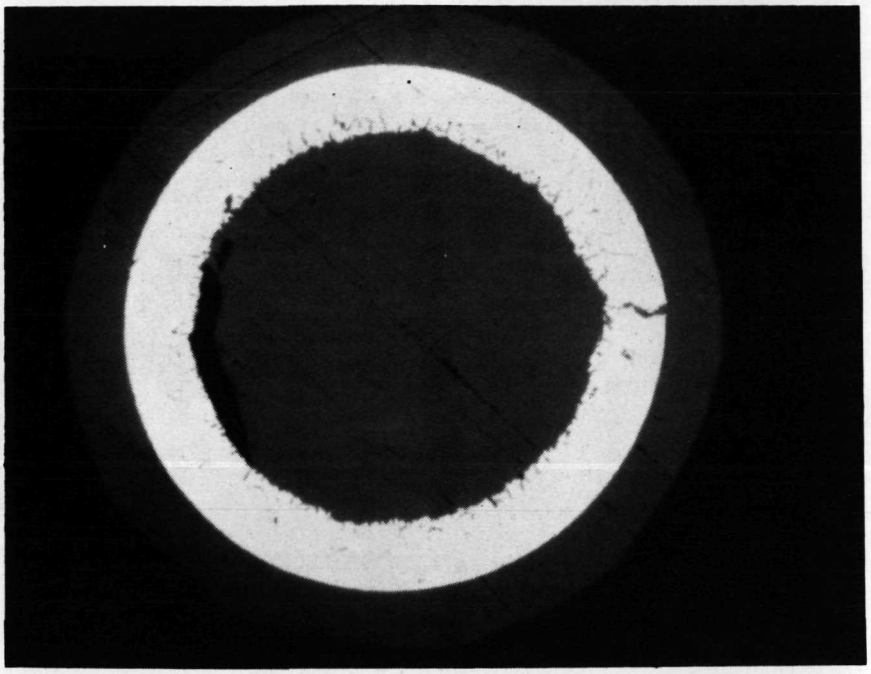

TEST L8-3A UNETCHED

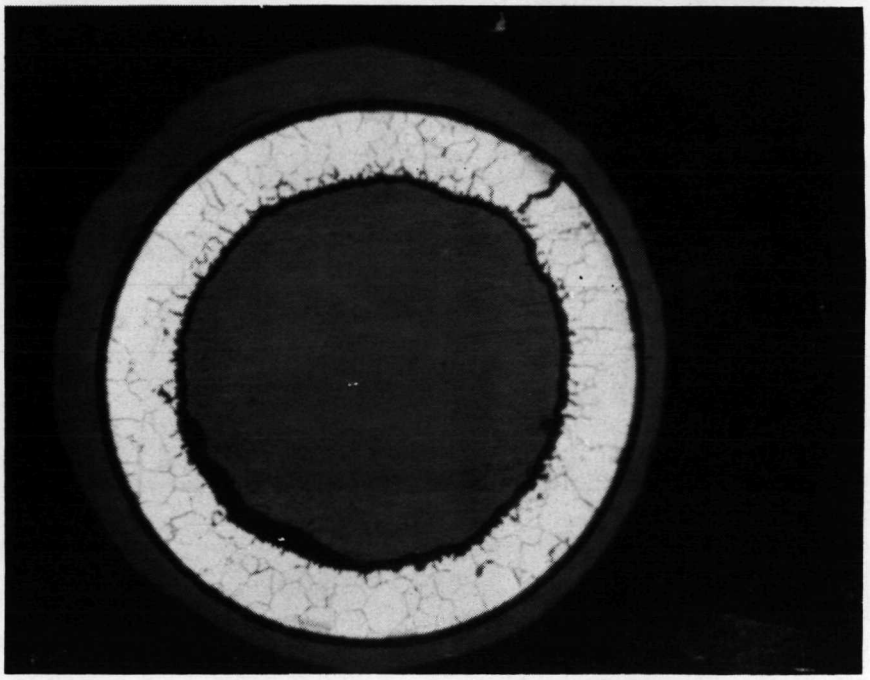

TEST L8-3A ETCHED

Figure 58

Pt-20Ir TUBE AFTER 160 HOURS WITH OXIDIZING PROPELLANT

1645 °K

X50

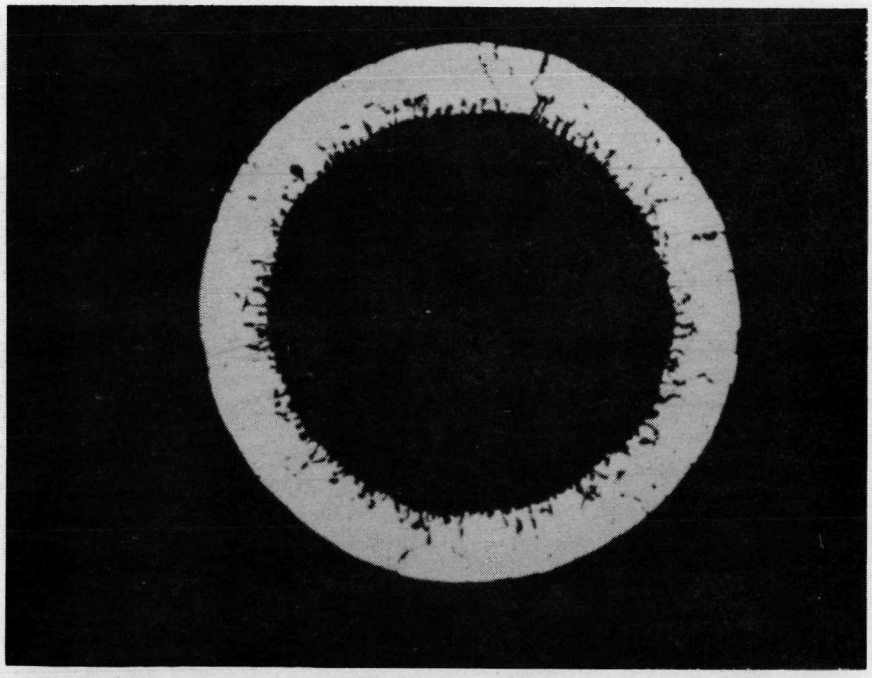

TEST L8-3B UNETCHED

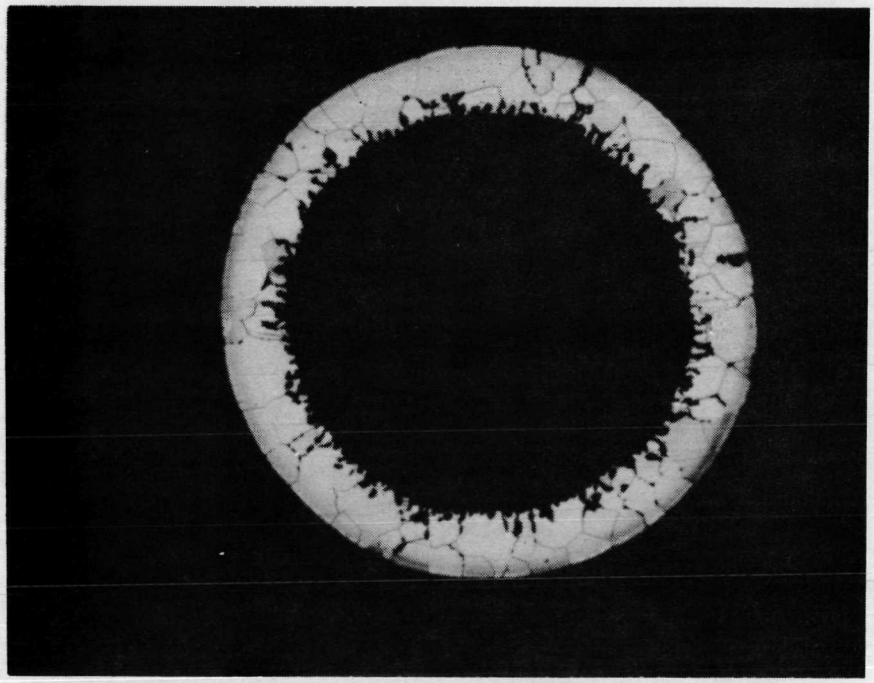

TEST L8-3B ETCHED

Figure 59

Pt-20Ir TUBE AFTER 160 HOURS AT 1330° K WITH OXIDIZING PROPELLANT

X50

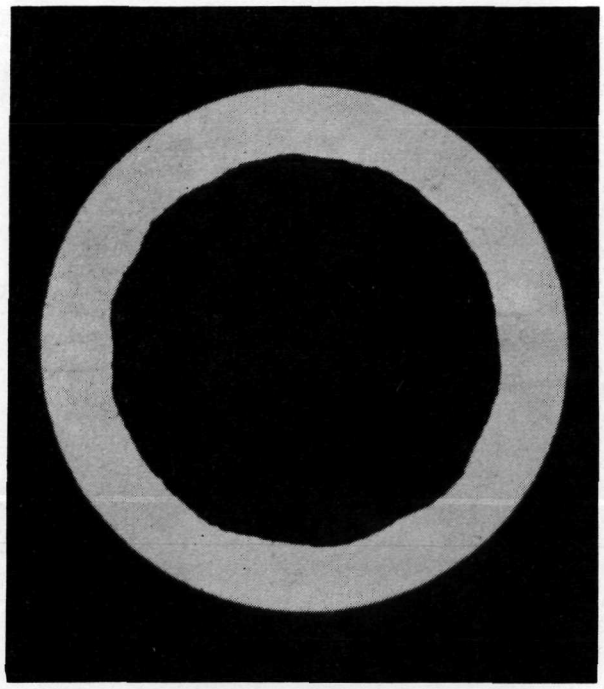

TEST L8-3AF UNETCHED

X50

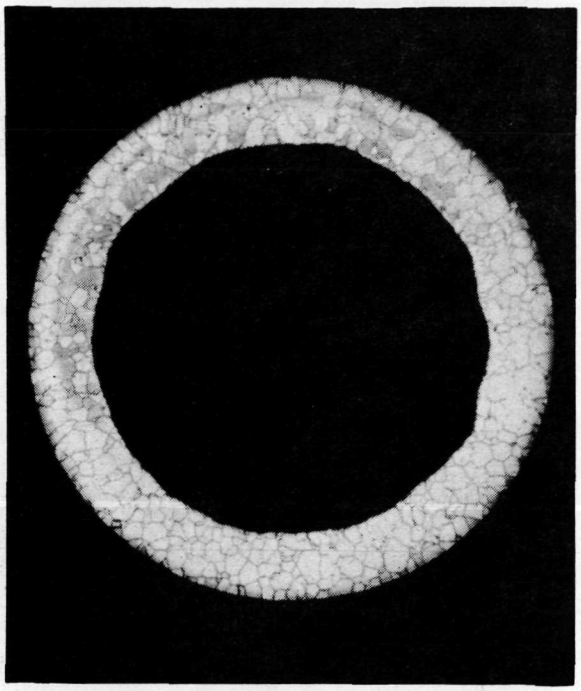

TEST L8-3AF ETCHED

X500

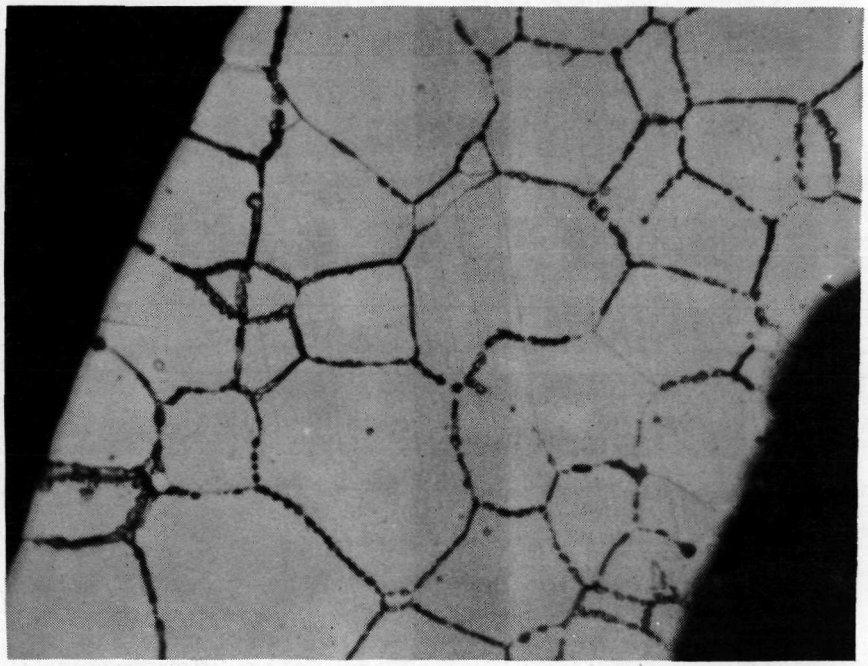

TEST L8-3AF ETCHED

Figure 60

Pt-20Ir TUBE AFTER 160 HOURS AT 1245° K WITH OXIDIZING PROPELLANT

X50

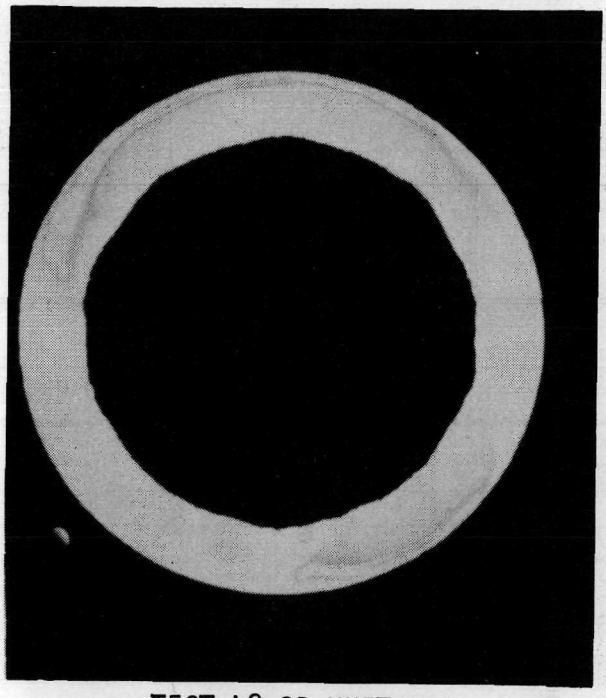

TEST L8-3D UNETCHED

X50

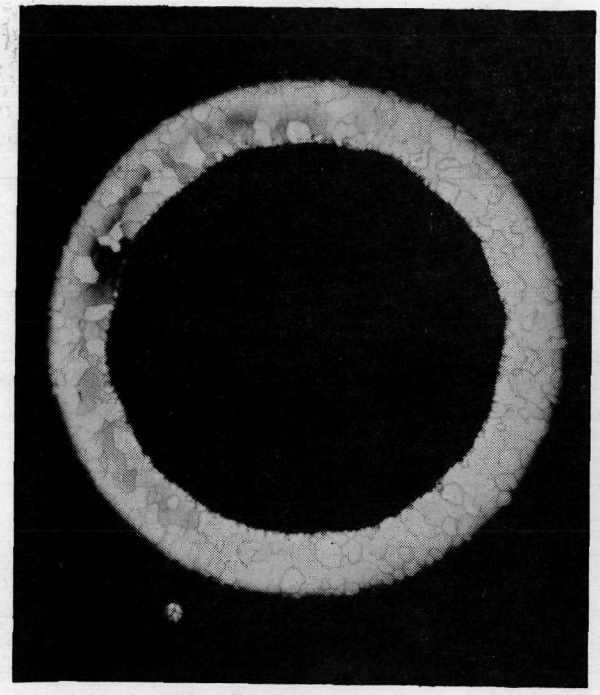

TEST L8-3D ETCHED

X500

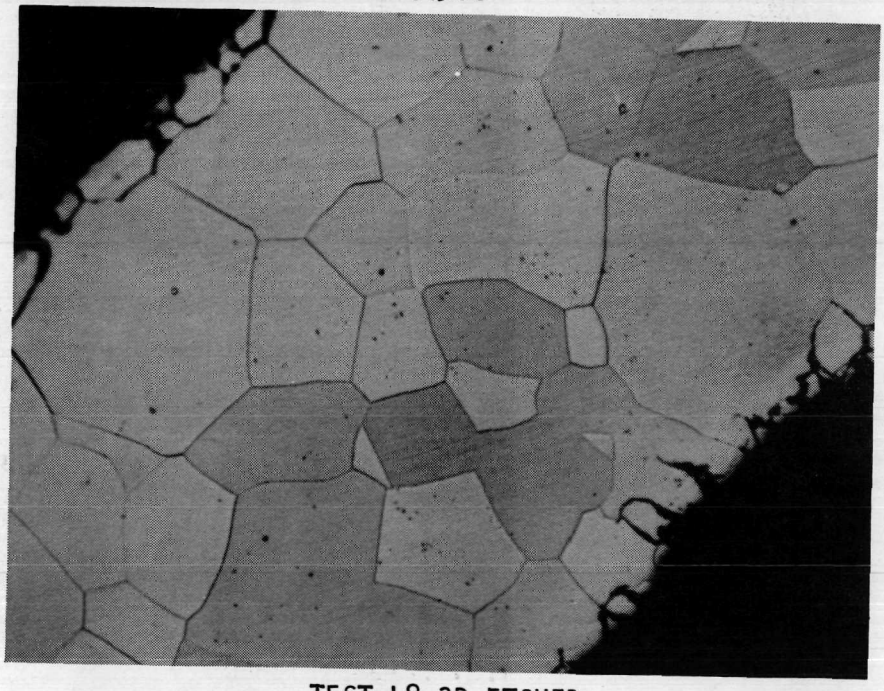

TEST L8-3D ETCHED

Figure 61

MECHANICAL DEFECTS IN Pt-30Ir TUBE AS RECEIVED - ETCHED - X200

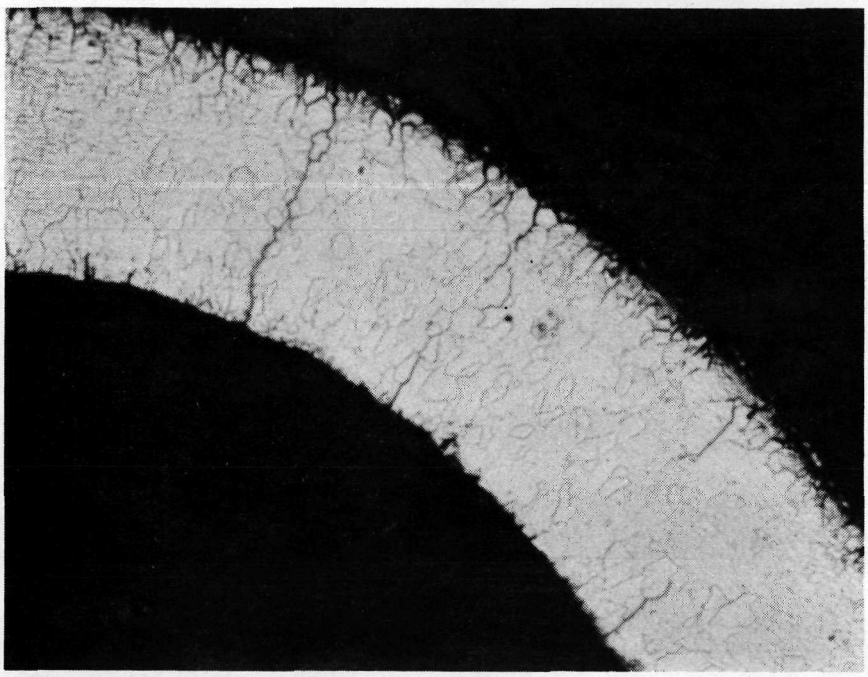

Figure 62

TEST R5 TUBES AFTER 100 HOURS AT 1400°K

CO_2 + 1.0% O_2

X 50

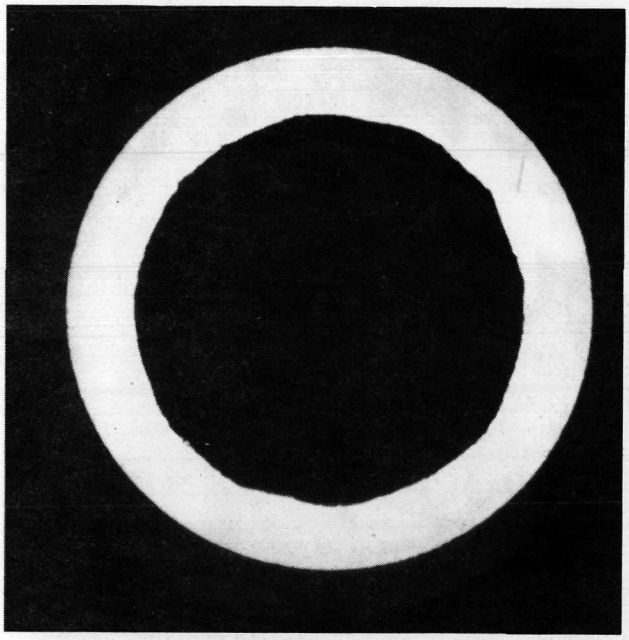

R5 -1 Pt -20 Ir (DRAWN)

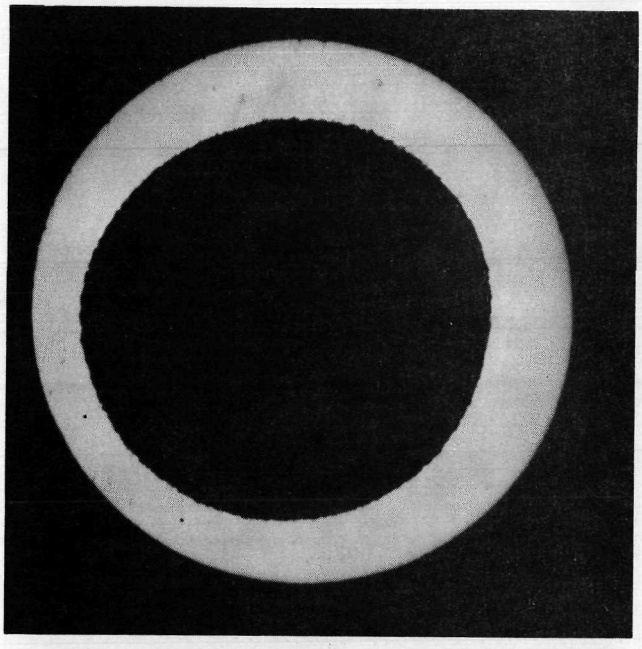

R5 -3 Pt -20 Ir (ELOXED)

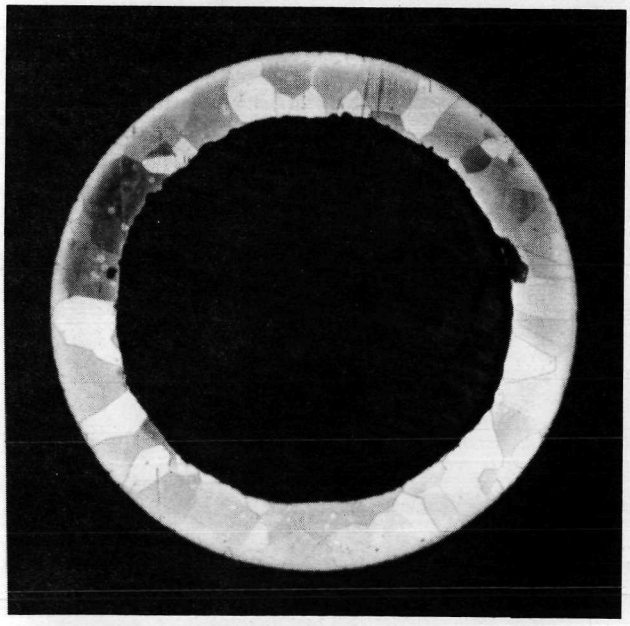

R5 -1 Pt -20 Ir (DRAWN) ETCHED

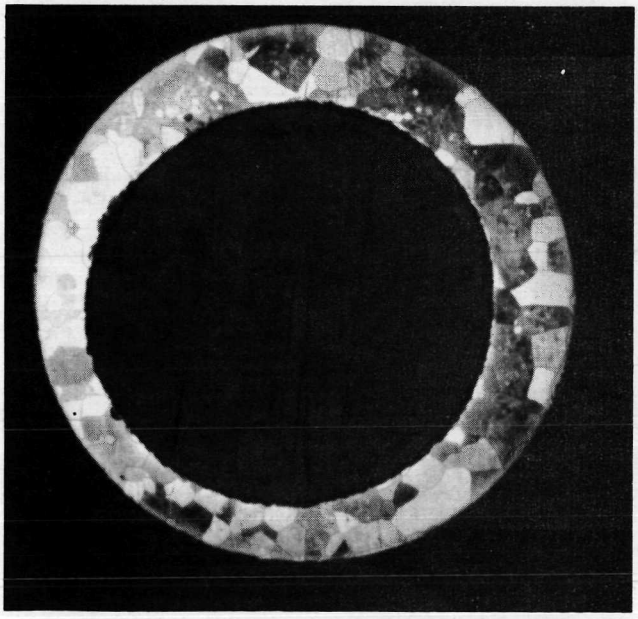

R5 -3 Pt -20 Ir (ELOXED) ETCHED

Figure 63

TEST R5 TUBES AFTER 100 HOURS AT 1500°K

CO_2 + 1.0% O_2

X 50

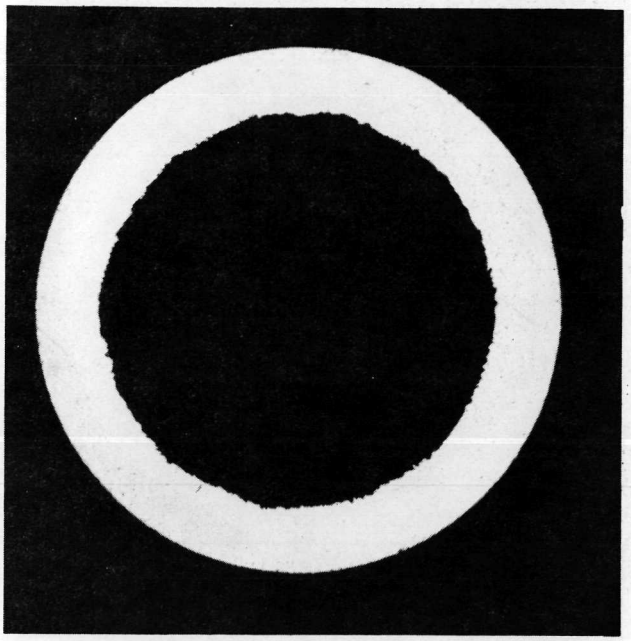

R5 -1 Pt -20 Ir (DRAWN)

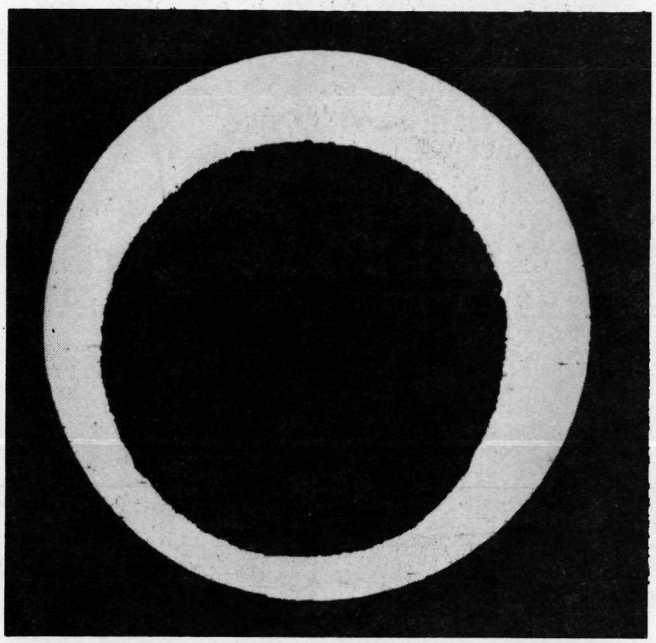

R5 -3 Pt -20 Ir (ELOXED)

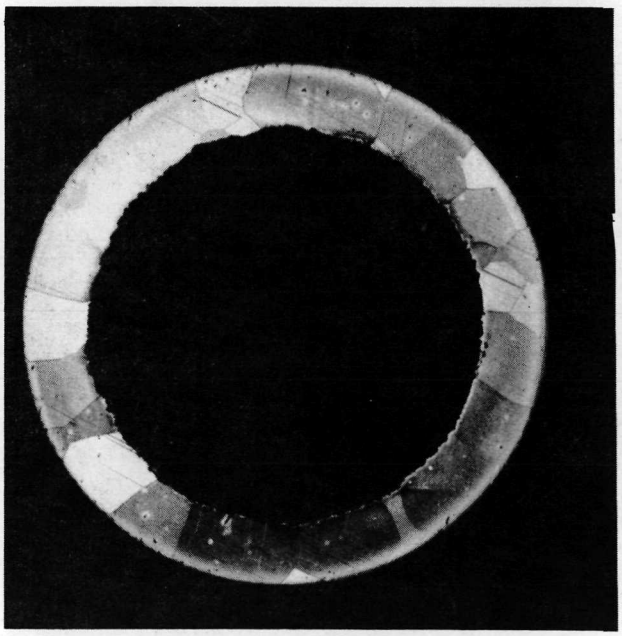

R5 -1 Pt -20 Ir (DRAWN) ETCHED

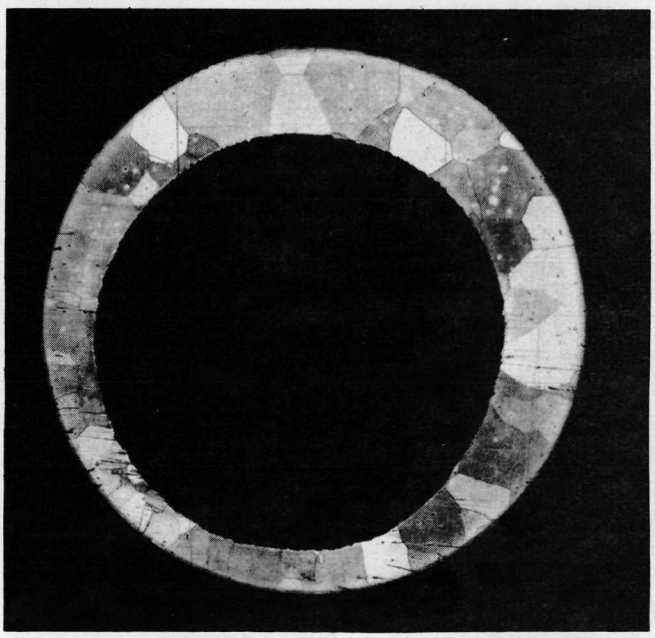

R5 -3 Pt -20 Ir (ELOXED) ETCHED

Figure 64

TEST R5 TUBES AFTER 100 HOURS AT 1570° K

CO_2 + 1.0% O_2

X 50

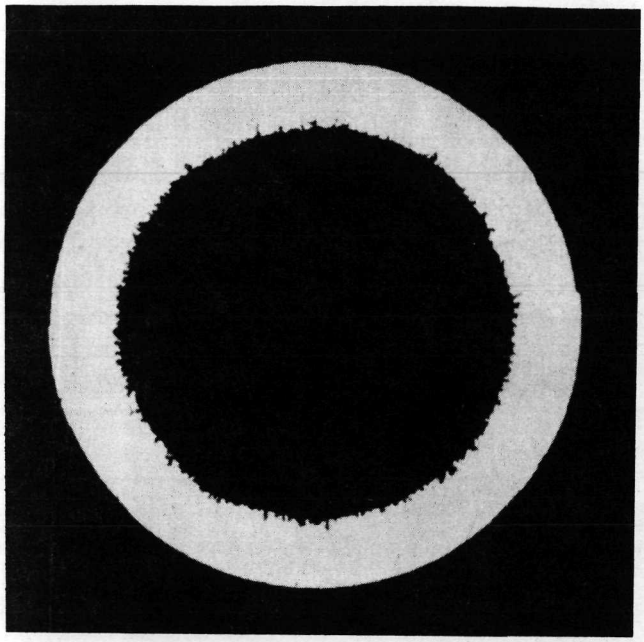

R5 -1 Pt -20 Ir (DRAWN)

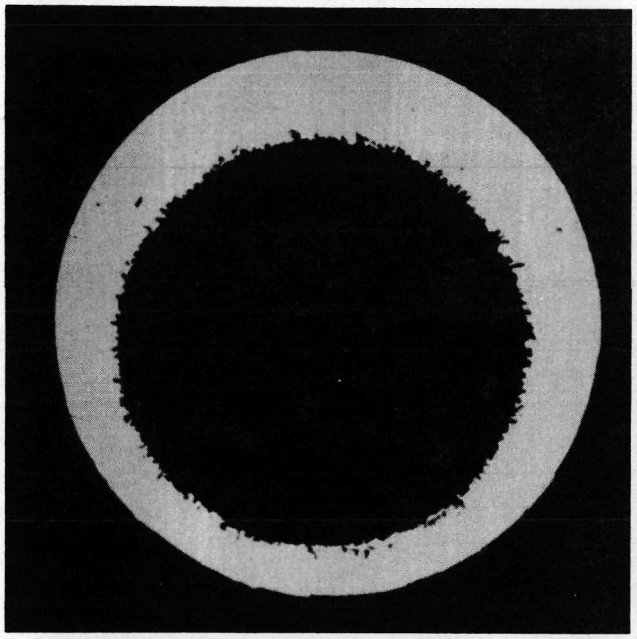

R5 -3 Pt -20 Ir (ELOXED)

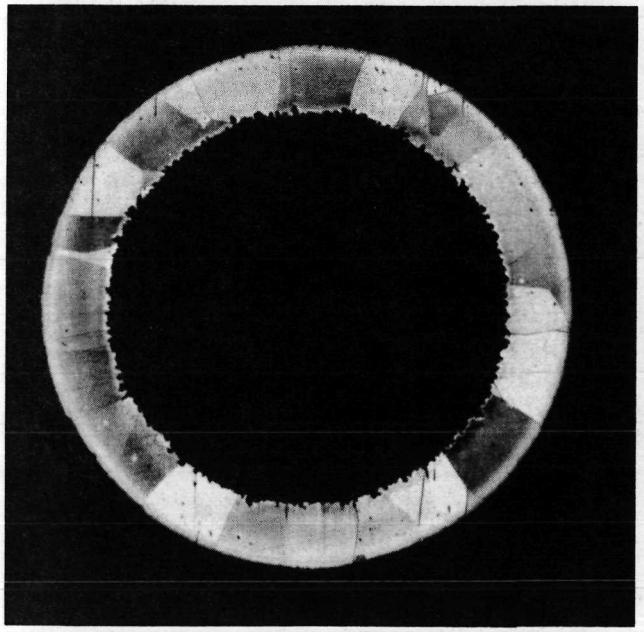

R5 -1 Pt -20 Ir (DRAWN) ETCHED

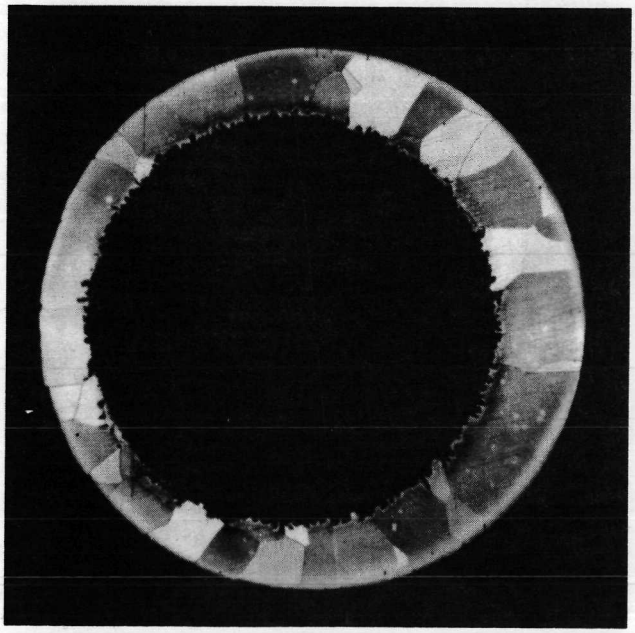

R5 -3 Pt -20 Ir (ELOXED) ETCHED

Figure 65

TEST R5 TUBES AFTER 100 HOURS AT 1400°K

CO_2 + 1.0% C_2

X500 ETCHED

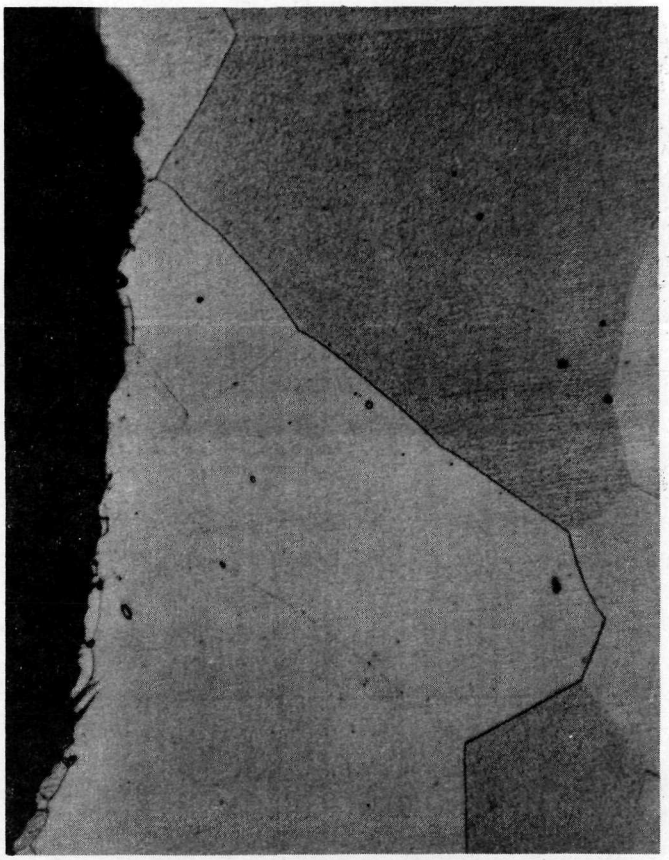

R5 -1 Pt -20 Ir (DRAWN)

R5 -3 Pt -20 Ir (ELOXED)

Figure 66

TEST R5 TUBES AFTER 100 HOURS AT 1570^{0}K

CO_2 + 1.0% O_2

X500 ETCHED

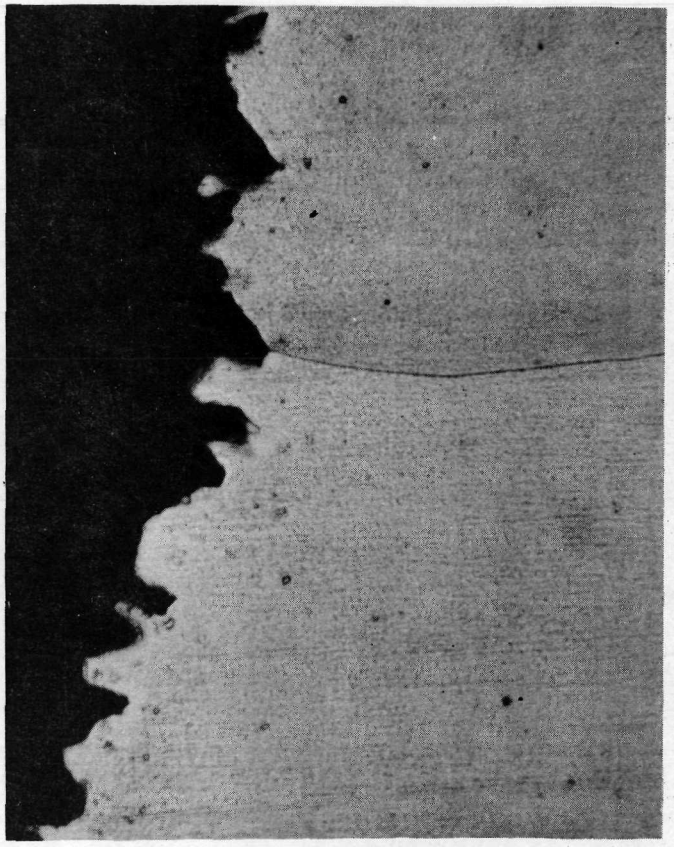

R5 -1 Pt -20 Ir DRAWN

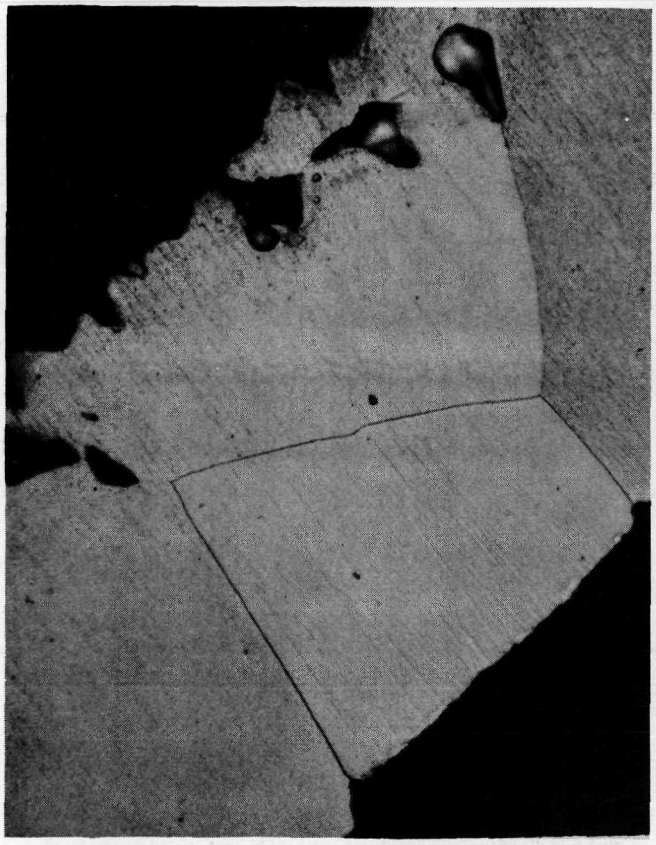

R5 -3 Pt -20 Ir (ELOXED)

Figure 67

PLATINUM - 20% PALLADIUM TUBE PRIOR TO TESTING

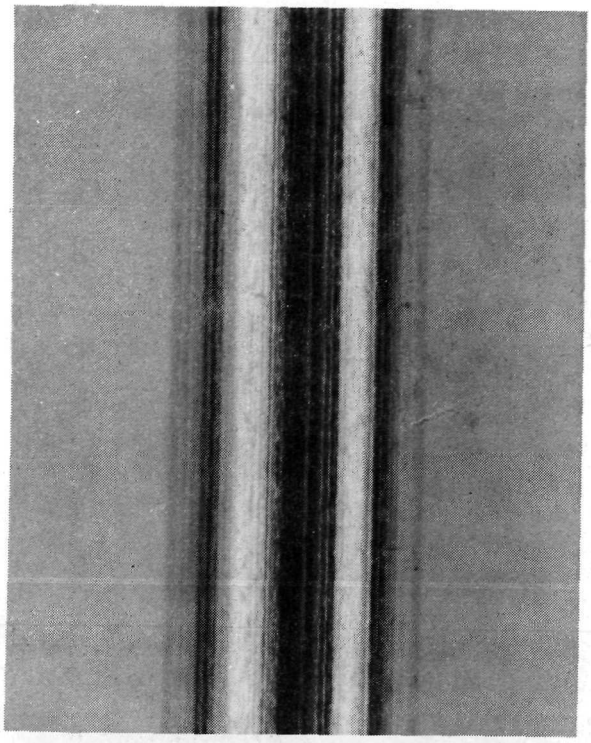

X25

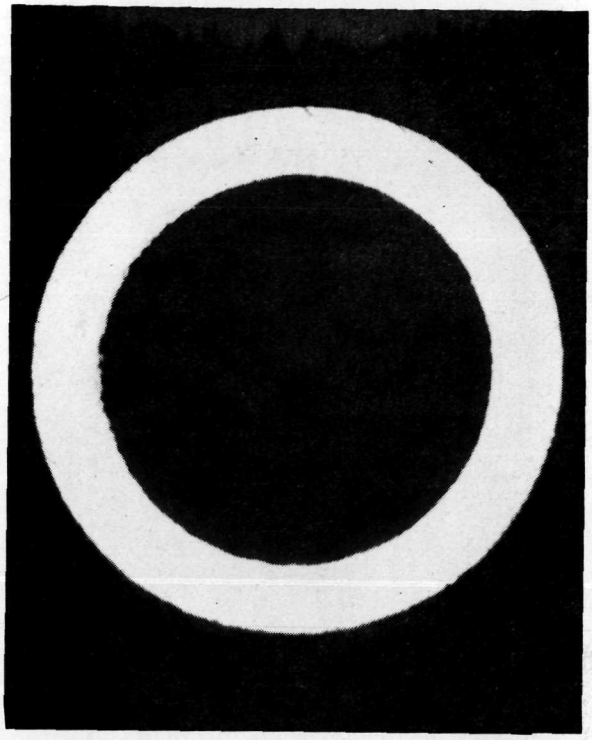

X50

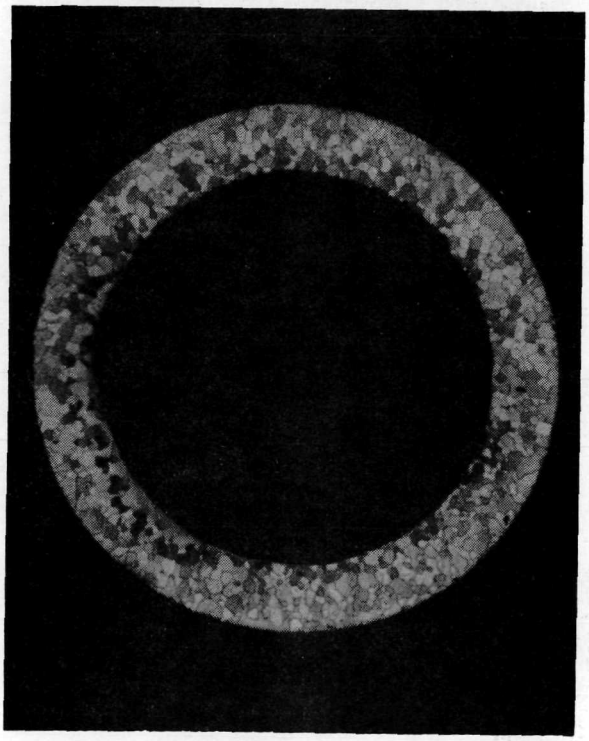

X50 ETCHED

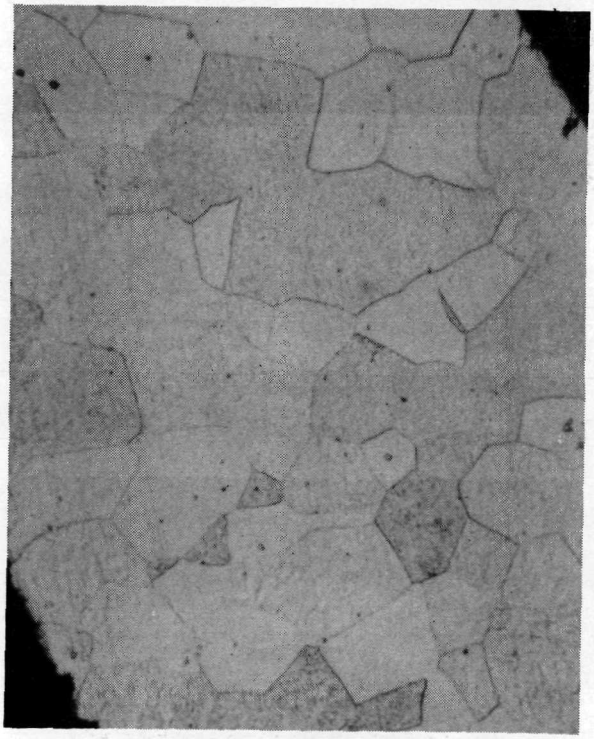

X500 ETCHED

Figure 68

TEST R6 Pt-20Pd TUBE AFTER 500 HOURS AT 1600° K

CO_2 + 1.5% O_2

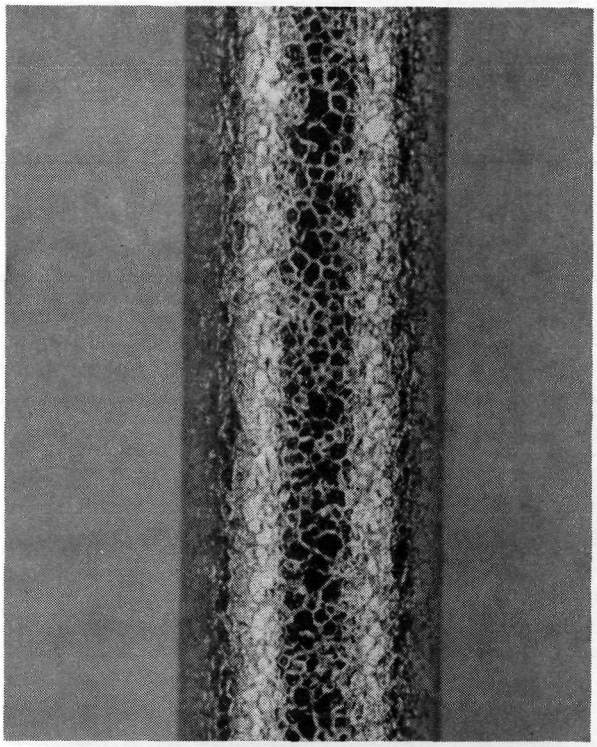

X 25

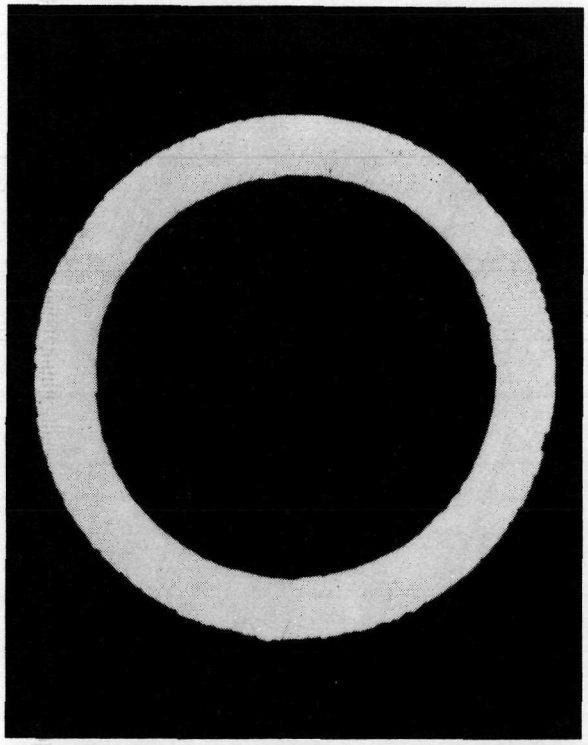

X 50

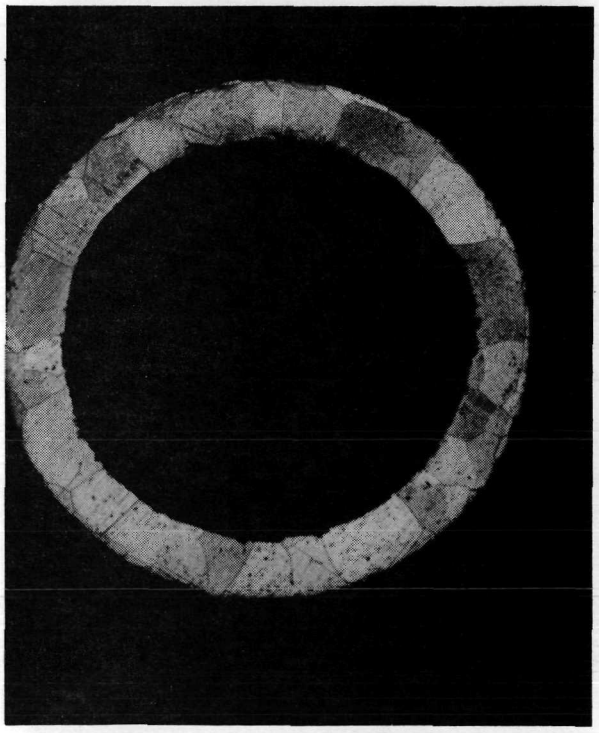

X 50 ETCHED

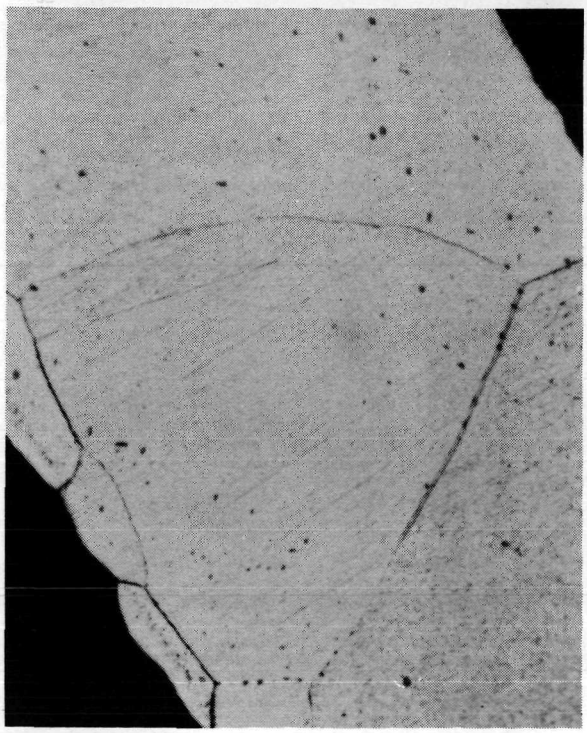

X 500 ETCHED

Figure 69

TEST L10-1 Pt-20Pd TUBE AFTER 1000 HOURS AT 1500° K

CO_2 + 1.5% O_2

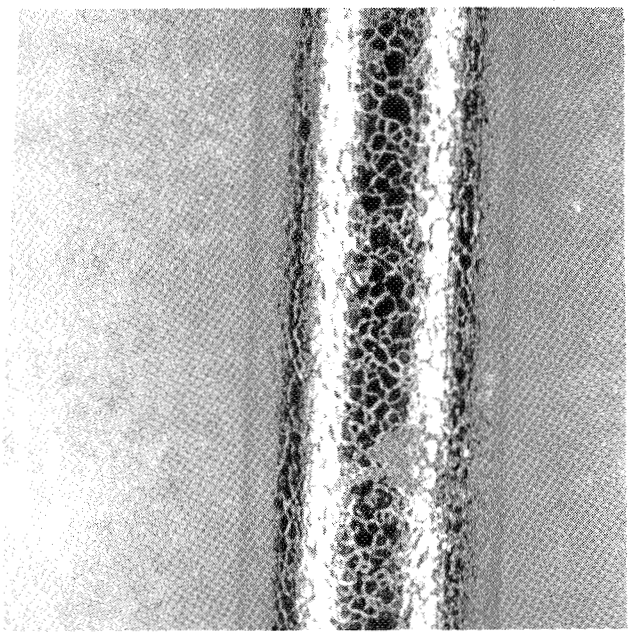

X 25

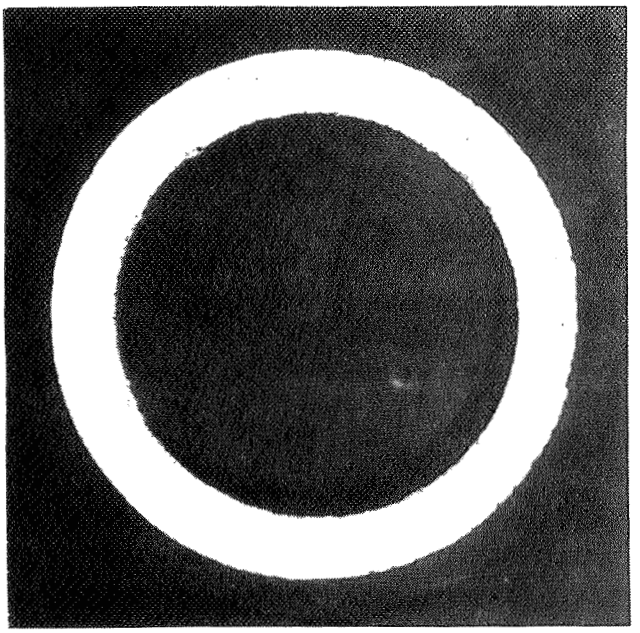

X 50

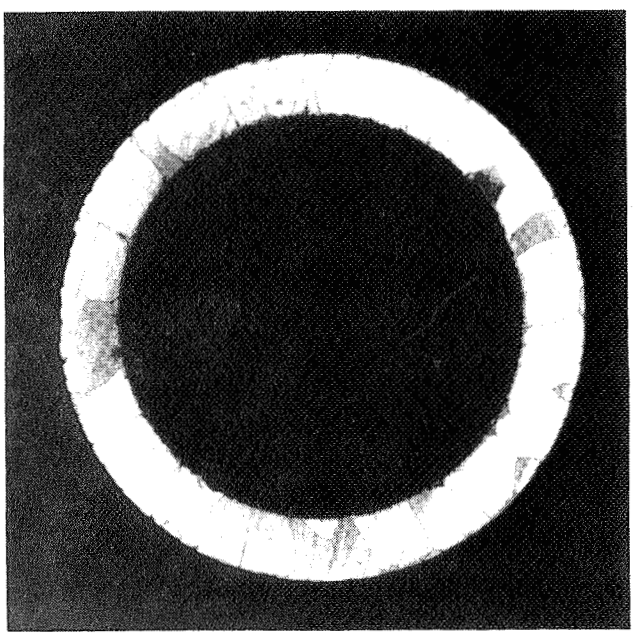

X 50 ETCHED

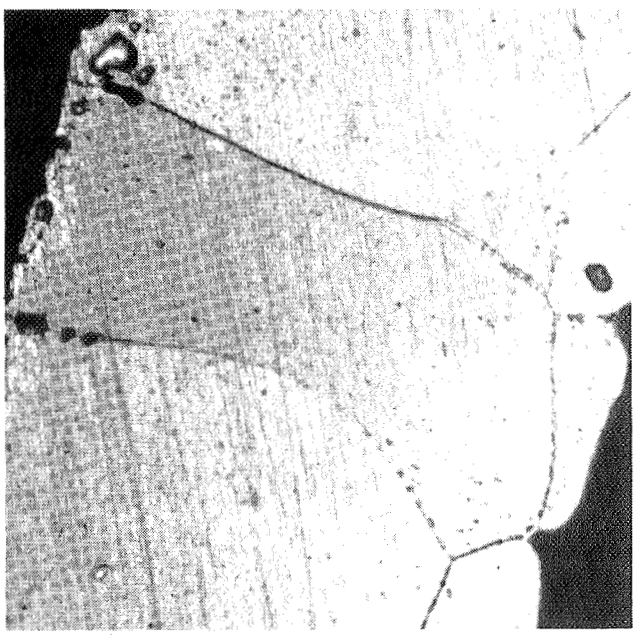

X 500 ETCHED

Figure 70

PLATINUM TUBE PRIOR TO TESTING

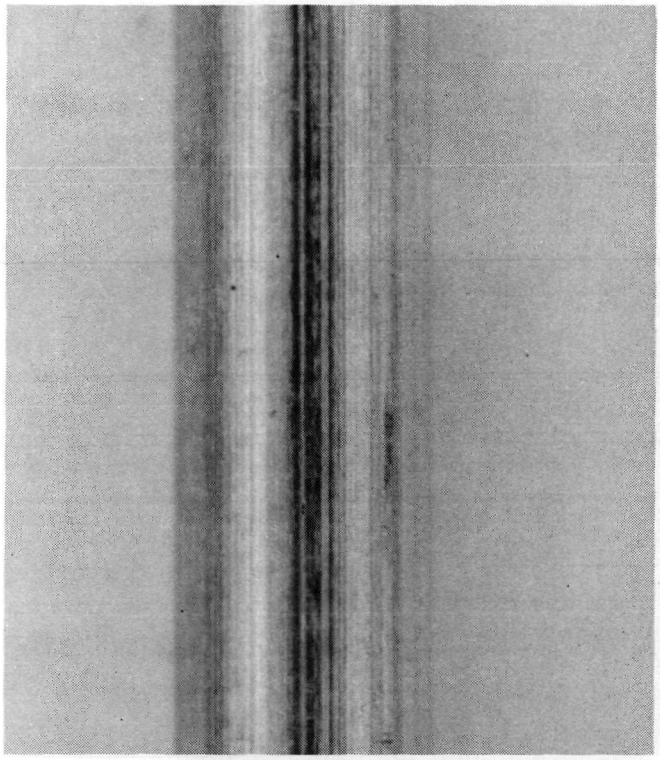

X25

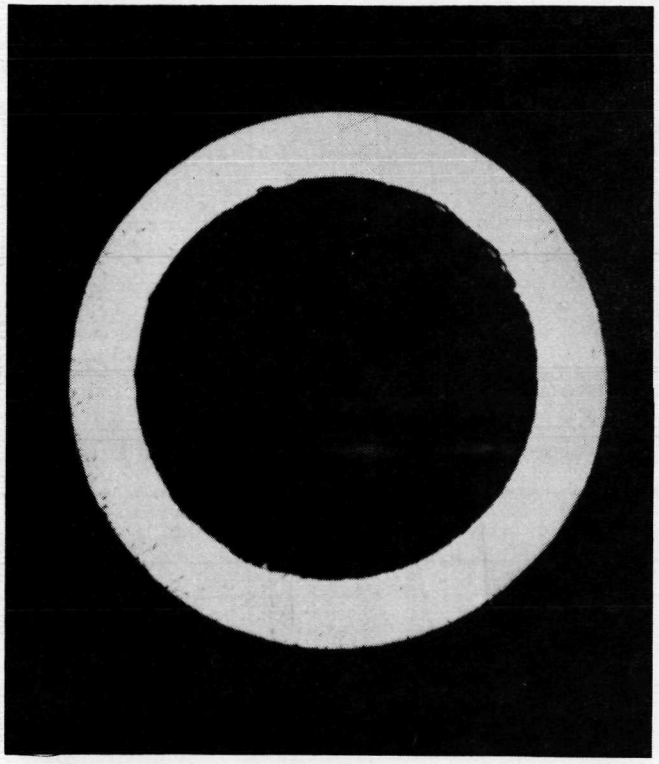

X50

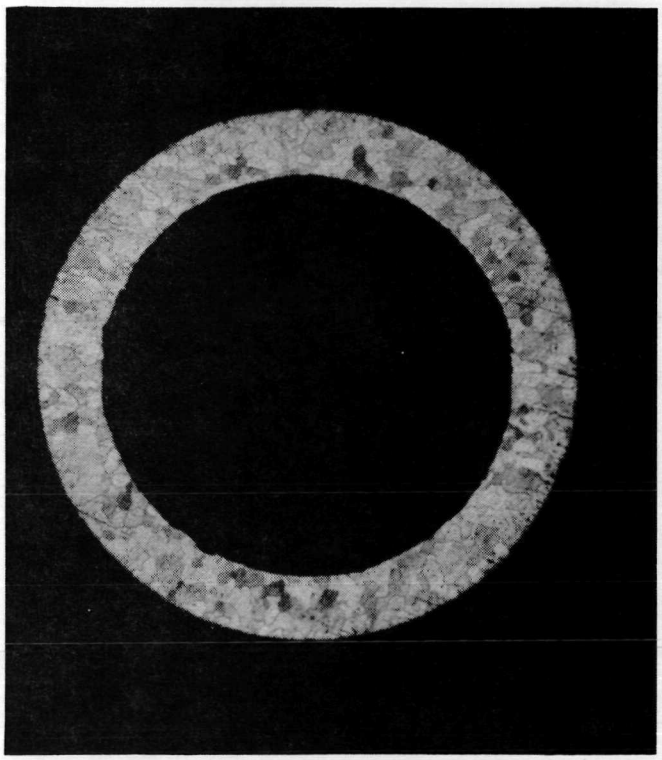

X50 ETCHED

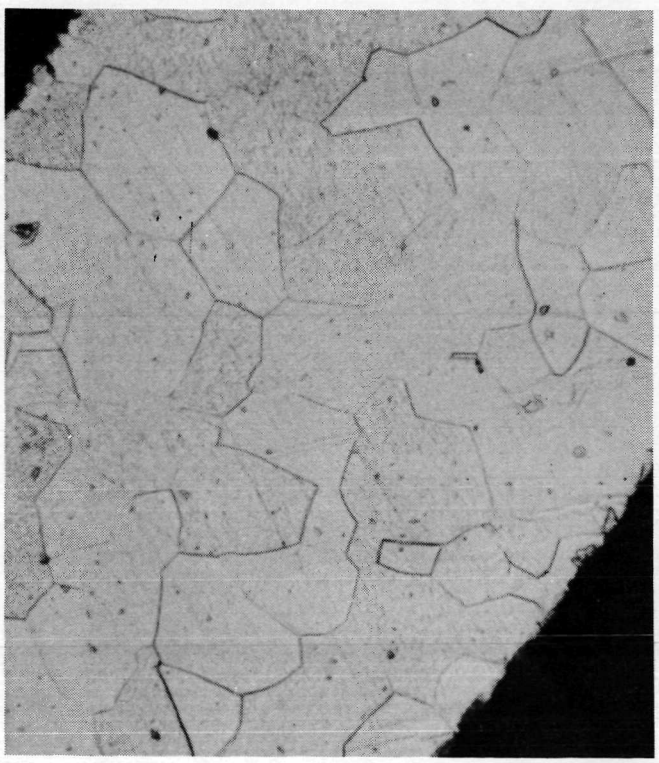

X500 ETCHED

Figure 71

TEST L10-3A PLATINUM TUBE AFTER 125 HOURS AT 1600° K

CO_2 + 1.5% O_2

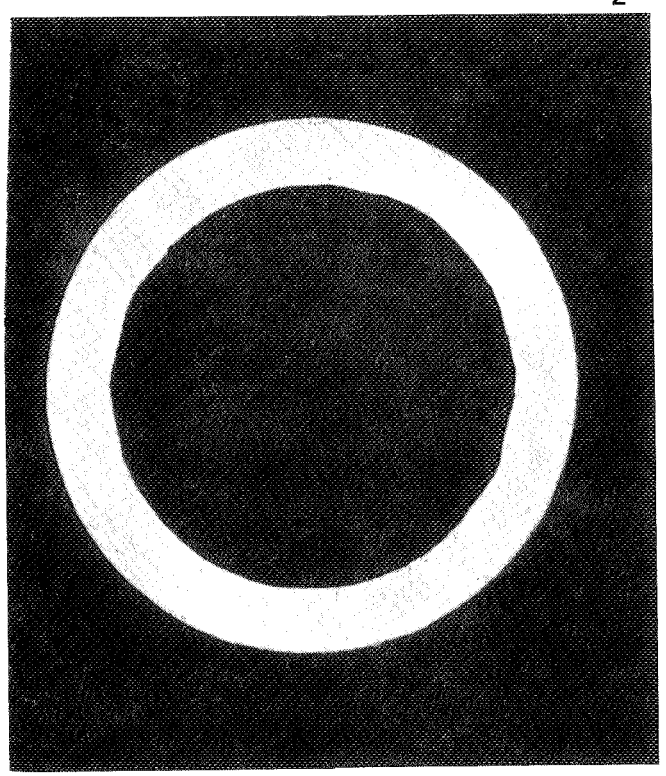

X 50

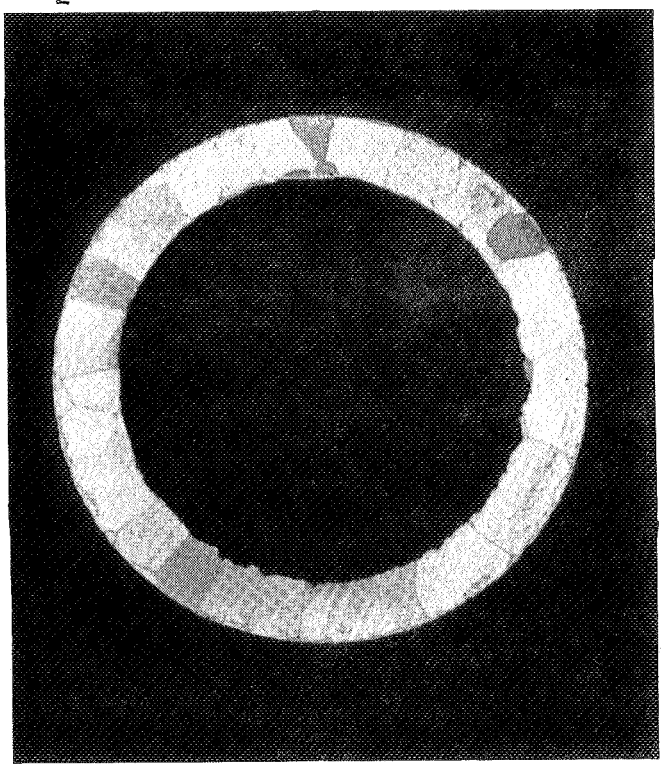

X 50 ETCHED

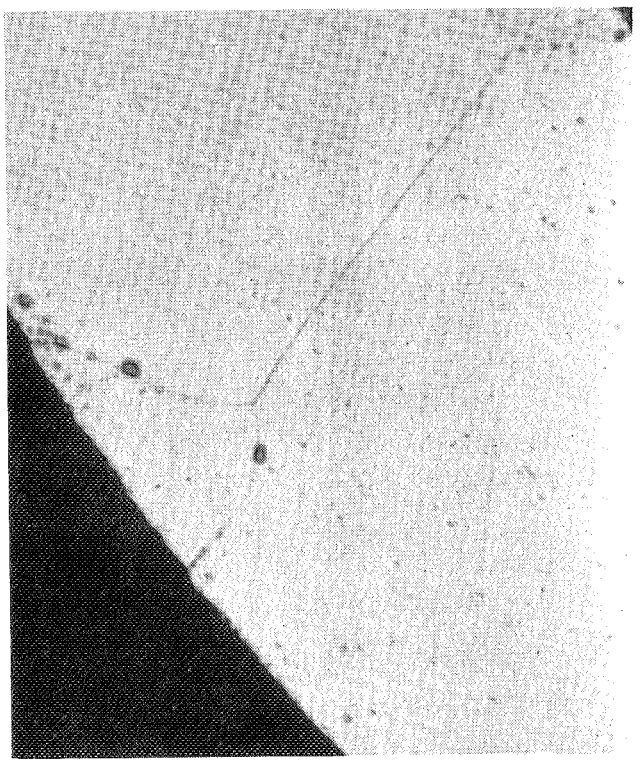

X 500 ETCHED

Figure 72

TEST L10-3 PLATINUM TUBE AFTER 800 HOURS AT 1500° K

CO_2 + 1.5% O_2

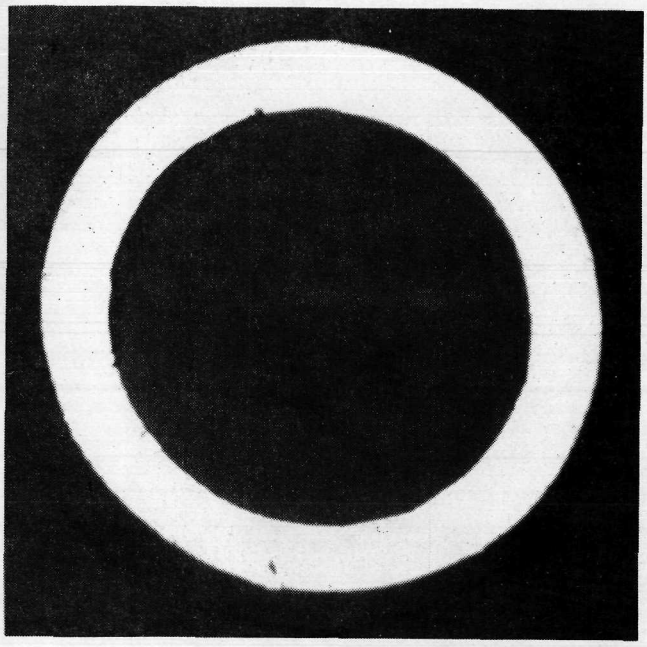

X 50

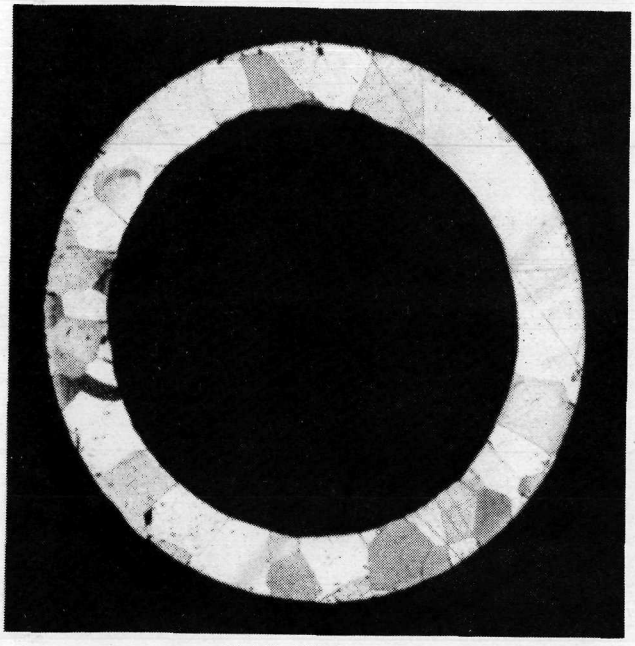

X 50 ETCHED

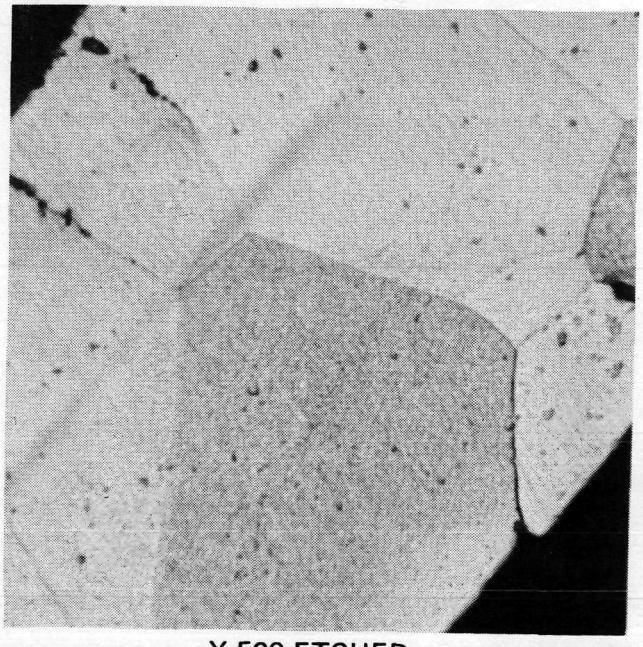

X 500 ETCHED

Figure 73

TEST L10-3 PLATINUM TUBE AFTER 800 HOURS AT 1600° K

CO_2 + 1.5% O_2

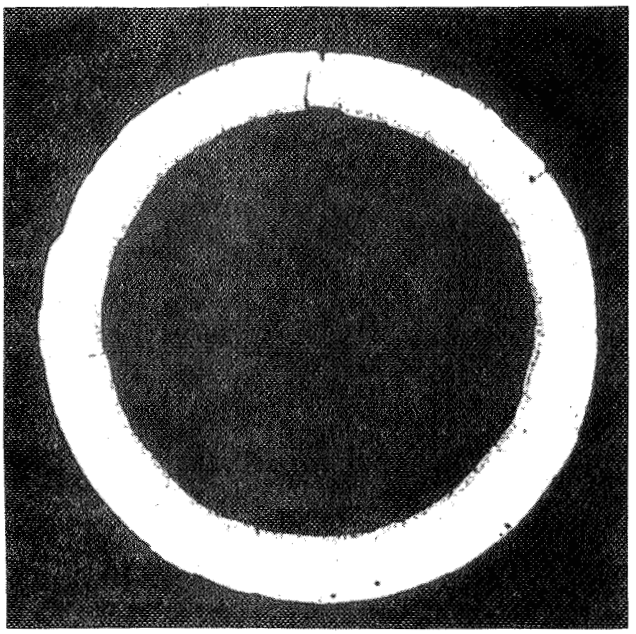

X 50

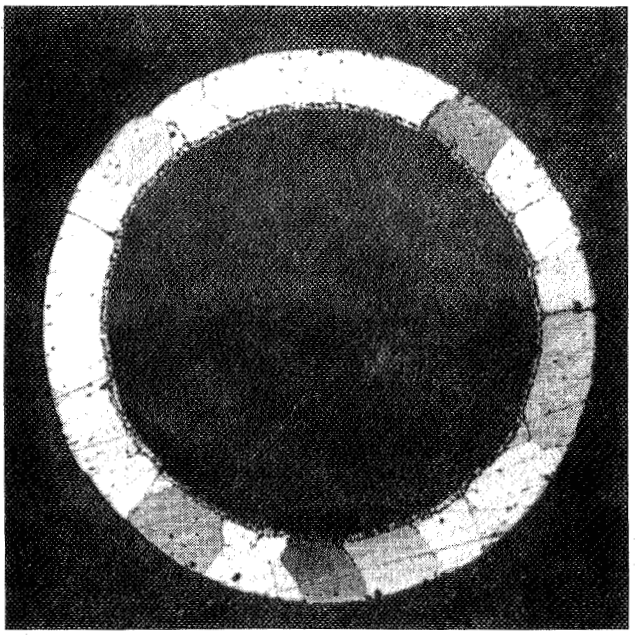

X 50 ETCHED

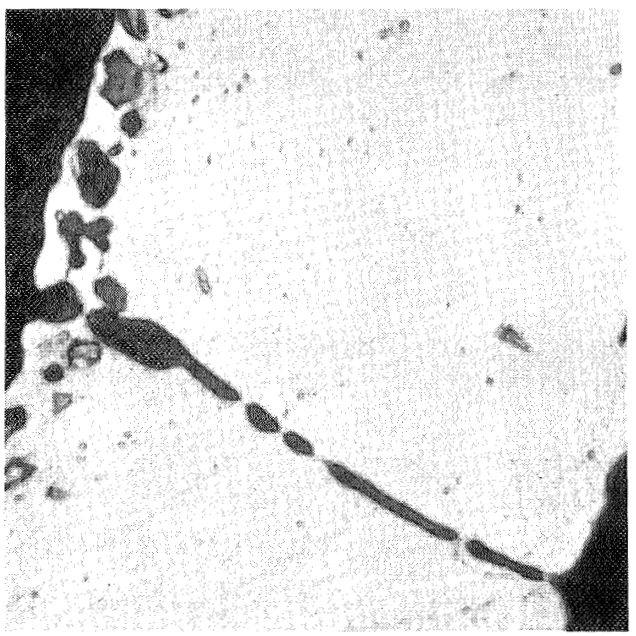

X 500 ETCHED

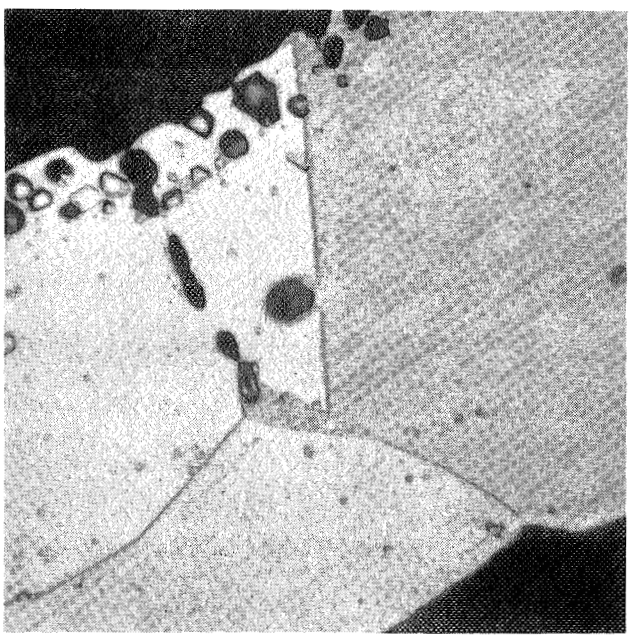

X 500 ETCHED

Figure 74

TEST R6 - 3 PLATINUM TUBE AFTER 1036 HOURS AT 1600°K

CO_2 + 1.5% O_2

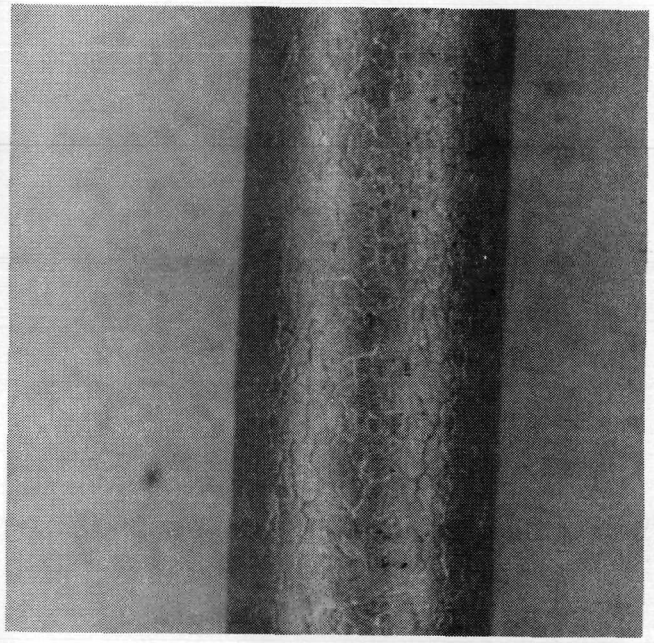

X 25

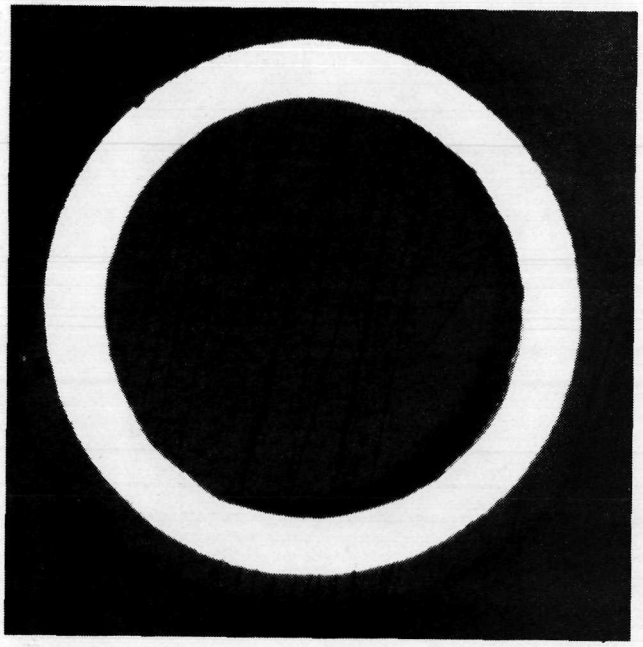

X 50

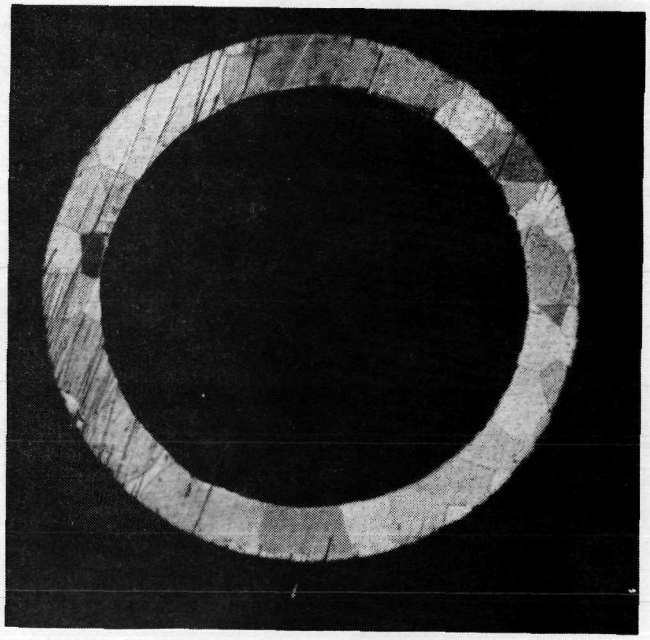

X 50 ETCHED

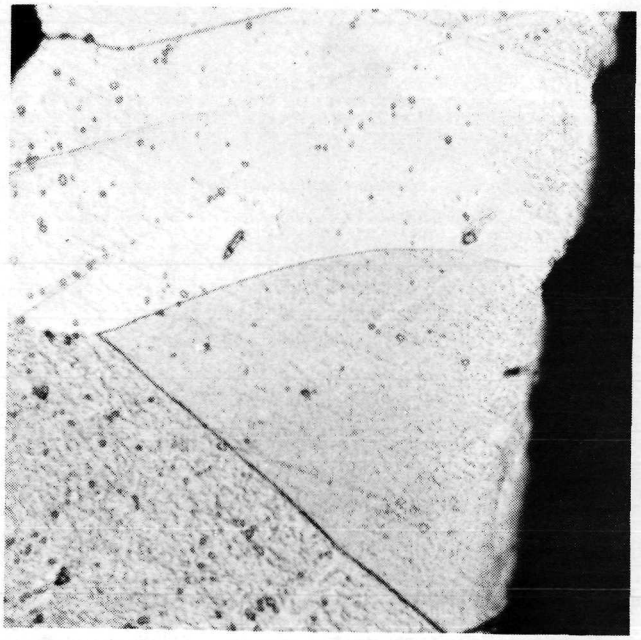

X 500 ETCHED

Figure 75

TEST R6-3 PLATINUM TUBE AFTER 1036 HOURS AT 1700° K

$CO_2 + 1.5\% O_2$

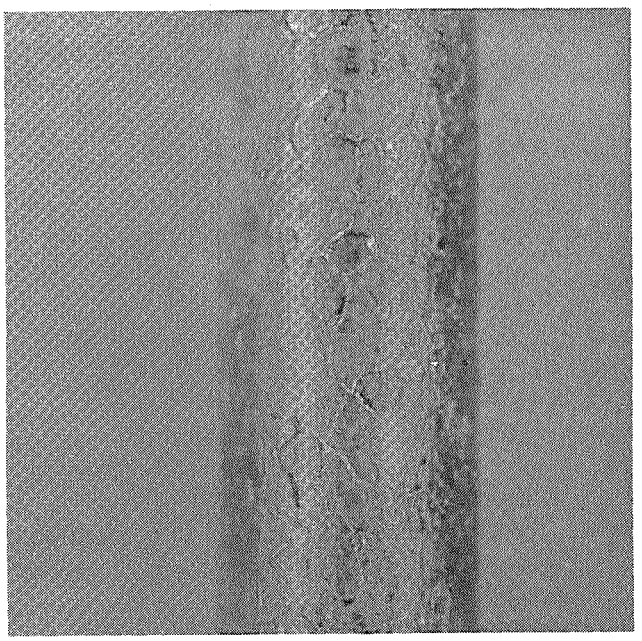

X 25

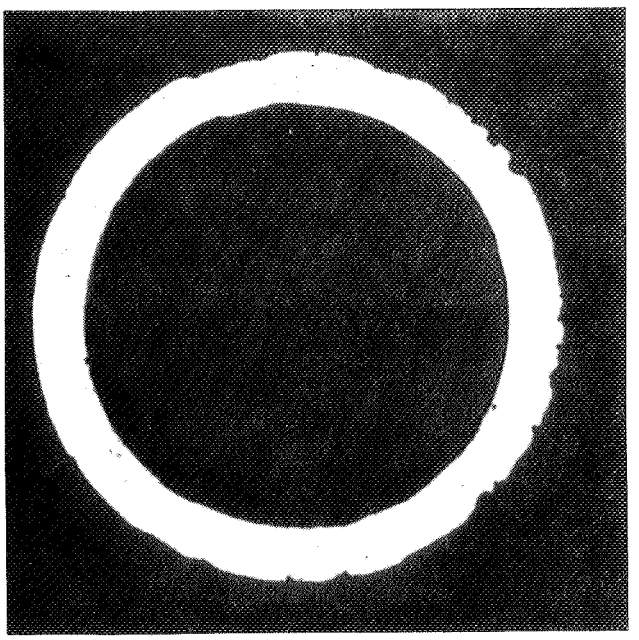

X 50

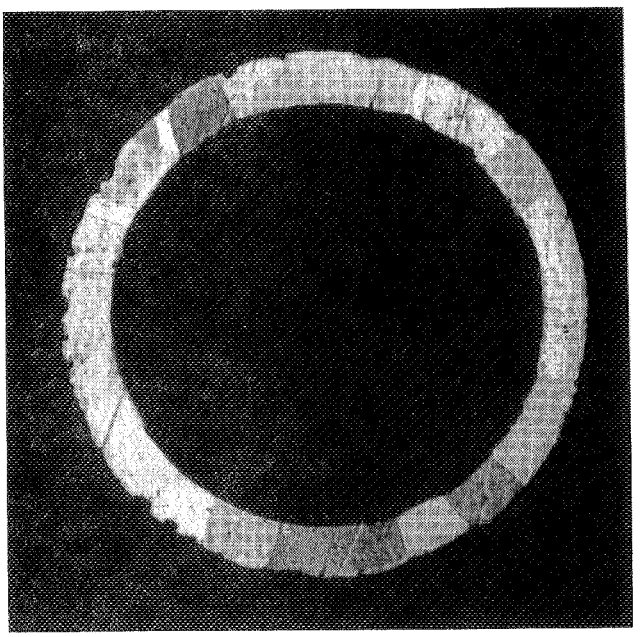

X 50 ETCHED

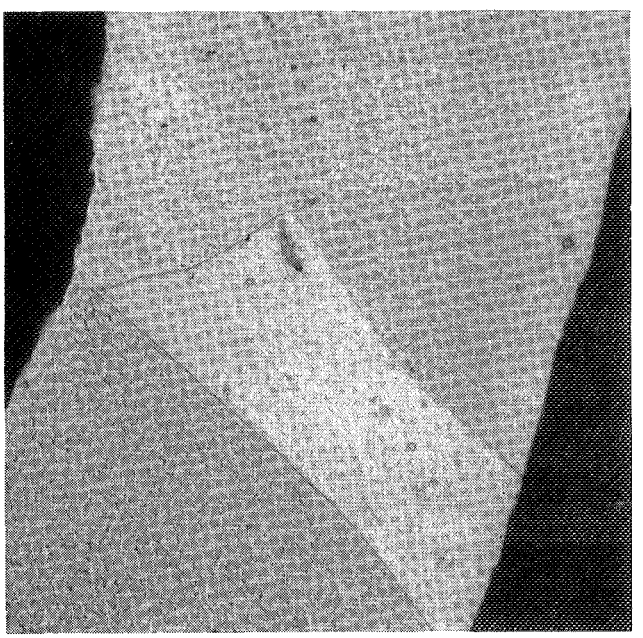

X 500 ETCHED

Figure 75

CROSS SECTIONS OF $Pt-ThO_2$ TUBES

X50 ETCHED

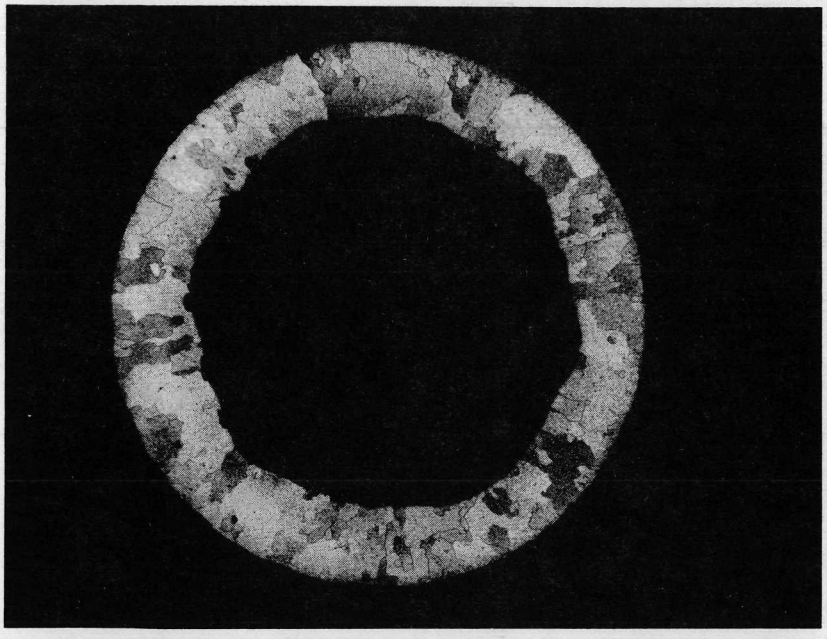

AS RECEIVED

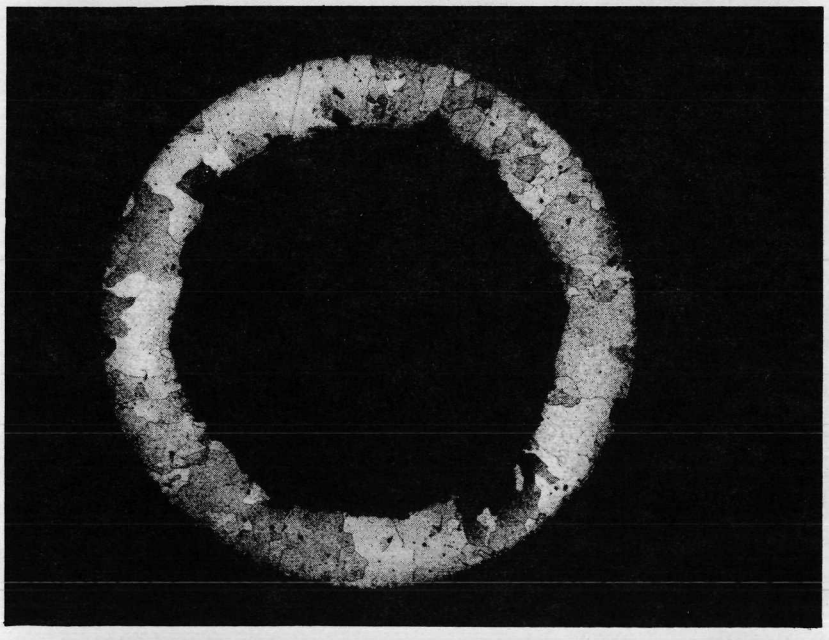

AFTER EXPOSURE TO CO_2 AT 1509 ^{o}K FOR 429 HOURS

Figure 77

PHOTOMICROGRAPHS OF 0.6% TD-Pt TUBE AS RECEIVED

X50

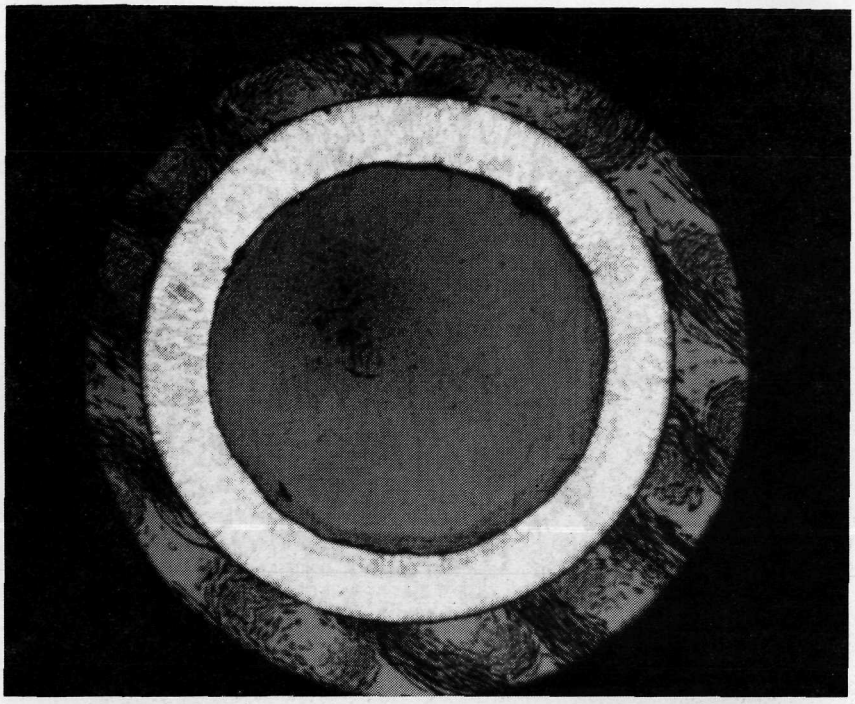

X500

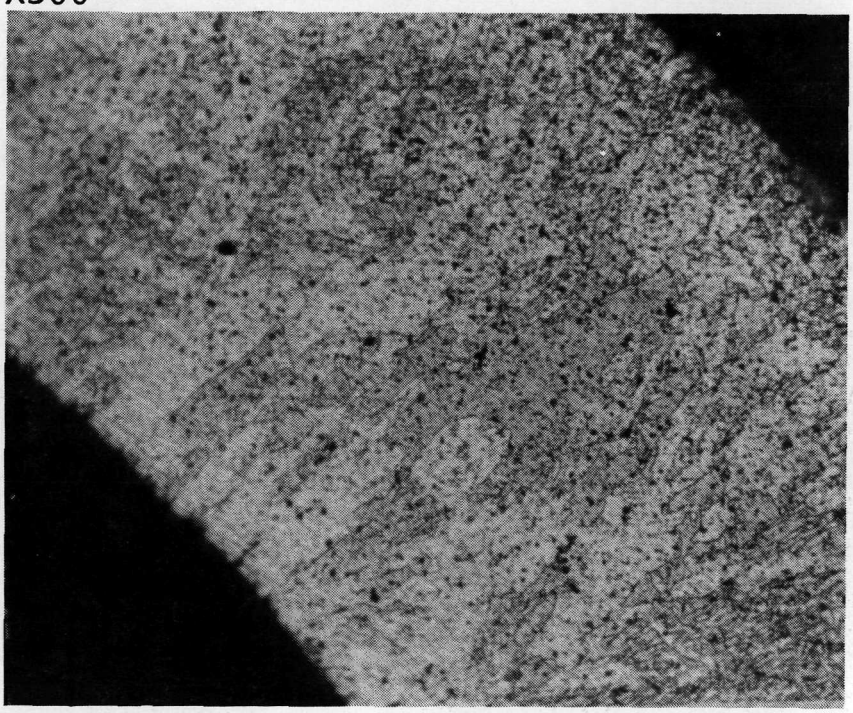

Figure 78

EXTERNAL SURFACE OF 0.6% TD-Pt TUBE AS RECEIVED

X50

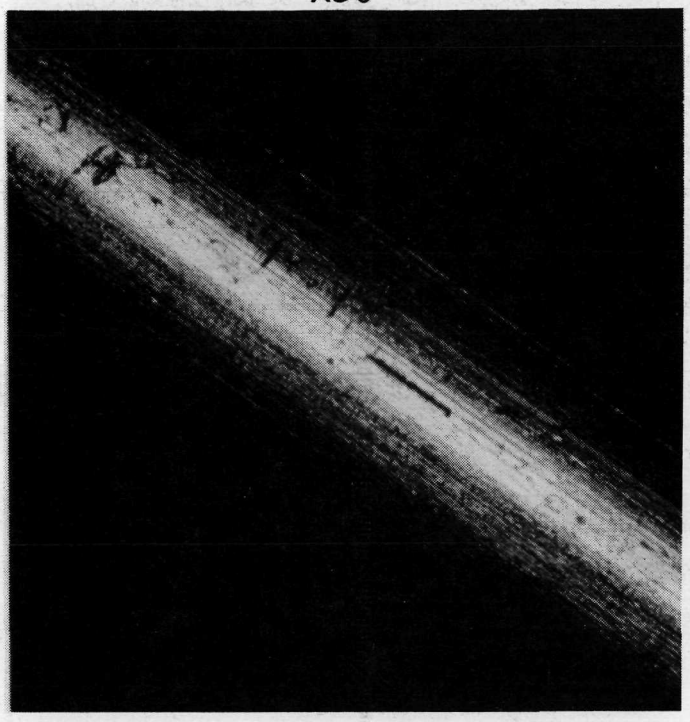

X200

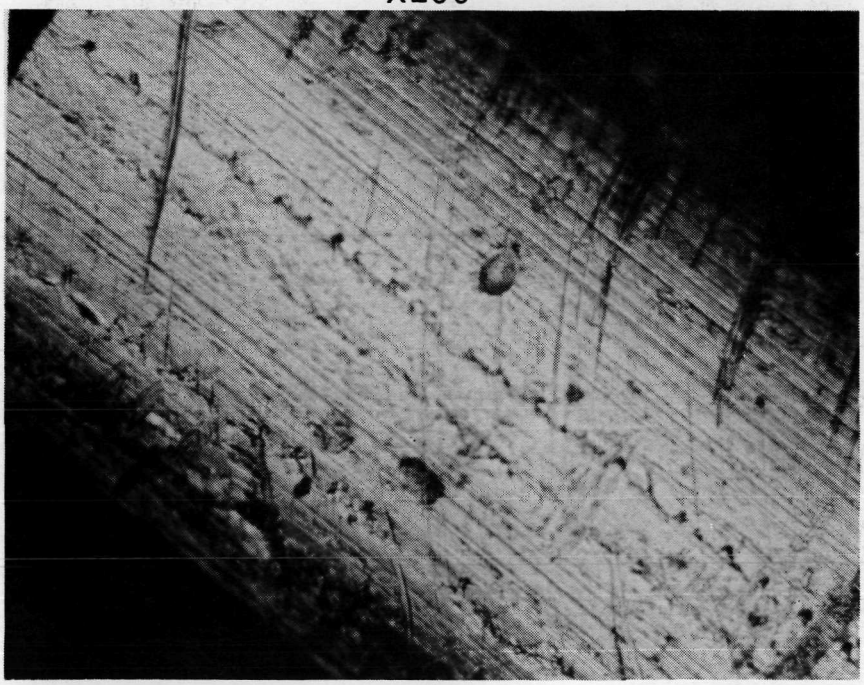

Figure 79

TEST R5
TUBE NO. 2 - AVERAGE TEST TEMPERATURE

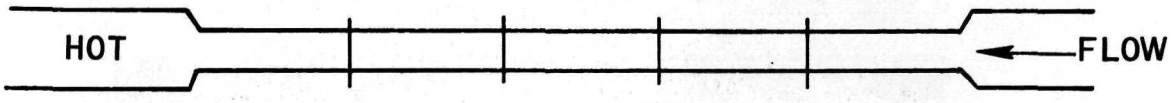

Pt-0.6ThO$_2$

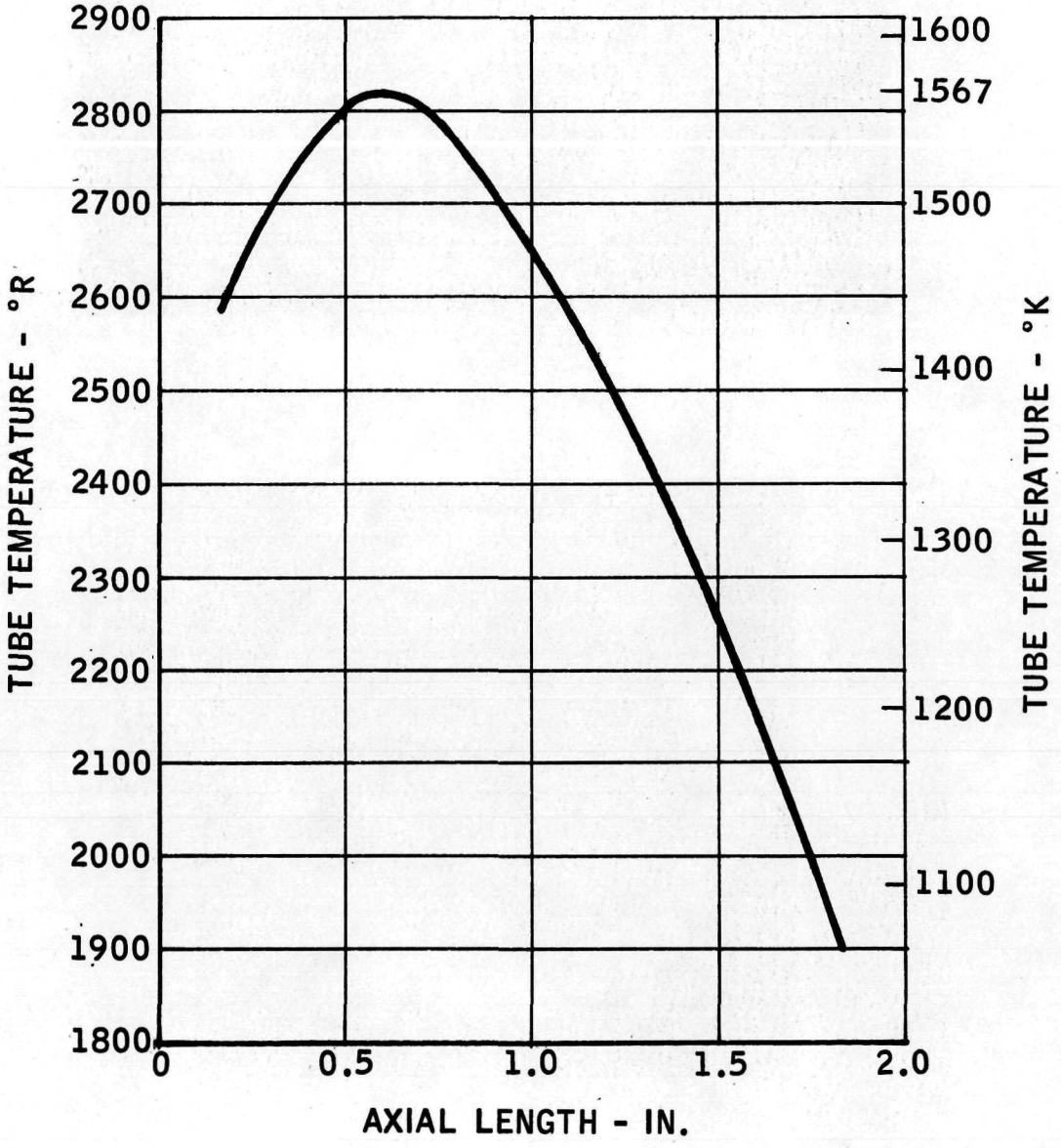

Figure 80

TEST R5 TD-Pt TUBE AFTER 100 HOURS AT 1400° K

CO_2 + 1.0% O_2

X 50

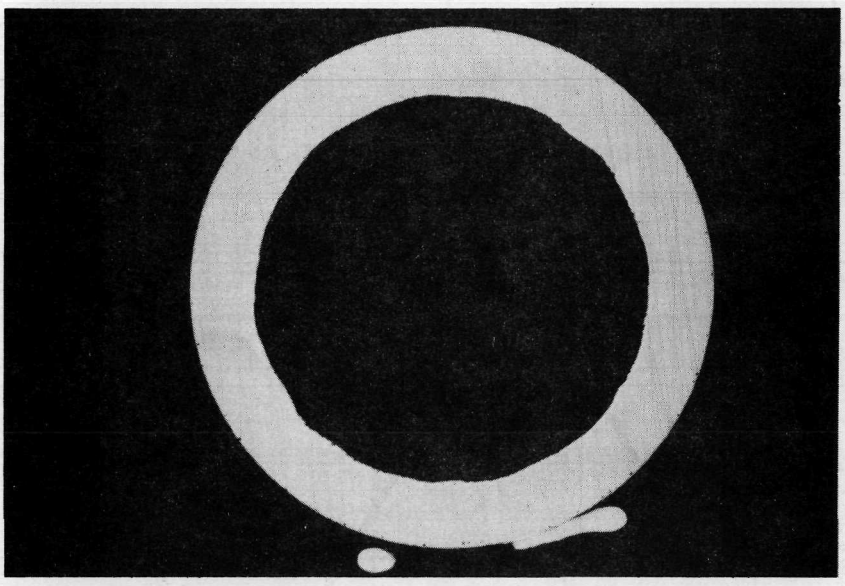

R5 -2

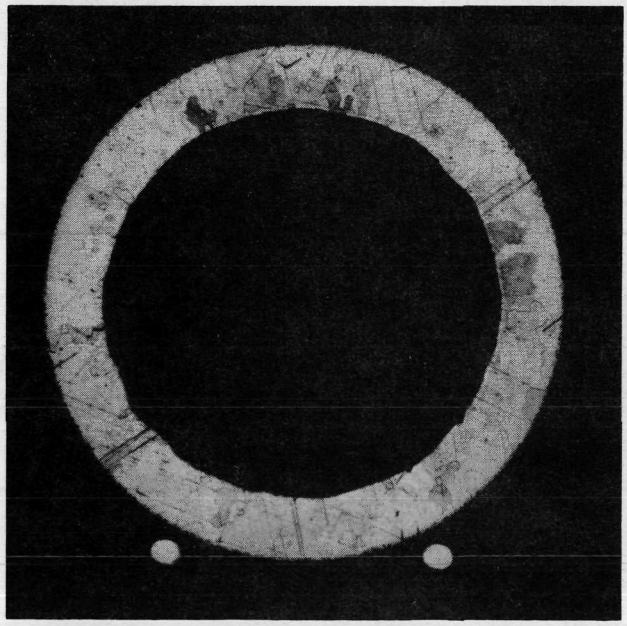

R5 -2 ETCHED

Figure 81

TEST R5 TD-Pt TUBE AFTER 100 HOURS AT 1500° K

CO_2 + 1.0% O_2

X 50

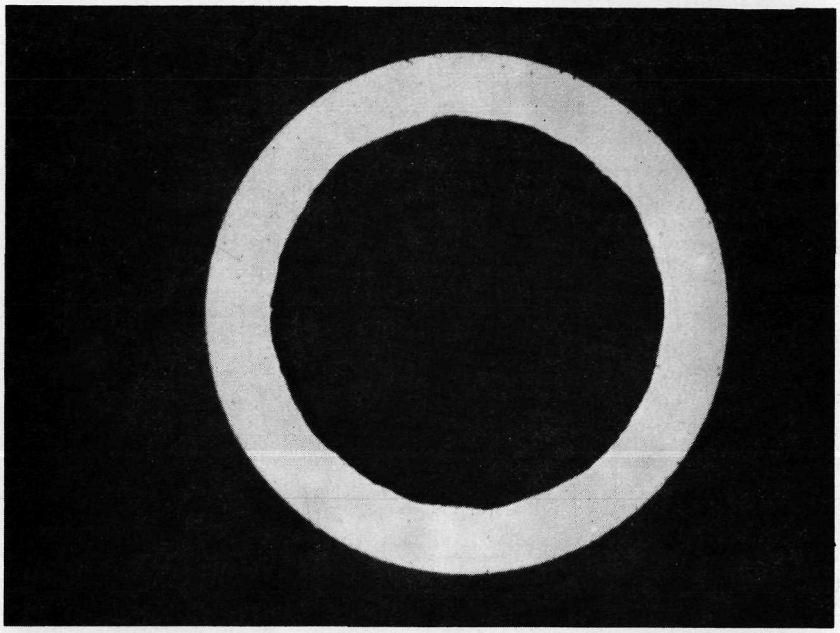

R5 -2

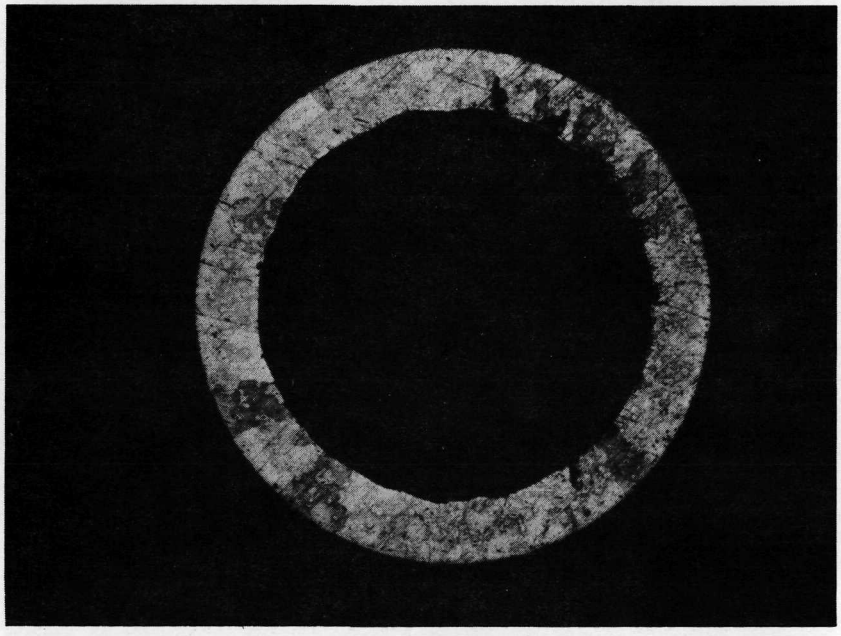

R5 -2 ETCHED

Figure 82

TEST R5 TD-Pt TUBE AFTER 100 HOURS AT 1570°K

CO_2 + 1.0% O_2

X 50

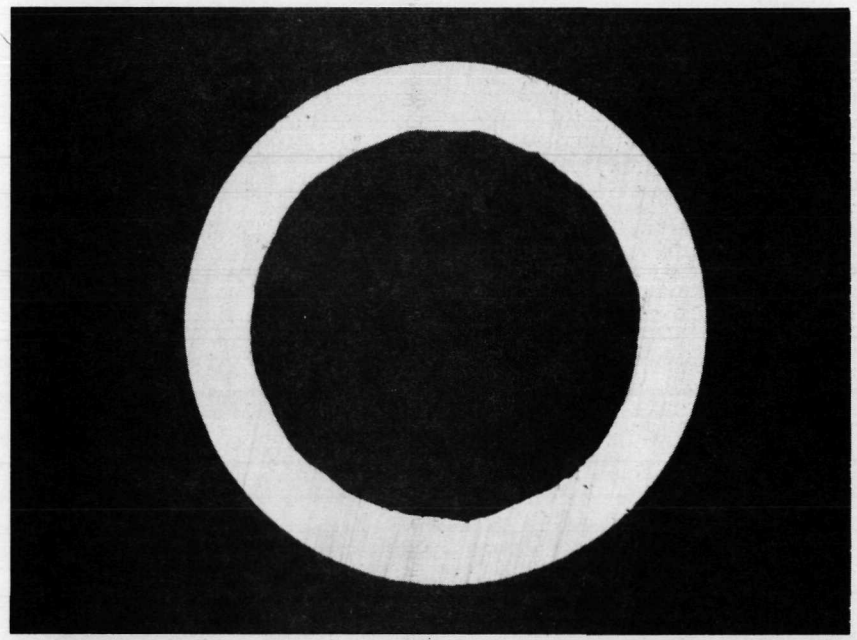

R5 -2

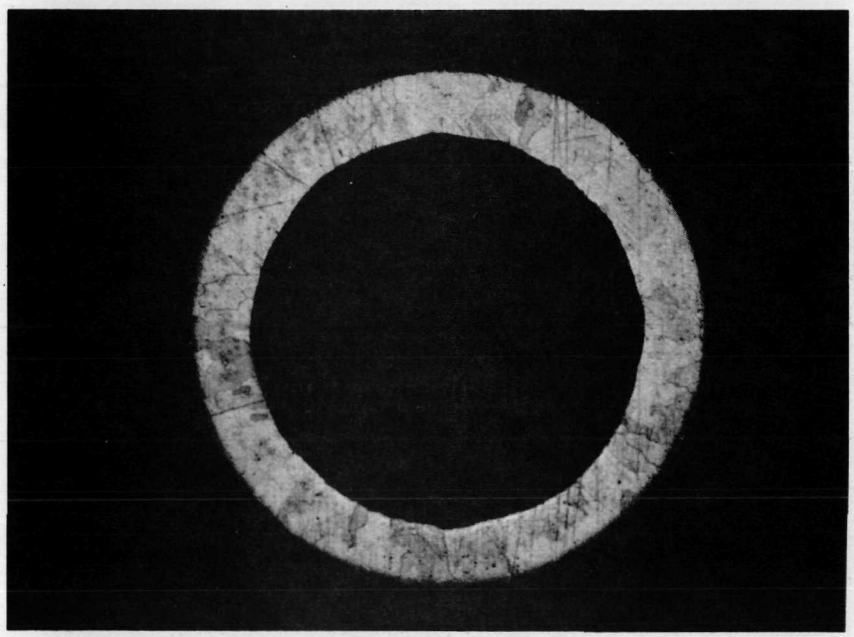

R5 -2 ETCHED

Figure 83

TEST R5 TD-Pt TUBES AFTER 100 HOURS

CO_2 + 1.5% O_2

X 500 ETCHED

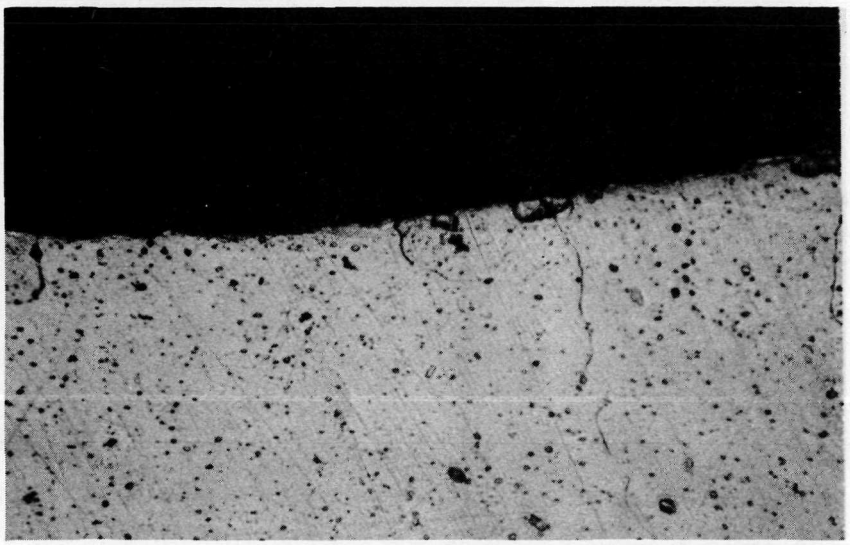

R5 -2 AT 1400 ^{o}K

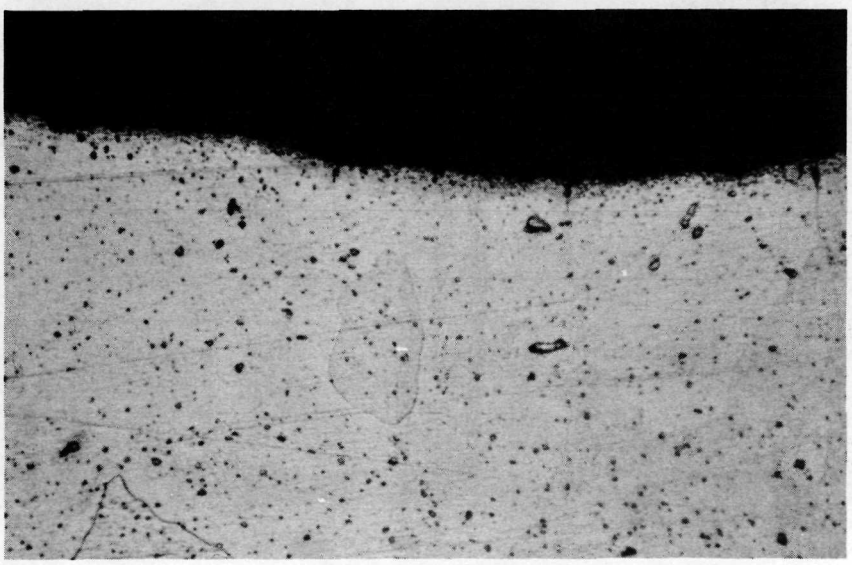

R5 -2 AT 1570 ^{o}K

Figure 84

TEST L9-3 AFTER 10 HOURS AT 1700° K
TD - Pt TUBE MATERIAL

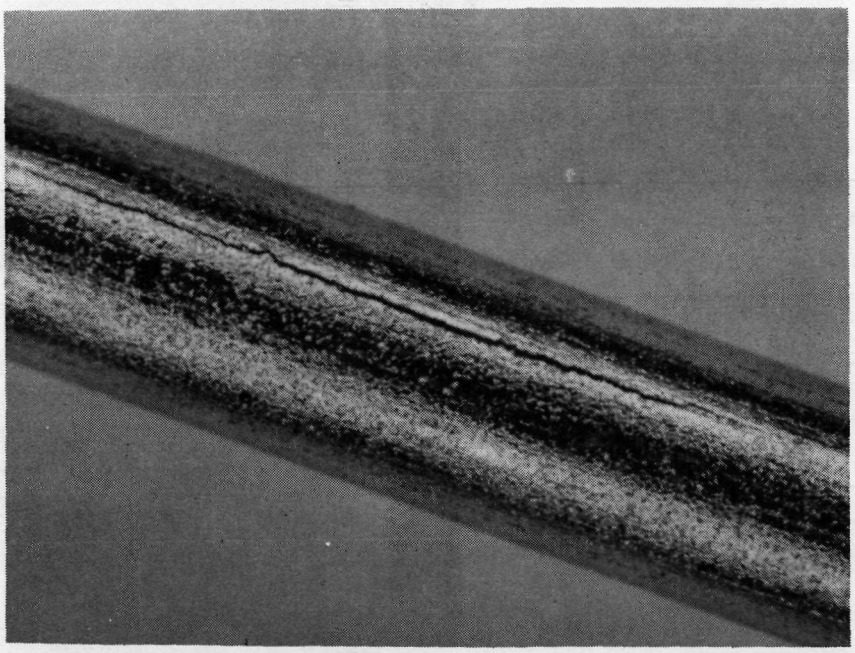

X25

X50

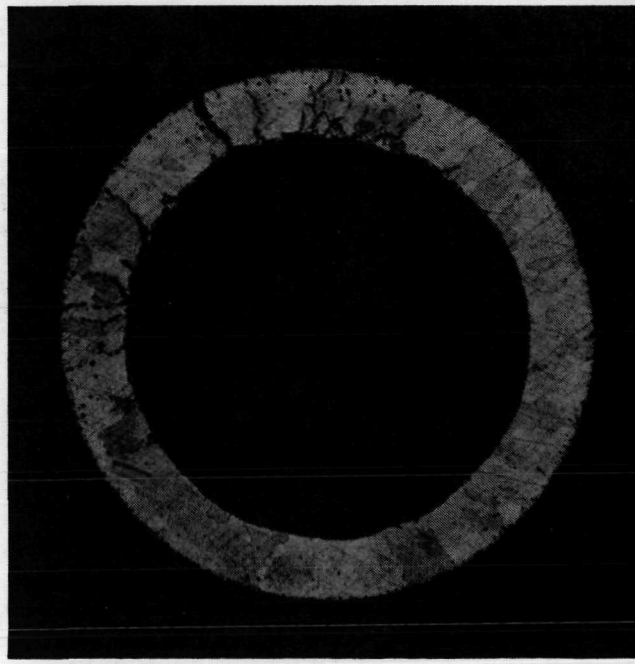

X50 ETCHED

Figure 85

TEMPERATURE PROFILE
TUBE TEST L10-2

TD-Pt TUBE 1007 HR CO_2 + 1.5% O_2

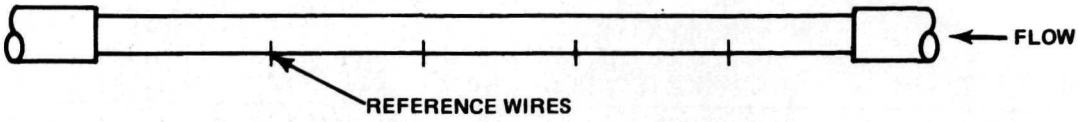

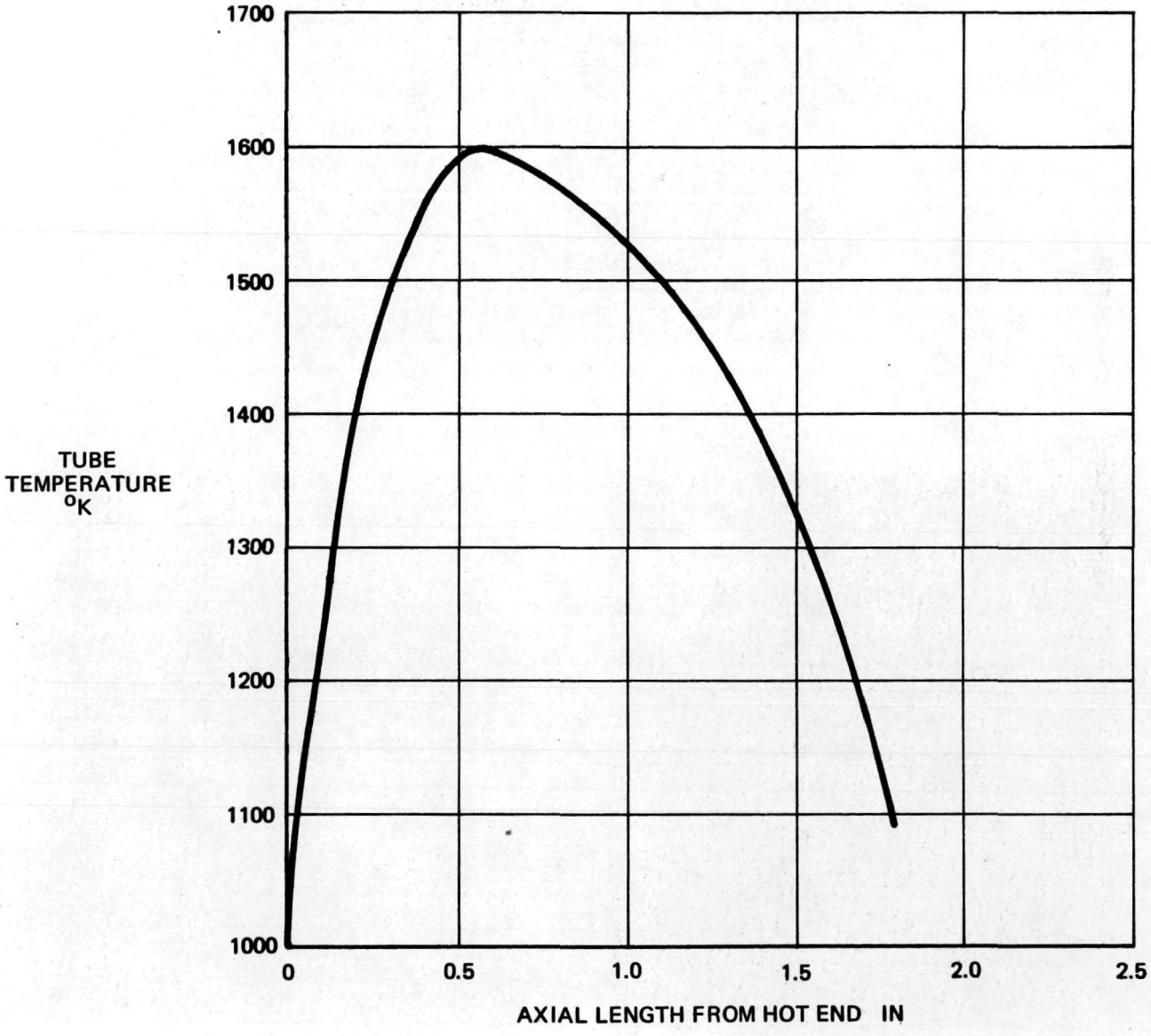

Figure 86

TEST L10-2 EXTERNAL VIEWS OF TD-Pt TUBE AFTER 1007 HOURS AT 1600° K

CO_2 + 1.5% O_2

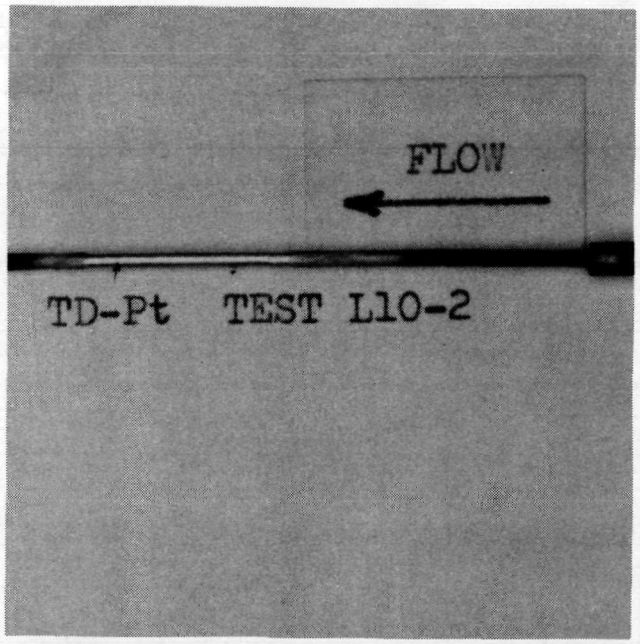

X 1.5

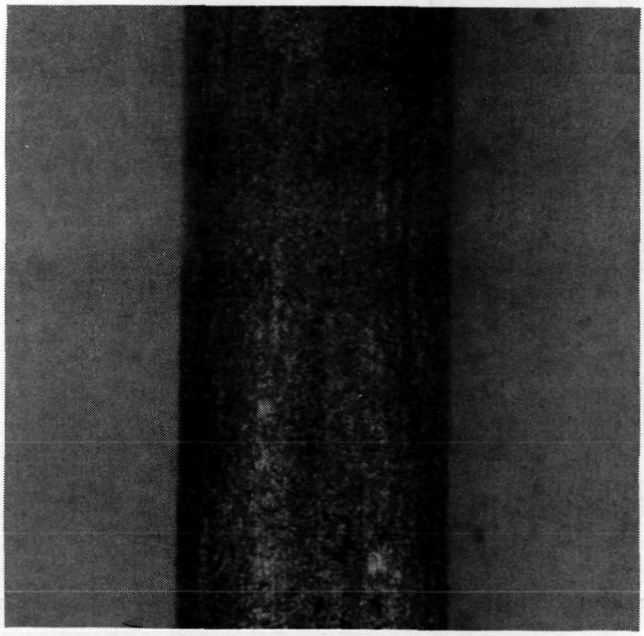

X 25 1500 °K

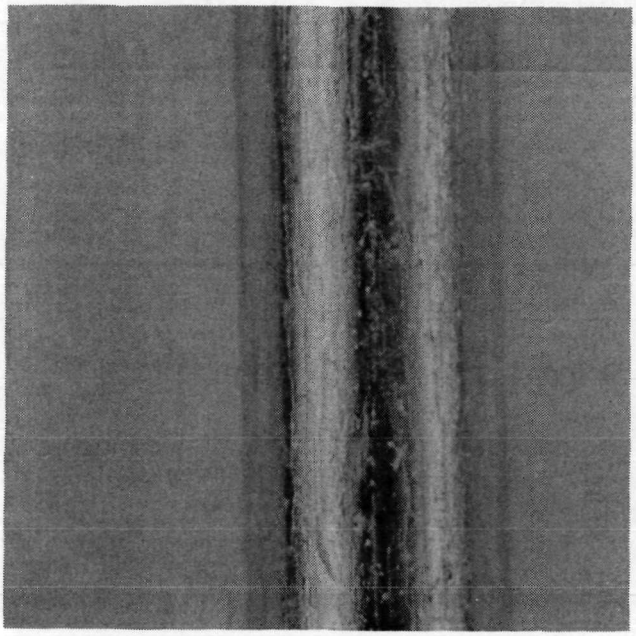

X 25 1600 °K

Figure 87

TEST L10-2 TD-Pt TUBE AFTER 1007 HOURS AT 1450° K

CO_2 + 1.5% O_2

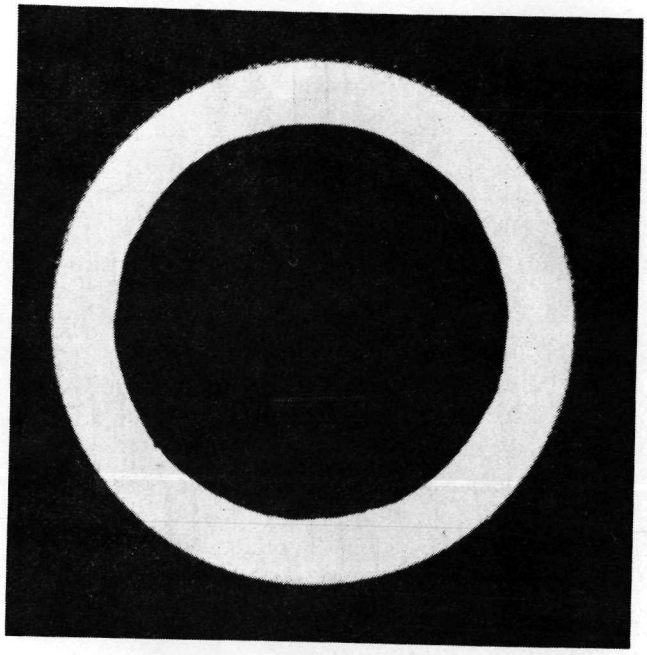

X 50

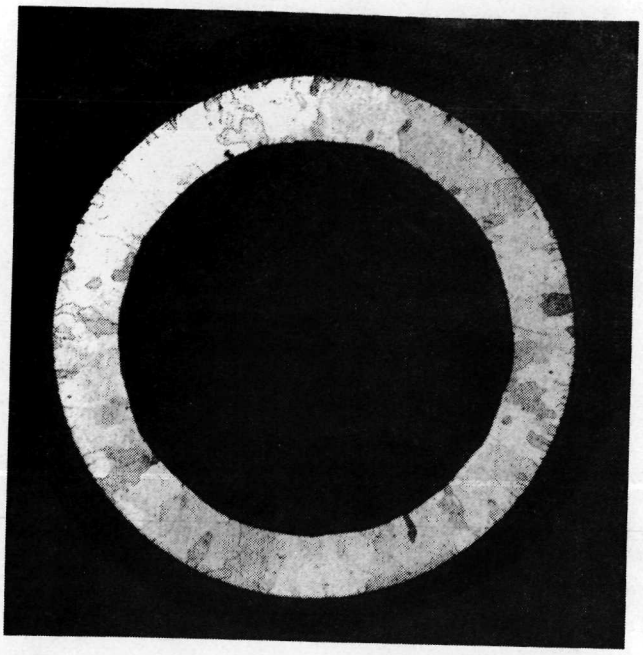

X 50 ETCHED

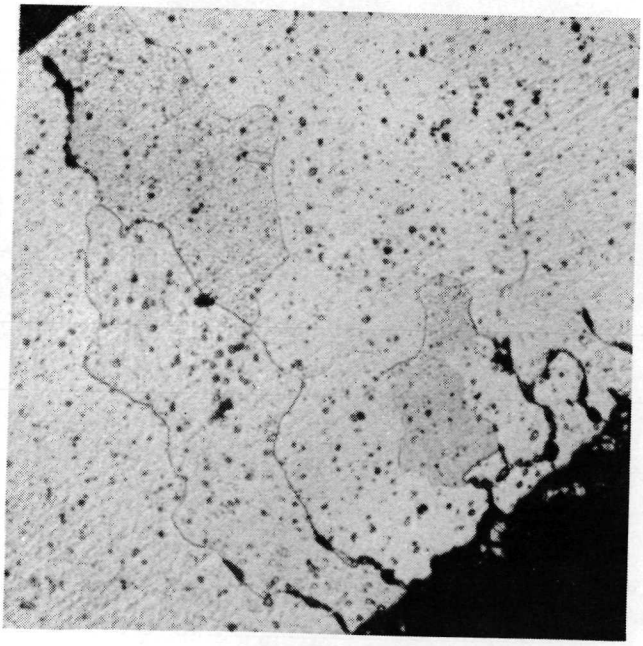

X 500 ETCHED

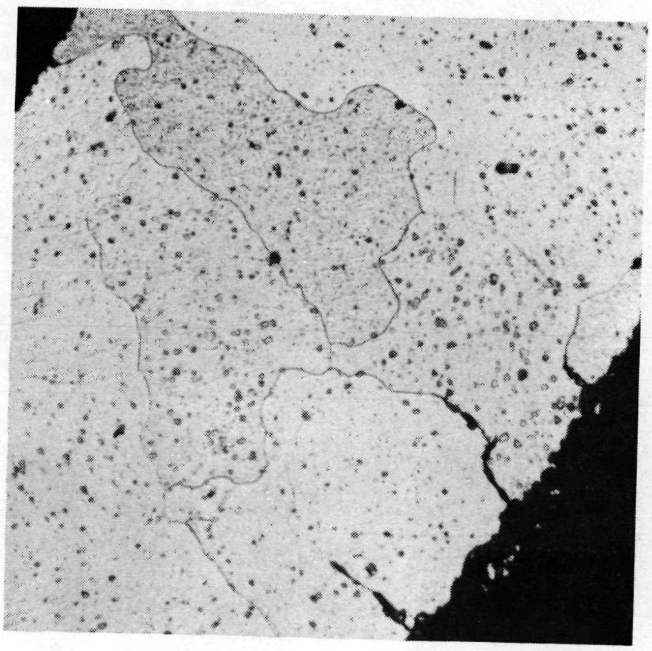

X 500 ETCHED

Figure 88

TEST L10-2 TD-Pt TUBE AFTER 1007 HOURS AT 1500° K

CO_2 + 1.5% O_2

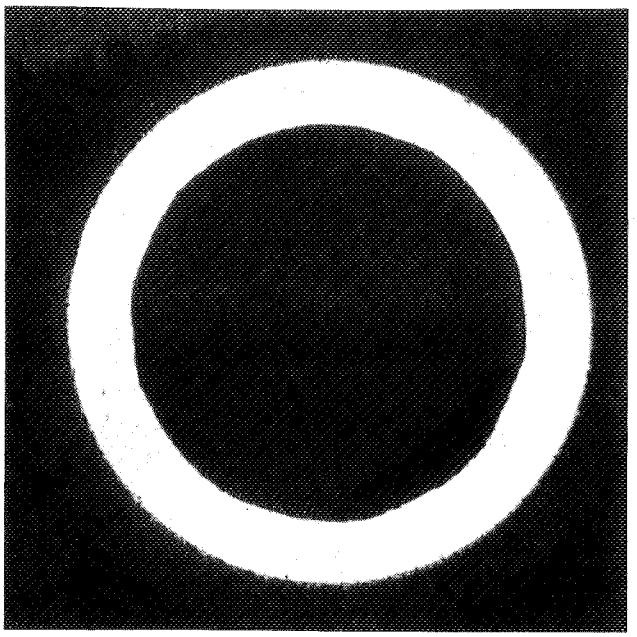

X 50

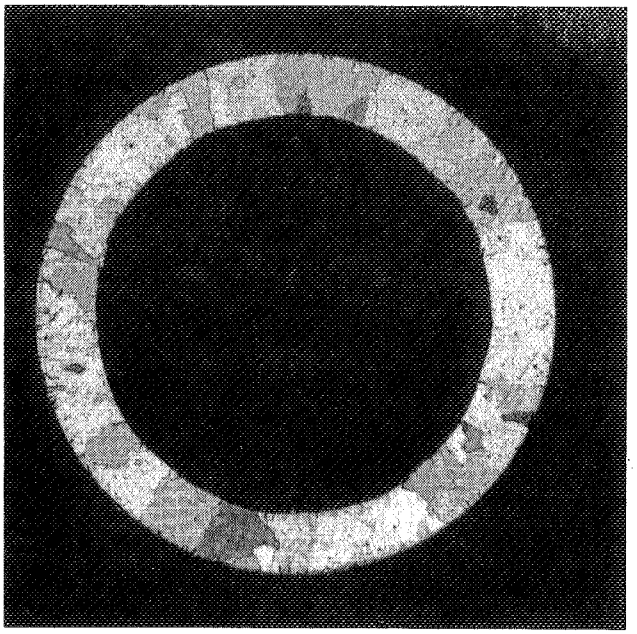

X 50 ETCHED

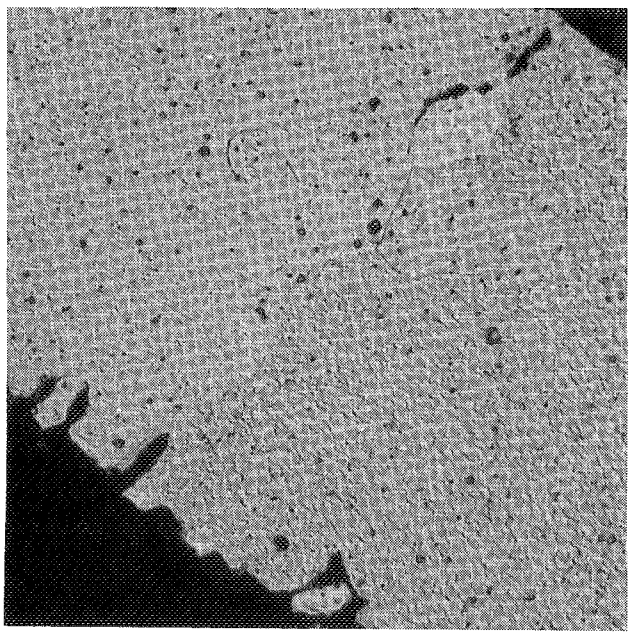

X 500 ETCHED

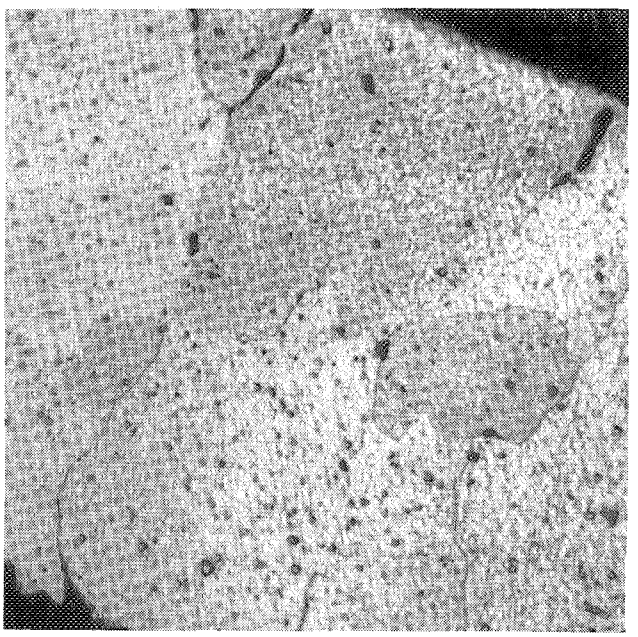

X 500 ETCHED

Figure 89

TEST L10-2 TD-Pt TUBE AFTER 1007 HOURS AT 1600° K

CO_2 + 1.5% O_2

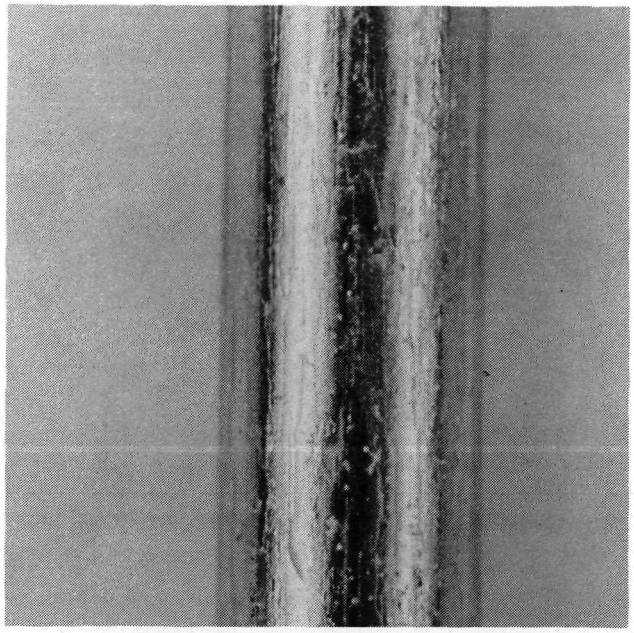

X 25

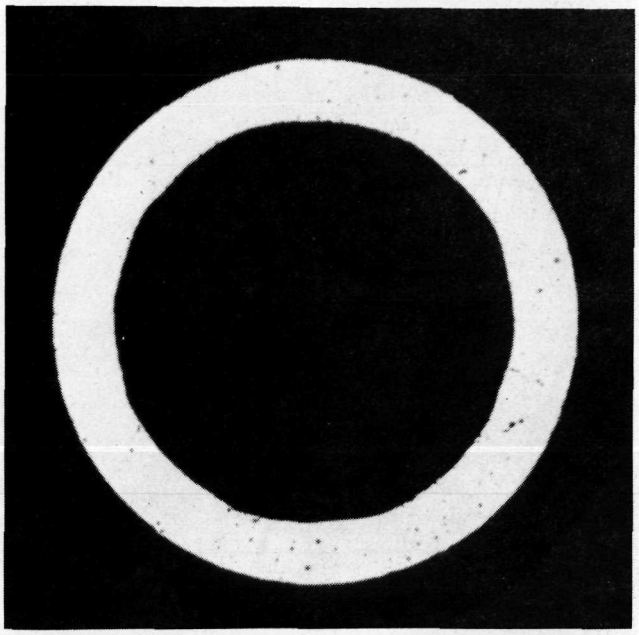

X 50

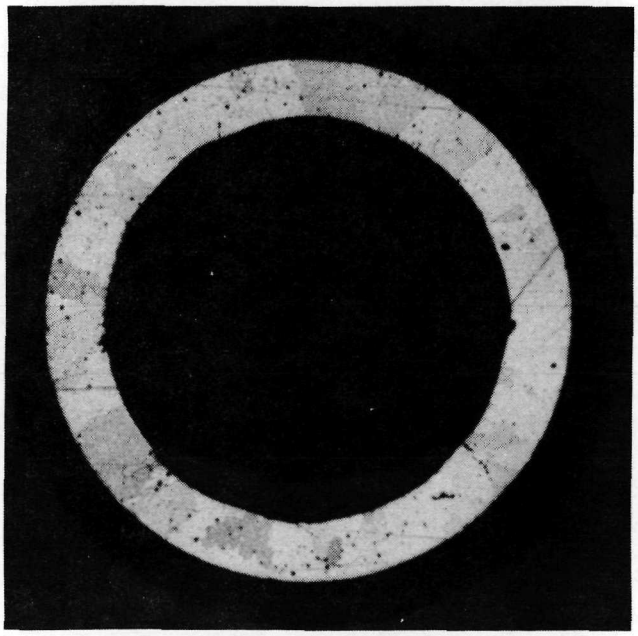

X 50 ETCHED

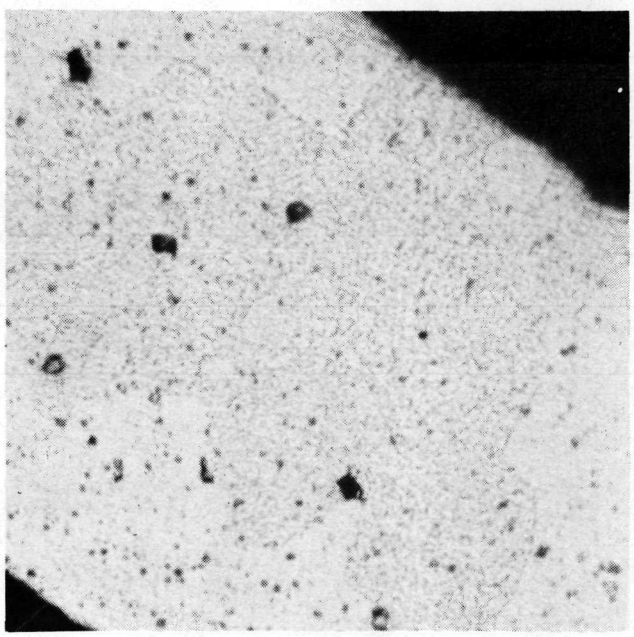

X 500 ETCHED

Figure 90

TD-PT TUBE PRIOR TO TESTING

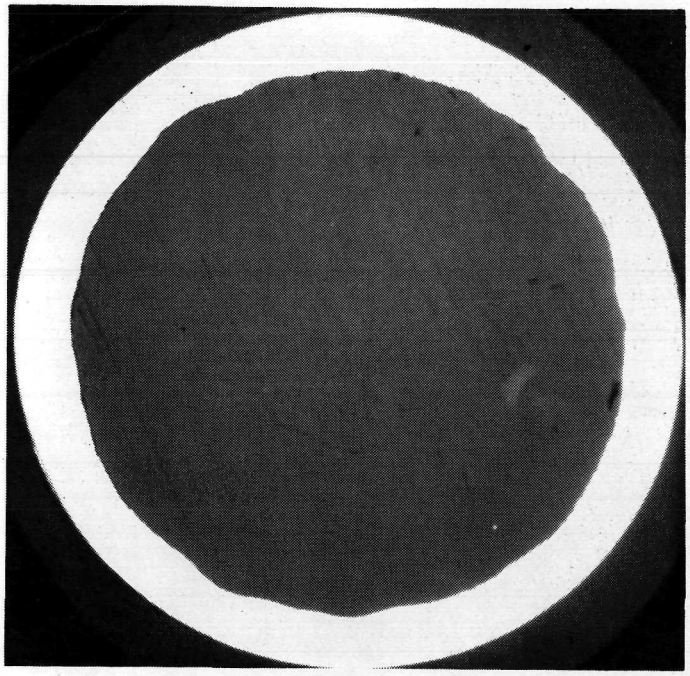

X 40

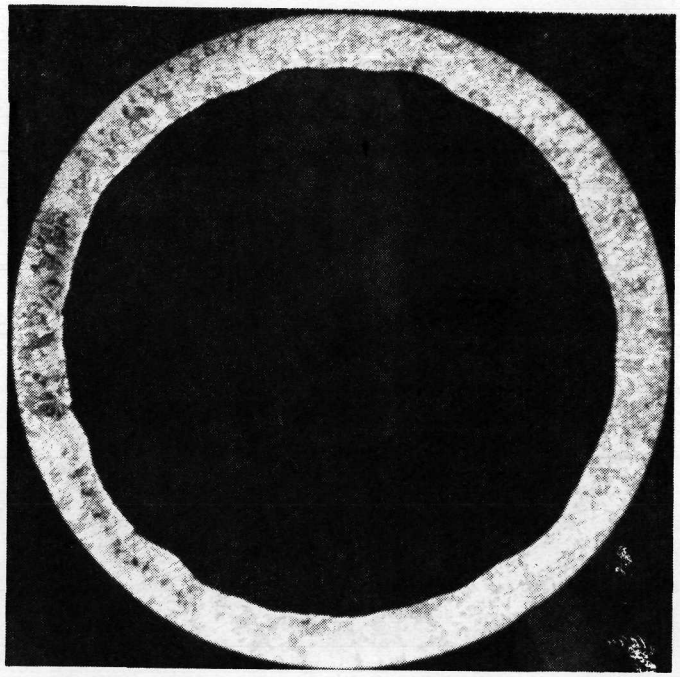

X 40 ETCHED

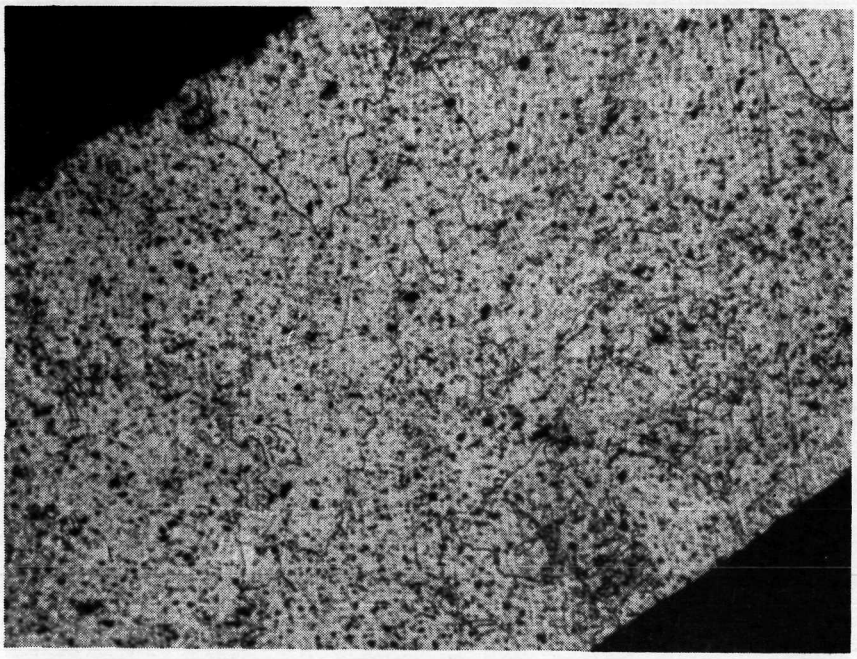

X 500 ETCHED

Figure 91

TEST L11-2 EXTERNAL VIEWS OF TD-Pt TUBE AFTER 1501 HOURS AT 1700° K

CO_2 + 0.25% O_2

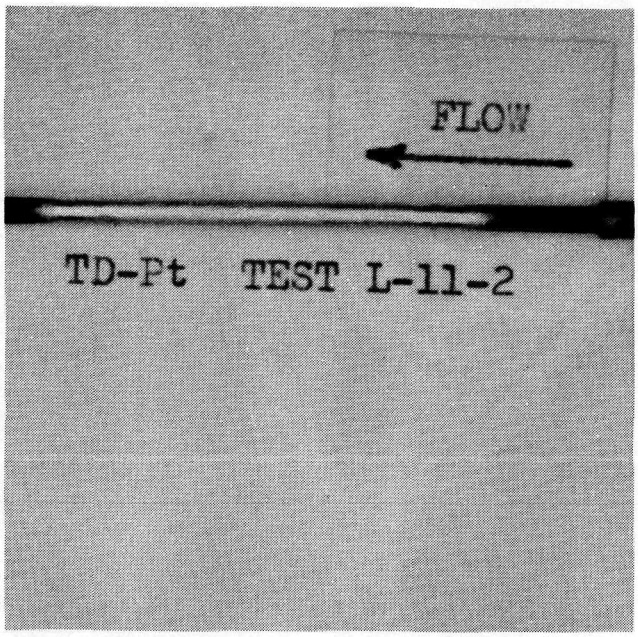

X 1.5

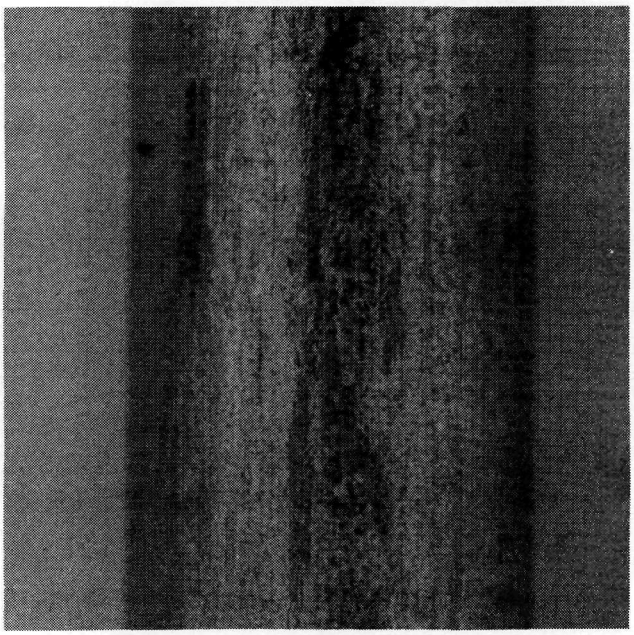

X 25 1600 °K

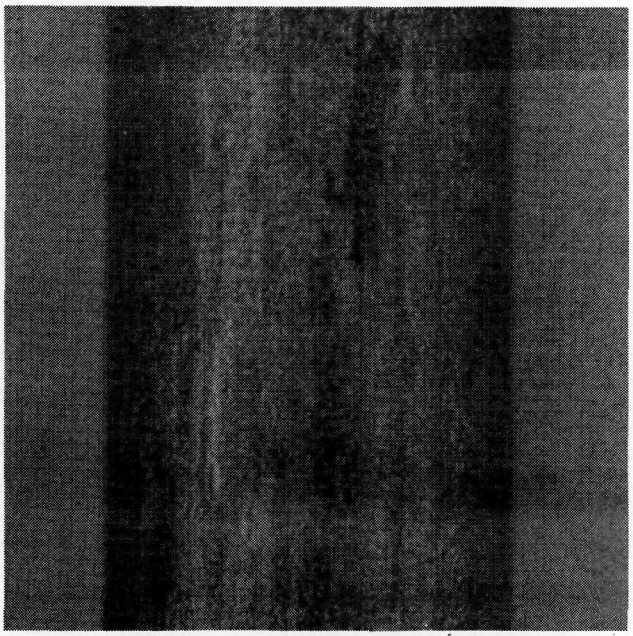

X 25 1700 °K

Figure 92

TEST L11-2 TD-Pt TUBE AFTER 1501 HOURS AT 1600° K

CO_2 + 0.25% O_2

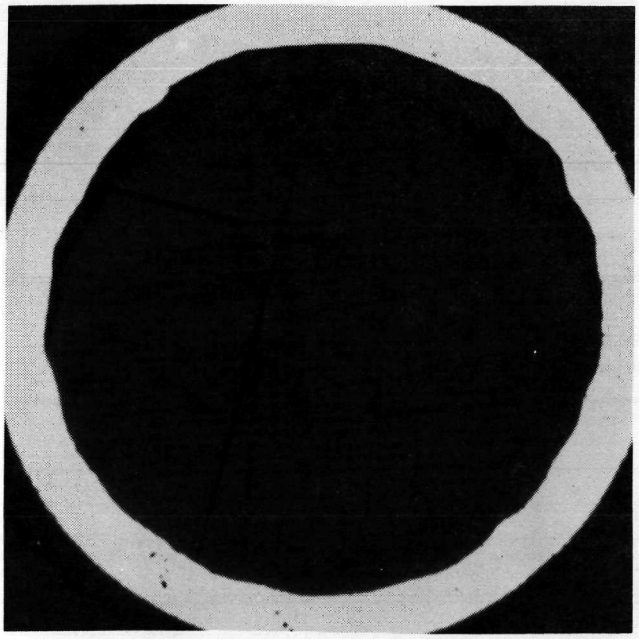

X 40

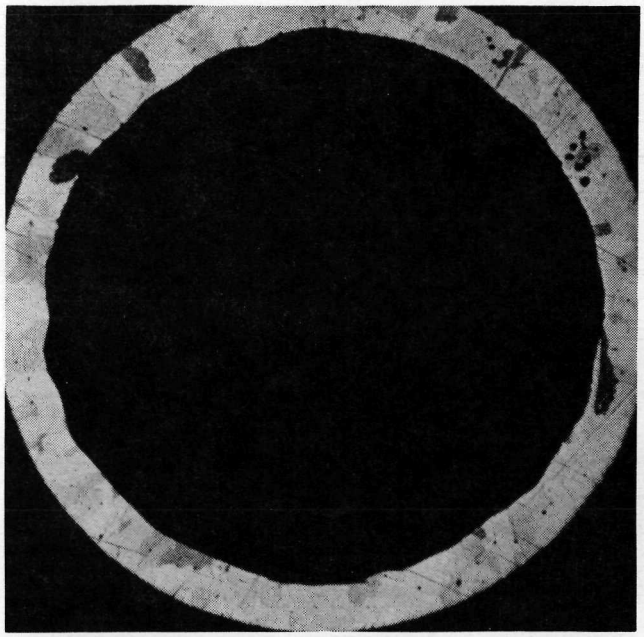

X 40 ETCHED

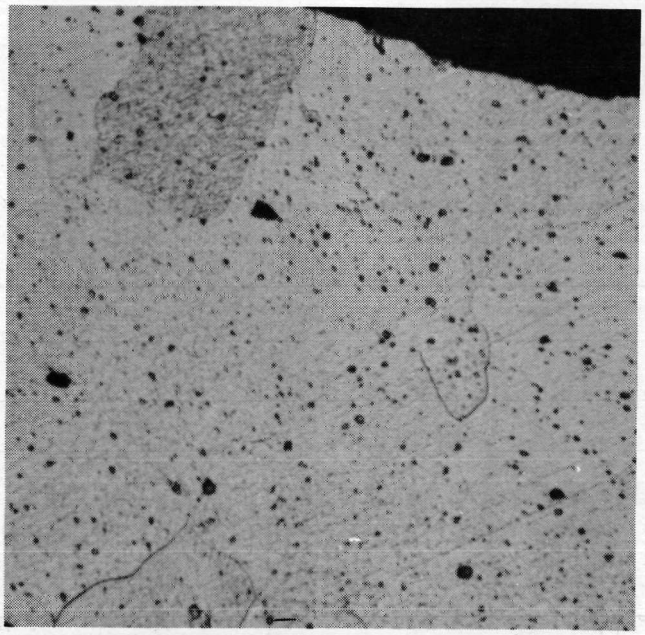

X 500 ETCHED

Figure 93

TEST L11-2 TD-Pt TUBE AFTER 1501 HOURS AT 1700° K

CO_2 + 0.25% O_2

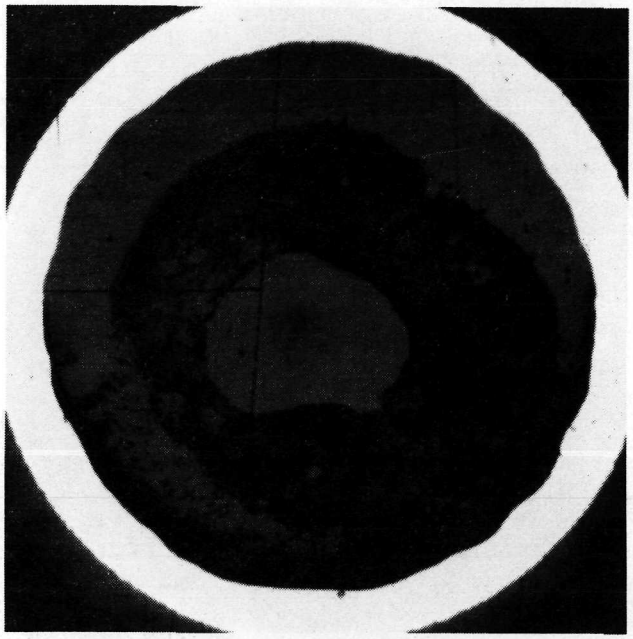

X 40

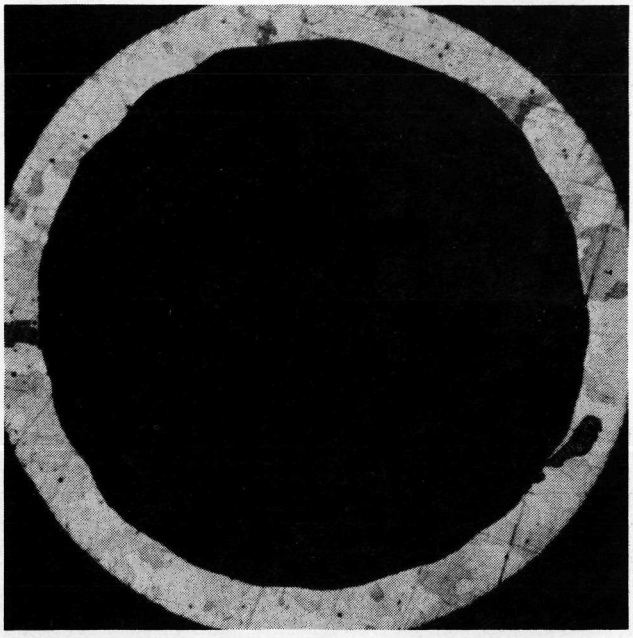

X 40 ETCHED

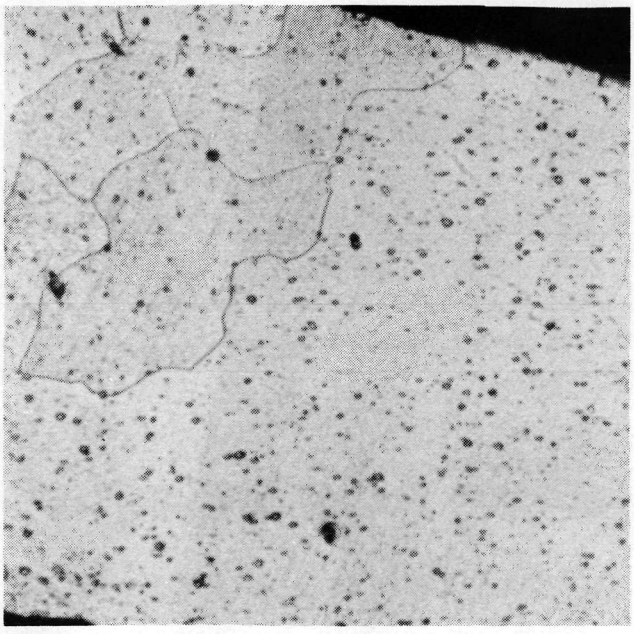

X 500 ETCHED

Figure 94

TEST R8-1

TD - PT TUBE AFTER 1500 HOURS AT 1600°K

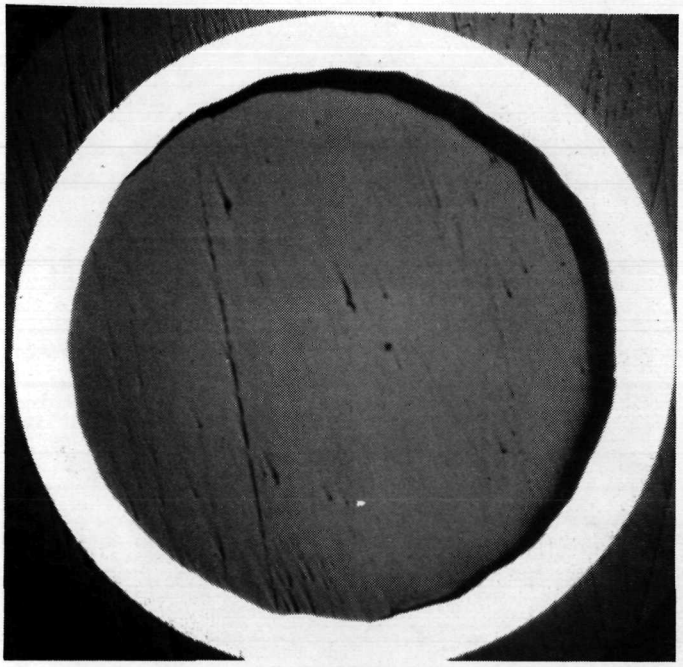

X 40

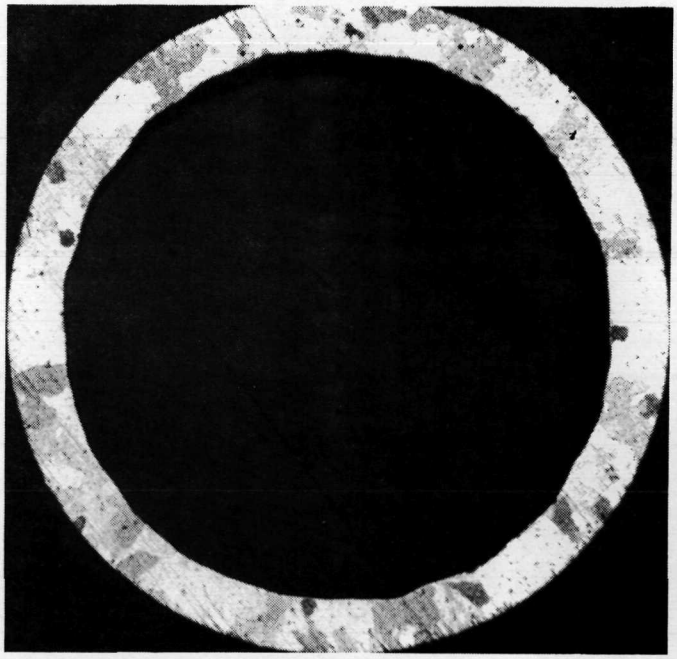

X 40 ETCHED

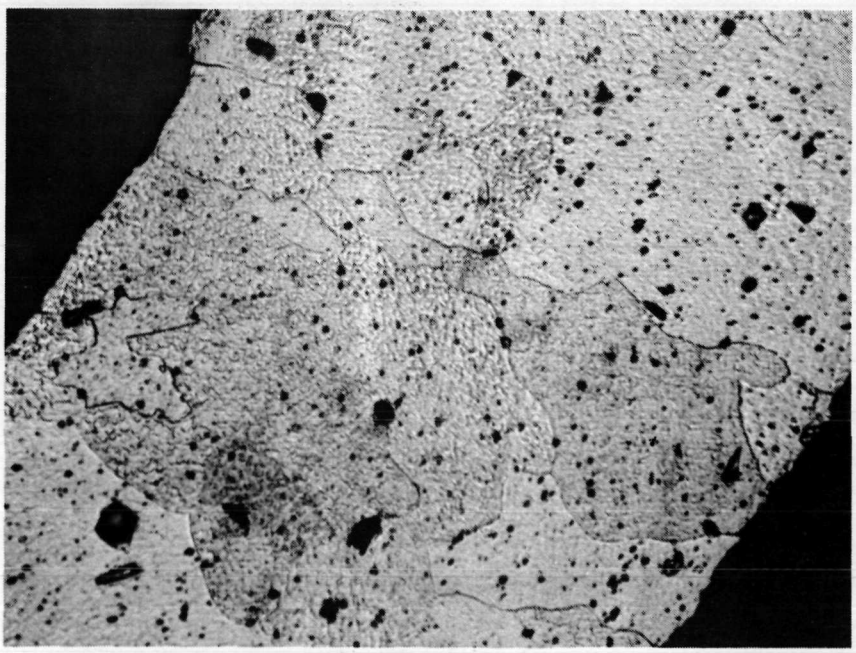

X 500 ETCHED

Figure 95

TEST R8-1

TD - PT AFTER 1500 HOURS AT 1600°K
LONGITUDINAL CROSS-SECTION

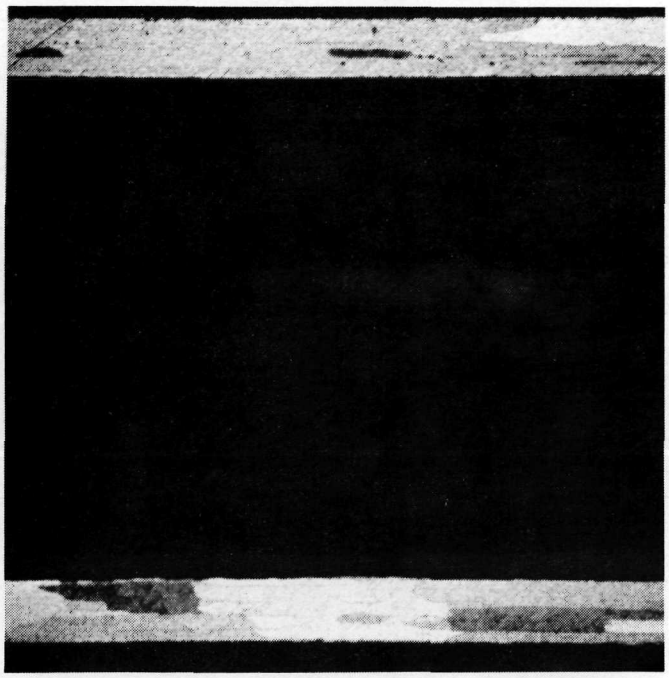

X 40 ETCHED

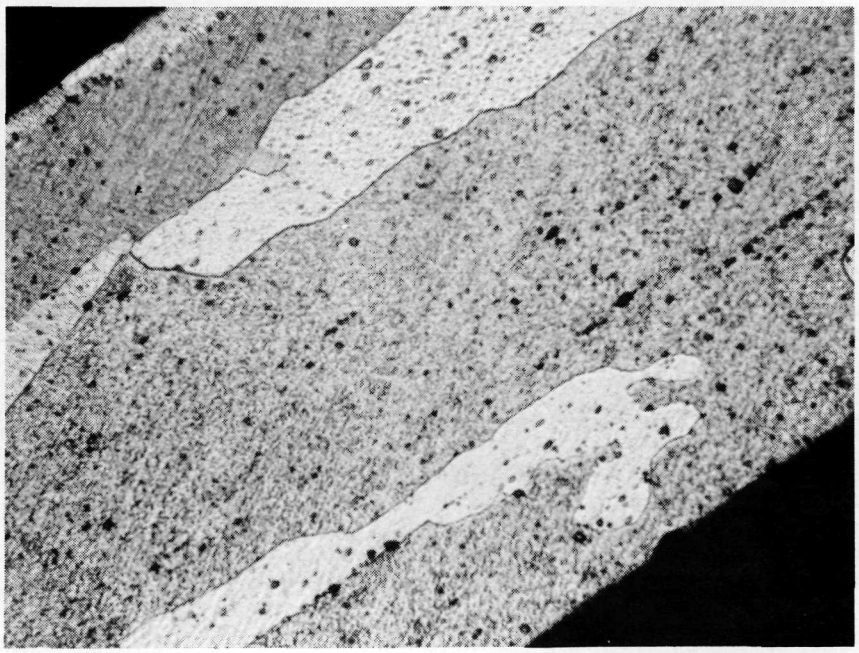

X 500 ETCHED

Figure 96

TEST R8-2 TD-Pt TUBE AFTER 1500 HOURS AT 1700° K

CO_2

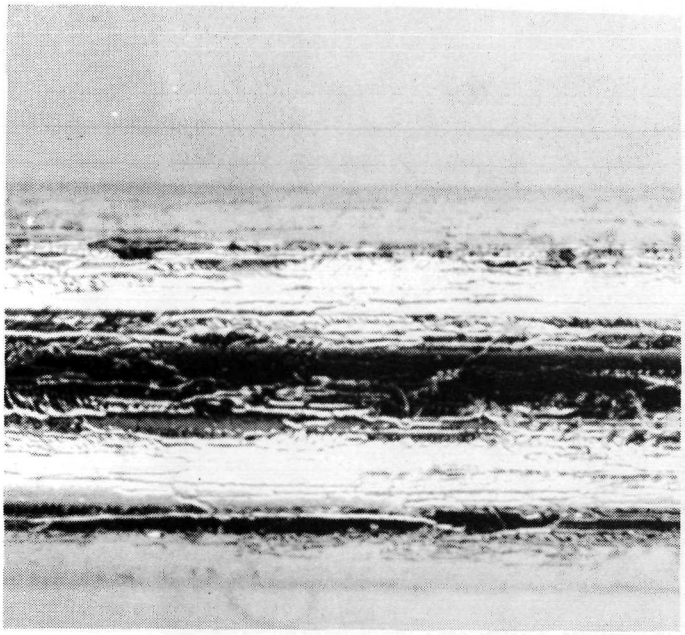

X 25

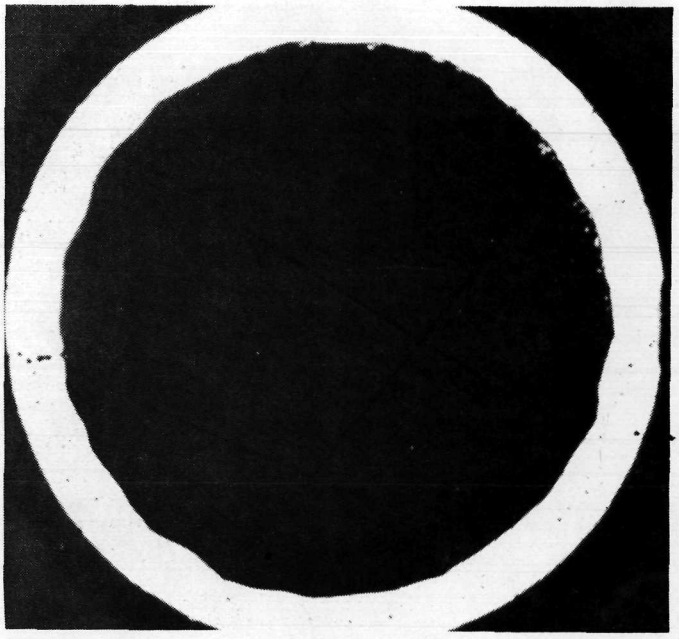

X 40

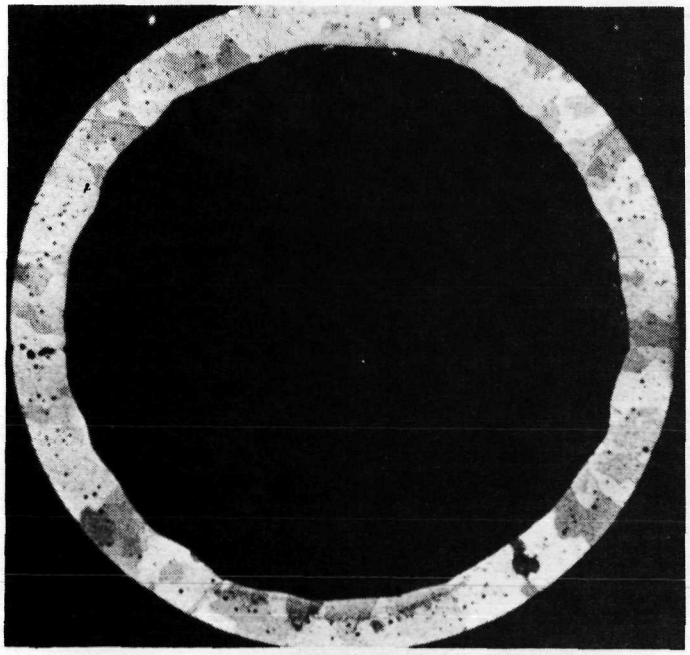

X 40 ETCHED

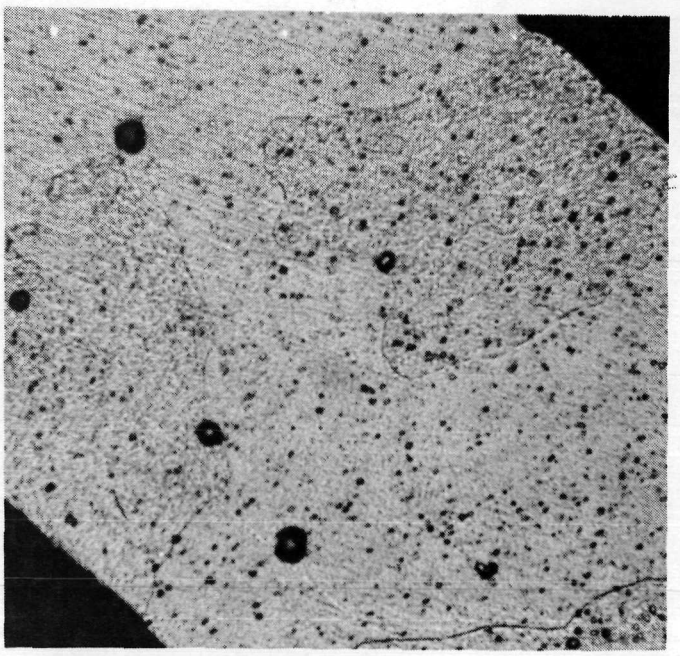

X 500 ETCHED

Figure 97

PYROLYTIC CARBON SAMPLE

POLARIZED LIGHT
100X

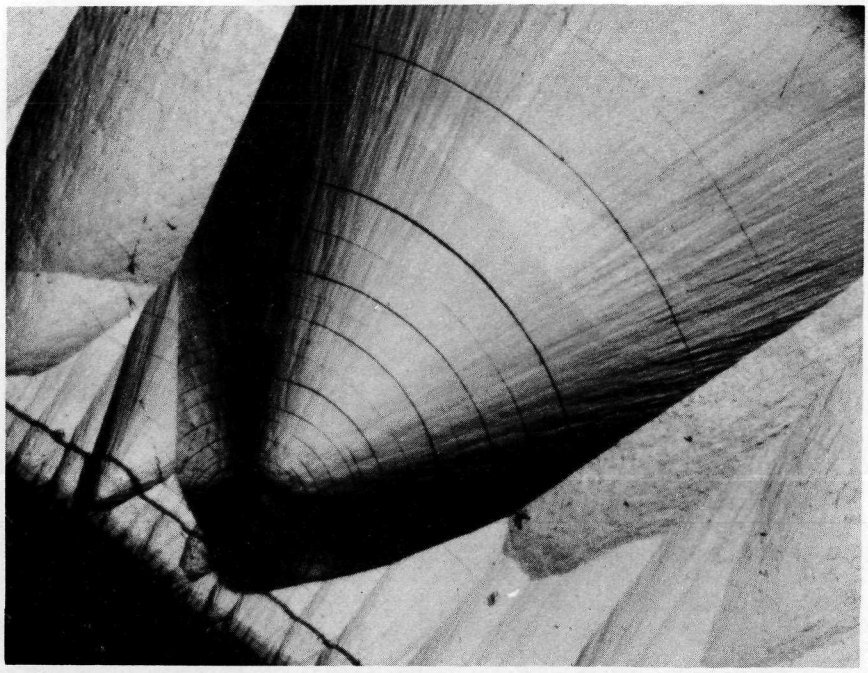

NEG. 9994-7

BRIGHT FIELD
100X

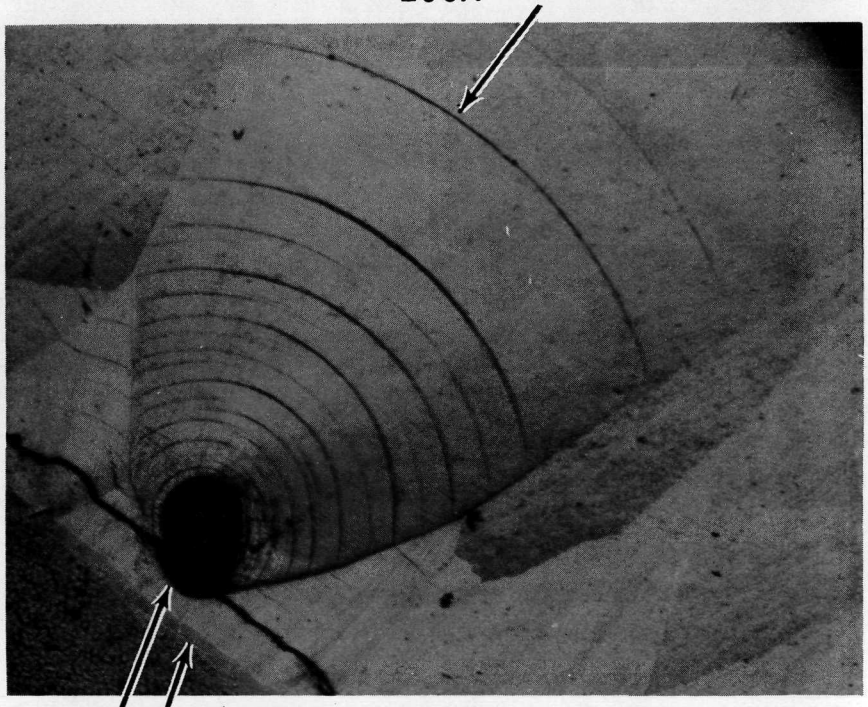

NEG. 9994-8

Figure A1

PYROLYTIC CARBON SAMPLE

POLARIZED LIGHT – 500X

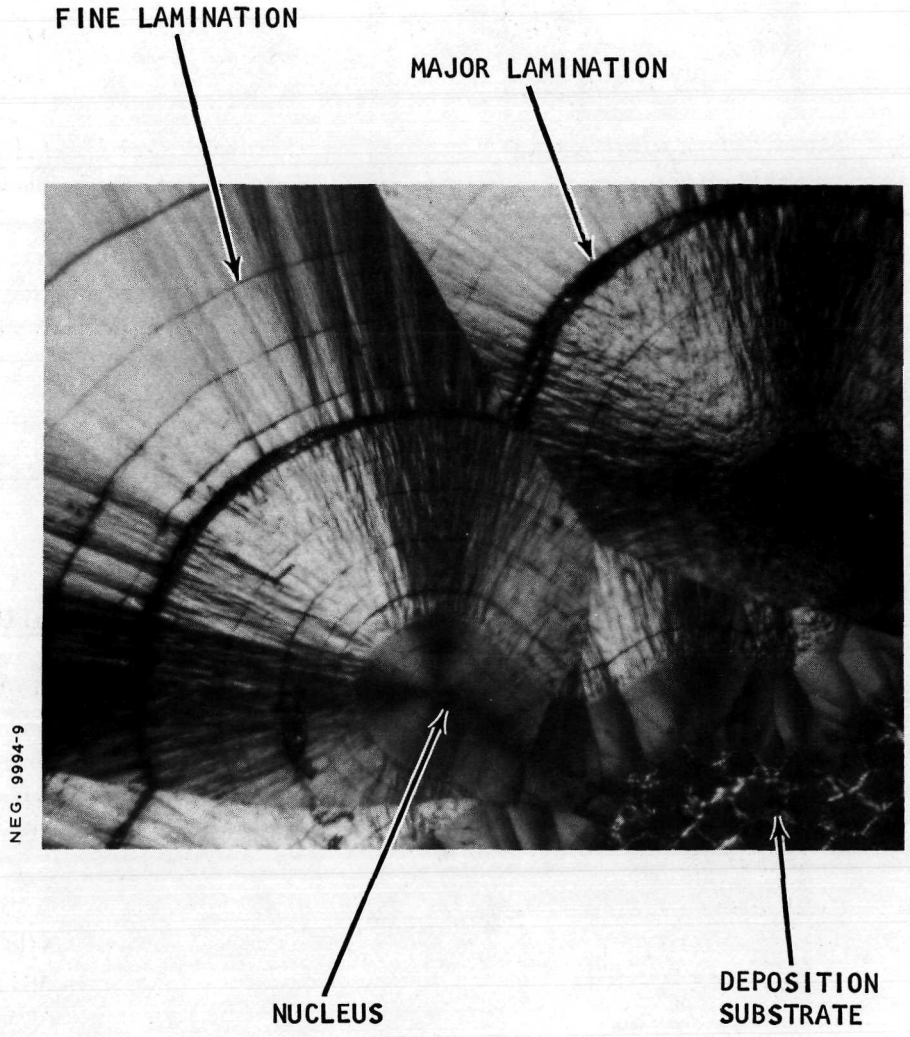

Figure A2

TABLE I

MATERIALS REVIEW FOR BIOWASTE RESISTOJET

Temperature Range, °K	Applicable Materials	Coating Requirement	Applicable* Coating Types	Remarks
Up to 1150	Stainless Steels, Nickel Alloys, etc.	None	-	Well within state-of-the-art
1150 - 1250	Stainless Steels, Nickel Alloys, Super Alloys	Advisable for long operating times	Ceramic slurries, aluminized, plated, etc.	Within present state-of-the-art
1250 - 1350	Super Alloys, Nickel Base, etc.	Required for long operating times	Ceramic slurries, aluminized, silicides, chrome coatings, etc.	Within state-of-the-art
1350 - 1600	Super Alloys	Yes	Same	Pushing state-of-the-art. May be time limited.
1350 - 1900	Refractory Metal Alloys and Graphite - Cb, Mo, Zr, Hf, V, Ir, Cr, Pt	Yes - Except for Ir, Pt, Cr	Silicide, Aluminide, SiC, Hf-Ta, Ir, Pt, Cr, etc.	Within state-of-the-art but reliability of most coating systems for long times at higher temperature is poor.
1350 - 2500	Ceramics - SiC, Al_2O_3, HfO_2, ThO_2, ZrO_2, etc.	No	-	Within materials environmental capability but limited by brittleness and thermal shock resistance.
1900 - 2500	Refractory Metal Alloys - Ta, W	Yes	Advanced coatings in experimental development	Feasible for short times - beyond current state-of-the-art for long times.

*Inspection of coatings on the interior of long, small diameter tubes is difficult.

TABLE II

BIOWASTE RESISTOJET CANDIDATE HEATER MATERIALS

PHYSICAL AND MECHANICAL PROPERTIES

		Austenitic Stainless Steel	Ferritic Stainless Steel	Iron-Chromium-Aluminum Alloys		Nickel Chromium Steel	Nickel Base Alloys (Less than 5% Cobalt)							
Material		Type 310	Type 446			N-155 (Multimet)	Hastelloy C	Hastelloy X	Nimonic 80A	Inconel X	Inconel 601	Nichrome	TD Nickel	TD Ni Cr
Composition		Fe - 25 Cr -20 Ni	Fe - 27 Cr -0.2 N	Fe - 23 Cr -5 Al	Fe - 37.5 Cr -7.5 Al	Fe - 20 Ni -20 Cr - 20 Co -3 Mo - 2.5 W -1 Cb	Ni - 16 Cr -16 Mo - 5 Fe -4 W	Ni - 22 Cr -18 Fe - 9 Mo -1.5 Co - 0.5W	Ni - 20 Cr -2 Ti - 1 Al	Ni - 15 Cr -7 Fe - 2.5 Ti -1 Cb - 0.7 Al	Ni - 23 Cr -14.1 Fe - 1.35 Al -0.5 Mn	Ni - 20 Cr	Ni - 2 ThO_2	Ni - 18 Cr -2 ThO_2
Melting Point °C		1430	1455	1520	1540	1275	1270	1290	1360	1410	1300	1400	1455	1400
Density grams/cm^3		7.9	7.6	7.2	6.9	8.3	8.9	8.2	8.2	8.25	8.1	8.4	8.9	8.5
Specific Heat cal/g-°C	25°C	.12	.12			.10	.09	.11	.10	.10	.11	.11	.11	
	800°C						.14	.16		.16	.16	.15		
Thermal Expansion Coefficient x 10^6/°C	25°C	14	10	11	18	13	11	14	11	12	11	13		
	800°C	18		17		18	15	16	15	16	17	17	16	
Thermal Conductivity cal-cm/sec-cm^2 - °C	25°C	.03	.05			.03	.02	.02	.03	.03	.03	.03	.21	.04
	800°C	.07				.06		.06	.06	.06	.06	.06	.11	.06
Electrical Resistivity microhm-cm	25°C	98	57	139	166	93	139	118	123	122	120	108	8	108
	800°C	128		147	170				125	127	127	114	46	
Ultimate Tensile Strength, kpsi		90	95	105		120	130	110	150	160	100	120	80	125
Yield Tensile Strength, kpsi		40	45			60	70	60	85	100	45	50	60	80
Modulus of Elasticity, x 10^6 psi		29	29			30	30	30	30	30	30	31	18	22

TABEL II (continued)

BIOWASTE RESISTOJET CANDIDATE HEATER MATERIALS

PHYSICAL AND MECHANICAL PROPERTIES

Material		Nickel Base Alloys (More than 5% Cobalt)					Cobalt Base Alloys			Hafnium-Tantalum Alloy	Molybdenum Disilicide
		Udimet 700 (Astroloy)	Nimonic 90	In - 100 (Haynes 100 / Rene' 100)	Rene' 41	MAR-M-200	L-605 (Haynes 25)	Haynes 188	MAR-M-302		
Composition		Ni - 18 Co -15 Cr - 5 Mo -4.5 Al - 3.5 Ti -0.03B	Ni - 20 Cr - 18 Co - 2.5 Ti -1.5 Al	Ni - 15 Co -10 Cr - 5.5 Al -4.7 Ti - 3 Mo -0.95 V	Ni - 19 Cr -11 Co - 10 Mo -3 Ti - 1.5 Al	Ni - 12.5 W -10 Co - 9 Cr -5 Al - 2 Ti -1 Cb + B + Zr	Co - 20 Cr -15W - 10 Ni	Co - 22 Cr -22 Ni - 14W	Co - 21.5 Cr -10W - 9 Ta	Hf-20 Ta - 2 Mo / *Hf-27 Ta	$MoSi_2$
Melting Point °C		1210	1360	1260	1320	1315	1330		1315	2200	1950
Density grams/cm^3		7.9	8.3	7.8	8.2	8.4	9.1	9.2	9.2		6.0
Specific Heat cal/g - °C	25°C	.14	.11		.06	.10	.09		.11		.10
	800°C	.14		.13	.17	.12					.13
Thermal Expansion Coefficient x 10^6/°C	25°C	14	12	13	12	11	13	11	11		9
	800°C	16	16	16	15	14	16	17	14	6	
Thermal Conductivity cal-cm/sec-cm^2 - °C	25°C	.04	.03		.03	.03	.03		.04	.03	.12
	800°C	.06	.06	.06	.05	.05	.06		.05	.06	.06
Electrical Resistivity microhm-cm	25°C	130	117				89				25
	800°C	150	125								150
Ultimate Tensile Strength, kpsi		200	160	150	180	120	150	130	130	156 *	
Yield Tensile Strength, kpsi		140	70	120	140	80	70	70	90	147 *	
Modulus of Elasticity, x 10^6 psi		32	33	31	31	31	33	33	36	26 *	

TABLE II (continued)

BIOWASTE RESISTOJET CANDIDATE HEATER MATERIALS

PHYSICAL AND MECHANICAL PROPERTIES

Material		Platinum	Platinum-Rhodium Alloys			Platinum-Iridium Alloys		
			10% Rh	20% Rh	30% Rh	10% Ir	20% Ir	30% Ir
Composition		Pt	Pt-10 Rh	Pt-20 Rh	Pt-30 Rh	Pt-10 Ir	Pt-20 Ir	Pt-30 Ir
Melting Point °C		1770	1830	1870	1900	1785	1810	1850
Density grams/cm^3		21.4	20.0	18.7	17.6	21.5	21.6	21.7
Specific Heat cal/g-°C	25°C	.03	.03	.04	.04	.03	.03	.03
	800°C	.04						
Thermal Expansion Coefficient x 10^6/°C	25°C	9.1	9.0	8.9	8.8	8.9	8.6	8.4
	800°C	10.3						9.5
Thermal Conductivity cal-cm/sec-cm^2-°C	25°C	.17						
	800°C	.16						
Electrical Resistivity microhm-cm	25°C	11	19	21	19	25	31	35
	800°C	43	48	45	43			55
Ultimate Tensile Strength, kpsi		18	45	70	78	55	100	160
Yield Tensile Strength, kpsi		2 - 5						90
Modulus of Elasticity, x 10^6 psi		25	28	32	34	31	37	43

TABLE III

BIOWASTE RESISTOJET CANDIDATE HEATER MATERIALS

1000 HOUR CREEP STRENGTH

Material	Temp °C	Stress for Creep Rupture kpsi	Stress for 1% Creep kpsi
Type 310 Stainless Steel	540 820 980	32 5 1.5	20 (10^4 hours) 1 (10^4 hour)
Type 446 Stainless Steel	540 820	6 1.1	6 (10^4 hours)
Iron-Chromium-Aluminum Alloys	1090	1.8 Yield	
N-155 (Multimet)	820 980	16 2	12
Hastelloy C	820 980	12 4	
Hastelloy X	820 980	10 3	8 3 (100 hours)
Nimonic 80A	820 900	10 3	9
Inconel X	820 980	17 1	15
Inconel 601	820 980 1090	6 4 1	4 1
Nichrome	1090	6 (Yield)	0.2 (10^4 hours)
TD Nickel	820 1090 1210	14 12 6	 6 4
TD N_i Cr	820 1090 1210	13 7 5	
Udimet 700 (Astroloy)	820 980	43 8	35 6
Nimonic 90	820 980	20 2	13

TABLE III (continued)

BIOWASTE RESISTOJET CANDIDATE HEATER MATERIALS

1000 HOUR CREEP STRENGTH

Material	Temp °C	Stress for Creep Rupture kpsi	Stress for 1% Creep kpsi
In-100 Haynes 100 Rene' 100	820 980 1090	55 16 4	46 14
Rene' 41	820 980	30 5	25
MAR-M-200	820 980 1090	60 30 6	40 12 5
L-605 (Haynes 25)	820 980 1090	16 4	10 2 2.8 (100 hours)
Haynes 188	820 980	16 4	
MAR-M-302	820 980 1090	32 11 4	 15 (100 hours) 2.5 (100 hours)
Hafnium-Tantalum			
Platinum	980 1300 1450	1 < 0.1	
Pt - 10 Rh	980 1300 1450	2 0.4 0.3	
Pt - 20 Rh	980 1300 1450	3 0.5	
Pt - 30 Rh	980 1300 1450	4	
Pt - 10 Ir	980 1300 1450	3 0.3 0.1	

TABLE III (continued)

BIOWASTE RESISTOJET CANDIDATE HEATER MATERIALS

1000 HOUR CREEP STRENGTH

Material	Temp °C	Stress for Creep Rupture kpsi	Stress for 1% Creep kpsi
Pt - 20 Ir	980 1300 1450	3 0.4 0.1	
Pt - 30 Ir	980 1300 1450	3	

Temperature Conversion	
°C	°F
540	1000
820	1500
980	1800
1090	2000
1210	2200
1300	2370
1450	2640

TABLE IV

EMISSIVITY OF TYPICAL BIOWASTE RESISTOJET CANDIDATE MATERIALS

Material	Surface Condition	Temperature °C	Emissivity
310 Stainless Steel	As received	870	0.7 (TH)
	Oxidized	870	0.95 (TH)
321 Stainless Steel	Polished	25	0.1 (NT)
	Polished	980	0.47 (NT)
	Oxidized	980	0.96 (NT)
	Polished	980	0.35 (S)
	Oxidized	980	0.6 (S)
Hastelloy C	Oxidized	1090	0.97 (TH)
	Polished	1090	0.4 (S)
Hastelloy X	Oxidized	1090	0.88 (TH)
Inconel X	Polished	1090	0.3 (NT)
	Oxidized	1090	0.9 (NT)
	Polished	1090	0.4 (NS)
	Oxidized	1090	0.8 (NS)
	Polished	--	0.5 (S)
	Oxidized	--	0.9 (S)
Nichrome	Polished	500	0.7 (TN)
	Oxidized	500	0.98 (TN)
Rene 41 L-605	Oxidized	1090	0.9 (TH)
TD Ni	Oxidized	1090	0.65 (TN)
Hafnium-Tantalum	Oxidized	1500	0.7 (TH & S)
Platinum	--	870	0.13 (TN)
	--	1090	0.16 (TN)
	--	1500	0.17 (TN)
	--	870	0.32 (S)
	--	1090	0.3 (S)
	--	1500	0.24 (S)
Thorium Oxide	--	870	0.40 (TN)
		1090	0.35 (TN)
Molybdenum Disilicide	--	--	0.77 (TN)
Graphite	--	--	0.7 - 0.8 (S)

S ~ Spectral
NS ~ Normal Spectral
NT ~ Normal Total
TH ~ Total Hemispherical

TABLE V

SUMMARY OF BIOWASTE RESISTOJET HEATER TUBE TESTS
SINGLE BELL JAR FACILITY

Internal Pressure = 2 to 3 Atmospheres External Pressure < 100 Microns

Test No.	Tube Material	Propellant	Mixture Weight Ratio CO_2/CH_4	Flow Rate grams/sec x 10^3	Test Duration hours	Wall Temperature °K (°R)	Carbon Deposit	Deposit Thickness in.x10^3	Average Deposition Rate inches/hr x 10^6
I	Pt-20 Rh	CO_2	-	30	100 100 300 500 Total	1300 (2340) 1450 (2610) 1675 (3010)	None	-	-
II	Pt-20 Rh	CO_2	-	29	570	1500 (2695)	None	-	-
II-I	Pt-30Ir	CO_2	-	29	706	1550 (2740)	None	-	-
III	Pt-ThO_2*	CO_2	-	29	429	1410 (2540)	None	-	-
VI	Hastelloy X	CO_2	-	3.5	579	1250 (2250)	None	-	-
VII	Hastelloy X	CH_4	-	5	509	1250 (2250)	Amorphous	0.5**	1
VIII-1	Hastelloy X	$CO_2 + CH_4$	1.1	3	250	1320 (2380)	Pyrolytic	6	24
VIII-1	Hastelloy X	$CO_2 + CH_4$	1.1	3	250	1255 (2260)	Pyrolytic	4	16
VIII-2	Hastelloy X	$CO_2 + CH_4$	1.1	3	250	1230 (2220)	Pyrolytic	2	8
VIII-2	Hastelloy X	$CO_2 + CH_4$	1.1	3	250	1145 (2060)	Pyrolytic	1.2	4.8
VIII-3	Hastelloy X	$CO_2 + CH_4$	1.1	3	250	1115 (2005)	Pyrolytic	0.6	2.4
VIII-3	Hastelloy X	$CO_2 + CH_4$	1.1	3	250	925 (1660)	None	-	-
IX-1	Pt-20 Rh	$CO_2 + CH_4$	1.1	4.9	214	945 (1700)	None	-	-
IX-1	Pt-20 Rh	$CO_2 + CH_4$	1.1	4.9	214	840 (1510)	None	-	-
IX-2	Pt-20 Rh	$CO_2 + CH_4$	1.1	4.9	214	1255 (2260)	Amorphous	0.3	1.4
IX-2	Pt-20 Rh	$CO_2 + CH_4$	1.1	4.9	214	1090 (1960)	None	-	-
IX-2	PT-20 Rh	$CO_2 + CH_4$	1.1	4.9	214	925 (1660)	None	-	-
X-1	Hastelloy X	$CO_2 + CH_4$	1.0	3.3	241	1255 (2260)	Pyrolytic	1.0	4.1
X-1	Hastelloy X	$CO_2 + CH_4$	1.0	3.3	241	1090 (1960)	None	-	-
X-2	Pt-20 Rh	$CO_2 + CH_4$	1.0	3.3	241	1255 (2260)	Pyrolytic	0.4	1.7
X-2	Pt-20 Rh	$CO_2 + CH_4$	1.0	3.3	241	1090 (1960)	None	-	-
X-3	Pt-20 Rh	$CO_2 + CH_4$	1.0	3.3	241	1440 (2590)	Pyrolytic	6.7	28
X-3	Pt-20 Rh	$CO_2 + CH_4$	1.0	3.3	241	1255 (2260)	Pyrolytic	0.7	2.9

* Less than 1.0% Thoria ** Also contained a 0.0035 inch thick blister like deposit.

TABLE VI

SUMMARY OF BIOWASTE RESISTOJET HEATER TUBE TESTS L1 TO L6

INTERNAL PRESSURE = 2 ATMOSPHERES EXTERNAL PRESSURE < 20 MICRONS OF Hg

TEST NO.	DATA POINT	TUBE MATERIAL	PROPELLANT	MIXTURE WEIGHT RATIO CO_2/CH_4	FLOW RATE GRAMS/SEC X 10^3	TEST DURATION HOURS	WALL TEMPERATURE ^oK (^oR)	TYPE CARBON DEPOSIT*	AVERAGE *DEPOSIT* THICKNESS IN. X 10^6	AVERAGE *DEPOSITION* RATE IN./HR. X 10^6
L1	1B	HASTELLOY X	$CO_2 + CH_4$	1.1	5.7	113.5	1270 (2290)	P	710	6.25
	1C						1195 (2150)		160	1.41
	2A						1250 (2245)		660	5.80
	2B						1185 (2130)		150	1.32
	2C						1110 (2000)		80	0.70
	3A						1185 (2130)		180	1.58
	3B						1110 (2000)		90	0.79
	3C						1065 (1915)		30	0.26
L2	1B	HASTELLOY X	$CO_2 + CH_4$	2.1	5.5	97.2	1305 (2350)	A	250	2.58
	1C						1310 (2360)	A + P	200	2.06
	1D						1280 (2300)	P	200	2.06
	2B						1240 (2230)	P	170	1.75
	2C						1195 (2150)	P	170	1.75
	2D						1160 (2090)	NONE	0	0
	3B						1185 (2130)	P	80	0.83
	3C						1155 (2080)	P	100	1.03
	3D						1115 (2010)	P	TRACE	≅ 0.1
L3	1A	HASTELLOY X	$CO_2 + CH_4$	3.0	6.0	125.0	1095 (1970)	P	60	0.48
	1B						1070 (1930)	P	30	0.24
	1C						1045 (1880)	NONE	0	0
	2A						1145 (2060)	P	100	0.80
	2B						1115 (2010)		80	0.64
	2C						1085 (1950)		60	0.48
	3A						1200 (2160)		125	1.00
	3B						1180 (2125)		100	0.80
	3C						1140 (2055)		75	0.60
L4	1A	HASTELLOY X	CH_4	--	5.0	122.0	1115 (2010)	A	150	1.23
	1B						1070 (1925)		100	0.82
	1C						1015 (1830)		50	0.41
	2B						1130 (2030)		150	1.23
	3A					92.0	1255 (2260)		330	3.59
	3B						1210 (2175)		180	1.96
	3C						1145 (2060)		140	1.52
L5	1A	HASTELLOY X	$CO_2 + CH_4$	2.0	6.0	140.5	1055 (1900)	A	160	1.14
	1B						1015 (1830)	A	240	1.71
	1C						978 (1760)	NONE	0	0
	2A						1130 (2030)	A	100	0.71
	2B						1090 (1965)	P	250	1.78
	2C						1030 (1860)	A + P	400	2.84
	3A						1200 (2160)	P	290	2.06
	3B						1160 (2090)	P	200	1.42
	3C						1110 (2000)	P	250	1.78
L6	1A	PLATINUM - 30% IRIDIUM	$CO_2 + CH_4$	2.0	6.0	185.0	1115 (2005)	P	100	0.54
	1B						1090 (1965)	P	80	0.43
	1C						1035 (1865)	A + P	110	0.60
	1D						995 (1790)	A	TRACE	≅ 0.1
	1E						1080 (1950)	P	40	0.22
	1F						1005 (1810)	A	20	0.11
	2A						1200 (2160)	P	100	0.54
	2B						1175 (2120)	P	80	0.43
	2C						1100 (1980)	P	TRACE	≅ 0.1
	2D						1035 (1865)	A	60	0.32
	2E						1150 (2070)	P	90	0.49
	2F						1045 (1880)	A	60	0.32
	3A						1280 (2300)	P	750	4.05
	3B						1265 (2275)	P	420	2.27
	3C						1175 (2115)	A + P	100	0.54
	3D						1100 (1980)	A	150	0.81
	3E						1240 (2235)	A + P	550	2.97
	3F						1115 (2005)	A	160	0.87

* A - AMORPHOUS, P - PYROLYTIC

TABLE VII

SUMMARY OF BIOWASTE RESISTOJET HEATER TUBE TESTS R1 TO R4

INTERNAL PRESSURE = 2 ATMOSPHERES — **EXTERNAL PRESSURE < 20 MICRONS OF Hg**

TEST NO.	DATA POINT	TUBE MATERIAL	PROPELLANT	MIXTURE WEIGHT RATIO H_2O/CH_4	FLOW RATE GRAMS/SEC X 10^3	TEST DURATION HOURS	WALL TEMPERATURE ^oK (^oR)	TYPE CARBON DEPOSIT*	AVERAGE DEPOSIT THICKNESS IN. X 10^6	AVERAGE DEPOSITION RATE IN./HR. X 10^6
R1	1A	HASTELLOY X	$H_2O + CH_4$	1.13	8	161.5	978 (1760)	NONE	0	0
	1B						1024 (1845)			
	1C						1082 (1950)			
	2A						1075 (1935)			
	2B						1139 (2050)			
	2C						1192 (2145)			
	3A						1133 (2040)			
	3B						1203 (2165)			
	3C						1250 (2250)			
	1D						955 (1720)	A + P	20	0.12
	2D						983 (1770)	A + P	50	0.31
	3D						1000 (1800)	A + P	80	0.50
R2	1A	HASTELLOY X	$H_2O + CH_4$	0.5	8	164.8	984 (1770)	NONE	0	0
	1B						1027 (1845)	A + P	TRACE	≃ 0.1
	1C						1062 (1910)		TRACE	≃ 0.1
	1D						945 (1700)		50	0.30
	2A						1063 (1915)		30	0.20
	2B						1137 (2045)		20	0.10
	2C						1182 (2125)		TRACE	≃ 0.1
	2D						970 (1750)		90	0.55
	3A						1128 (2030)		20	0.10
	3B						1207 (2170)		TRACE	≃ 0.1
	3C						1240 (2230)		TRACE	≃ 0.1
	3D						1000 (1800)		120	0.73
R3	1A	HASTELLOY X	$H_2O + CH_4$	0.26	8	140.4	1218 (2190)	A + P	TRACE	≃ 0.1
	1B						1270 (2285)	A + P	150	1.07
	1C						1308 (2355)	P	430	3.06
	1D						1062 (1910)	P	360	2.56
	2A						1175 (2115)	NONE	0	0
	2B						1228 (2210)	A + P	30	0.21
	2C						1255 (2260)	A + P	20	0.14
	2D						1045 (1880)	P	270	1.92
	3A						1110 (1995)	NONE	0	0
	3B						1172 (2110)	A + P	30	0.21
	3C						1200 (2160)	A + P	20	0.14
	3D						1028 (1850)	A + P	175	1.25
R4	1A	TD PLATINUM	$H_2O + CH_4$	0.5	8	97.8	1045 (1880)	NONE	0	0
	1B						1175 (2115)	NONE	0	0
	1C	(0.6% ThO_2)					1260 (2270)	A + P	40	0.41
	1D						1060 (1905)	P	TRACE	≃ 0.1
	2A						1062 (1910)	NONE	0	0
	2B						1230 (2215)	P	TRACE	≃ 0.1
	2C						1340 (2410)	P	240	2.45
	2D						1130 (2035)	P	60	0.61
	3A						1128 (2030)	NONE	0	0
	3B						1320 (2375)	A + P	120	1.22
	3C						1418 (2550)	P	630	6.44
	3D						1172 (2110)	P	200	2.04

* A - AMORPHOUS, P - PYROLYTIC

TABLE VIII

SUMMARY OF BIOWASTE HEATER TUBE TESTS L7 TO L11

TUBE PRESSURE 32 PSIA

Test No.	Tube No.	Tube Material	Propellant	Percent Oxygen	Bell Jar Press.	Flow Rate g/sec x 10^4	Test Duration Hours	Wall Temperature °K (°R)	Result
L7		Pt-20Ir	$H_2+CO_2+H_2O$ .73/.22/5	-	5μ	8	734	1640 (2950)	Large grain growth with pits and voids on grain boundaries mostly toward outer edge. (May be reaction with air at 5μ in bell jar.)
	3	Pt-20Ir	↓	-	5μ	8	734	1690 (3040)	
L8	2	Pt-20Ir	$CO_2+O_2+H_2O$ 98.3/1.3/0.4	1.2-1.4	10μ	10	137	1600 (2880)	Failed at grain boundaries
	3	Pt-20Ir		↓	↓	↓	160	1700 (3060)	Failed at grain boundaries
L9	1	TD-Pt*	CO_2+Air	1.0	1 μ	10	26	1600 - 1700	Failed by longitudinal crack
	2	↓	↓	↓	↓	↓	17	1700 - 1800 (3060-3240)	Failed by longitudinal crack
	3						10	1700 - 1800 (3060-3240)	Tube failed by longitudinal crack
L10	1	Pt-20 Pd	CO_2 + Air	1.5	1 atm	10	860	1500 (2700)	Significant Pd vaporization occurred.
	2	TD-Pt	↓	↓	↓	↓	887	1600 (2880)	Some attack at 1500°K station.
	3	Pt					765	1600 (2880)	Significant oxidation occurred.
L11	1	Pt-10Rh	CO_2 + Air	0.25	1 atm	10	1501	1700 (3060)	Some grain boundary attack
	2	TD-Pt	↓	↓	↓	↓	1501	1700 (3060)	Tube in excellent condition
	3	Pt					24.5**	1600 (2880)	Developed leak

*Contains 0.6% ThO_2

**Previously tested in Test L10

TABLE IX

SUMMARY OF BIOWASTE HEATER TUBE TESTS R5 TO R-8

TUBE PRESSURE 32 PSIA

Test No.	Tube No.	Tube Material	Propellant	Percent Oxygen	Bell Jar Press.	Flow Rate g/sec x 10^4	Test Duration Hours	Wall Temperature °K (°R)	Result
R5	1	Pt-20Ir	CO_2 + Air	1.0	8-12 μ	10	100	1570 (2826)	Large grain growth and internal oxidation.
	2	TD - Pt						1570 (2826)	Unaffected by test
	3	Pt-20Ir (Eloxed)						1570 (2826)	Large grain growth and internal oxidation.
R6	3	Pt	CO_2 + Air	1.5	1 atm	10	1036	1700 (3060)	Surface oxidation occurred.
	2	Pt-10Rh					500	1700 (3060)	Large grain growth and metal evaporation.
	1	Pt-20Pd					500	1600 (2880)	Large grain growth and metal evaporation.
R7	1	TD-Pt	CH_4	-	5 μ	10	189	1100-1200 (1980-2160)	Deposited carbon in tube
	2	TD-Pt	CH_4	-	5 μ		189	1200 (2160)	" " " "
	1	TD-Pt	CO_2 + Air	1.5	1 atm.		313	1600 (2880)	Removed carbon
	2	TD-Pt	CO_2 + Air	1.5	1 atm.		313	1600 (2880)	" "
R8	1	TD-Pt	CO_2	-	1 atm	10	1213*	1600 (2880)	Tube in excellent condition.
	2	TD-Pt		-	1 atm		1500	1700 (3060)	Tube in excellent condition.
	3	Pt-5Rh		-	1 atm		1500	1700 (3060	Tube in excellent condition.

*Previously tested in Test R7